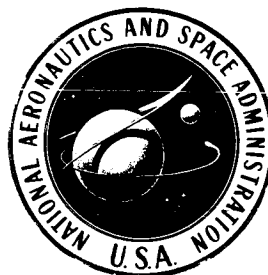


**NASA CONTRACTOR REPORT**



**NASA CR-66660**

**NASA CR-66660**

**FINAL REPORT**  
**STUDY OF DIRECT VERSUS ORBITAL ENTRY**  
**FOR MARS MISSIONS**

**Volume II - Parametric Studies, Final Analyses, and Conceptual Designs**

*Prepared by*

**MARTIN MARIETTA CORPORATION**  
**DENVER, COLORADO**

*for*

*Langley Research Center*

**NATIONAL AERONAUTICS AND SPACE ADMINISTRATION • WASHINGTON, D.C. • AUGUST 1968**

NASA CR-66660

FINAL REPORT

STUDY OF DIRECT VERSUS ORBITAL ENTRY FOR MARS MISSIONS

VOLUME II: PARAMETRIC STUDIES, FINAL ANALYSES,  
AND CONCEPTUAL DESIGNS

By Raymond S. Wiltshire

Distribution of this report is provided in the interest of information exchange. Responsibility for the contents resides in the author or organization that prepared it.

Prepared under Contract No. NAS1-7976 by  
MARTIN MARIETTA CORPORATION  
Denver, Colorado

for

NATIONAL AERONAUTICS AND SPACE ADMINISTRATION

### FOREWORD

This Final Report for the "Study of Direct Versus Orbital Entry for Mars Missions" (NASA Contract NAS1-7976) is provided in accordance with Part III A.4 of the contract schedule as amended. The report is in six volumes as follows:

- NASA CR-66659 - Volume I - Summary;
- NASA CR-66660 - Volume II - Parametric Studies, Final Analyses, and Conceptual Designs;
- NASA CR-66661 - Volume III - Appendix A - Launch Vehicle Performance and Flight Mechanics;
- NASA CR-66662 - Volume IV - Appendix B - Entry and Terminal Phase Performance Analysis;
- NASA CR-66663 - Volume V - Appendix C - Entry Configuration Analysis;
- NASA CR-66664 - Volume VI - Appendix D - Subsystem Studies and Parametric Data.

## CONTENTS

	<u>Page</u>
FOREWORD . . . . .	ii
CONTENTS . . . . .	iii
	thru
	vii
SUMMARY . . . . .	1
INTRODUCTION . . . . .	3
SYMBOLS AND ABBREVIATIONS . . . . .	5
PART I -- PARAMETRIC STUDIES SUMMARY . . . . .	19
1. MISSION ANALYSIS . . . . .	19
2. SUBSYSTEM STUDIES . . . . .	91
PART II -- FINAL ANALYSES AND CONCEPTUAL DESIGNS . . . . .	133
1. CONFIGURATION 1A DESCRIPTION, OUT OF ORBIT . . . . .	133
2. CONFIGURATION 2A DESCRIPTION, DIRECT ENTRY . . . . .	235
3. CONFIGURATION 1B DESCRIPTION, OUT OF ORBIT . . . . .	249
4. CONFIGURATION 2C DESCRIPTION, AUTONOMOUS CAPSULE . . . . .	259
5. CONFIGURATION 3 DESCRIPTION . . . . .	275
6. CONFIGURATION COMPARISONS . . . . .	291
CONCLUSIONS . . . . .	295
REFERENCES . . . . .	297

### Figure

1	Optimum Capsule System Weight, Entry from Orbit . .	23
2	Optimum Capsule System Weight, Direct Entry, Orbiter . . . . .	24
3	Optimum Capsule System Weight, Entry from Orbit, with and without Orbit Positioning . . . . .	25
4	Relay Communication Link during Entry . . . . .	27
5	Entry Location (Direct Mode) . . . . .	28
6	Ejection $\Delta V$ Requirements . . . . .	29
7	Targeting Boundary, Direct Mode . . . . .	31
8	Summary of Entry Locations (Orbit Mode) . . . . .	32
9	$\Delta V_D$ versus Lead Angle . . . . .	34
10	Targeting Boundary, Orbit Mode . . . . .	35
11	Approach Trajectory Geometry . . . . .	36
12	Possible $V_{HE}$ Vector Positions . . . . .	38
13	Possible Landing Area, Direct Mode . . . . .	40
14	Launch Date/Encounter Date . . . . .	43
15	Entry and Touchdown Dispersions, Direct Mode . . . .	44
16	Entry and Touchdown Dispersions, Orbit Mode . . . .	46
17	Peak Load Factor Limits, Orbit and Direct Modes . .	48
18	Entry Time Limits, Orbit and Direct Modes . . . . .	50



	<u>Page</u>
19 Downrange Angle Limits, Orbit and Direct Modes . .	51
20 Altitude at Mach 2.0 . . . . .	52
21 Altitude at Mach 3.0 . . . . .	53
22 Altitude at Mach 5.0 . . . . .	54
23 Altitude at Mach 2.0 . . . . .	55
24 Altitude at Mach 3.0 . . . . .	56
25 Altitude at Mach 5.0 . . . . .	57
26 Mars Skipout Boundary . . . . .	59
27 Landed Equipment Weight . . . . .	61
28 Aerodecelerator Performance, Entry from Orbit . . .	63
29 Terminal Phase Summary, Aeroshell Diameter = 8.5 ft . . . . .	65
30 Terminal Phase Summary, Aeroshell Diameter = 15 ft . . . . .	66
31 Terminal Phase Summary, Landed Equipment Weight = 600 lb . . . . .	67
32 Terminal Phase Summary, Landed Equipment Weight = 600 lb . . . . .	69
33 Terminal Phase Summary, Entry Weight = 1500 lb . .	70
34 Terminal Phase Summary, Entry Weight = 1500 lb . .	71
35 Maximum $W_{LE}$ , 10% Margin . . . . .	73
36 Maximum $W_{LE}$ , 10% Margin . . . . .	74
37 Orbit Mode, Aeroheating Sensitivities, VM-7, Cone Edge . . . . .	76
38 Direct Mode, Aeroheating Sensitivities, VM-7, Cone Edge . . . . .	78
39 Direct Mode, Aeroheating Sensitivities, VM-4, Cone Edge . . . . .	79
40 Maximum Heating Rate Comparison, $B = 0.30$ , Diameter = 15 ft, Cone Edge . . . . .	81
41 Total Heating Rate Comparison, $B = 0.30$ , Diameter = 15 ft, Cone Edge . . . . .	82
42 Performance Summary, Aeroshell Diameter = 8.5 ft .	85
43 Performance Summary, Aeroshell Diameter = 15 ft . .	86
44 Performance Summary, $W_{LE} = 600$ lb . . . . .	87
45 Performance Summary, $W_{LE} = 1500$ lb . . . . .	89
46 Results of Entry Science Error Analysis for Three Groups of Sensors . . . . .	94
47 Specific Humidity versus Frostpoint at the Martian Surface Showing Range of Present Estimates . . . .	97
48 Sampler and Analyzer Arrangement . . . . .	100
49 Aeroshell Structural Weight Comparison . . . . .	102
50 Parameter Layout Study, 15-ft Diameter Fixed Aeroshell with Flaps . . . . .	103

	<u>Page</u>
51 Projected Area versus Number of Simple Flaps on a 15-ft Fixed Cone . . . . .	105
52 Parametric Layout Study, 15-ft Diameter Fixed Aeroshell with Airmat Extension . . . . .	107
53 Comparison of Regulated and Blowdown Pressuriza- tion Subsystems . . . . .	111
54 Navigation Accuracy Effect on Entry Angle . . . . .	114
55 Planetary Approach Guidance Geometry . . . . .	116
56 Mars Lander Solar Array Output, 17° S Slope . . . . .	125
57 Thermal Control System Weight versus Lander Size (2-Day Life), Solid Chemical Energy Source . . . . .	129
58 Thermal Control System Weight versus Lander Size (2-Day Life), Battery Heat Source . . . . .	130
59 System Block Diagram, Configurations 1A, 1B, and 2A . . . . .	137
60 Space Vehicle Integration, Configuration 1A . . . . .	147
61 Atmosphere Structure Quantities from Entry Science Measurements . . . . .	149
62 Ratio of O/O <sub>2</sub> Ion Currents from Mass Spectrometer Measurements . . . . .	151
63 Viewing Geometry and Coverage . . . . .	153
64 Proposed Variable Parameter Facsimile Camera . . . . .	154
65 Examples of Surveyor I Photography for Visualizing Imaging Resolution Requirements . . . . .	156
66 Meteorology Package Concept . . . . .	157
67 Surveyor V Alpha Scattering Instrument . . . . .	158
68 Science Subsystem Functional Block Diagram . . . . .	164
69 Power Profile and Sequence Description . . . . .	165
70 Configuration 1A . . . . .	173
71 Landing Propulsion System . . . . .	181
72 Terminal Descent Profile and Propellant Utilization . . . . .	183
73 Deorbit Propulsion System . . . . .	185
74 Attitude Control System . . . . .	187
75 Development Status . . . . .	190
76 Guidance and Control Subsystem Block Diagram . . . . .	191
77 Inertial Measurement Unit Block Diagram . . . . .	193
78 Terminal Descent and Landing Radar Block Diagram . . . . .	194
79 Phase II Sequencer Block Diagram . . . . .	196
80 Telecommunications Subsystem Configuration . . . . .	200
81 Communications Subsystem Performance, Reference Orbit . . . . .	204
82 Communications Subsystem Performance, Alternative Orbit . . . . .	205
83 Communications Subsystem Performance, Reference Orbit . . . . .	206

	<u>Page</u>
84	Communications Subsystem Performance, Alternative Orbit . . . . . 207
85	Power Subsystem Block Diagram . . . . . 213
86	Entry Load Profile . . . . . 214
87	Landed Operations Load Profile . . . . . 215
88	Mars Lander Solar Array Output, 17° S Slope . . . . 217
89	Isolated Single-Point Ground . . . . . 219
90	Simplified Block Diagram, Lander Pyrotechnic Subsystem . . . . . 222
91	Thermal Control Subsystem . . . . . 224
92	Isotope Heater Control Concept . . . . . 227
93	Insulation Effective Conductivity . . . . . 229
94	Phase Change Packaging Concept . . . . . 230
95	Lander Temperature as a Function of Time, Hot Environment . . . . . 231
96	Lander Temperature as a Function of Time, Cold Environment, 100% N <sub>2</sub> Atmosphere . . . . . 232
97	Space Vehicle Integration, Configuration 2A . . . . 239
98	Configuration 2A . . . . . 241
99	Space Vehicle Integration, Configuration 1B . . . . 253
100	Configuration 1B . . . . . 255
101	System Block Diagram, Configuration 2C . . . . . 262
102	Configuration 2C . . . . . 267
103	Autonomous Capsule Thermal Control . . . . . 270
104	Space Vehicle Integration, Configuration 2C . . . . 274
105	Configuration 3 . . . . . 279
106	System Block Diagram, Configuration 3 . . . . . 283
107	Space Vehicle Integration, Configuration 3 . . . . 290

Table

1	Part II Point Designs . . . . .	4
2	Optimum Capsule System Weight for Entry from Orbit, Fixed Spacecraft, 30-Day Launch Period . . . . .	22
3	Optimum Direct Entry Capsule System Weight, Fixed Orbiter Propulsion, 30-Day Launch Period . . . . .	22
4	Flight Capsule Mission Objectives, Science Requirements, and Science Measurements . . . . .	92
5	Measurement Accuracies and Sampling Rates . . . . .	95
6	Summary of Extension to '73 Science Equipment for 1975 and 1977 Missions . . . . .	98
7	Planetary Approach Guidance Summary of Results . . . . .	117
8	Comparison of Direct-Link Performance . . . . .	122
9	Thermal Control Parameters . . . . .	127
10	Configuration 1A Performance Parameters . . . . .	135
11	Configuration 1A Sequential Weight Statement . . . . .	145

	<u>Page</u>
12 Science Instrument Summary, 1973 . . . . .	159
13 Equipment Status . . . . .	161
14 Science Sequence of Events . . . . .	167
15 Detailed Weight Statement . . . . .	170
16 Propulsion Subsystem Characteristics . . . . .	186
17 Attitude Control System . . . . .	188
18 GCC Functional Requirements . . . . .	195
19 G&C Weight, Power, and Volume . . . . .	197
20 Subsystem Performance ( $3\sigma$ ) . . . . .	198
21 Component Performance . . . . .	198
22 Telemetry Subsystem Predicted Weight, Power, and Volume . . . . .	202
23 Entry Link . . . . .	208
24 Initial Postland Contact (Impact + 10 min) . . . .	209
25 UHF Communication Subsystem Weight, Power, and Volume . . . . .	210
26 S-Band Communication Subsystem Weight, Power, and Volume . . . . .	211
27 Power Subsystem Weights . . . . .	220
28 Pyrotechnic Subsystem Weights . . . . .	223
29 Thermal Environments . . . . .	225
30 25 to 30 W Isotope Heater Summary . . . . .	226
31 Configuration 2A Performance Parameters . . . . .	236
32 Configuration 2A Sequential Weight Statement . . .	238
33 Configuration 2A Propulsion Subsystem Character- istics . . . . .	247
34 Configuration 2A Attitude Control System . . . . .	248
35 Configuration 1B Performance Parameters . . . . .	250
36 Configuration 1B Sequential Weight Statement . . .	251
37 Configuration 1B Propulsion Subsystem Character- istics . . . . .	257
38 Configuration 1B Attitude Control System . . . . .	258
39 Configuration 2C Performance Parameters . . . . .	260
40 Configuration 2C Sequential Weight Statement . . .	272
41 Configuration 3 Performance Parameters . . . . .	276
42 Extended Capsule Mission Objectives and Science Requirements, 1975 and 1977 . . . . .	278
43 Configuration 3 Sequential Weight Statement . . . .	289
44 Mission, Sequential Weight, and Subsystem Parameters, Configurations 1A, 1B, and 2A . . . . .	292
45 Summary Weight Comparison . . . . .	294

## FINAL REPORT

### STUDY OF DIRECT VERSUS ORBITAL ENTRY FOR MARS MISSIONS

#### VOLUME II: PARAMETRIC STUDIES, FINAL ANALYSES, AND CONCEPTUAL DESIGNS

By Raymond S. Wiltshire  
Martin Marietta Corporation

#### SUMMARY

This report documents the results of all the work in the Study of Direct versus Orbital Entry for Mars Missions. The contract tasks were divided into two general parts:

- Part I - Parametric studies of the problems associated with the direct entry mode. Payload capability of a wide range of capsules (500 to 10 000 lb) to be determined and compared with data developed for the out-of-orbit mode;
- Part II - Refinement of selective representative capsules together with their conceptual design. Three conceptual designs were emphasized, covering a range of capsule weights and including integration with a launch vehicle. Three additional designs were carried only to the point where Langley Research Center and Martin Marietta felt further study would not be fruitful.

Mission analyses, considering launch vehicle performance, launch period selection, targeting capability, entry corridors, terminal phase, and aerothermodynamics, were conducted.

The launch vehicles considered were Titan IIIC, Titan IIIF/Stretched Transtage, Titan IIIC/Centaur, and Titan IIIF/Centaur. The basic launch capability has been evaluated as a function of launch date and encounter date for each of the launch opportunities (1973, 1975, and 1977) for both Type I and Type II transfers. The 30-day launch periods that optimize launch vehicle performance have been identified. Orbiters weighing 600 and 900 lb were investigated in orbits of 1000x15 000 and 1000x33 070 km to determine allowable flight capsule weights.

The Titan IIIC/Centaur launch vehicle is required for either mission mode when an orbiter science capability is desired.

Targeting capability and landing footprint size were determined for each mission mode. The targeting capability is the same in either mission mode when considering only flight profile constraints. However, superimposing any time or orientation constraints decreases the direct mode landing site selection flexibility. For example, if multistation tracking is required at encounter, the achievable longitudes are limited in the direct mode. The orbit mode allows selection of orbits more desirable from an orbiting science mission viewpoint without compromising the landing site selection. The accuracy analysis shows smaller entry dispersions and landing footprints for the orbit mode.

The terminal phase systems considered included subsonic parachute plus vernier, tuckback ballute plus vernier, all retropropulsion, and two-burn propulsion with and without a parachute. The Mach 2 parachute is the most efficient from a weight standpoint, while the ballutes are favored from the aeroshell diameter standpoint. The Mach 2 parachute is preferred on the basis of more straightforward packaging and release considerations. A bulbous shroud is definitely required for direct mode, and is probably required for the out-of-orbit mode when providing margin.

For a 500- to 650-lb landed equipment weight (845- to 950-lb useful landed weight) configuration having approximately the same coast time and communication range, the mission mode choice has a negligible effect on the science, telecommunication, power, propulsion, and thermal control subsystems.

The out-of-orbit mode provides more in-flight mission flexibility than the direct mode by providing site survey prior to separation, opportunity to correct malfunctions prior to separation from the orbiter, targeting change capability, and higher landed weights within a given aeroshell diameter. The out-of-orbit mode avoids several problems of the direct mode resulting from more severe entry environment (acceleration, heating rate), approach guidance instruments required on orbiter, and a more rapid sequence of events.

## INTRODUCTION

The present study was conceived to provide data as a basis for judgment as to whether the direct entry or out-of-orbit mission modes should be used for Mars landing missions. This study is based on the Titan III family of launch vehicles. The basis for conducting the study was to draw heavily on the Voyager Phase B study in providing parametric data for the out-of-orbit mode.

Specifically, the objectives of the present study were to (1) obtain data on the net science payload weight available for capsules utilizing the direct mode, and (2) evaluate the capsule mode, direct and out-of-orbit, for soft lander missions. The Martin Marietta study is believed to be in complete response to the requirements established by Langley Research Center, National Aeronautics and Space Administration. Specifically the study has:

- 1) Completed the Part I mission analysis and profiles and capsule analytical studies;
- 2) Developed the Part II final analyses and conceptual designs relating to the mission definition, flight capsule, and spacecraft/launch vehicle integration;
- 3) Conducted the other mission, system, and subsystem investigations required by the contract;
- 4) Selected a recommended mission mode and configuration from the conceptual designs that best satisfy the study objectives, guidelines, and constraints and emphasizes the availability for the 1973 launch opportunity.

Performance data have been generated for the Titan IIIC, Titan IIIF/Stretched Transtage, Titan IIIC/Centaur, and Titan IIIF/Centaur. The entry corridor and landing site footprint have been analyzed. Parametric analyses were also conducted in mission design areas to determine the effect of mission mode choice on targeting, deorbit/deflection velocity increment, entry flightpath angle, required aeroshell ballistic coefficient, parachute size, parachute deployment altitude, time on parachute, required vernier ignition altitude, and landing terrain height.

Parametric analyses were made on each of the capsule subsystems over the range necessary to accommodate 500- to 10 000-lb flight capsule weights. In addition to developing parametric weight equations, different design approaches were investigated.

The parametric analyses are summarized in Part I of this volume and are discussed in more detail in the appendixes.

Based on the Part I parametric analysis, three point designs were selected by Langley Research Center to be further defined in the Part II final analysis and conceptual designs. These are shown in table 1.

TABLE 1.- PART II POINT DESIGNS

	1	2			3
		2A	2B	2C (autonomous)	
Landed equipment weight, lb	500 to 600	← 500 to 600 →			1200 to 1500
Useful landed weight, lb	845	← 914 to 950 →			1600 to 1900
Capsule system weight, lb	1500 to 1700	1900 to 2000		2100	4000
Mission mode	Orbital	Direct (Orbital S/C)		Direct	Orbital
Aeroshell Diameter, ft	8.5	10.75		11.5 11	12 to 15
Entry flightpath angle, $\gamma_E$ , deg	18	24	24	24	18
Spacecraft	950-lb Mariner	950-lb Mariner	600-lb Mariner	Auto- capsule	950-lb Mariner
Launch vehicle	Titan IIIC/ Centaur	Titan IIIC/ Centaur	Titan IIIF/ St. Trans.	Titan IIIC	Titan IIIC/ Centaur
Surface lifetime	> 2 days	← > 2 days →			> 6 months

Configuration 1 (since designated 1A), using the out-of-orbit mission mode, fits within the existing Titan III shroud and requires the Titan IIIC/Centaur launch vehicle. The 500- to 600-lb landed equipment weight is the minimum required to meet the study goals of science, data, and lifetime. Solar array/battery power is used on the configuration with an expected lifetime greater than two days.

Configurations 2A and 2B are for a direct entry of the capsule with the orbiter being placed into orbit following landing of the capsule.



The autonomous (2C) capsule varies significantly from the previous configuration because of its additional orbiter role. It has the advantage of requiring the smallest launch vehicle, but has several serious shortcomings in satisfying this mission.

Configuration 3 is representative of later mission capsules using the out-of-orbit mode. Its 1200- to 1500-lb landing weight represents a significant increase in science capability and lifetime. The Titan IIIC/Centaur with a bulbous shroud is required to accommodate this configuration.

As a result of the second oral progress report given at Langley Research Center, May 28, 1968, the emphasis of the conceptual designs was modified to replace Configuration 2C with a new Configuration 1B and eliminate Configuration 2B. Configuration 1B is a 500- to 600-lb landed equipment weight and out-of-orbit mode, with the aeroshell diameter sufficiently increased over that of Configuration 1A to provide weight and operational margins. Guidelines include a nominal entry ballistic coefficient of 0.35, parachute deployment at 20 000 ft above terrain, and an assumption of zero terrain elevations. This results in system comparisons between Configuration 1A (previously 1), 1B, and 2A.

Configurations 2C (autonomous) and 3 have been documented in this report as they existed when we, with Langley Research Center's concurrence, stopped that portion of the study.

#### SYMBOLS AND ABBREVIATIONS

A	aerodynamic reference area, square feet; pre-exponential constant, seconds <sup>-1</sup> ; 3x3 matrix relating planet-oriented axis with stability axis
a	semimajor axis, kilometers; slant length of cone extended to the apex
ACS	attitude control system
AM0	air mass zero
AMR	altitude measuring radar
A <sub>v</sub>	Avogadro's number, $6.02 \times 10^{23}$ molecules/g mol

$a_x$	acceleration along flightpath
B	ballistic coefficient, slugs/foot <sup>2</sup> ; activation energy, °R
b	impact parameter asymptote, kilometers
$B_{DEC}$	aerodecelerator ballistic coefficient, slugs/foot <sup>2</sup>
$B_E, B_e$	entry ballistic coefficient, slugs/foot <sup>2</sup>
BER	bit error rate
BF	flange width, inches
BF(br)	flange width on aeroshell intermediate frames
bps	bits per second
BS	frame spacing, inches
BS(bs) <sup>(b)</sup>	intermediate frame spacing on cone
BW	web depth, inches
BW(br)	web depth on aeroshell intermediate frames
c	heat capacity, Btu/pound °F
$C_D$	drag coefficient
C(K)	local instability coefficient
$C_p$	pressure coefficient
$c_p$	ablator specific heat, Btu/pound °R
$c_{p_g}$	vapor specific heat, Btu/pound °R
$C_3$	earth escape energy, kilometers <sup>2</sup> /second <sup>2</sup>
d	one-half honeycomb core thickness

DAS	data automation system
$D_{A/S}$	diameter of aeroshell, feet
$D_{DEC}$	diameter of aerodecelerator, feet
DLA	declination of departure asymptote, degrees
D/O	deorbit
$dp/ds$	local pressure gradient, pound/inch <sup>2</sup> inch
DSIF	Deep Space Instrumentation Facility
DSS	Deep Space Station
E	modulus of elasticity
e	orbit eccentricity; edge
$E_B$	energy of battery, watt-hours
ERP	effective radiated power
$E_T$	radiation intensity, watts/centimeter <sup>3</sup>
ETR	Eastern Test Range
F	thrust; matrix of partial derivatives
f	volatile fraction of ablator
FSK	frequency shift keying
G,g	gravitational acceleration
G	universal gravitational constant, kilometer <sup>2</sup> /second <sup>2</sup>
g.	earth gravitational constant, 32.174 feet/second <sup>2</sup>
G&CC	guidance and command control
h	altitude, feet

$h_E$	entry altitude, 800 000 feet
$h_p$	periapsis altitude of orbiter, kilometers
$h_T$	terrain height, feet; tropopause altitude
$H_w$	wall enthalpy, Btu/pound
$H_\gamma$	recovery enthalpy, Btu/pound
$I$	moment of inertia of structure over a width $b$
$i$	orbiter inclination, degrees
$i_{PIS}$	orbiter inclination to plane normal to Earth/Mars line of sight, degrees
$I_{sp}$	specific impulse, seconds
$K$	optimal linear gain
$k$	thermal conductivity, Btu/hour foot $^{\circ}F$ ; ablator thermal conductivity, Btu/inch-second- $^{\circ}R$
$kb$	kilobits
$kbps$	kilobits per second
$L$	liquid; slant length of cone
$LAZ$	launch azimuth (ETR), degrees
$L_p$	heat of pyrolysis, Btu/pound
$LRM$	liquid rocket motor
$M$	Mach number; Mars; mass, slugs
$m$	total mass of entry vehicle

$\bar{m}$	mean molecular weight
$m_a$	mass of air containing $m_v$
M/C	midcourse
$\dot{m}_c$	mass loss rate of surface material, pounds/inch <sup>2</sup> -second
MFS	multiple frequency shift
MFSK	multiple frequency shift keying
MMH	monomethylhydrazine
$M_o$	molecular weight
MR	mixture ratio
$m_v$	mass of water vapor
$\dot{m}_v$	pyrolysis vapor mass flow at x, pounds/inch <sup>2</sup> -second
n	load factor; reaction order
$n_k$	number density for k <sup>th</sup> species
OSE	operational support equipment
P	pressure, pounds/foot <sup>2</sup> ; ambient pressure; power, watts; covariance matrix of state vector
p	structural design pressure
PC	time for battery charging
$P_c$	battery charging power, watts
$P_c$	chamber pressure
$P_f$	final tank pressure

$P_i$	initial tank pressure
P/L	payload
PN	pseudorandom noise
PRIME	Precision Recovery including Maneuvering Entry
$P_S$	source power, watts; surface pressure; stagnation pressure
PSK/PM	phase shift keying/phase modulation
$P_1$	continuous power, watts
$P_2$	peak power, watts
$P_{\Delta}$	power delta (peak power minus continuous power), watts
Q	thermal energy, Btu; integrated heating, Btu/foot <sup>2</sup>
$\dot{Q}$	heat rate, Btu/hour
q	specific humidity; random noise in measurement; dynamic pressure
$\dot{q}$	heating rate, Btu/foot <sup>2</sup> -second
$\dot{q}_r$	radiation heating rate, Btu/inch <sup>2</sup> -second
R	radius of curvature; local body radius, inches
R;R*	universal gas constant, $8.3 \times 10^7$ erg/mol °K
r	radius vector to point of transfer injection, kilometers; distance from vehicle to planet center; radius, feet
$R_B$	aeroshell base radius, inches
$R_C$	rate of charge, hours

$R_{EJ}$	ejection distance for direct mode, kilometers
$R_o$	base radius of nose cap
$r_o$	radius of planet
$r_p$	radius vector to Mars-orbit periapsis; periapsis radius, kilometers
RTG	radioisotope thermoelectric generator
$R_\phi$	radius of Mars (3393 km)
S/C	spacecraft
SFC	squib firing circuit
SNR	signal-to-noise ratio
SRM	solid rocket motor
T	ambient temperature, degrees
t	time; temperature, °R or °F; nose cap thickness
$\bar{t}$	smear thickness of structure over a width b
$t_c$	coast time (from ejection/deorbit to entry), hours
$t_D$	time of daylight
TDLR	terminal descent and landing radar
TF	frame thickness
TGA	thermogravimetric analysis
tm	monocoque skin thickness
T/M	telemetry
$t_N$	time of night

$t_p$	time of periapsis passage
TS	skin thickness
$T_s$	stagnation temperature; surface temperature
TS(ts)	aeroshell skin thickness, inches
$T_u$	tropopause temperature
$T_w$	surface temperature
T/W	thrust-to-weight ratio
TWT	traveling wave tube
TWTA	traveling wave tube amplifier
$t_1$	continuous power period, hours
$t_2$	peak power period, hours
TIIC	Titan IIIC
TIIF	Titan IIIF
$u$	tangential velocity $\left( \tau \int \frac{1}{\mu} dy + \left( \frac{dp}{ds} - \rho_g \sin \theta \right) \int \frac{x}{\mu} dx \right)$ , inches/second
$V$	velocity, feet/second or kilofeet/second
$v$	speed along flightpath; easterly component of horizontal velocity
VCO	voltage control oscillator
VDA	valve drive amplifiers
$V_E$	entry velocity, feet/second
$V_{HE}$	Mars approach energy, kilometers/second; hyperbolic excess velocity vector, kilometers/second



$V_{\text{INJ}}$	velocity required for Mars transfer injection, kilometers/second
$W$	weight, pounds
$w$	northerly component of horizontal velocity; argument of periapsis, degrees
$W_A$	spacecraft-to-capsule weight, pounds
$W_{\text{ACS-E}}$	ACS weight, expended, pounds
$W_{\text{ACS-F}}$	ACS weight, fixed, pounds
$W_{\text{A/D-E}}$	aerodecelerator weight, expended, pounds
$W_{\text{A/D-F}}$	aerodecelerator weight, fixed, pounds
$W_{\text{A/S}}$	aeroshell weight, pounds
$W_{\text{BF}}$	backface shield weight, pounds
$W_C$	canister weight, pounds
$W_{\text{C/S}}$	capsule system weight, pounds
$W_{\text{DP}}$	deorbit propulsion system (including propellant) weight, pounds
$W_{\text{DS}}$	deorbit structure weight, pounds
$W_E$	entry weight, pounds
$W_{\text{E/L}}$	adapter electrical weight, pounds
$W_{\text{F/B}}$	flyby spacecraft useful weight, pounds
$W_{\text{G/C-T}}$	terminal guidance weight, pounds
$W_i$	initial weight, pounds

$W_j$	weight after maneuver, pounds
$W_L$	sterilization canister weight, pounds; landed weight, pounds
$W_{LE}$	landed equipment weight, pounds
$W_{LS}$	lander structure weight, pounds
$W_o$	weight before maneuver, pounds
$W_{OR}$	useful in-orbit orbiter weight, pounds
$W_P$	propellant weight, pounds
$W_{PI}$	propulsion system unit weight, pounds
$W_{PIL}$	useful in-orbit weight, pounds
$W_{PY}$	pyrotechnic control weight, pounds
$W_S$	capsule system weight, pounds; propulsion module structural weight, pounds
$W_{S-A/S}$	weight of science in aeroshell, pounds
$W_{S/C}$	spacecraft weight, pounds
$W_{TE}$	telecommunication cabling weight, pounds
$W_{TG}$	terminal guidance system weight, pounds
$W_{TH}$	thermal control weight, pounds
$W_V$	verniered weight, pounds
$W_{V_o}$	system weight at vernier ignition, pounds

$W_{VP-E}$	vernier propellant weight, expended, pounds
$W_{VP-F}$	vernier propellant weight, fixed, pounds
$X$	state vector
$x$	length, feet
$X_R$	crossrange angle (from ejection/deorbit to entry), degrees
$Y$	measurement vector
$\alpha$	angle of attack, degrees; thermal absorptivity
$\alpha_{CE}$	capsule antenna aspect angle at entry, degrees
$\alpha_E$	capsule angle of attack at entry, degrees
$\alpha_{CTD}$	capsule antenna aspect angle at touchdown, degrees
$\beta$	entry location parameter (between entry point and orbit periapsis measured positively opposite direction of of motion), degrees; sideslip angle, degrees
$\gamma$	relative flightpath angle, degrees; ratio of specific heats
$\gamma_A$	flightpath angle relative to atmosphere, degrees
$\gamma_E$	entry flightpath angle, degrees
$\delta_{HE}$	declination of $\vec{V}_{HE}$ with respect to the Martian equator, degrees
$\Delta H_r$	heat of reaction, Btu/pound
$\Delta V$	velocity change; velocity increment

$\Delta V_D$	deorbit impulse, meters/second
$\Delta V_{D_{MIN.}}$	minimum deorbit impulse, meters/second
$\Delta V_{EJ}$	ejection impulse for direct mode, meters/second
$\Delta V_{OI}$	Mars orbit insertion velocity increment, kilometers/ second
$\Delta W_{FJ}$	jettisoned weight, pounds
$\Delta W_{PIL}$	launch-vehicle payload increment, pounds
$\Delta \beta$	variation in entry location parameter, $\beta$ , degrees
$\Delta(\Delta V_{O.I.})$	incremental velocity required for periapsis shift, degrees
$\Delta \omega$	argument of periapsis shift at orbit insertion, degrees
$\epsilon$	Mars orbit eccentricity; emissivity
$\zeta_p$	angle between $\vec{V}_{HE}$ and Mars-sun vector, degrees
$\eta_B$	battery charge acceptance efficiency
$\eta_C$	battery charger efficiency
$\eta_D$	diode efficiency
$\eta_R$	regulator efficiency
$\theta$	thrust vector angle, degrees; time, Mars-days
$\theta_D$	true anomaly of deorbit, degrees
$\theta_{FM}$	fading margin angle (between reflected signal from cap- sule to surface to orbiter and local vertical at re- flection point), degrees

$\lambda$	orbiter lead angle, degrees; propulsion system mass fraction, $\frac{\text{propellant weight}}{\text{total weight}}$
$\lambda(x)$	nondimensional density, $\frac{\rho(x) - \rho_{\text{char}}}{\rho_{\text{vp}} - \rho_{\text{char}}}$
$\mu$	Poisson's ratio; universal gravitational constant x mass; melt viscosity, pound-seconds/inch <sup>2</sup>
$\mu_{\text{M}}$	gravitational parameter of Mars, 42 830 km <sup>3</sup> /sec <sup>2</sup>
$\rho$	density, slugs/foot <sup>3</sup>
$\rho_{\text{CE}}$	capsule-to-orbiter communication distance at entry, kilometers
$\rho_e^H C_H$	net heat-transfer coefficient, pounds/inch <sup>2</sup> -second
$\rho_k$	mass density for k <sup>th</sup> species
$\rho_o$	density constant, 0.0025 slug/foot <sup>3</sup>
$\rho_{vq}$	ablator virgin density, pounds/inch <sup>3</sup>
$\rho(x)$	ablator density at x, pounds/inch <sup>3</sup>
$\sigma$	standard deviation; roll angle, degrees; Stephan-Boltzmann constant, Btu/inch <sup>2</sup> -seconds °R
$\tau$	aerodynamic shear stress, pounds/inch <sup>2</sup> ; shear stress, pounds/foot <sup>2</sup>
$\tau'$	central angle between $\vec{V}_{\text{HE}}$ and orbiter periapsis, degrees
$\tau_{\text{EJ}}$	ejection angle, degrees
$\phi_E$	downrange angle traversed from ejection/deorbit to entry, degrees

$\phi_L$  central angle from  $\vec{V}_{HE}$  to landing site, degrees

$\Omega$  right ascension of ascending node, degrees;  
rotation rate of planet

$\theta_c$  1/2 included cone angle, degree

Subscripts:

A/S aeroshell

B base

C convective

D deployment conditions

DEC decelerator

E entry; entry conditions

F final conditions

I initial conditions

Lam laminar

N nose

R radiative

S solid;  
stagnation point

T terminal

Turb turbulent

$\infty$  free-stream conditions

$\oplus$  Earth

$\circ$  Mars

2 conditions behind normal shock

PART I

PARAMETRIC STUDIES SUMMARY

## 1. MISSION ANALYSIS

The mission analysis discussion presented summarizes the parametric analyses of the launch vehicle performance, the launch period selection, targeting analysis, error analysis, entry trajectory analysis, terminal phase system comparisons, and aerothermodynamic analysis. Most of the detailed data associated with these analyses are presented in Appendix A, Launch Vehicle Performance and Flight Mechanics; Appendix B, Entry and Terminal Phase Performance Analysis; and Appendix C, Entry Configuration Analysis.

### Objectives and Constraints

The objectives of these analyses were to evaluate the various aspects of the Mars missions in the 1973 to 1977 period both from the point of view of mission mode (i.e., direct mode or entry from the approach trajectory, and orbit mode or entry from orbit), and comparison of types of delivery systems. The delivery system analysis includes launch vehicle selection at one end of the mission and the terminal phase system at the other end of the mission. The launch vehicles considered are the Titan IIIC, Titan IIIF/Stretched Transtage, Titan IIIC/Centaur, and Titan IIIF/Centaur. Basic definitions of these vehicles are given in Appendix A. The terminal phase systems considered include subsonic-type parachute plus vernier, tuckback ballute plus vernier, all retropropulsion landing system, and two-burn systems with a solid rocket motor for braking prior to parachute or all-retro system deployment.

The range of variables defined for this analysis include:

- 1) Flight capsule system weights from 500 to 5000 lb (orbit mode) and 500 to 10 000 lb (direct mode);
- 2) Entry velocities up to 16 000 fps (orbit mode) and 24 000 fps (direct mode);
- 3) Entry flightpath angles up to  $-\gamma_E = 20^\circ$  (orbit mode) and  $-\gamma_E = 38^\circ$  (direct mode).

Other constraints imposed on the analysis are:

- 1) Maximum launch vehicle shroud diameter of 16 ft;
- 2) Orbit sizes of 1000x15 000 km (periapsis by apoapsis altitude) and 1000x33 070 km;



- 3) 1973, 1975, and 1977 launch opportunities, both Type I and Type II transfers;
- 4) Landing sites near the equator and  $30^\circ$  from the (evening) terminator.

The shroud size limitation has been interpreted in this parametric analysis to limit the aeroshell diameter to approximately 15 ft for the hammerheaded 16-ft shroud. Aeroshell diameters greater than 15 ft are obtained by deploying flaps or extendible afterbodies.

The parametric analyses performed are summarized for the various mission phases studied. The integration of these results into a mission mode comparison follows the description of the parametric analyses. It must be understood that the mission mode comparison presented in this section deals only with the parametric analyses results. The influence of hardware design, development status, etc. appear in subsequent sections of this report.

#### Summary of Parametric Analyses

The parametric analyses summarized are grouped into:

- 1) Launch vehicle capability;
- 2) Launch period selection and targeting analysis;
- 3) Entry corridor and landing footprints;
- 4) Entry trajectory and terminal phase system analysis;
- 5) Aerothermodynamic analysis.

Because so much data have been generated in each of these areas, they are, for the most part, presented in Appendixes A, B, and C. Only the more significant factors that enter into the mission mode comparison are presented in this subsection.

Launch vehicle capability. - The launch vehicles considered in this analysis are the Titan IIIC, Titan IIIF/Stretched Transtage, Titan IIIC/Centaur, and Titan IIIF/Centaur. The Titan IIIC vehicle corresponds to the Article 19 vehicle and includes 5-segment strap-on solid rocket motors. The Titan IIIF vehicle has 7-segment solid rocket motors and a stretched Stage I. A stretched (tank) Transtage is assumed for the Titan IIIF/Stretched Transtage configuration to allow the use of a circular Earth parking orbit. The vehicle characteristics are defined in more detail in Appendix A, section 1.

The basic launch vehicle capability has been evaluated as a function of launch date and encounter date for each of the launch opportunities (1973, 1975, and 1977) and for both Type I and Type II (heliocentric) transfers. These data are given as allowable cruise weight contours after midcourse correction. The data assume a launch azimuth of  $115^\circ$  where launch azimuths of  $90^\circ$  to  $115^\circ$  are possible, and a required launch azimuth up to a minimum limit of  $45^\circ$  for launch date/encounter date combinations requiring launch azimuths that do not lie in the range from  $90$  to  $115^\circ$ . An arbitrary midcourse  $\Delta V$  capability is conservatively assumed to be 75 m/sec. The data are corrected for spacecraft adapter and shroud losses (defined in Appendix A).

From these data the 30-day launch periods that optimize launch vehicle performance have been identified. The resultant optimum launch vehicle performance is summarized in tables 2 and 3 for the orbit and direct modes, respectively. The data shown have been reduced to allowable capsule system weight for two sizes of orbiter. Capsule system weight, as defined here, includes the entry vehicle, deorbit/ejection module, capsule-to-orbiter adapter, and sterilization canister. The two orbiter sizes identified in these tables are 890 lb and 620 lb. This weight is useful orbiter weight and does not include the orbit insertion motor dry weight. Orbiter propulsion characteristics (propellant plus system weight) are sized for the maximum requirement over the launch period. Orbit propulsion system  $I_{sp} = 309$  seconds. Data for two orbit eccentricities are also presented. The  $e = 0.785$  corresponds to the  $1000 \times 33\,070$ -km orbit and the  $e = 0.614$  corresponds to the  $1000 \times 15\,000$ -km orbit.

The general characteristics exhibited in tables 2 and 3 are that the 1973-I, 1975-II, and 1977-II opportunities maximize the performance capability. The 1973-II capability is low because of higher Earth departure energy requirements ( $C_3$ ). The 1975-I and 1977-I opportunities require launch azimuths up to  $45^\circ$ .

The data shown in tables 2 and 3 are summarized in figures 1 and 2 for the 1973-I, 1975-II, and 1977-II opportunities. These data illustrate that the combination of launch vehicle, orbiter size, and orbit selection can be selected for capsule system weights from a few hundred pounds to over 5000 lb for the orbit mode, and up to 10 000 lb for the direct mode. A final consideration is the potential need for orbit positioning to improve the targeting flexibility with the orbit mode (discussed below). This possible requirement increases the orbit insertion  $\Delta V$  with the payload penalty shown in figure 3. This payload penalty is quite small.

TABLE 2.- OPTIMUM CAPSULE SYSTEM WEIGHT FOR ENTRY FROM ORBIT, FIXED SPACECRAFT, 30-DAY LAUNCH PERIOD

Mission opportunity	Transfer type	Orbit eccentricity	Capsule system weight (lb)*			
			TIIIC	TIIIF/T	TIIIC/C	TIIIF/C
1973	I	0.785	350/620	1010/1280	3550/3820	5060/5330
		0.614	220/490	825/1095	3140/3410	4530/4800
	II	0.785	90/360	630/900	2900/3170	4170/4440
		0.614	----/230	480/750	2550/2820	3680/3950
1975	I	0.785	----/----	----/230	1760/2030	2650/2920
		0.614	----/----	----/110	1360/1630	2210/2480
	II	0.785	500/770	1180/1450	3860/4130	5490/5760
		0.614	360/630	985/1255	3440/3710	4920/5190
1977	I	0.785	----/----	----/----	1830/2100	2830/3100
		0.614	----/----	----/----	1420/1690	2260/2530
	II	0.785	850/1120	1620/1890	4600/4870	6440/6710
		0.614	680/950	1370/1640	4110/4380	5820/6090
*890-lb orbiter/620-lb orbiter.						

TABLE 3.- OPTIMUM DIRECT ENTRY CAPSULE SYSTEM WEIGHT, FIXED ORBITER PROPULSION, 30-DAY LAUNCH PERIOD

Mission opportunity	Transfer type	Orbit eccentricity	Capsule system weight (lb)*			
			TIIIC	TIIIF/T	TIIIC/C	TIIIF/C
1973	I	0.785	450/940	1570/2060	5920/6390	8590/9060
		0.614	270/790	1390/1910	5740/6250	8340/8840
	II	0.785	125/660	1235/1765	5590/6110	8235/8775
		0.614	----/500	1050/1610	5410/5960	7985/8535
1975	I	0.785	----/----	----/450	4210/4770	6490/7080
		0.614	----/----	----/270	3880/4570	6250/6920
	II	0.785	750/1210	1870/2340	6220/6670	8870/9310
		0.614	560/1070	1690/2190	6040/6525	8690/9190
1977	I	0.785	----/----	80/630	4360/4920	6630/7180
		0.614	----/----	----/470	4170/4750	6420/7030
	II	0.785	1280/1700	2570/2910	6790/7220	9580/10 000
		0.614	1100/1575	2300/2770	6640/7090	9420/9910
*890-lb orbiter/620-lb orbiter.						

Fixed spacecraft propulsion  
30-day launch period

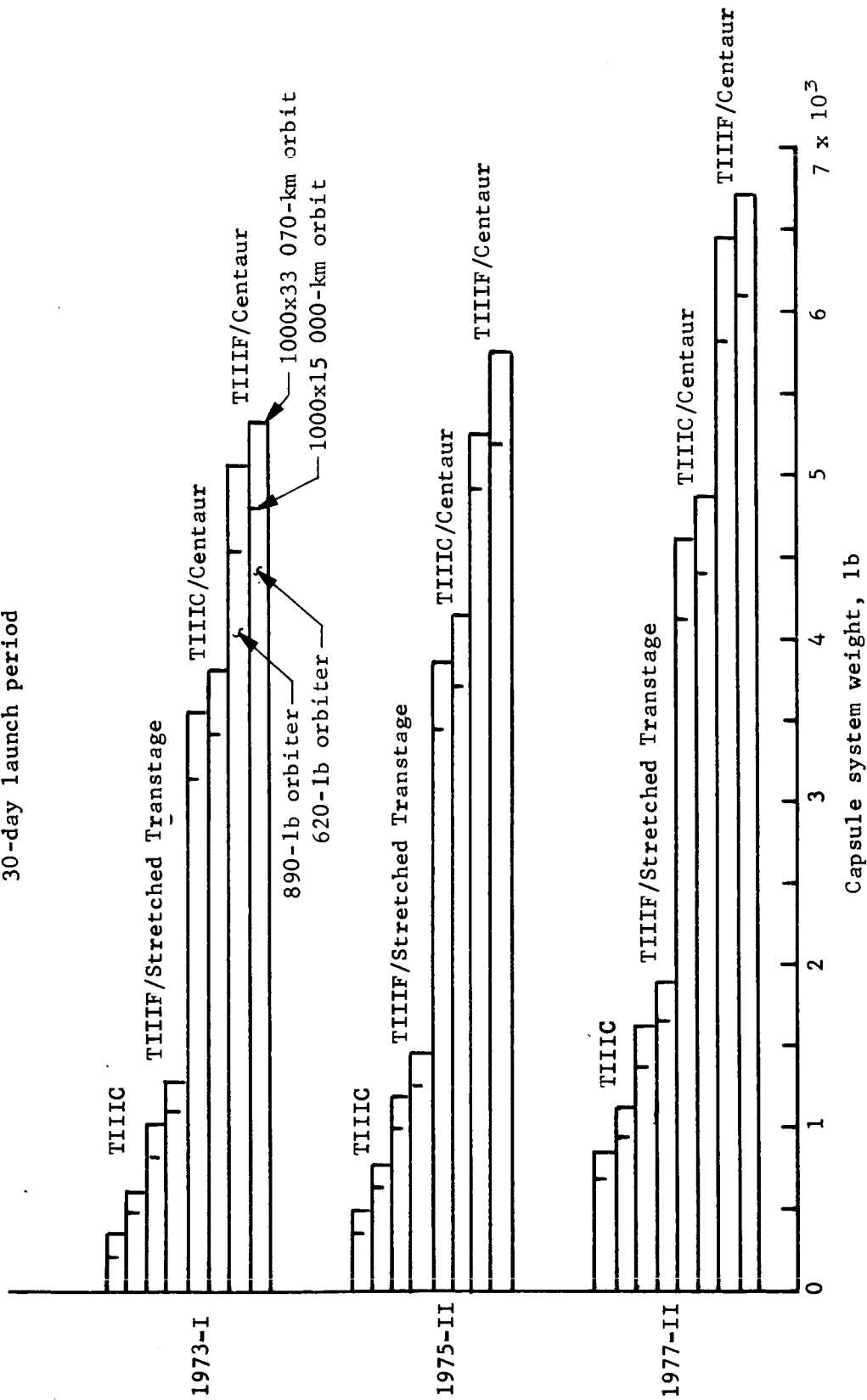


Figure 1.- Optimum Capsule System Weight, Entry from Orbit

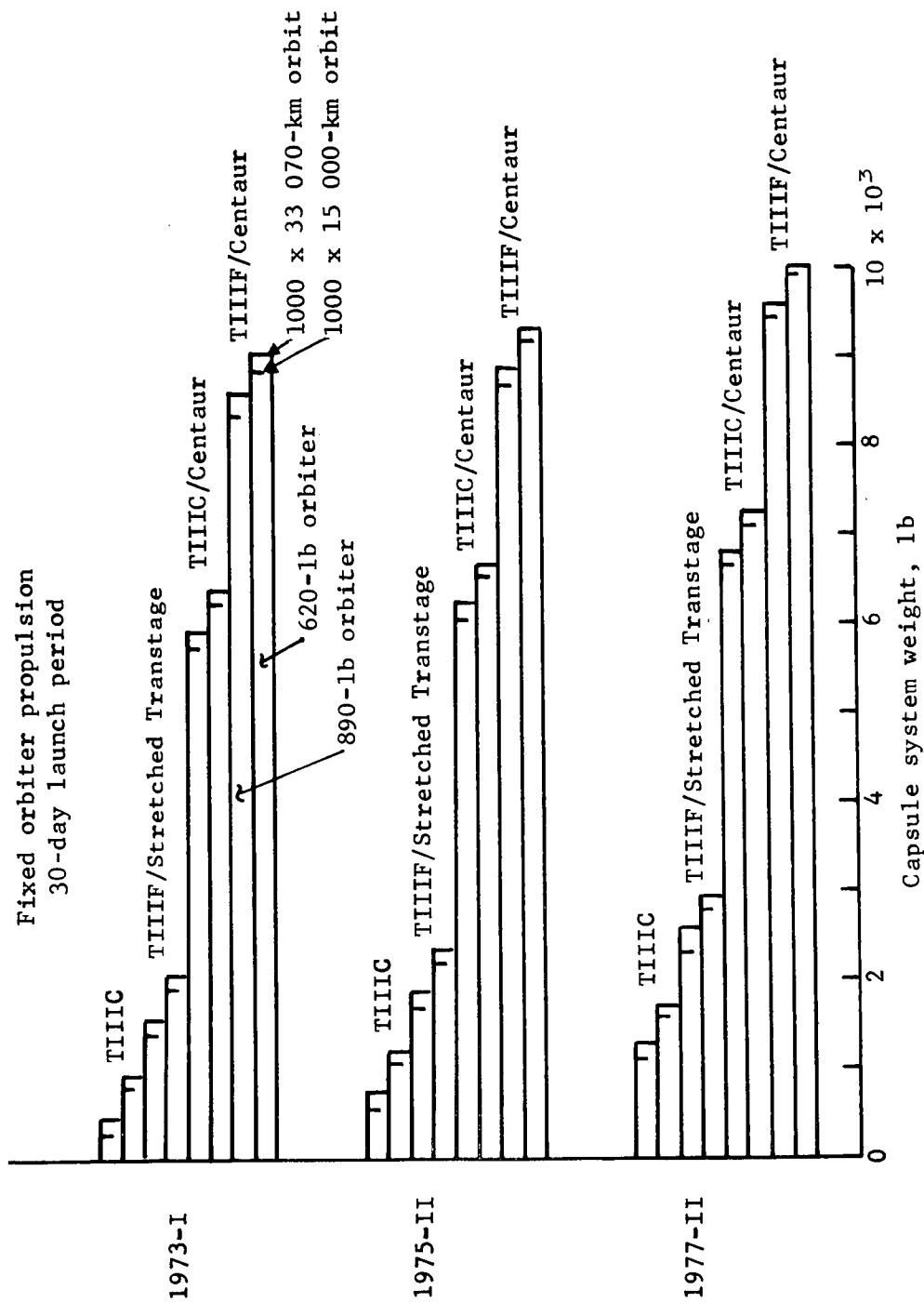


Figure 2.- Optimum Capsule System Weight, Direct Entry, Orbiter

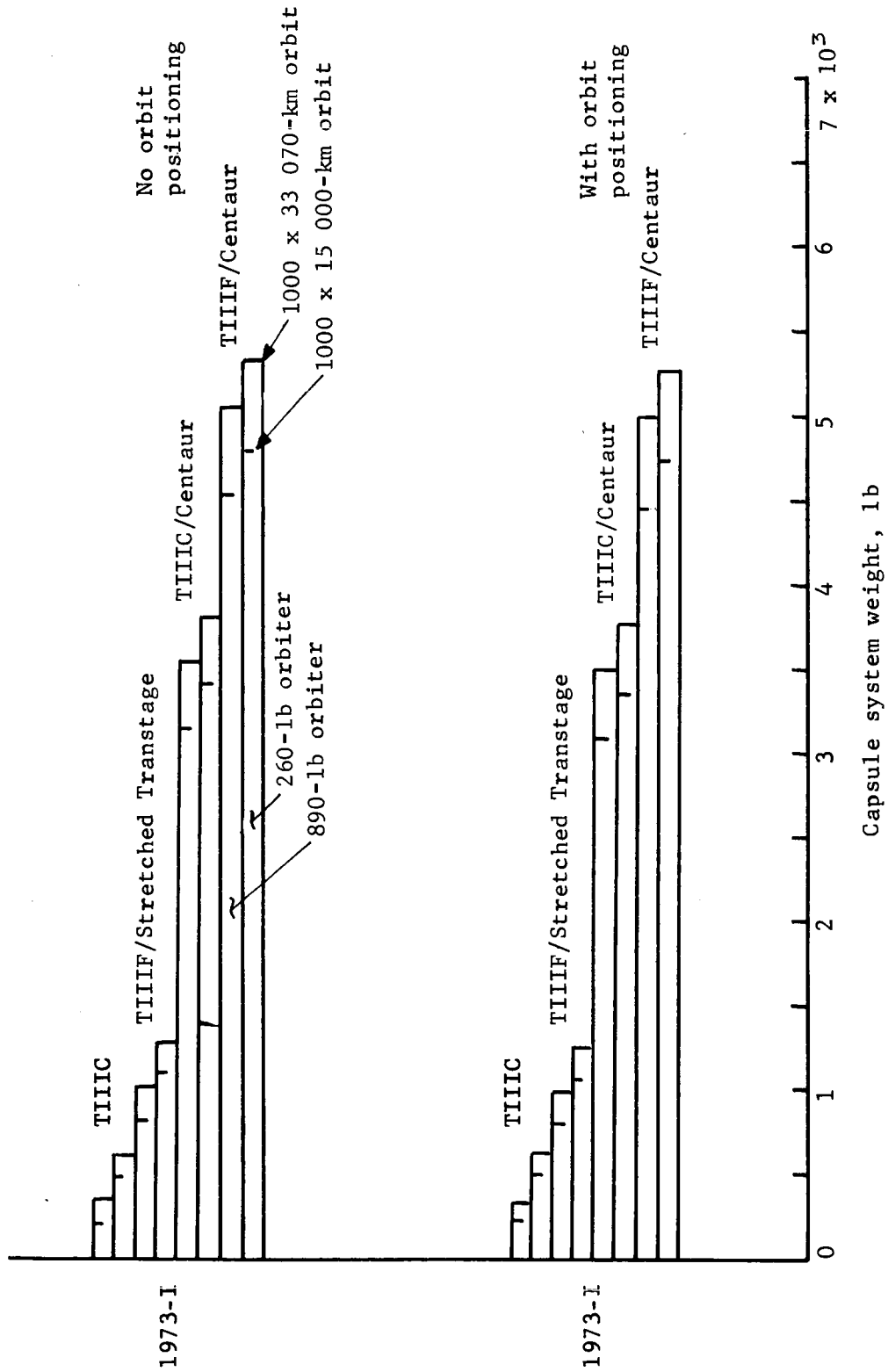


Figure 3.- Optimum Capsule System Weight, Entry from Orbit, with and without Orbit Positioning

The analyses presented in the following subsections derive the required payload capabilities for the various landed science complements and mission modes. It soon becomes apparent that the Titan IIIC and Titan IIIF/Stretched Transtage capabilities are too low and that the Titan IIIC/Centaur is the only launch vehicle that satisfies both the orbit and direct mode missions.

Launch period selection and targeting analysis. - The launch vehicle analysis just summarized was based on the selection of a 30-day launch period (launch date/encounter date combinations) that maximized launch vehicle capability. However, variations in launch date/encounter date combinations are directly reflected in variations in approach trajectory geometry and, ultimately, in targeting capability. Thus, the launch period selection must be a compromise between launch vehicle performance, capsule landed science, and orbiter science. The factors involved in this trade-off are summarized here and discussed in more detail in Appendix A, section 2.

The first factor involved in the targeting analysis is the definition of possible landing areas relative to the approach trajectory (direct mode) or orbit (orbit mode). The parameters used throughout this analysis are illustrated in figure 4. The targeting parameter  $\beta$  defines the entry point relative to the subperapsis point of the approach trajectory (direct mode) or orbit (orbit mode). The spacecraft lead angle  $\lambda$  defines the orbiter position relative to the capsule at the time of entry. The  $\beta$  can be varied by adjusting the deorbit/ejection  $\Delta V$  or entry flightpath angle. The lead angle  $\lambda$  can be adjusted by deorbit/ejection  $\Delta V$  and firing angle.

For the direct mode, the parametric ejection analysis in Appendix A, section 2 shows that the achievable  $\beta$  are directly a function of entry flightpath angle  $\gamma_E$ . This relationship (for ejection distance  $R_{eject}$  greater than 50 000 km) is summarized in figure 5. The fact that landed payload for Martian entries is highly sensitive to entry flightpath angle (discussed in the following subsection) makes it difficult to use  $\gamma_E$  as a targeting parameter to obtain flexibility. A representative  $\lambda$  variation with  $\Delta V_{eject}$  and firing angle  $\tau$  is shown in figure 6. For large  $R_{eject}$ ,  $\tau$  can be varied over a wide range. However, the entry flightpath angle dispersions due to maneuver pointing uncertainty are also sensitive to  $\tau$  (Appendix A, section 2) and  $\tau > 40^\circ$  are generally required.

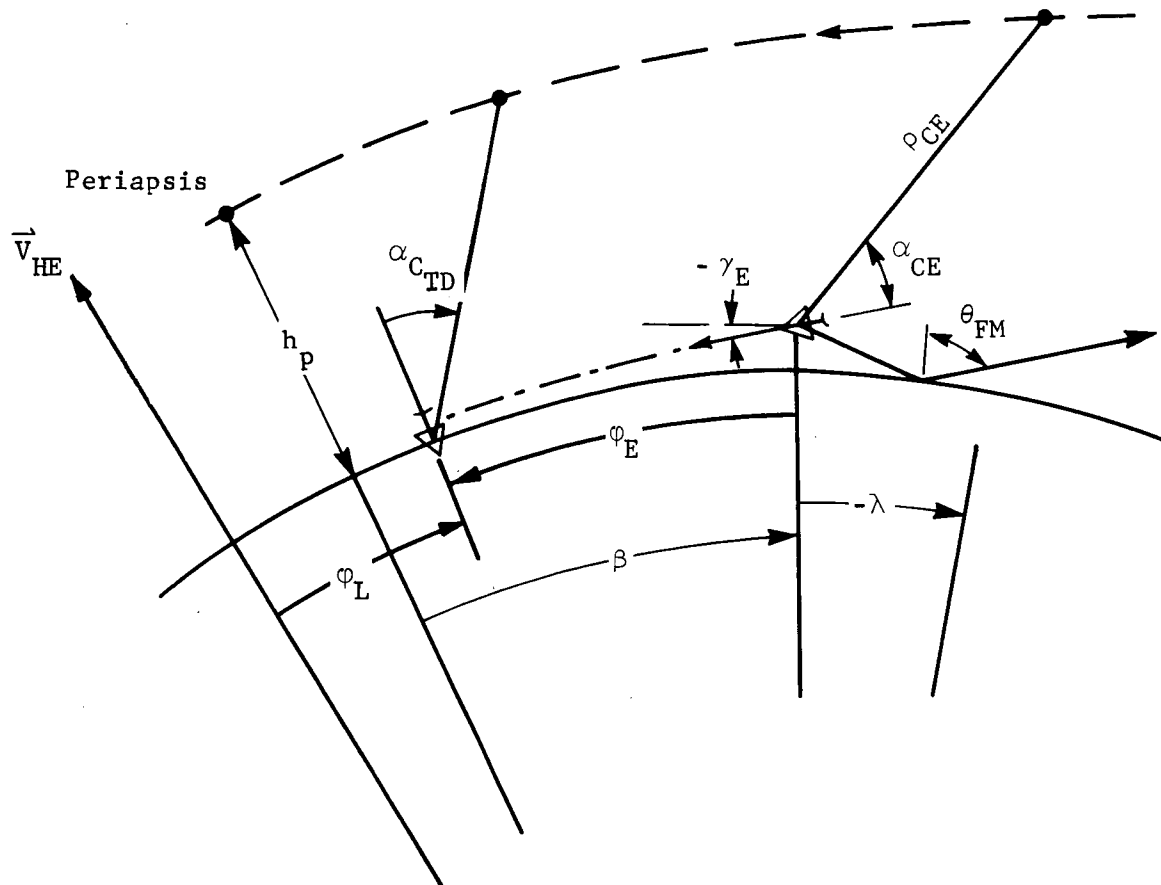


Figure 4.- Relay Communication Link during Entry



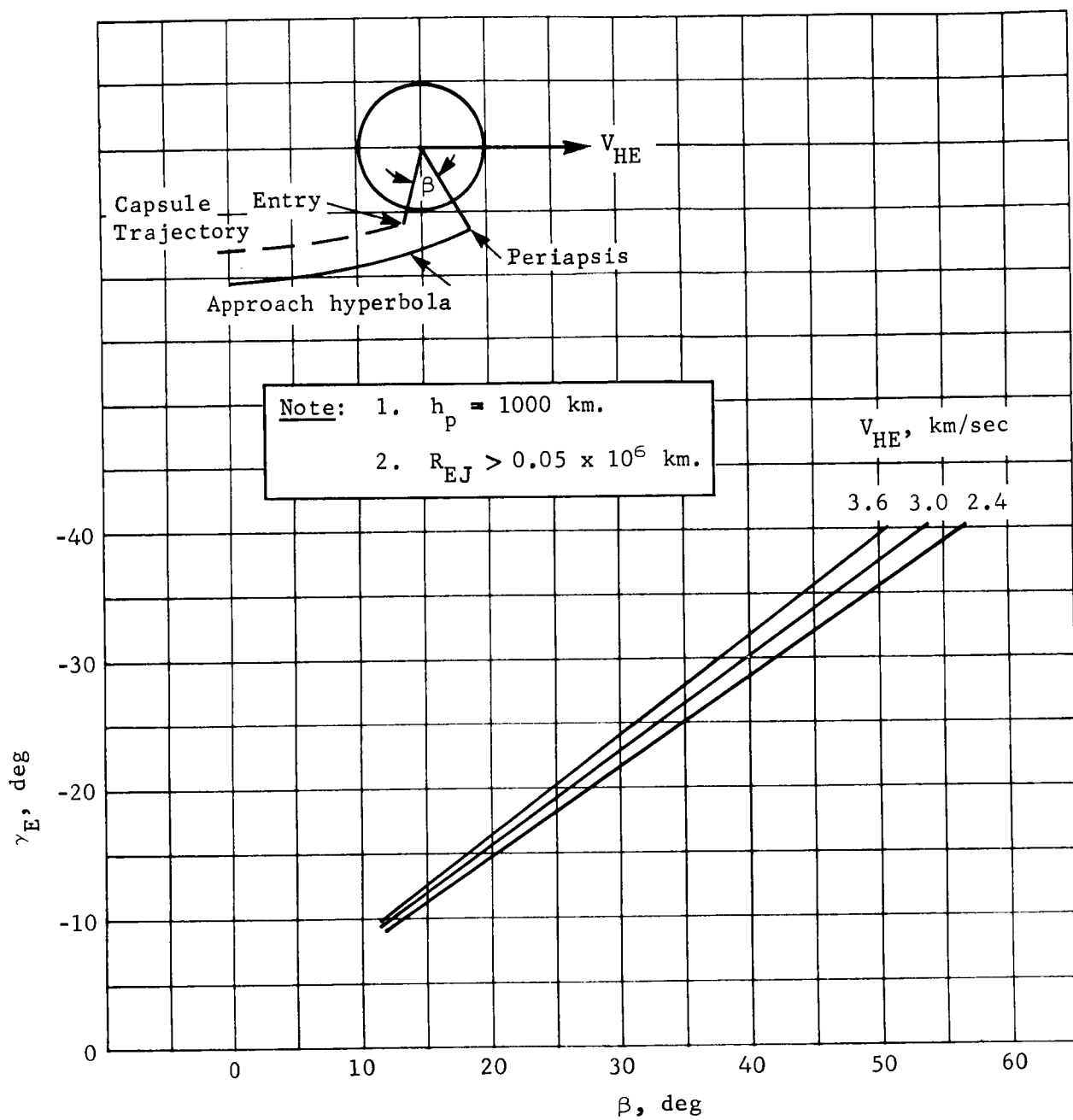


Figure 5.- Entry Location (Direct Mode)

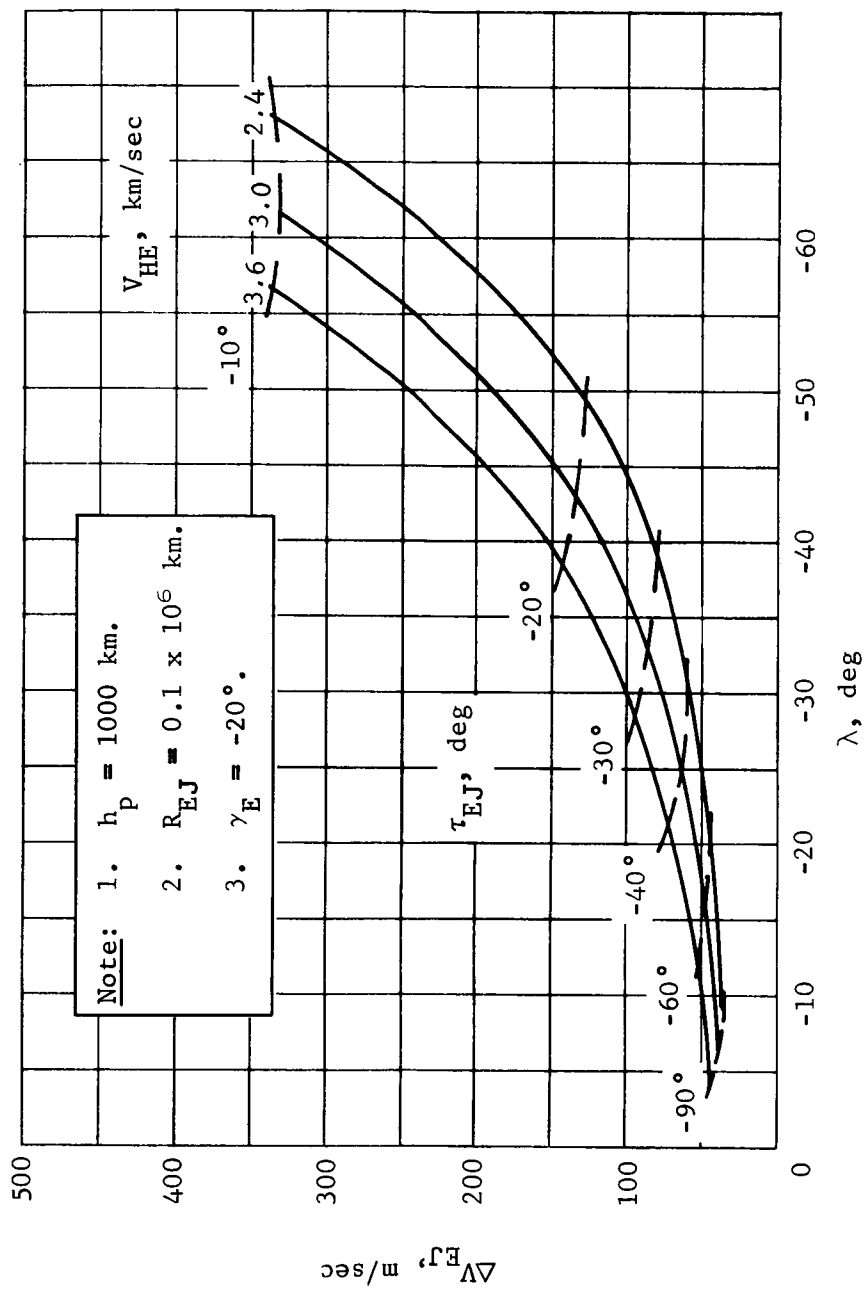


Figure 6.- Ejection  $\Delta V$  Requirement

Although  $\beta$  and  $\lambda$  can be varied by properly varying the ejection maneuver characteristics, the final selection of possible  $\beta$  and  $\lambda$  depend on other system constraints. An example of a direct mode targeting boundary map is shown in figure 7. Other parameters entering the analysis are maximum relay communication range,  $\rho_{CE}$ ; capsule relay antenna aspect angle,  $\alpha_{CE}$ ; fading margin boundary,  $\theta_{FM}$ ; posttouchdown relay link time,  $t_{T,D}$ ; and elevation angle at touchdown  $\alpha_{C_{TD}}$ . It is desirable to minimize

the communication range to minimize power requirements. A goal of less than 5000 km is used here. The antenna aspect angle at entry should be minimized so excessively broad antenna patterns are not required. This is particularly true at entry where the communication range tends to be near maximum and the signal propagated toward the ground and reflected back to the orbiter receiver can lead to multipath interference. A maximum  $\alpha_{CE}$  at entry of  $50^\circ$  is used here. The elevation mask at touchdown is  $34^\circ$  (orbiter behind lander). This insures a good link at touchdown from both an elevation mask viewpoint and capsule antenna aspect angle. Finally, the initial posttouchdown relay link should be as long as possible (5 to 10 min min.) to allow time for deployment of landed science and possible transmission of a few initial pictures.

The direct mode targeting boundary shown in figure 7 shows that a large range of  $\beta$  is acceptable for  $\lambda \approx -17.5^\circ$ . The limitation on targeting flexibility ( $\Delta\beta$ -capability) will be the effect of allowable  $\gamma_E$  on landed payload. More detailed targeting boundaries showing the effects of approach energy  $V_{HE}$ , entry flightpath angle,  $\gamma_E$ , and atmosphere uncertainty are presented in Appendix A, section 2. Typically, the  $\gamma_E$  limitation will restrict the allowable  $\beta$  for the direct mode to approximately  $27^\circ$ .

The range of possible  $\beta$  for the orbit mode is a function of both entry flightpath angle and deorbit impulse,  $\Delta V_D$ . An example for the two orbits considered is shown in figures 8a and 8b. Here the magnitude of  $\Delta V_D$  is a strong parameter (negligible for the direct mode). Although the minimum  $\Delta V_D$  required for deorbit ( $\Delta\beta = 0$ ) is lower for the 1000x33 070-km orbit than for the 1000x15 000-km orbit, sizing the deorbit impulse greater than minimum pays off faster in terms of greater  $\Delta\beta$  capability ( $\Delta\beta = \beta_{max} - \beta_{min}$ ) for the less eccentric orbit.

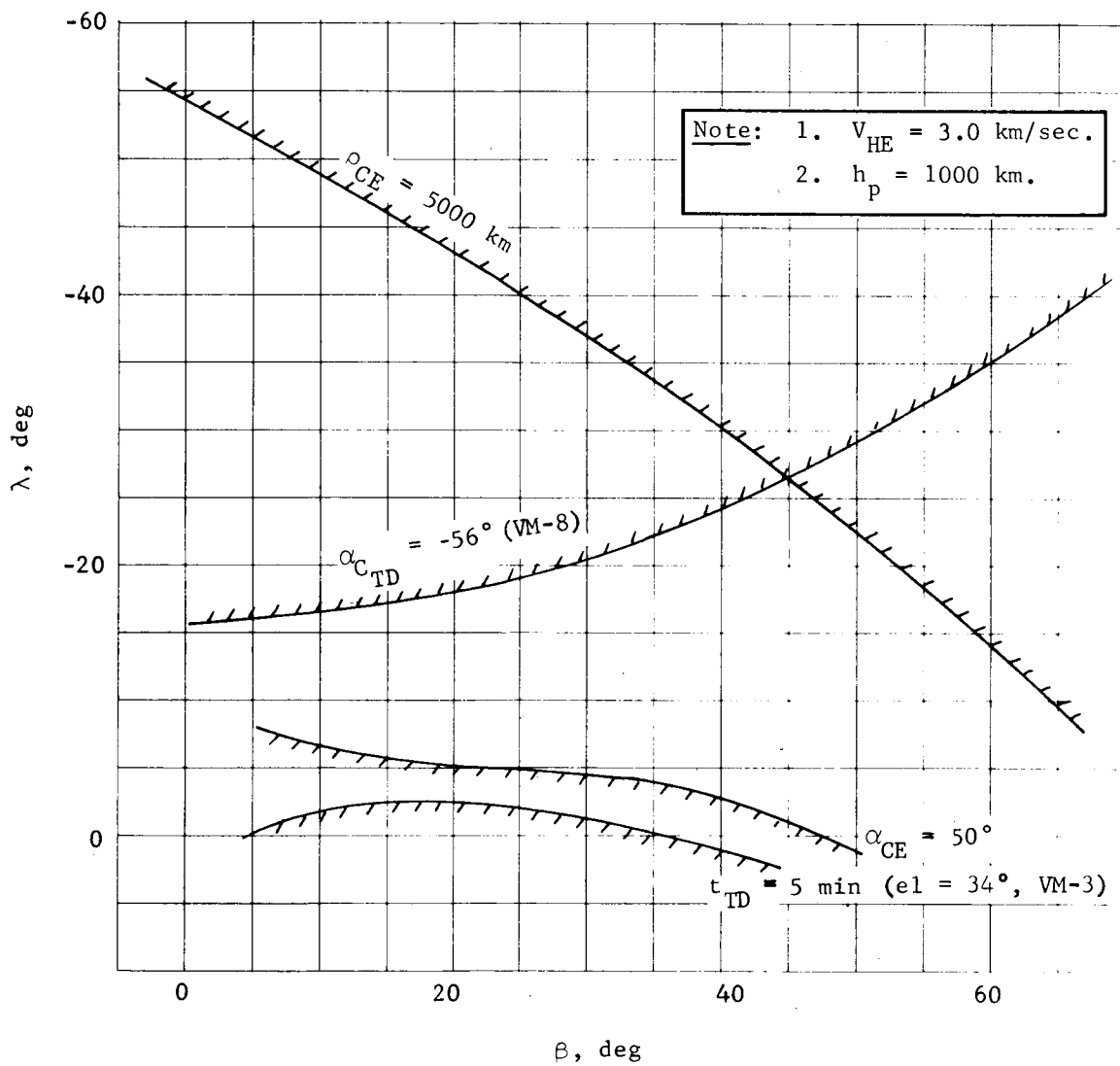


Figure 7. - Targeting Boundary, Direct Mode

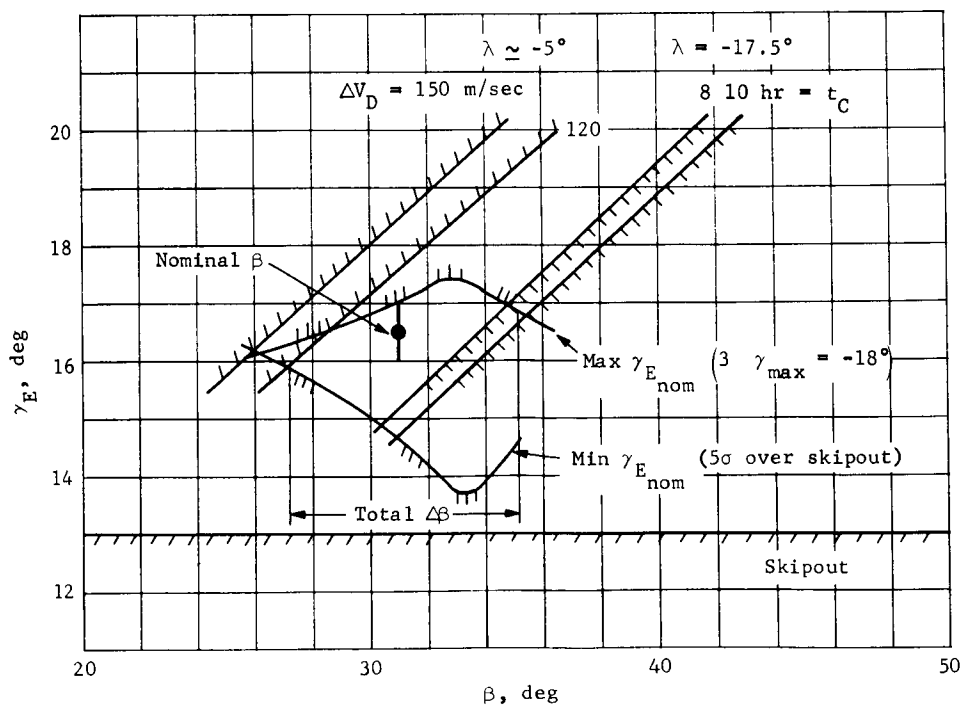
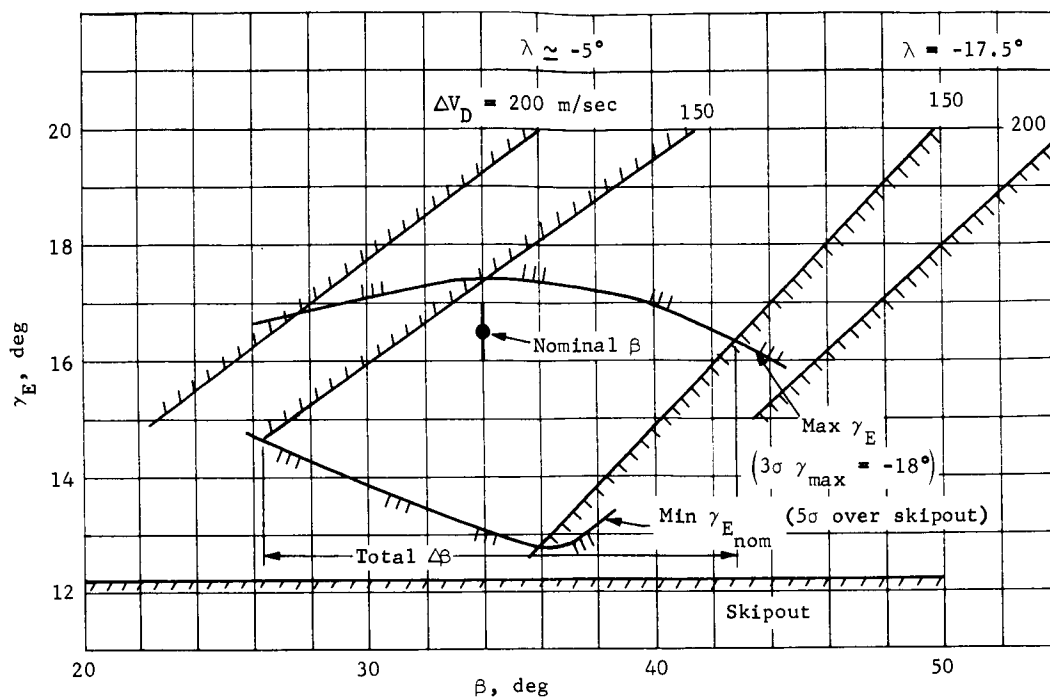


Figure 8.- Summary of Entry Locations (Orbit Mode)

A typical  $\Delta V_D$  versus  $\lambda$  is shown in figure 9. As above, a wide range of  $\lambda$  can be achievable by properly selecting the deorbit location  $\Delta V_D$  and firing angle. The parametric deorbit analysis from which these limited examples were extracted are presented in Appendix A, section 2.

Targeting boundaries analogous to those described for the direct mode are illustrated in figure 10 for the orbit mode. The same communication link constraints are in evidence for the orbit mode, but now the range of possible  $\beta$  is restricted by the  $\Delta V_D$  capability. Another constraint is also shown -- maximum coast time from deorbit to entry  $t_C$ . The goal here is to limit the coast time to less than 8 hr to minimize the power requirements of the attitude control system (ACS). This constraint limits the effectiveness of  $\Delta V_D$  on  $\Delta\beta$  capability by eliminating the higher  $\beta$ . Similar boundaries showing the effects of entry flight-path angle and atmosphere uncertainty are presented in Appendix A, section 2. Typically, the  $\beta$  ranges shown in figure 8 are achievable.

The analysis just discussed dealt with the possible entry point locations relative to the approach trajectory for the direct mode or orbit for the orbit mode. The resulting limitations on  $\beta$  are relatively rigid for the communication and  $\Delta V$  constraints assumed. The next step in the analysis is to interpret the  $\beta$  limitations in terms of where on the planet the landing can be made. Before this is done, the fundamental concept of the approach trajectory hyperbolic excess velocity vector ( $V_{HE}$ ) will be reviewed. This vector, whose magnitude and orientation are strictly a function of Earth departure date and Mars encounter date, defines the orientation of the Mars hyperbolic approach trajectory asymptote. Although all approach trajectories for a given departure date/encounter date have the same magnitude and orientation  $V_{HE}$  vector, the actual penetration point of the approach trajectory on Mars sphere of influence (in a patched-conic sense) is arbitrary. However, the plane of the approach trajectory must contain the center of the planet. Thus, the allowable planet approach trajectory geometry is dictated by the  $V_{HE}$  vector as illustrated in figure 11. The planet approach can be made from above or below the planet (as illustrated) or in three dimensions, anywhere along the surface of a "hyperboloid" whose centerline is an axis drawn through the planet center and parallel to the  $V_{HE}$  vector.

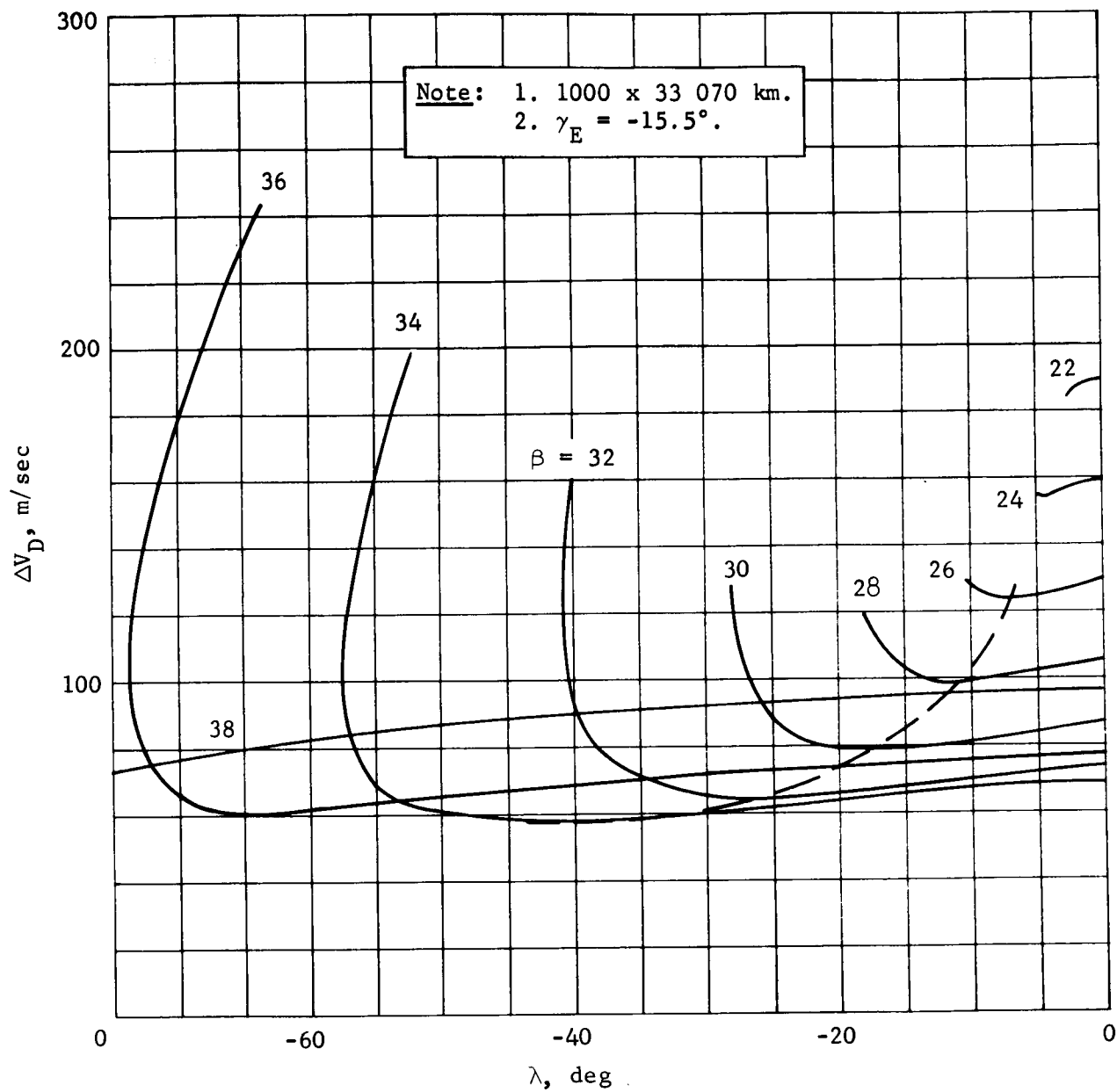


Figure 9.-  $\Delta V_D$  versus Lead Angle (Orbit)





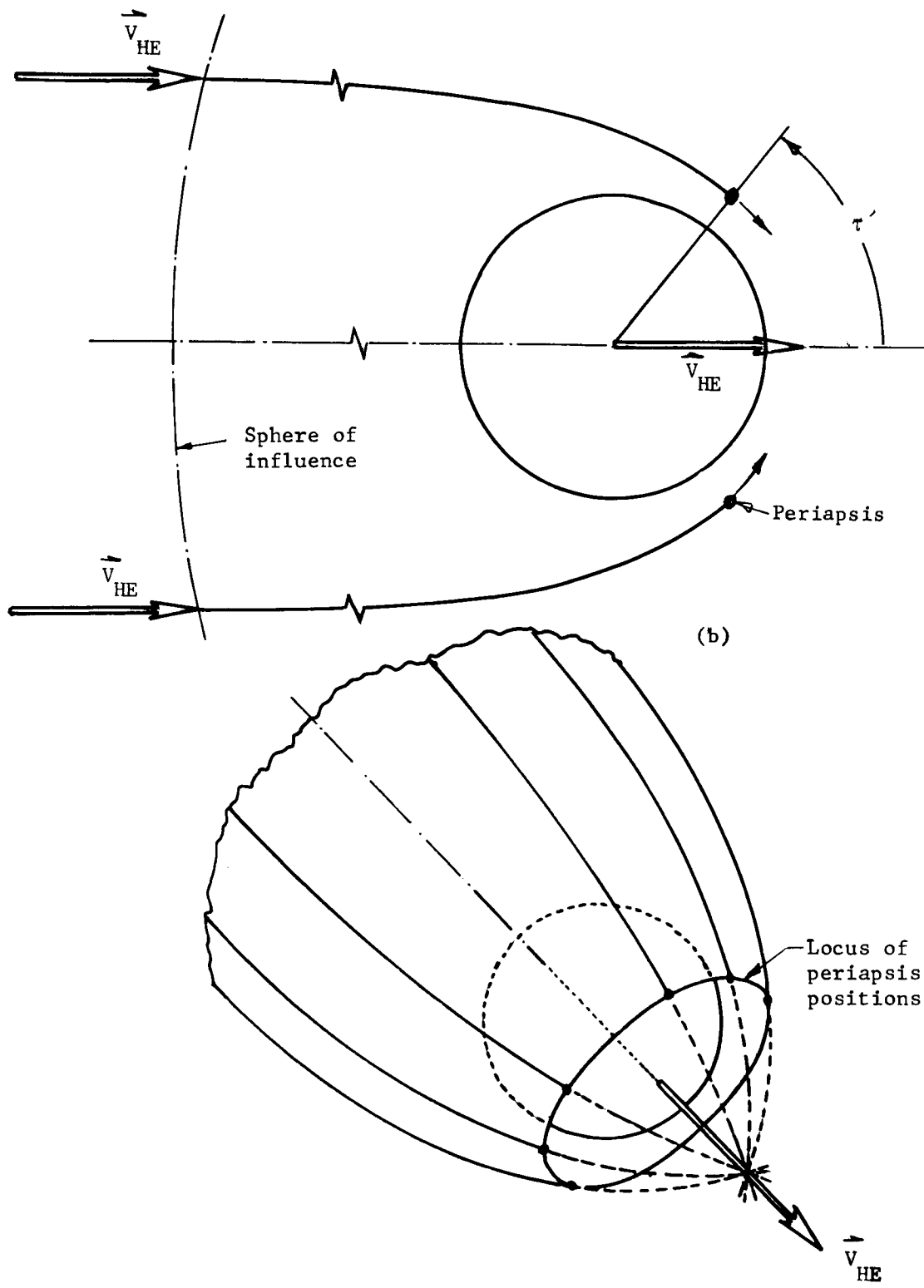


Figure 11.- Approach Trajectory Geometry

In all cases, the plane of the approach trajectory must contain the  $V_{HE}$  vector drawn from the center of the planet. A final consideration, before proceeding, is the location of the periapsis of the approach trajectory. This is identified in figure 11a by the angle  $\tau'$  measured (opposite to the direction of flight) from the  $V_{HE}$  vector. This angle is given by

$$\tan \tau' = \left( \frac{V_{HE}}{V_{SP}} \right) \sqrt{\left[ \frac{V_{HE}}{V_{SP}} \right]^2 + 2}$$

where

$$V_{SP}^2 = \left[ \frac{u}{r_p} \right] \quad \begin{array}{l} u = \text{planet gravitational constant} \\ r_p = \text{periapsis radius} \end{array}$$

Thus  $\tau'$  is only a function of the magnitude of the  $V_{HE}$  vector and the periapsis radius of the approach trajectory. The value of  $\tau'$  for a periapsis altitude of 1000 km varies from 52.5 to 58.5° for  $V_{HE}$  from 2.5 to 3.0 km/sec.

With this background, consider the possible range of  $V_{HE}$  vector magnitudes and orientations. The data in Appendix A illustrate contours of constant  $C_3$  (Earth departure energy) and  $V_{HE}$  (Mars approach energy) as a function of departure date and encounter date. Launch vehicle performance is directly related to  $C_3$ . Typically, a  $C_3 = 30 \text{ (km/sec)}^2$  is a good upper limit. Similarly, the orbit insertion  $\Delta V$  at Mars is directly related to  $V_{HE}$ . Typically, a  $V_{HE} \approx 3.5 \text{ km/sec}$  is a desirable upper limit. Using these limits for the 1973-I opportunity, the locus of possible  $V_{HE}$  vector orientations has been evaluated and is shown in figure 12. The figure illustrates the potential regions where the  $V_{HE}$  vector, drawn from the center of the planet, can pierce the planet surface for launch dates between approximately June 30, 1973 to September 5, 1973, and encounter dates between January 16, 1974 to May 25, 1974. The locus is shown relative to the Mars equator and the evening terminator. Thus, by selecting the proper launch date/encounter date combination within the above limits, the  $V_{HE}$  vector can be fixed anywhere within the illustrated contour. Similarly, for a given  $V_{HE}$  vector, any approach trajectory plane containing the  $V_{HE}$  vector (and planet center) is possible.

Note:  $C_3$  in  $(\text{km/sec})^2$ ;  
 $V_{HE}$  in  $\text{km/sec}$ .

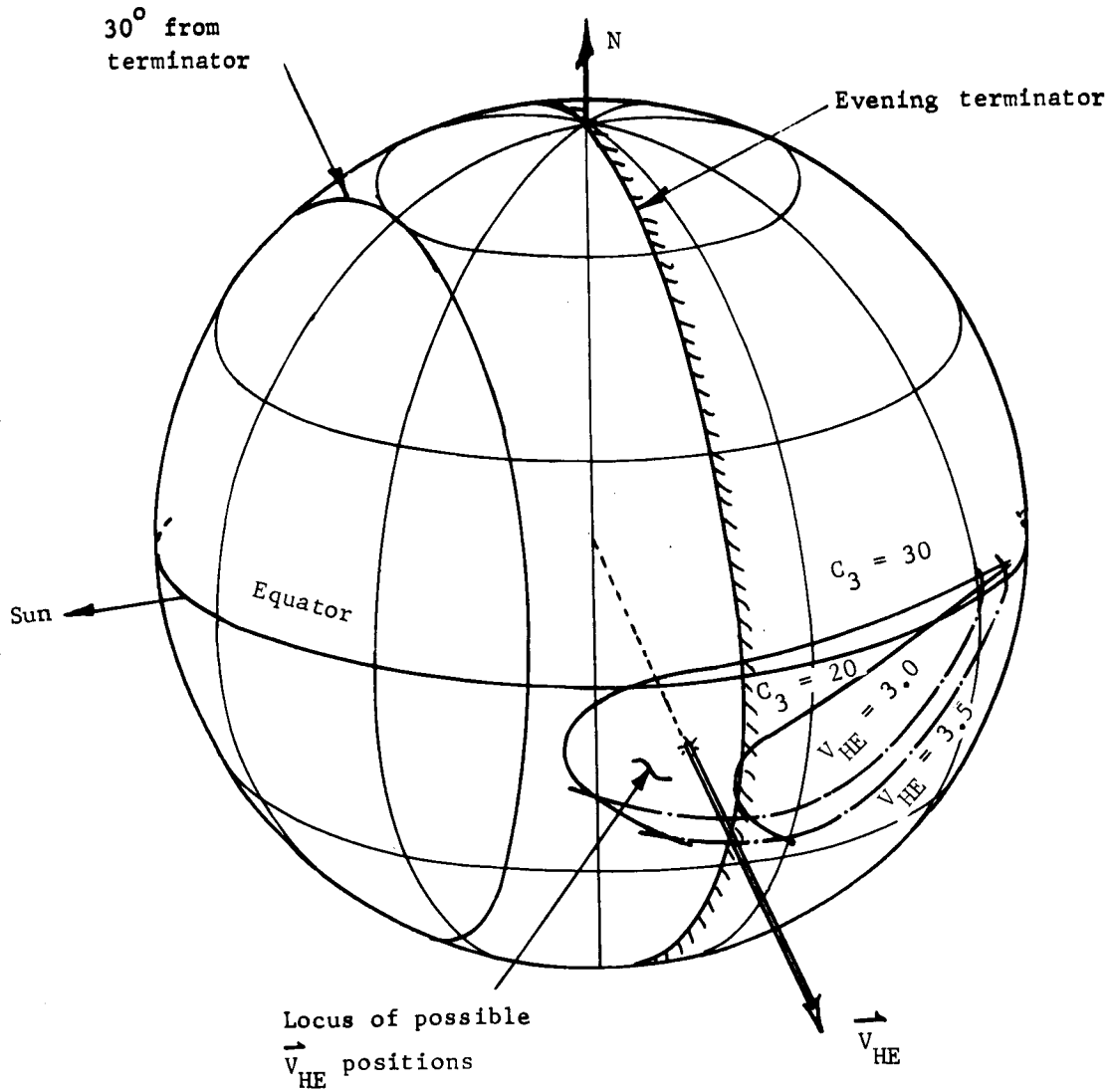


Figure 12.- Possible  $V_{HE}$  Vector Positions

These data can be interpreted directly in terms of possible landing areas for the direct mode. From the data presented, the periapsis of the approach trajectory  $\tau'$  is approximately  $55^\circ$  from the  $V_{HE}$  vector. Also from these data, the entry point location  $\beta$  measured from periapsis, is approximately  $27^\circ$  for  $\gamma_E = -21^\circ$ . Thus, the entry point is approximately  $27 + 55 = 82^\circ$  from the  $V_{HE}$  vector. From entry to touchdown, the capsule travels approximately  $12^\circ$  central angle. Thus, the touchdown point is approximately  $70^\circ$  from the  $V_{HE}$  vector. The loci of possible landing areas,  $70^\circ$  from the contours in figure 12, are shown in figure 13. Two representative approach trajectories are illustrated for a typical  $V_{HE}$  vector location with the resultant direct mode touchdown points illustrated. It is obvious that landing site latitudes are obtained by a combination of launch date/encounter date selection ( $V_{HE}$  vector orientation) and approach trajectory inclination. The landing site longitude is achieved by controlling the encounter time of day (i.e., planet rotation).

A contour of  $30^\circ$  from the evening terminator is also shown in figure 13. As can be seen, it lies within the band of possible landing areas. The special case of landing on the equator and  $30^\circ$  from the terminator is also illustrated by showing a locus of required  $V_{HE}$  vector orientation contour on the right side (encounter dates near the end of January, 1974). However, since the orbit plane must pass through both the landing site and  $V_{HE}$  vector, it is clear from the picture that low-inclination orbits are required (assuming no plane change as part of the orbit insertion maneuver).

The same logic used in defining the direct mode targeting capability can be applied to the orbit mode. For the orbit mode, the allowable  $\beta$  are  $28$  to  $32^\circ$  for the  $1000 \times 33$  070-km orbit and  $28$  to  $40^\circ$  for the  $1000 \times 15$  000-km orbit vs  $27^\circ$  for the direct mode. The central angle traveled by the capsule during entry is approximately  $16^\circ$  for the orbit mode vs  $12^\circ$  for the direct mode. Thus, the location of the touchdown point from the  $V_{HE}$  vector is  $67$  to  $70^\circ$  (variable after orbit insertion) vs  $70^\circ$  (fixed) for the direct mode. This means that the possible landing area map for the orbit mode is virtually the same as that shown in figure 13 for the direct mode. The differences are that the right side boundary (encircling the  $V_{HE}$  position locus) contracts toward the  $V_{HE}$  region an additional  $3^\circ$  while the left side advances an additional  $9^\circ$  away from the  $V_{HE}$  region. The differences in targeting capability at this point are relatively minor.

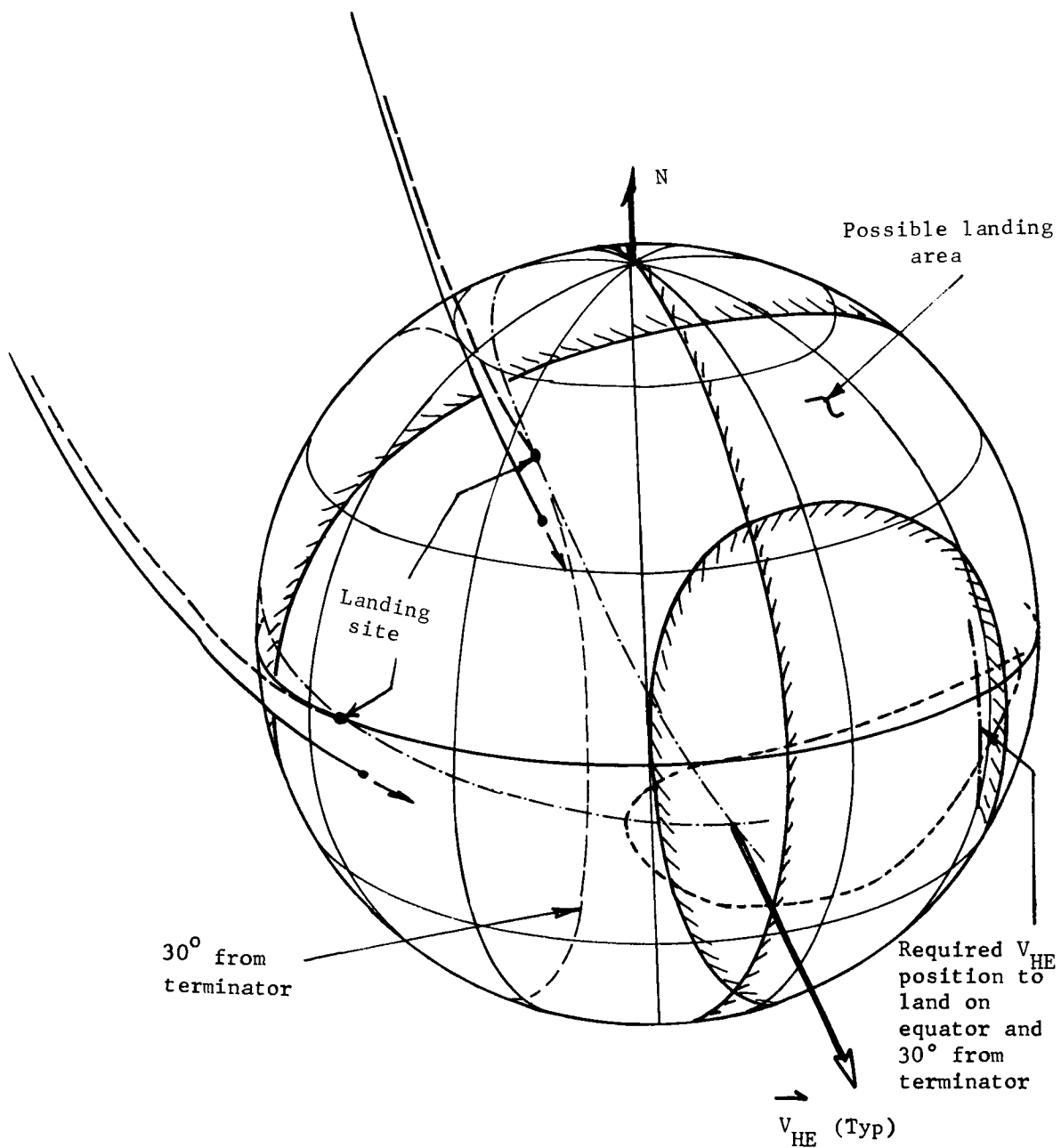


Figure 13.- Possible Landing Area  
Direct Mode

The comparison cannot end at this point, however. Two other factors must be considered -- technique for getting longitude control, and the effect of orbit orientation shift as part of the orbit insertion maneuvers. The technique used with the orbit mode to acquire a given landing site longitude is to adjust the orbit period and the time in orbit (i.e., let the planet rotate under the orbit until deorbit time). The direct mode controls longitude by time of day at encounter. Both techniques achieve the same end result, but the direct mode targeting capability can be compromised by the requirement for spacecraft tracking at or just prior to encounter by either a particular DSIF station or two DSIF stations simultaneously. Should this become a requirement, the allowable time of day at encounter will be restricted, also restricting the longitudes that can be acquired with the direct mode. The orbit mode is insensitive to DSN requirements at encounter. The selection of orbital period and time in orbit are variables that can be used to acquire any longitude.

The second factor is the usefulness of an orbit shift maneuver as part of the orbit insertion maneuver. The data in Appendix A, section 2 show that the location of the orbit periapsis relative to the  $V_{HE}$  vector can be modified from the natural location (at the location  $\tau'$ , fig. 11a) by changing the time of orbit insertion and increasing the  $\Delta V$  for orbit insertion. Typically, shifts of  $45^\circ$  in periapsis location (relative to the natural location) can be achieved with an additional 0.26 km/sec for the 1000x15 000-km orbit and 0.40 km/sec for the 1000x33 070-km orbit (this compared to a nominal  $\Delta V$  of 1.2 to 1.7 km/sec). Designing this additional capability into the orbit insertion motor will shrink the inaccessible region surrounding the  $V_{HE}$  locus region in figure 13 to nothing. This, in itself, has not bought anything. The use of orbit shift for the orbit mode can be significant, however, when considering the orbiter mapping mission. This mission desires a  $V_{HE}$  vector near the terminator and a high inclination orbit that has a long segment of its ground track within the good surface lighting region, 15 to  $40^\circ$  from the terminator. Targeting to such an orbit would leave the landing site latitude between  $40$  to  $50^\circ$  (north) for the direct mode with no ability to get anything different. The orbit mode, however, can acquire any latitude (zero to polar; north) by making use of both its natural  $\Delta\beta$  flexibility and orbit periapsis shift. Thus, the additional variables available with the orbit mode allow greater targeting flexibility while being better able to satisfy particular DSN requirements and orbiter science desires.

The preceding discussion described possible landing areas relative to  $V_{HE}$  vector orientation. The locus of the  $V_{HE}$  vector shown in figure 12 is reproduced in figure 14 with contours of constant launch date and encounter date superimposed. The  $V_{HE}$  vector must be near the right-hand boundary for near-equatorial landings  $30^\circ$  from the terminator. Therefore, the launch period will be early July, 1973, with encounter at the end of January, 1974. The good orbiter mapping mission, on the other hand, will use launch dates during July and early August, 1973, with encounter during late March and early April, 1974. For reference, the launch period that maximizes launch vehicle performance is superimposed.

Entry corridor and landing footprints. - Entry corridors are defined in terms of entry flightpath angle. The criterion used in this analysis to define entry corridor is that the shallowest nominal (or aimed at) entry flightpath angle that can be used for mission planning or targeting analysis shall be  $5\sigma$  over skipout. The entries are purposely biased away from the skipout limit with this criterion because entries near skipout:

- 1) Increase total heat load (heat shield design);
- 2) Increase potential entry communication blackout times (data storage);
- 3) Increase landing dispersions;
- 4) Increase atmosphere determination uncertainty dispersions.

Thus, by defining an entry corridor as  $3\sigma$  flightpath angle dispersions around a nominal, the skipout boundary will be avoided by at least  $2\sigma$  with a  $3\sigma$  probability.

On this basis, the entry corridor for the direct mode is shown in figure 15a. The data are presented as a function of b-vector uncertainty. The range of b-vector uncertainty used in this study is presented in Appendix A, section 2 as a function of time before encounter. Minimum and maximum limits are identified where maximum error is consistent with the current DSN capability and minimum is an assumed DSN capability in 1973. The limits shown in figure 15a correspond to the minimum and maximum values for an ejection distance of 100 000 km. From figure 15a, the nominal entry flightpath angle will vary from  $-21$  to  $-26^\circ$  as a function of DSN capability in 1973 and the steepest flightpath angle will vary from  $-24$  to  $-33^\circ$ .

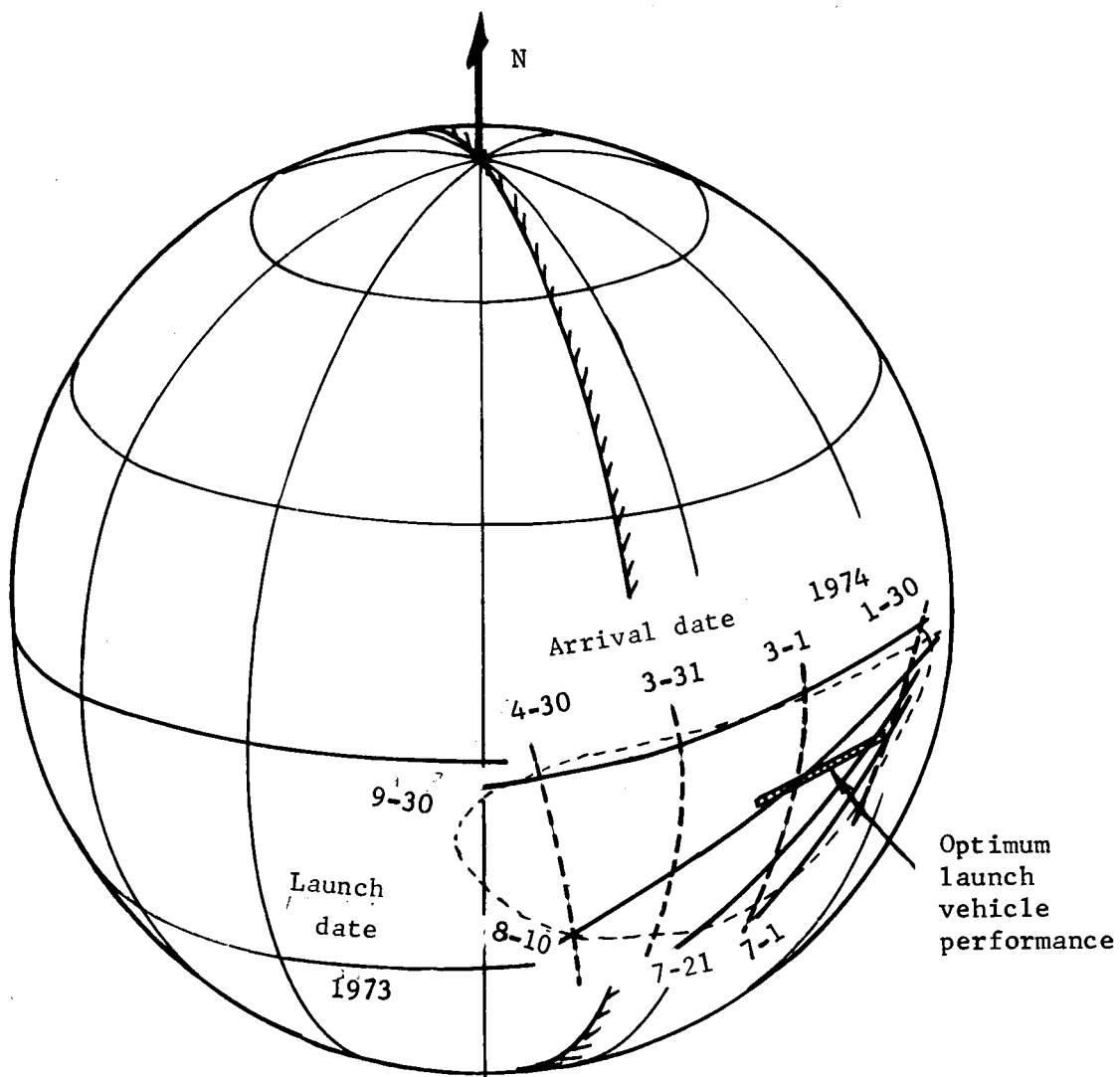
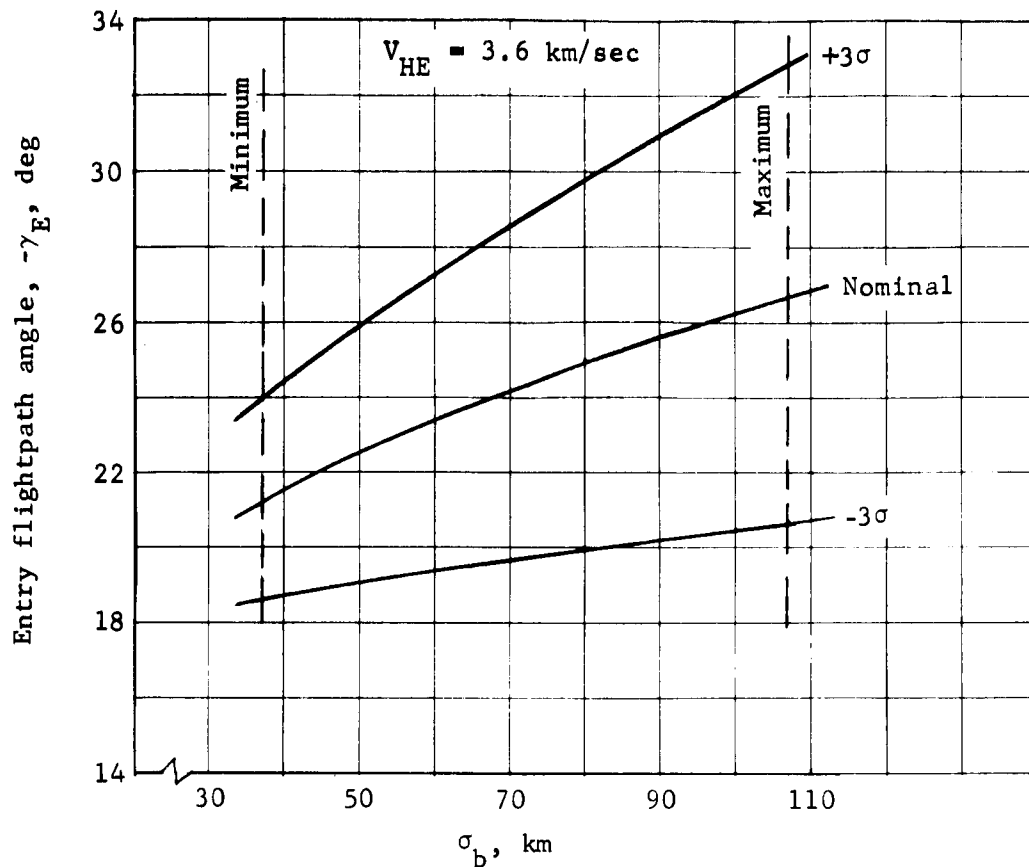
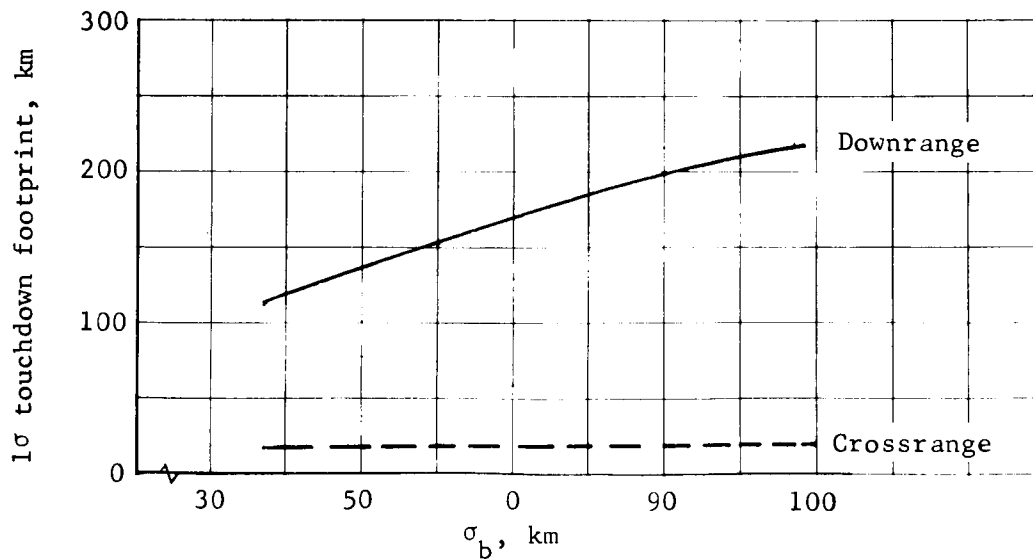


Figure 14.- Launch Date/Encounter Date





(a) Allowable Entry Corridor



(b)  $1\sigma$  Touchdown Footprint

Figure 15.- Entry and Touchdown Dispersions, Direct Mode

The following discussion will show that the use of sun-star-planet trackers aboard the spacecraft will result in sufficiently accurate information to reduce the b-vector uncertainty to the "minimum" level in figure 15a even if the maximum DSN errors are assumed. Thus, the "minimum" limit is achievable either by DSN improvement or approach guidance (onboard sensors).

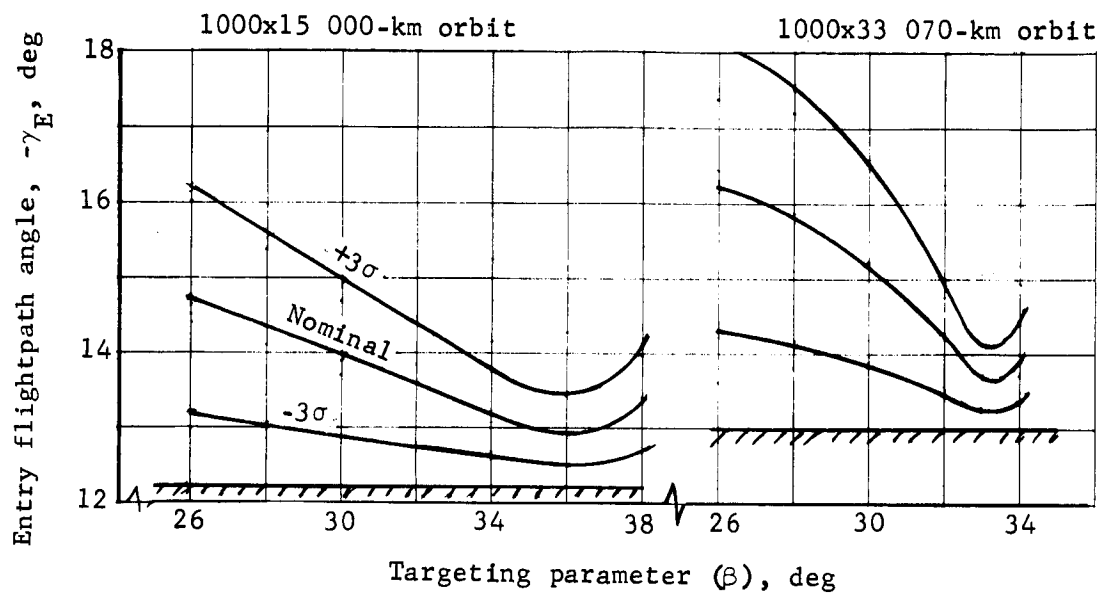
The landing footprint for the direct mode will have the  $1\sigma$  downrange and crossrange dispersions shown in figure 15b. These dispersions can vary from approximately 120 km for the "optimistic" b-vector uncertainty to 220 km with current DSN capability. Again, the 120 km ( $1\sigma$ ) dispersion is most likely.

Similar data for the orbit mode are shown in figures 16a and 16b for each of the two orbits considered. The orbit ephemeris and maneuver uncertainties used in this analysis are presented in Appendix A, section 3. The entry corridors for the two orbits are shown in figure 16a as a function of targeting parameter  $\beta$ . The nominal  $\gamma_E$  is lower for the smaller orbit because of the inherently lower entry velocity associated with this orbit and its effect on a shallower  $\gamma_E$  skipout limit. The variation is primarily a result of the navigation uncertainty at deorbit. Typically, the  $\beta$  range for the 1000x15 000-km orbit is  $26$  to  $43^\circ$  and  $27$  to  $35^\circ$  for the 1000x33 070-km orbit. Thus, the design entry flightpath angles for these two orbits will be  $-16.7$  and  $-16.5^\circ$  for the 1000x15 000-km and 1000x33 070-km orbits, respectively.

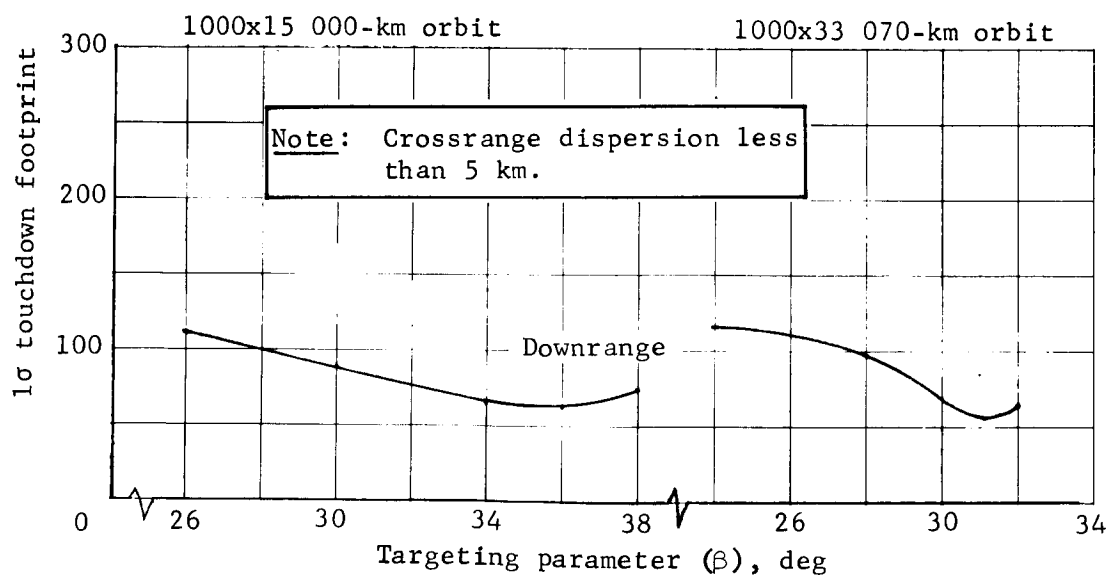
The downrange dispersion at touchdown is shown in figure 16b for the orbit mode. Its peak ( $1\sigma$ ) values are 110 and 115 km for the  $\beta = 27^\circ$  end of the targeting capability for the 1000x15 000-km and 1000x33 070-km orbits, respectively. Dispersions as low as 60 km are possible by selecting higher values for the nominal  $\beta$ . In all cases, the  $1\sigma$  crossrange dispersion is less than 5 km.

The landing footprints for the orbit and direct modes are comparable in size only when the most adverse  $\beta$  is targeted to for the orbit mode and the most optimistic navigation uncertainty is assumed for the direct mode. Most favorable  $\beta$  selection for the orbit mode will result in smaller landing footprints for this mode.

Entry trajectory and terminal phase system analysis. - The parametric entry trajectory and terminal phase system analysis is presented in detail in Appendix B. This subsection will only present the more important summary data that affect the choice of the terminal phase system and mission mode.



(a) Allowable Entry Corridor



(b) 1σ touchdown footprint, km

Figure 16.- Entry and Touchdown Dispersions, Orbit Mode

The entry trajectory analysis included generation of entry trajectory time histories over the following range of parameters:

Orbit mode

$$14\ 000 \leq V_E \leq 16\ 000 \text{ fps}$$

$$14 \leq -\gamma_E \leq 24^\circ$$

$$0.1 \leq B_E \leq 0.6 \text{ slugs/ft}^2$$

Direct mode

$$18\ 000 \leq V_E \leq 24\ 000 \text{ fps}$$

$$20 \leq -\gamma_E \leq 40^\circ$$

$$0.1 \leq B_E \leq 0.6 \text{ slugs/ft}^2$$

This range of parameters was investigated for the VM-3, VM-7, and VM-8 atmospheres. Selected runs were made in other atmospheres to verify that these three are critical for all aspects of the entry trajectory analysis with the exception of aerodynamic heating.

The most obvious difference between the direct and orbit modes from an entry trajectory viewpoint is the peak entry load factor. The peak load factors for the most adverse and least adverse atmosphere/velocity combinations are shown in figure 17 for both the orbit and direct modes. They vary from 5 to 31 (Earth) g for the orbit mode and 11 to 84 g for the direct mode. If the maximum entry flightpath angle is limited to  $-20^\circ$  (orbit) and  $-30^\circ$  (direct), the maximum values are 23 and 65 g for the two modes, respectively. It is apparent from the data shown in figure 17 that the peak load factors for the odd VM atmospheres are insensitive to entry ballistic coefficient,  $B_E$ . The peak load factor occurs at an altitude above the tropopause where the VM atmosphere scale height is constant. The scale height of the even VM atmospheres is low enough that the peak acceleration occurs at altitudes below the tropopause for the higher  $B_E$ ,  $\gamma_E$  combinations, resulting in the variations shown.

Two other factors of importance are the time from entry to terminal phase initiation and downrange angle traveled during this time. These data affect the comparison of relay communication link geometry and, in the case of downrange angle, the landing footprint dispersions.

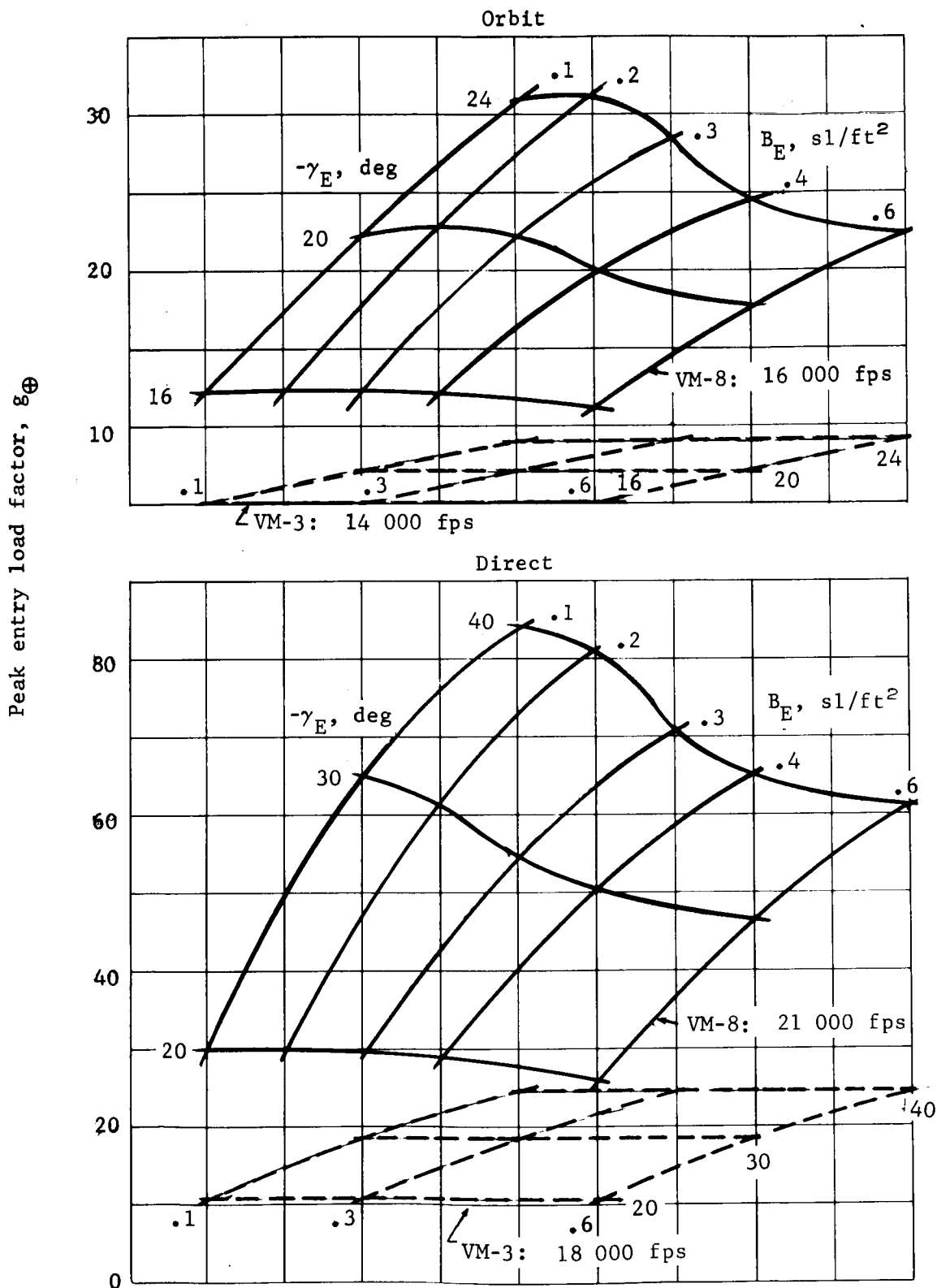


Figure 17.- Peak Load Factor Limits, Orbit and Direct Modes

These data are shown in figures 18 and 19 for the most adverse and least adverse atmosphere/velocity combinations. The time uncertainties caused by atmosphere uncertainties are approximately 1 to 2½ minutes for the orbit mode and up to 2 minutes for the direct mode. Downrange angle uncertainties vary up to 4° for the orbit mode and 3° for the direct mode. The direct mode uncertainties are generally smaller for these parameters because of the steeper entry flightpath angles.

The data shown in figures 17, 18, and 19 are composites only intended to show the range of values. The actual curves are presented separately for the three atmospheres and range of parameters quoted above in Appendix B, section 1.

The final aspect of the entry trajectory analysis is the altitude at deployment of the aerodecelerator terminal phase systems. Examples of these data are shown in figures 20, 21, and 22, showing altitude at Mach 2, 3, and 5 for  $V_E = 16\ 000$  fps, and in figures 23, 24, and 25 for  $V_E = 21\ 000$  fps. Data for other entry velocities are presented in Appendix B, section 1. The VM-8 atmosphere is critical in defining the Mach no.-sensitive deployment conditions because of its lowest upper altitude density (above 44 000 ft; results in highest velocities) and its low speed of sound.

These data become the inputs to the terminal phase system analysis. The systems considered in this study were:

- 1) Mach 2 deployed subsonic-type parachute with monopropellant or bipropellant type of vernier landing rocket motors;
- 2) Mach 3 and 5 tuckback ballutes with monopropellant vernier motors;
- 3) All retropropulsion bipropellant decelerator and vernier system (three-engine arrangement);
- 4) "Two-burn" system employing a high-thrust solid rocket motor in front of either the  $M_D = 2$  parachute or the all-retro system.

The detailed parametric analysis of these systems is given in Appendix B, section 2. The basic results of the analysis for the first three systems are summarized in the following paragraphs. The "two-burn" system is discussed only in the appendix. It did not offer any payload advantage and required excessively high thrust-to-weight ratios.

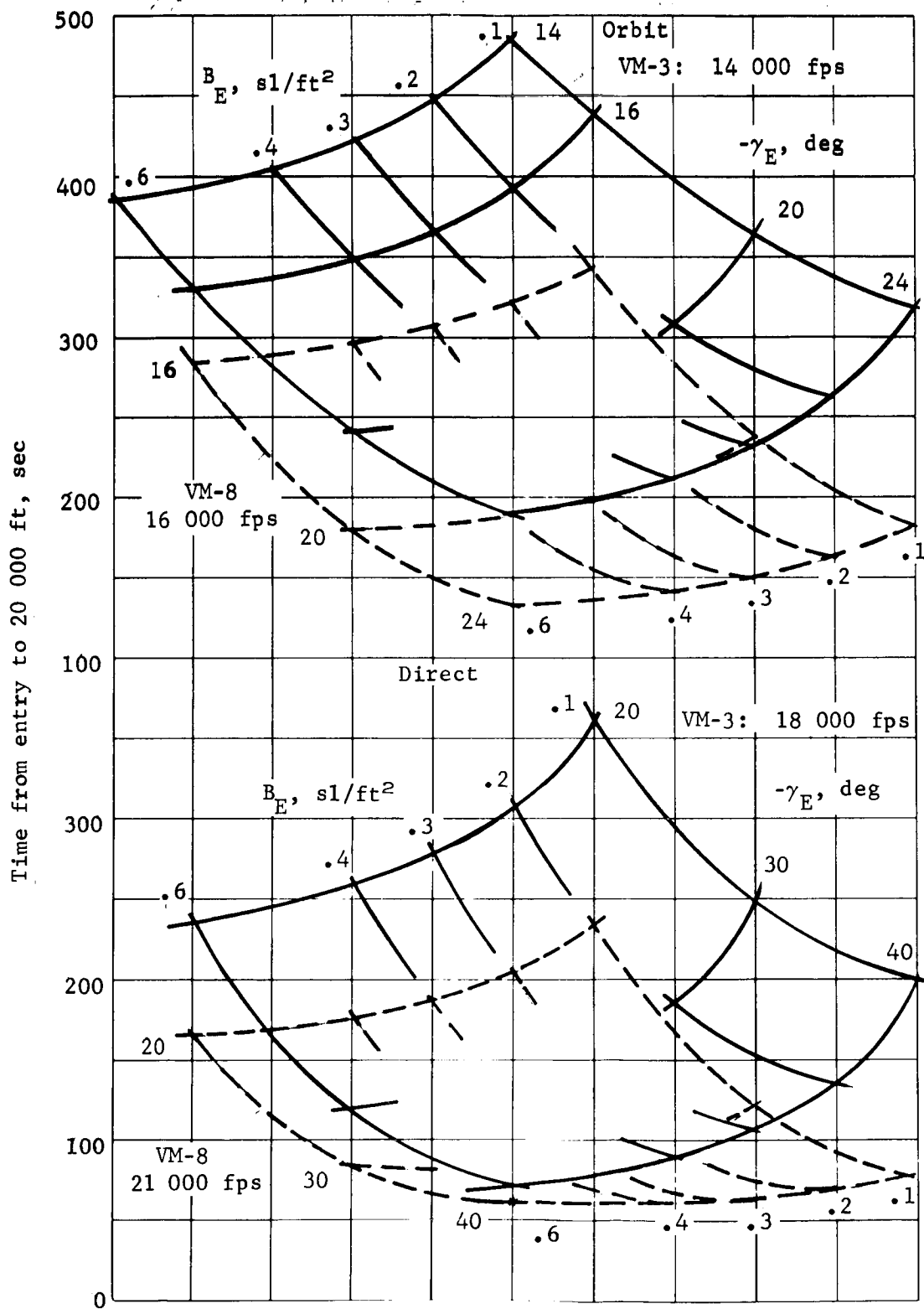


Figure 18.- Entry Time Limits, Orbit and Direct Modes

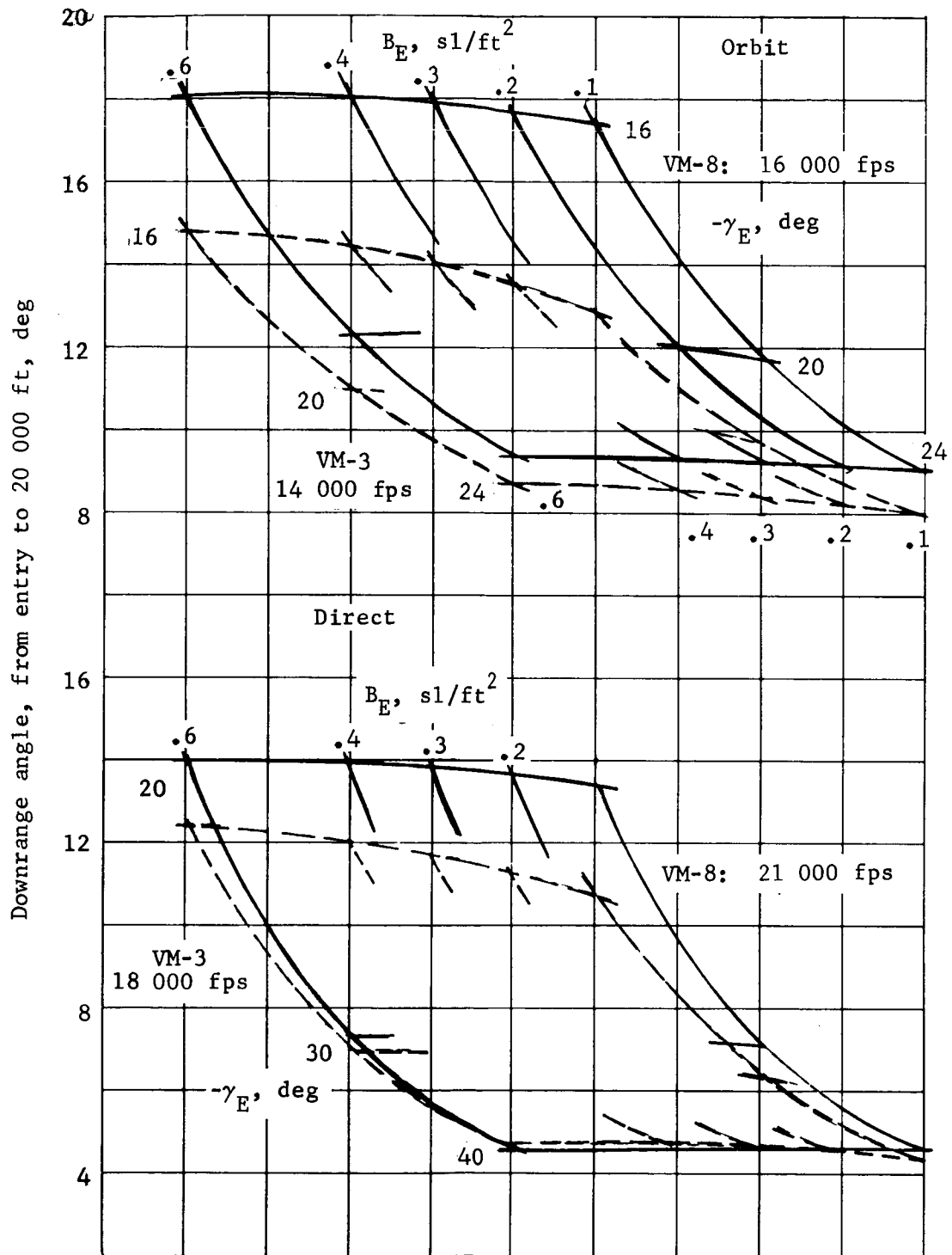


Figure 19.- Downrange Angle Limits, Orbit and Direct Modes



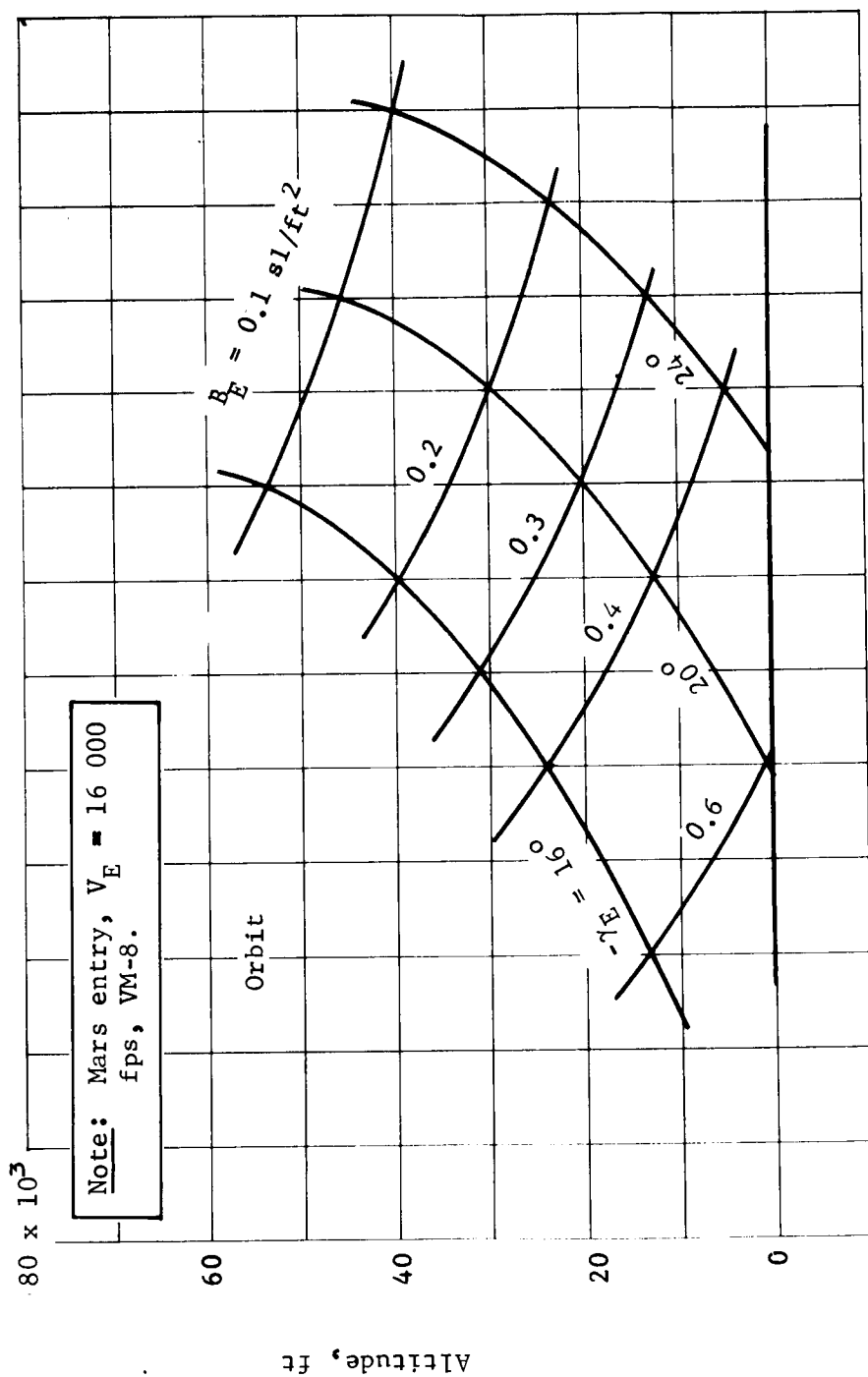


Figure 20. - Altitude at Mach 2.0

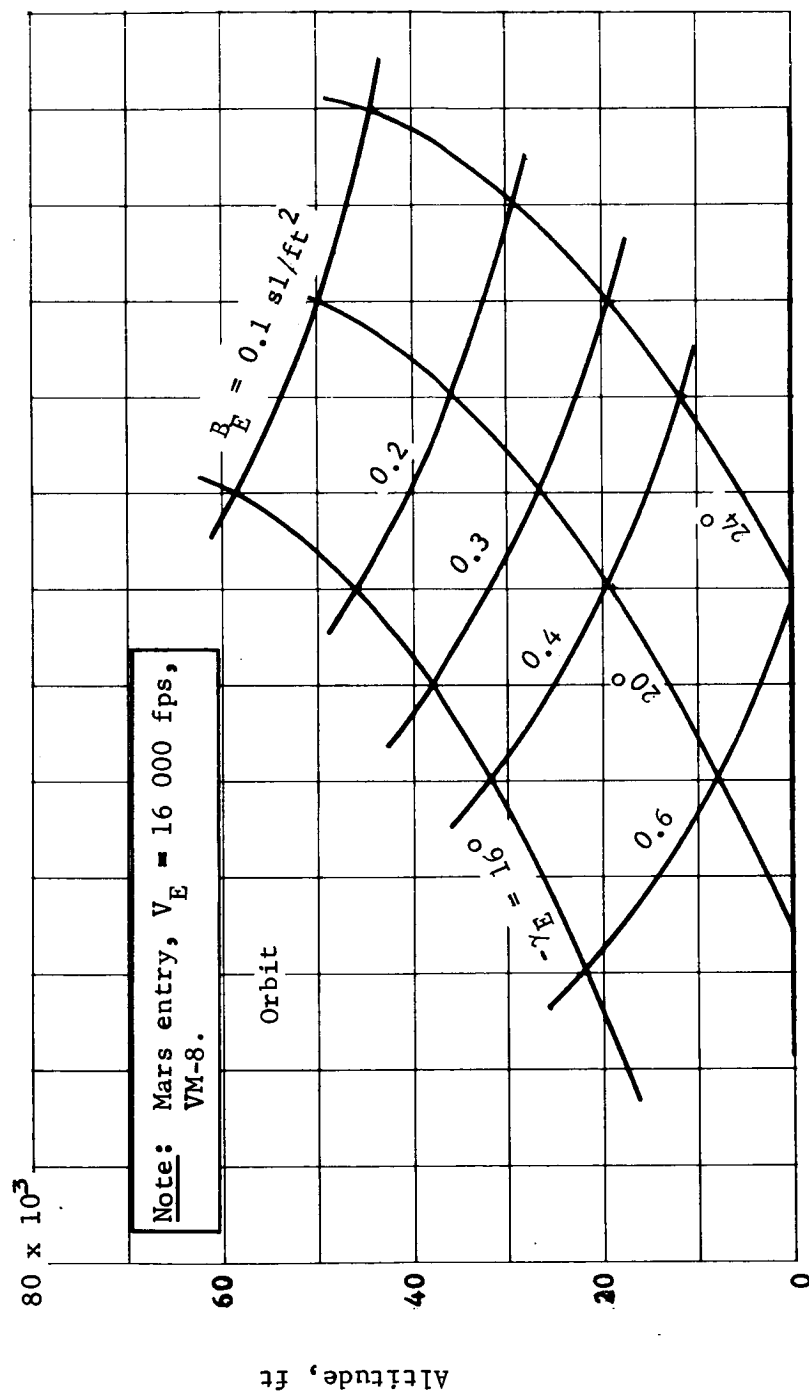


Figure 21.- Altitude at Mach 3.0

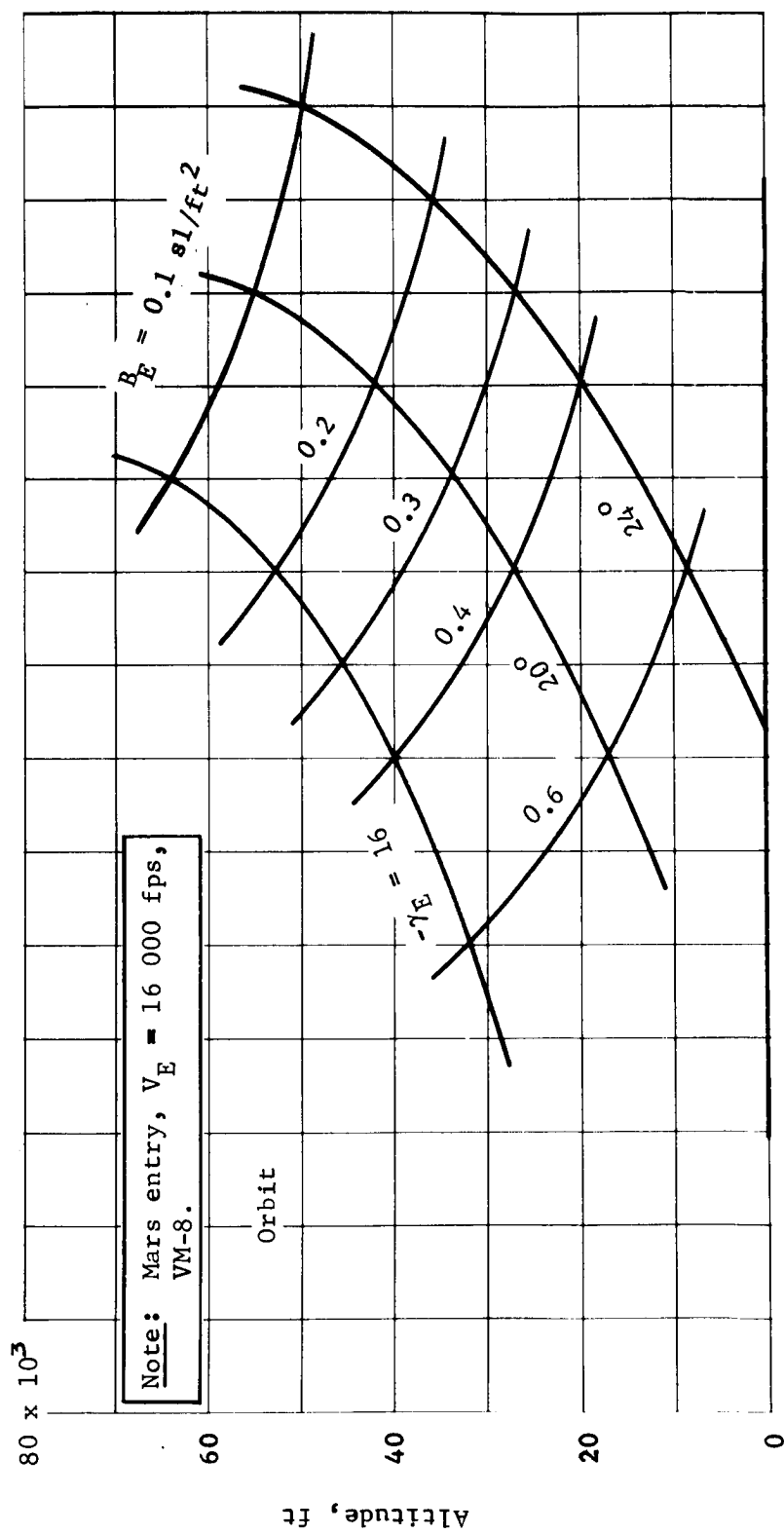


Figure 22.- Altitude at Mach 5.0

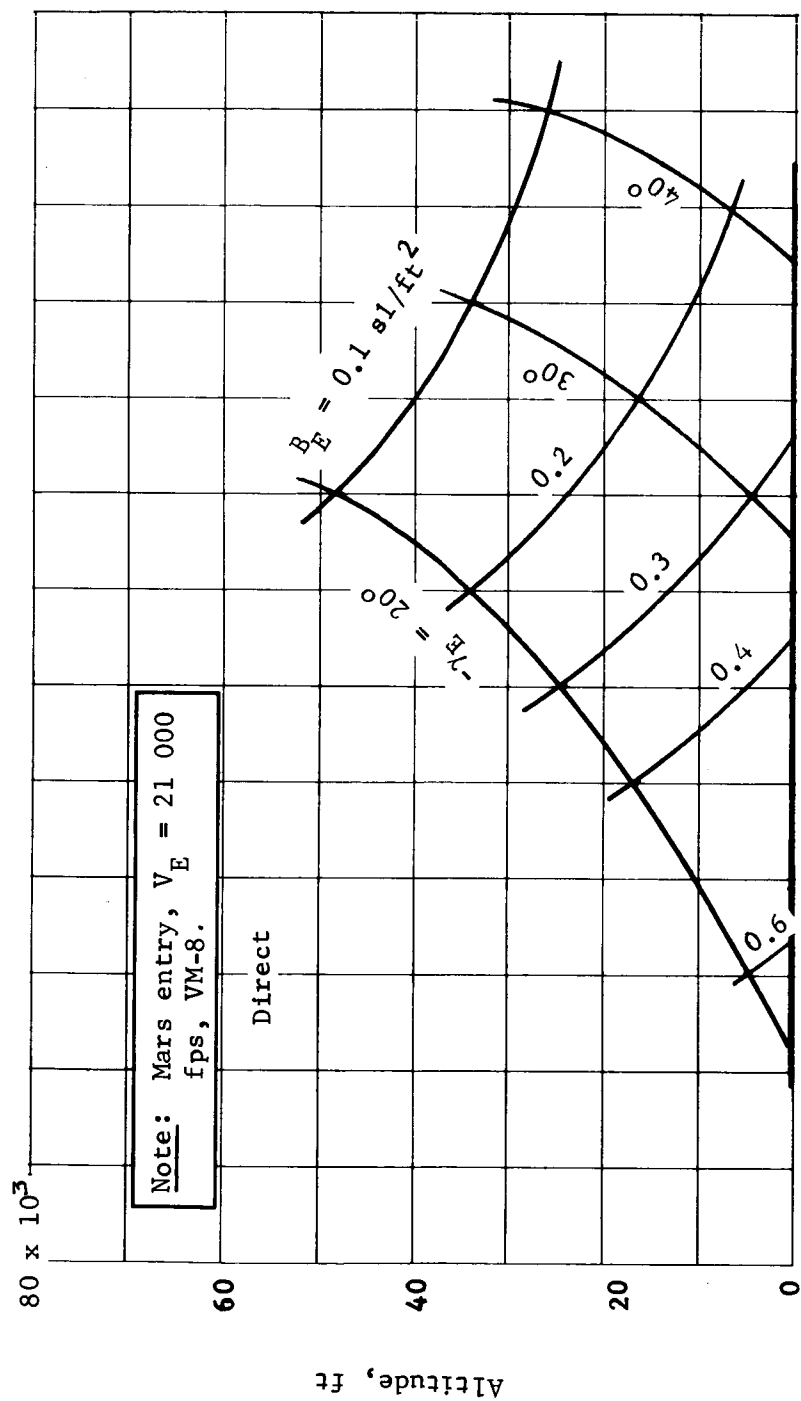


Figure 23.- Altitude at Mach 2.0

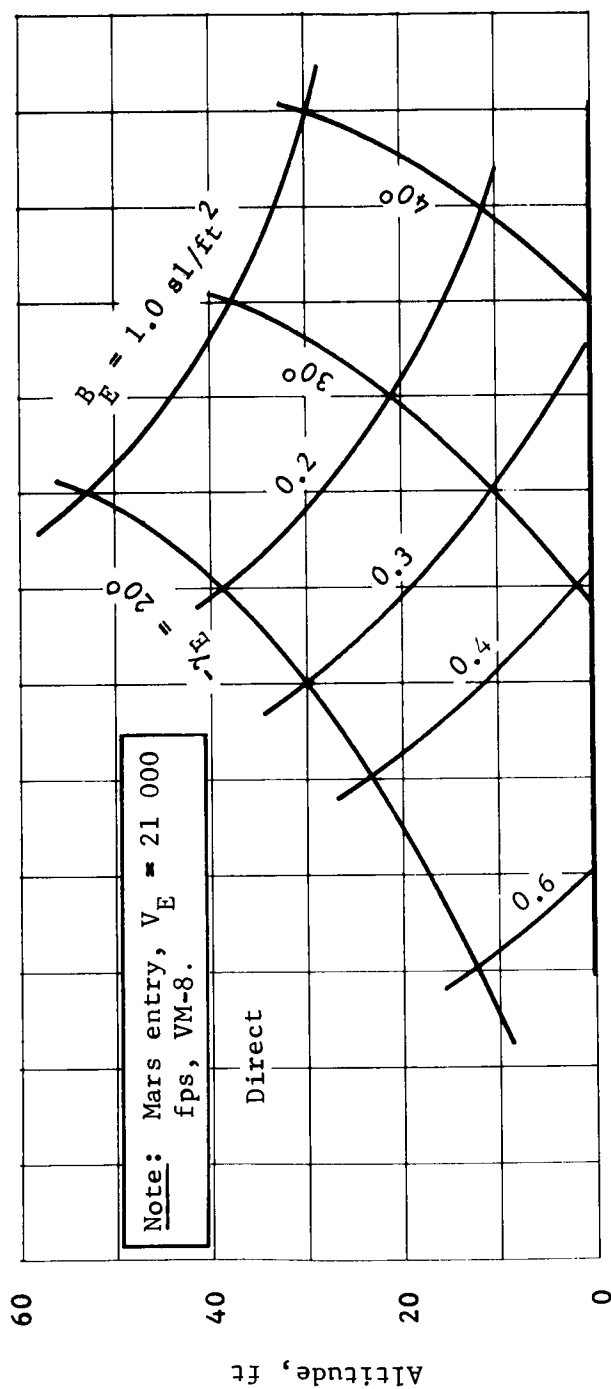


Figure 24.- Altitude at Mach 3.0

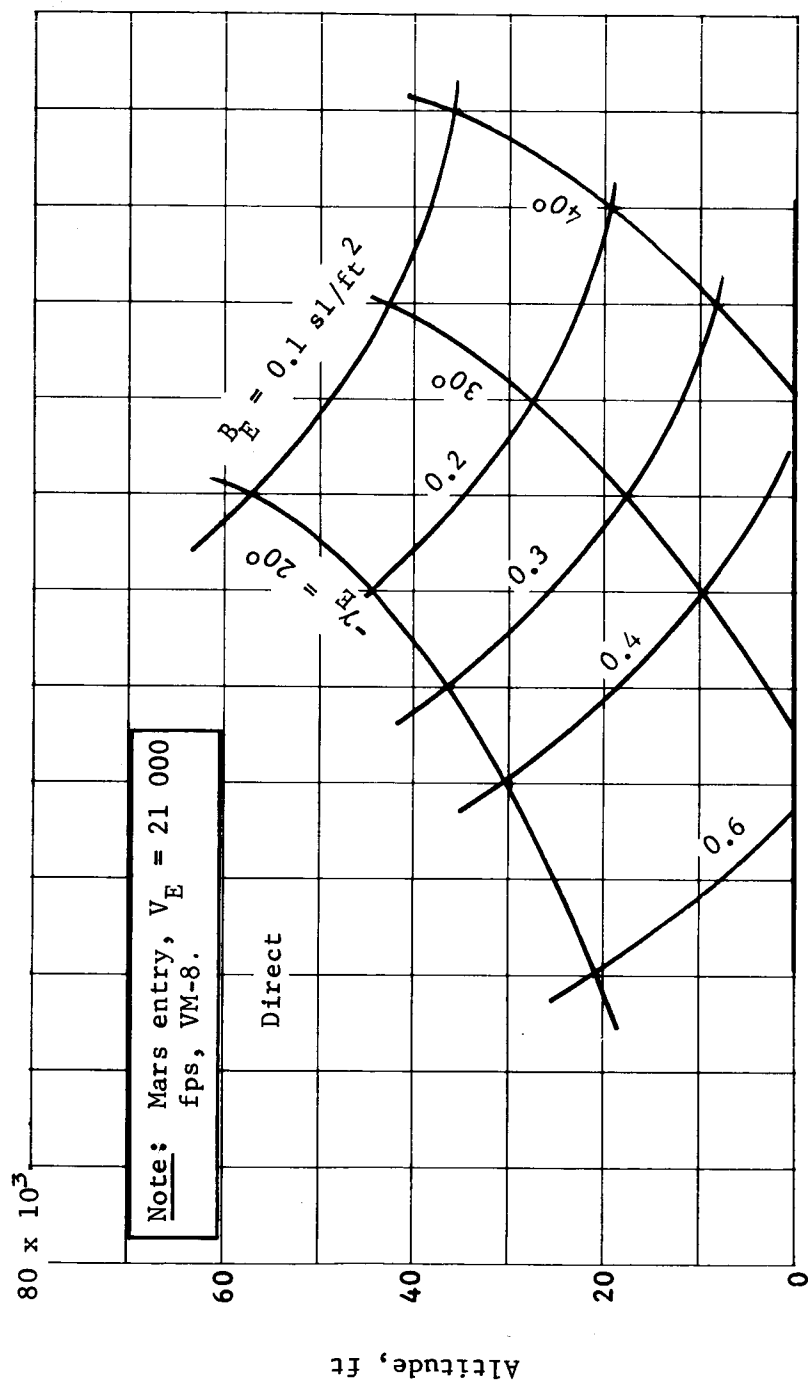


Figure 25.- Altitude at Mach 5.0

Before discussing the terminal phase system analysis results, a word of explanation is required relative to the philosophy adopted for defining the entry flightpath angle vs entry velocity profile to be used for the deorbit/ejection maneuver strategy. The analyses performed during our Voyager Phase B effort indicate the sensitivity of landed payload to entry flightpath angle. To avoid the problem of analyzing terminal phase system performance as a function of entry velocity and entry flightpath angle as well as system parameters, the maneuver strategy was devised, which desensitized the terminal phase system initial conditions to  $V_E$  and  $\gamma_E$ . An example is shown in figure 26. These data show that there are  $V_E, \gamma_E$  contours that result in essentially identical flight conditions below 30 000 ft. All of the targeting analysis discussed previously and in Appendix A are based on  $V-\gamma$  contours that have these characteristics. It is essential here to relate quoted entry flightpath angles in preceding sections to those that appear in this subsection. For example, the entry corridors defined previously for the two orbits considered were a maximum  $-\gamma_E$  of  $16.2^\circ$  and  $18.1^\circ$  for the  $1000 \times 15\,000$ -km and  $1000 \times 33\,070$ -km orbits, respectively. These  $-\gamma_E$  occur at entry velocities of approximately 14 400 and 15 100 fps, respectively. The terminal phase system analysis was based on an entry velocity of 4.5 km/sec (14 764 fps). The  $\gamma_E$  to be used in the terminal phase system comparison is obtained by taking the above values and following the trend shown in figure 26 from the actual  $V_E$  to 4.5 km/sec. Thus, the entry corridor limits for the two orbits change from  $-16.2$  and  $-18.1^\circ$  to  $-16.6$  and  $-17.8^\circ$  as far as the following discussion is concerned.

With this understood, we can proceed with the terminal phase system comparison. The basic ground rules used in this analysis included:

- 1) Aerodecelerator systems,
  - a) Landings at planet mean surface level ( $R_\phi = 3393$  km) and 6000 ft over mean surface level,
  - b) Aerodecelerator completed its job at 4000 ft above terrain,
  - c) Flightpath angle at aerodecelerator separation must be steeper than  $-60^\circ$ ,

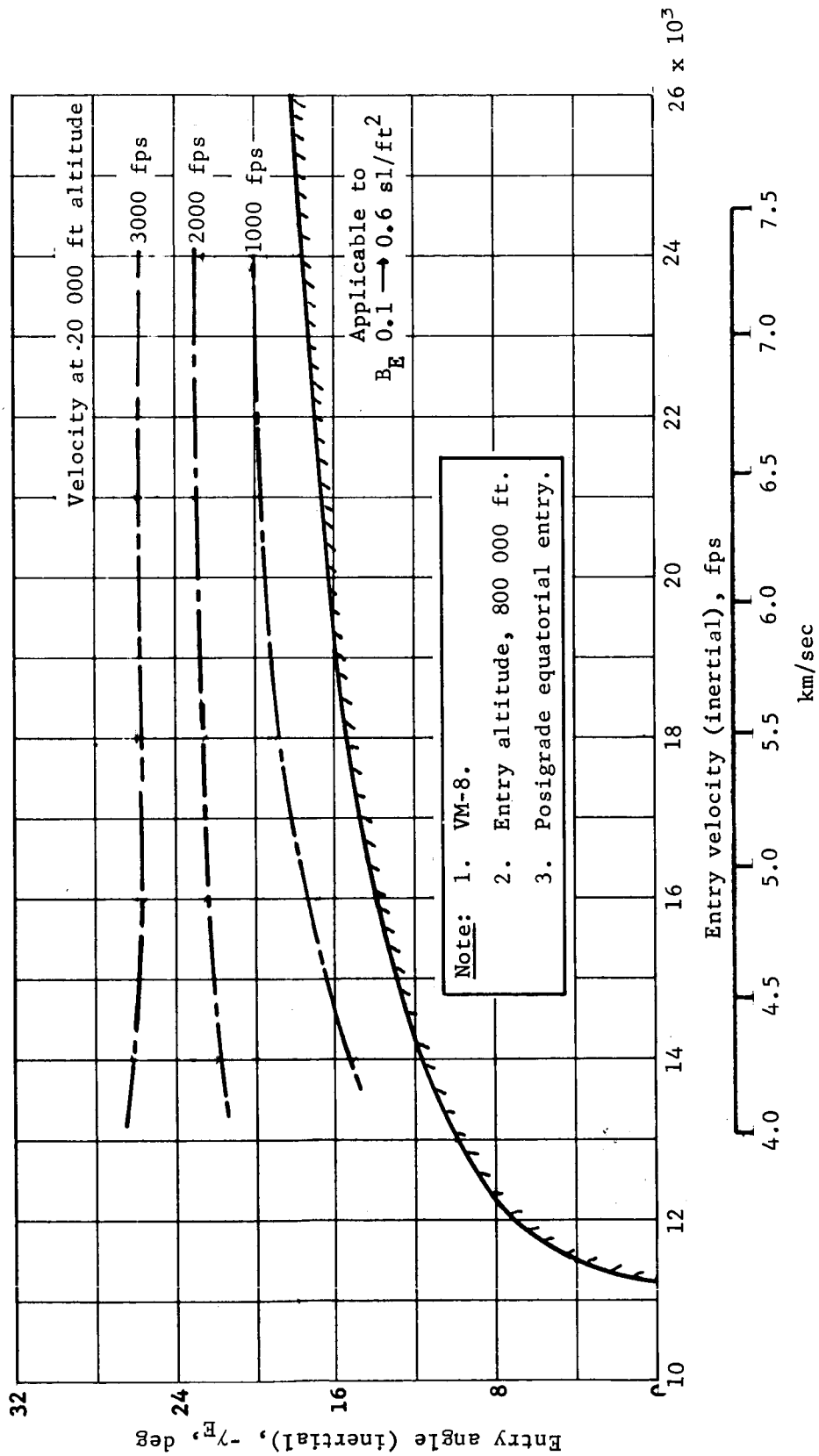


Figure 26.- Mars Skipout Boundary



- d) Time on aerodecelerator must be at least 16 sec or longer,
  - e) The  $M_D = 2$  system must be sized to accomplish c) and d) or to separate the aeroshell, whichever is larger;
- 2) All-retro systems,
- a) Terrain heights of zero and 6000 ft (as above),
  - b) High-thrust braking phase to zero horizontal velocity, with thrust vector aligned along velocity vector at initiation,
  - c) Vertical drop at 1 Mars g for 3 sec followed by 3 Mars g braking to zero velocity,
  - d) Initial thrust for high-thrust braking phase provides an acceleration equal to the drag acceleration (i.e., minimum allowable thrust-to-weight ratio);
- 3) General,
- a) Wind velocity of 220 fps at either aerodecelerator separation or retromotor ignition,
  - b) Analysis performed for aeroshell diameters of 6.5, 8.5, 12.0, 15.0, 20.0, 25.0, and 30.0 ft. Diameters above 15.0 ft are obtained by deployable afterbodies (flaps or inflatable).

The vernier system characteristics used for the aerodecelerator systems were based on the parametric results of our Voyager Phase B study with realistic control laws. They are described in Appendix B, section 2. All of the assumptions used were derived during our Phase B effort and have been demonstrated to be slightly conservative when compared to actual controlled maneuvers.

Much of the following data are presented in terms of  $W_{LE}$  (landed equipment weight). This is defined with the aid of figure 27, which illustrates the components subtracted from entry weight,  $W_E$ , to arrive at  $W_{LE}$ . The  $W_{LE}$  is defined as entry weight minus:

- 1) Aeroshell weight: function of diameter, ballistic coefficient,  $\gamma_E$ ;
- 2) Total aerodecelerator system: function of size and deployment dynamic pressure, Mach no., etc.;

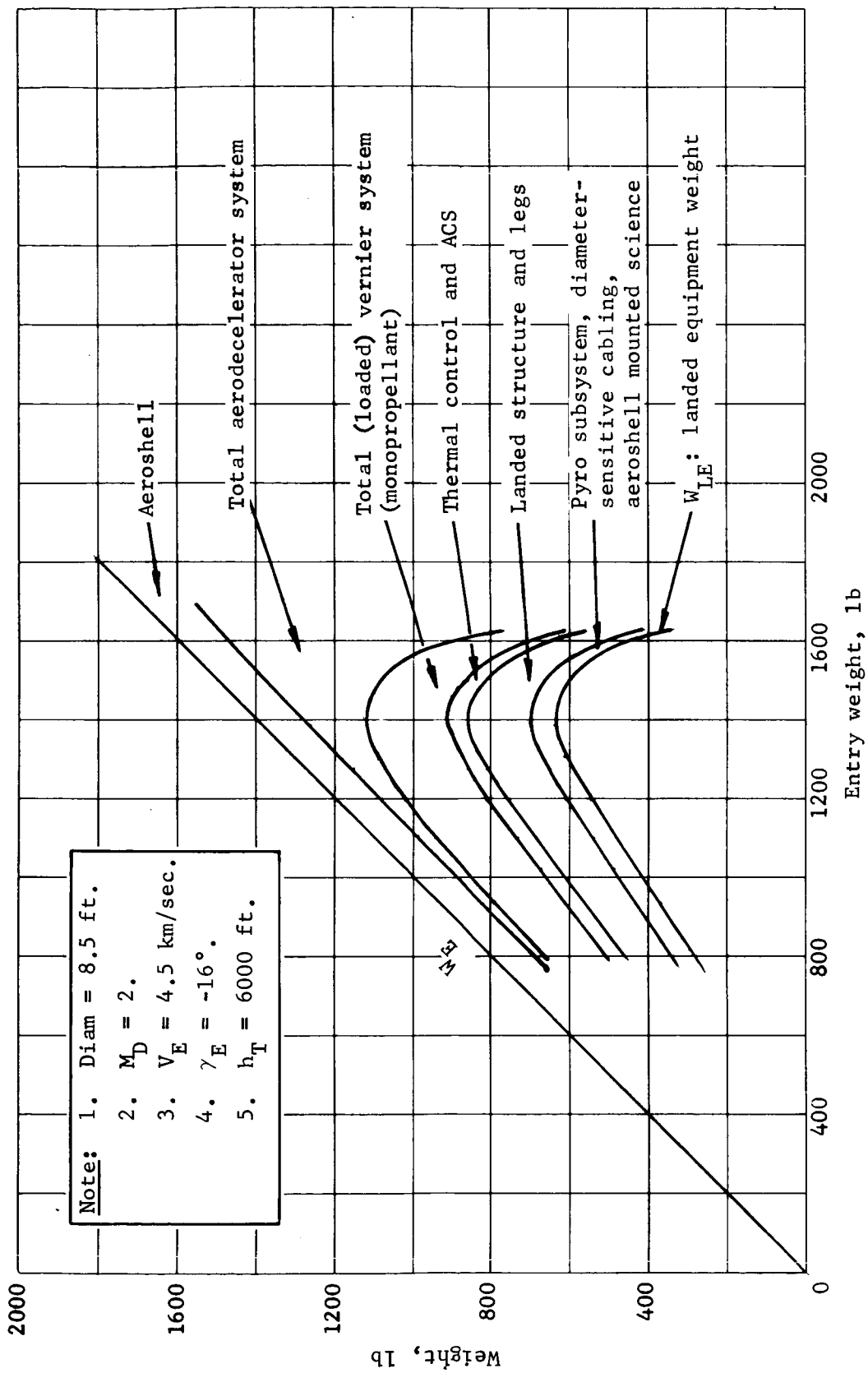


Figure 27.- Landed Equipment Weight

- 3) Vernier or retrosystem: function of thrust level and propellant loading;
- 4) Entry thermal control and ACS: function of diameter and weight;
- 5) Landed structure and legs: function of landed weight;
- 6) Pyro subsystem, cabling, etc.: constant plus function of diameter.

Thus,  $W_{LE}$  is the effective usable weight on the ground comprising entry guidance and control, all communication and data handling subsystems, power subsystems, surface thermal control, and surface science subsystems. The parametric weight equations used for the delivery system weights (i.e.,  $W_E - W_{LE}$ ) are given in Appendix D, section 1. The breakdown of  $W_{LE}$  is presented later in this report.

The basic parametric data presented in Appendix B, section 2 is of the form of  $W_{LE}$  vs  $W_E$ . An example is shown in figure 28 for a  $M_D = 2$  parachute system. Three specific contours are identified on the figure. The first is maximum  $W_{LE}$  for each diameter. This contour is the maximum system performance for any given diameter. The second contour is really the envelope of the curves. The contour describes the maximum  $W_{LE}$  for any given  $W_E$ . The price paid for using this contour is increased aeroshell diameter (i.e., minimum ballistic coefficient). The third contour lies between the first two and is a locus of maximum  $W_{LE}/W_E$  ratio for any given diameter. This contour is one that defines the most efficient system in terms of maximum lb on the ground/lb entry for any given diameter. These three contours are referred to as maximum  $W_{LE}$  contour, maximum  $W_{LE}$  envelope, and maximum  $W_{LE}/W_E$  ratio contour, respectively. Many of these contours are presented in Appendix B, section 2 for all of the terminal phase systems and several of the initial conditions (i.e., velocity, flightpath angle).

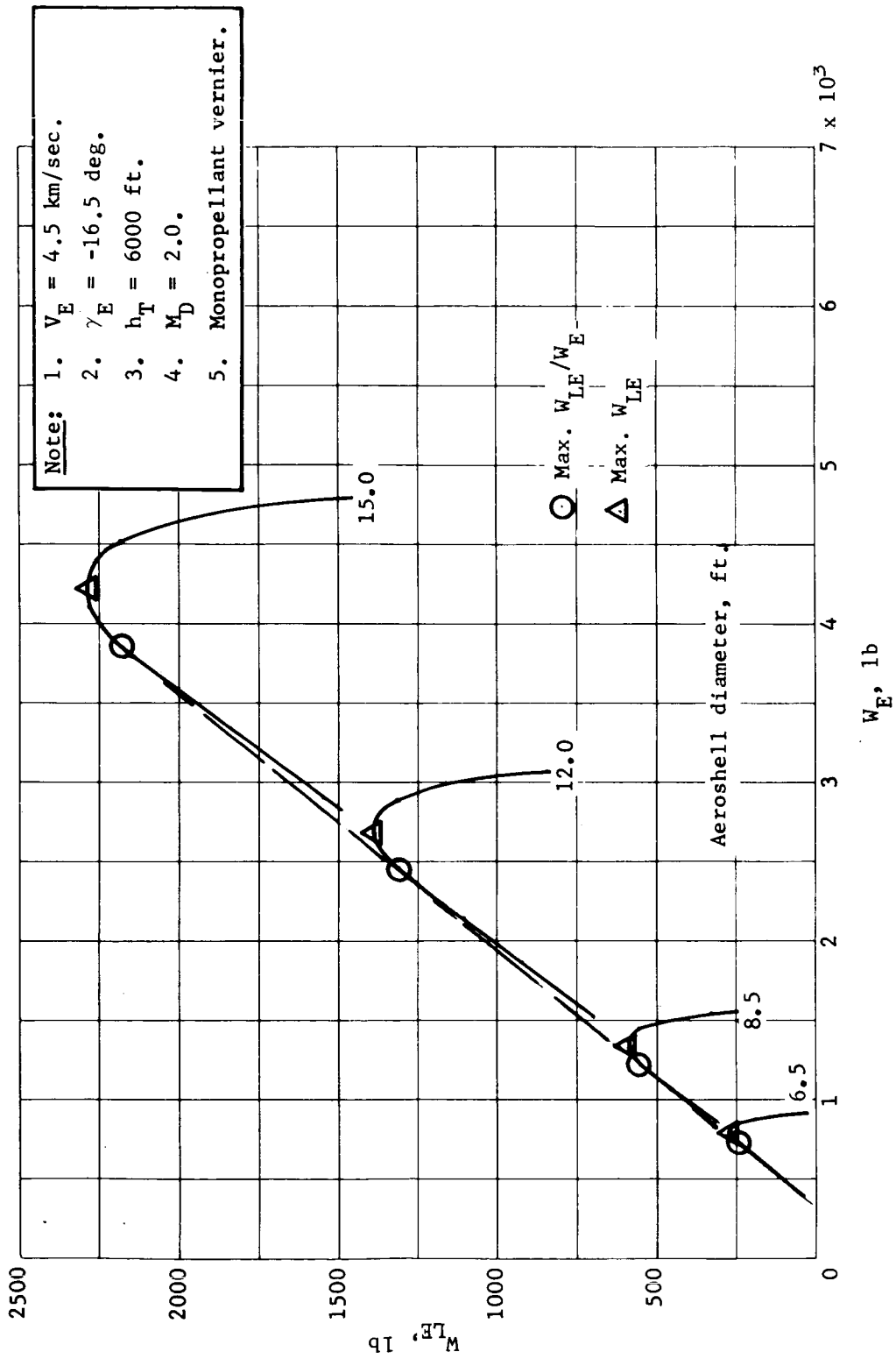


Figure 28.- Aerodecelerator Performance Entry from Orbit

The terminal phase system capabilities are summarized as a function of assumptions. The basic  $W_{LE}$  capability is shown in figures 29 and 30 for fixed diameters of 8.5 and 15.0 ft. The data are based on the maximum  $W_{LE}$  contour and therefore represent maximum  $W_{LE}$  for the given diameters. The data shown in figure 29 for the 8.5-ft diameter compare the orbit mode and direct mode for the various systems. Both entry weight and  $W_{LE}$  are shown as well as the sensitivity of both of these parameters to entry flightpath angle. For the orbit mode, the Mach 5 ballute provides the highest performance per diameter but also has the greatest entry weight. The retrosystem is slightly better than the  $M_D = 2$  parachute system. The direct mode data show the same trends except the retrosystem is relatively better. None of the direct mode performance is acceptable at a diameter of 8.5 ft. Similar data are shown in figure 30 for a 15-ft diameter. The orbit mode data show high performance capability with the same characteristics across systems as was exhibited for the 8.5-ft diameter data. The direct mode data, for a  $\gamma_E$  maximum of  $-24$  to  $-26^\circ$ , show acceptable performance, with the retrosystem showing the best performance capability. It is clear from these data that any of the systems can deliver useful payloads ( $W_{LE}$ ) in the 600-lb class with diameters in the 8.5- to 15.0-ft range. Generally, the ballute performance is superior for the orbit mode, while all-retro systems are most favorable for the direct mode. At fixed diameter, the orbit mode provides the greatest  $W_{LE}$  and continues to provide maximum lb on the ground/lb entry weight.

The second comparison is made on the basis of a fixed landed equipment weight of  $W_{LE} = 600$  lb. This is summarized in figure 31 in terms of minimum required entry weight. Once again the sensitivity to entry flightpath angle is indicated by the shaded portion of the bars. For the orbit mode, the  $M_D = 2$  parachute case requires the lightest entry weight, with the all-retro system a close second. For the direct mode, all of the required entry weights are greater than for the orbit mode, with the retro system requiring the smallest entry weight. The retro system data as presented are somewhat deceiving relative to the data's apparent insensitivity to  $\gamma_E$ . In reality, the data presented in Appendix B show that the variation in  $\gamma_E$  requires a wide variation in the required thrust-to-weight ratio.

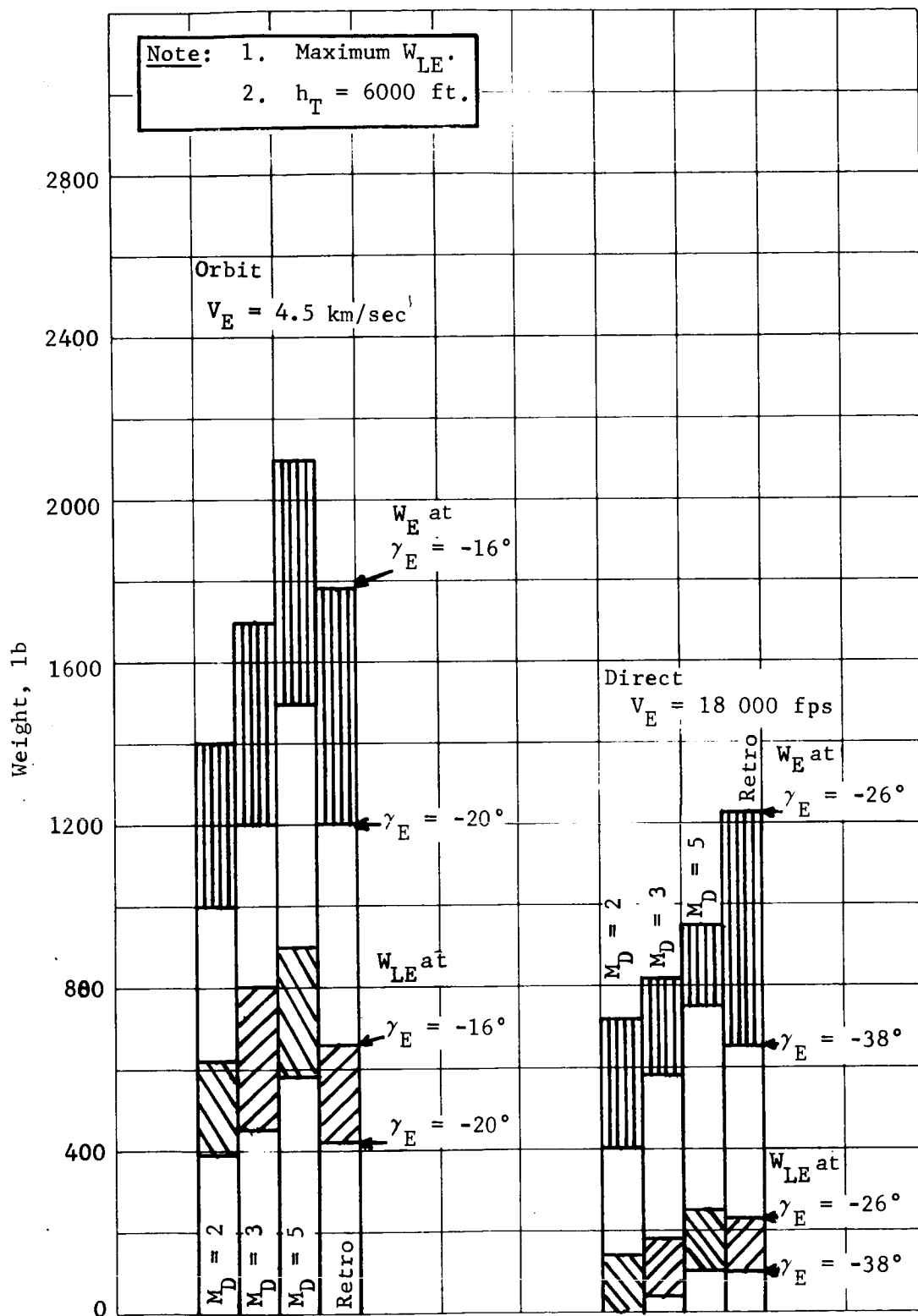


Figure 29.- Terminal Phase Summary, Aeroshell Diameter = 8.5 ft

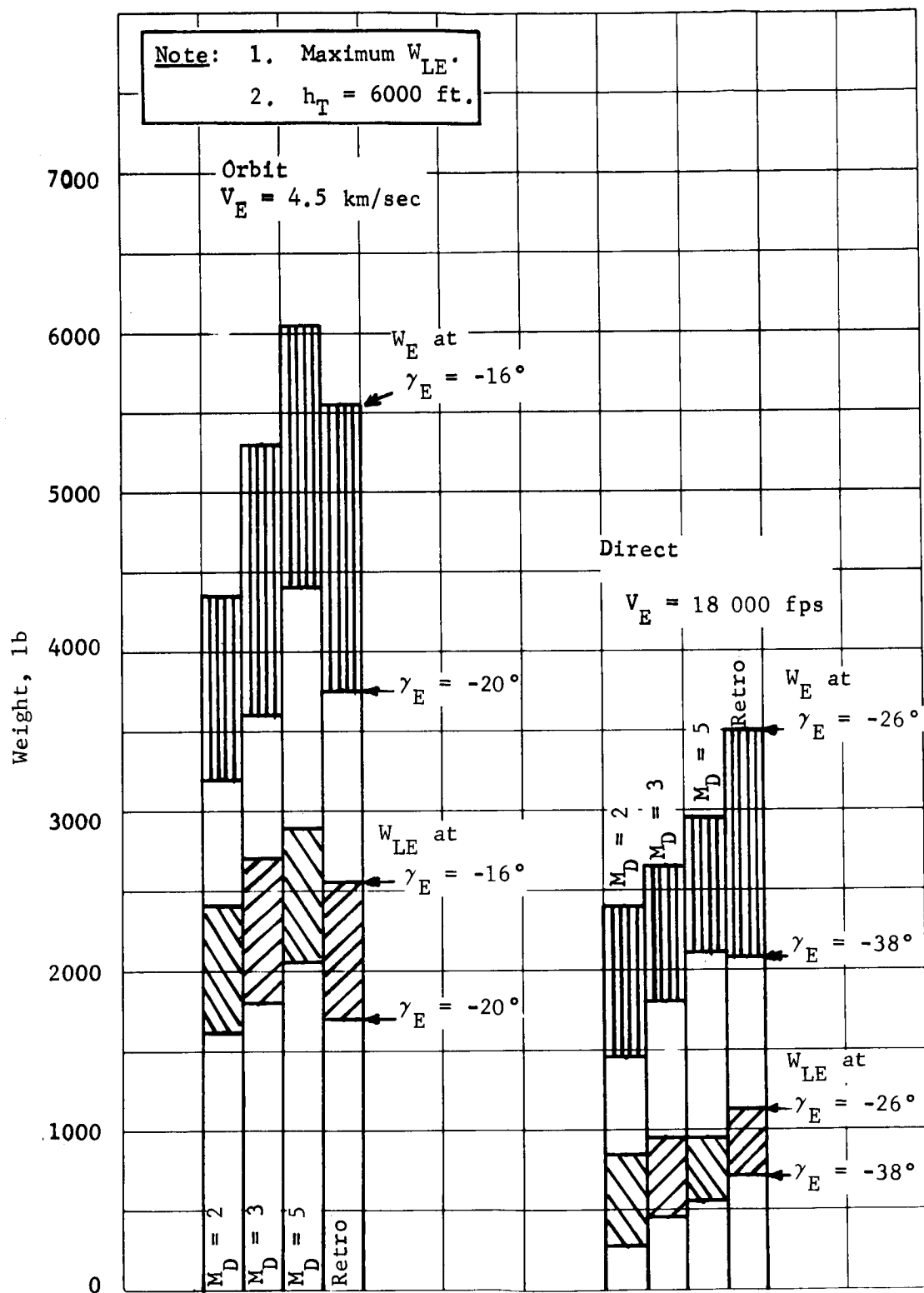


Figure 30.- Terminal Phase Summary, Aeroshell Diameter = 15 ft

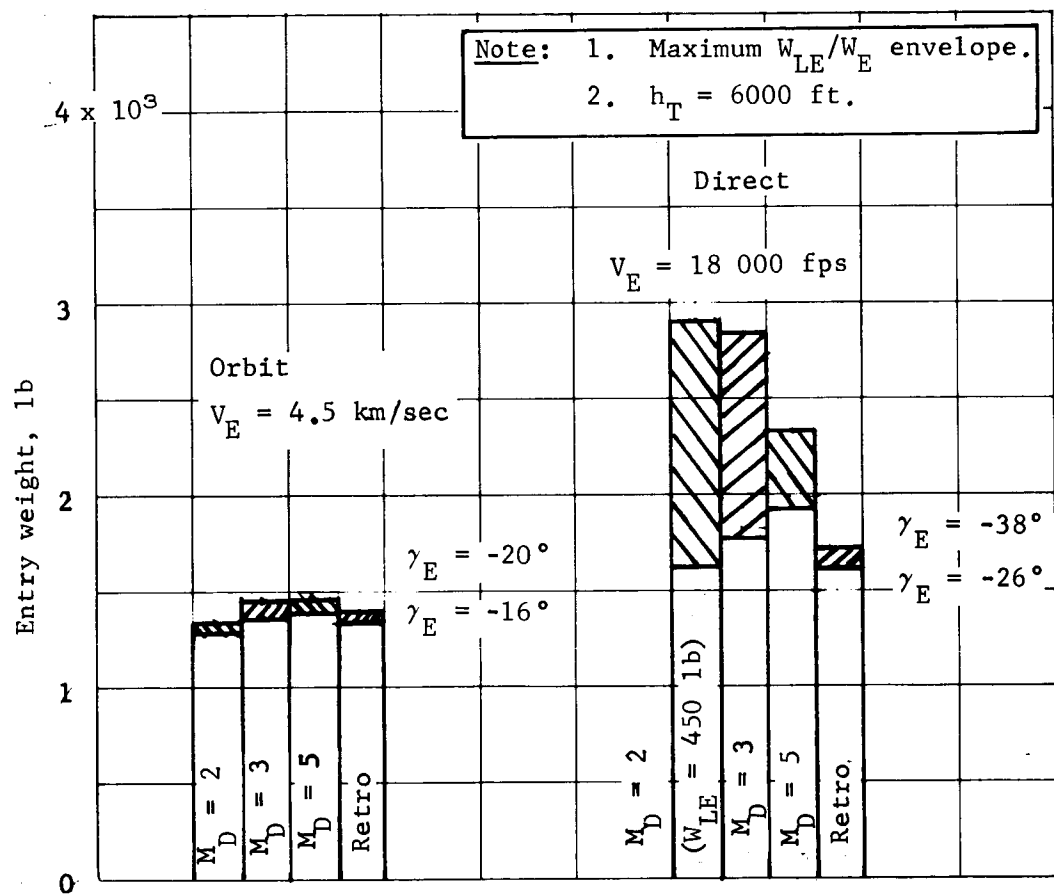


Figure 31.- Terminal Phase Summary, Landed Equipment  
Weight = 600 lb



The required aeroshell diameters for the above comparison are shown in figure 32. For the orbit mode, the all-retro system requires the greatest diameter. Once again the retro data can be somewhat misleading because they are based on using the minimum useful thrust-to-weight ratio. There is a tradeoff between thrust level and diameter. For the direct mode, the required diameters are all greater than those for the orbit mode. Again assuming  $-\gamma_E$  maximum of  $18^\circ$  for the orbit mode and  $26^\circ$  for the direct mode, the corresponding diameter ranges are 8.1 to 9.5 for the orbit mode aerodecelerators and 12.3 to 13.6 ft for the direct mode. These data correspond to the case of landing 600 lb of  $W_{LE}$  at the lowest entry weight  $W_E$  without regard to aeroshell diameter.

The final comparison made here (others are presented in Appendix B, section 2) is on the basis of a fixed entry system weight of 1500 lb. The maximum allowable landed weights for the systems and the mission modes are shown in figure 33. The efficiency of the  $M_D = 2$  parachute is once again apparent in providing the greatest lb on the ground/lb entry weight for the orbit mode, while the all-retro system is best for the direct mode. The corresponding required diameters are shown in figure 34. Once again, the orbit mode diameters are smaller than the direct mode cases, with the  $M_D = 2$  requiring the largest diameters.

The variations in these results are only indicative of the kinds of tradeoffs that can be made. A generalization that can be drawn from the analysis is that the  $M_D = 2$  parachute is best when compared on the basis of lb on the ground/lb entry weight. The supersonic ballutes provide the maximum lb on the ground/ft of aeroshell diameter. The all-retro systems are always competitive, but care must be taken in their evaluation to consider their high sensitivity to required thrust-to-weight ratios.

Before concluding this summary discussion of the data in Appendix B, section 2, we should mention the degree of conservatism implied in the analysis from a mission profile point of view. Two aspects to this question are discussed here. The first is that all of the results presented above are based on all of the following things occurring simultaneously:

- 1) The VM-8 atmosphere plus design terrain height define the altitude mark to trigger aerodecelerator deployment;

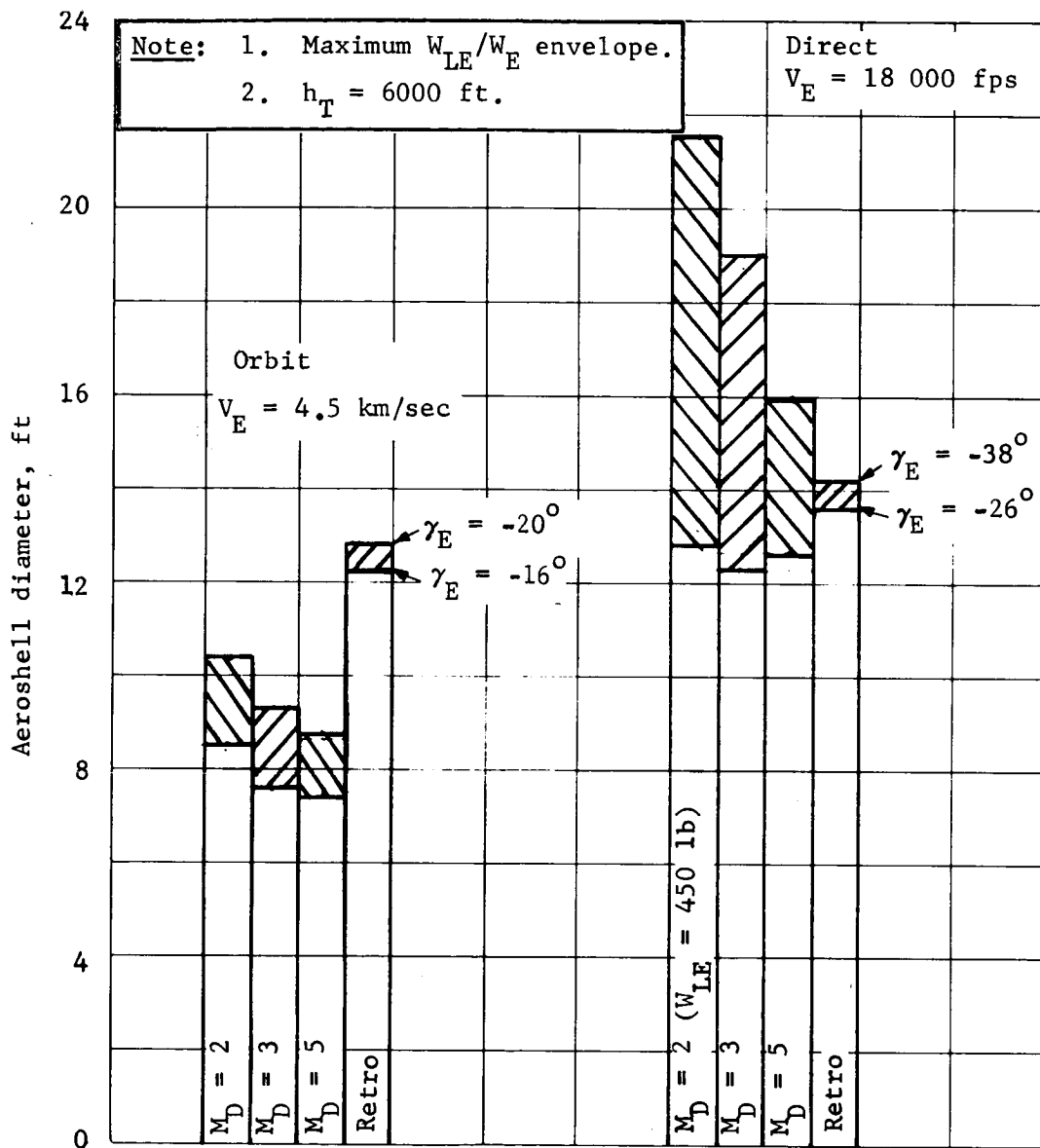


Figure 32.- Terminal Phase Summary, Landed Equipment Weight = 600 lb

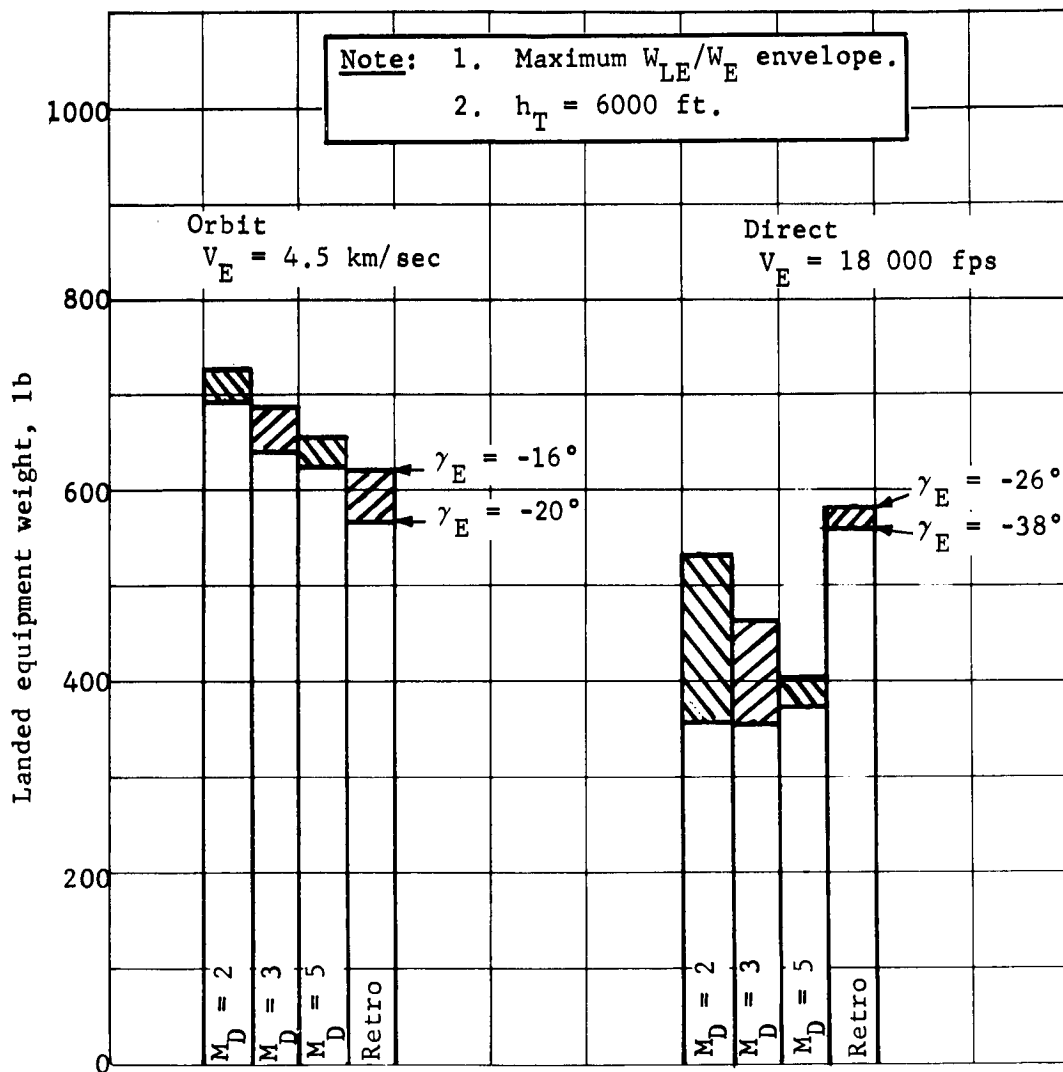


Figure 33.- Terminal Phase Summary, Entry Weight = 1500 lb

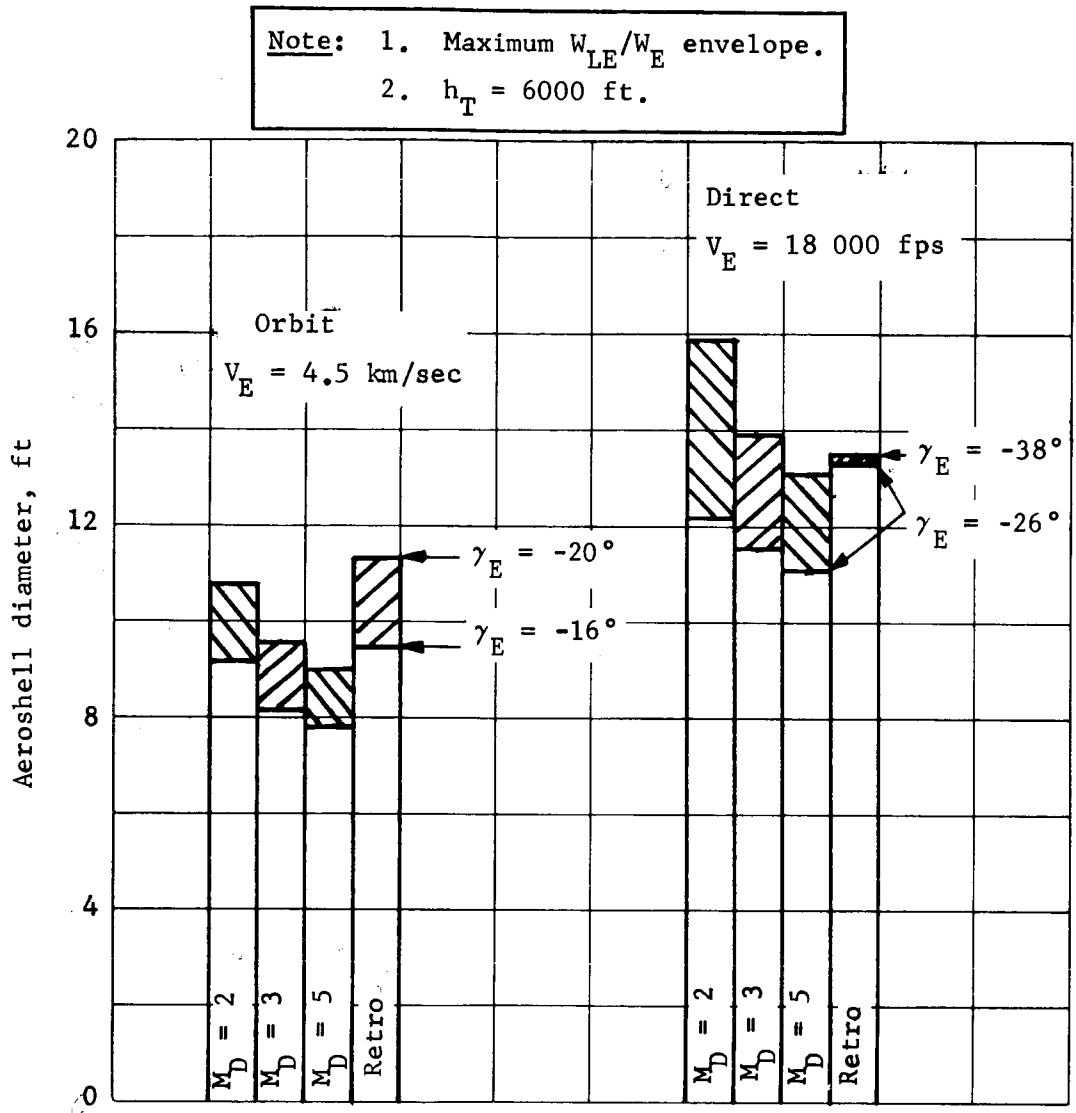


Figure 34.- Terminal Phase Summary, Entry Weight = 1500 lb

- 2) The VM-7 atmosphere in combination with a 220-fps horizontal wind define the aerodecelerator size and vernier requirements. The VM-8 atmosphere defines the deployment altitude and design dynamic pressure;
- 3) The  $3\sigma$  steepest entry flightpath angle is used in conjunction with  $3\sigma$  orbit or approach trajectory ephemeris uncertainty.

These constraints really fall into two categories from a design viewpoint. The first is that the worst entry flightpath angle and atmosphere are assumed in direct combination. The system might still work if either one or the other is worse than expected. The second category is the definition of altitude mark for aerodecelerator deployment. This must be based on an assumed design terrain height and worst atmosphere. If the terrain height is higher than assumed, the probability of successful landing is low. An altitude mark must be set prior to flight and there is less inherent adaptability in the system to cope with surprises. Even so, the combination of events that must happen simultaneously, as assumed in this analysis, should reflect as some degree of conservatism in the results.

The second aspect of conservatism that has been partially investigated here is the uncertainty in the weight equations. The  $M_D = 2$  parachute has been used as an example. The data shown in figure 35 show the "corrected  $W_{LE}$ " as a function of aeroshell diameter for the maximum  $W_{LE}$  contour in the case where all of the delivery systems have been arbitrarily increased by a net factor of 10%. This chart can be entered at the design  $W_{LE}$  plus 10% to arrive at a conservatively established aeroshell diameter. For example, assume a design  $W_{LE}$  of 600 lb. Entering figure 35 at  $W_{LE} = 660$  lb and  $\gamma_E = -16^\circ$  results in a required diameter of 9.0 ft for a design terrain height of 6000 ft. The nominal data from Appendix B call for 8.3 ft. A similar example for the direct mode, using figure 36 and  $-26^\circ$ , results in diameters of 14.7 and 13.1 ft for the 10% margin and nominal cases. Designs based on the increased diameters will allow a net growth of 10% in all systems before something must be offloaded. A procedure of this type must almost certainly be followed for a real design. A diameter margin of approximately 10% should be used.

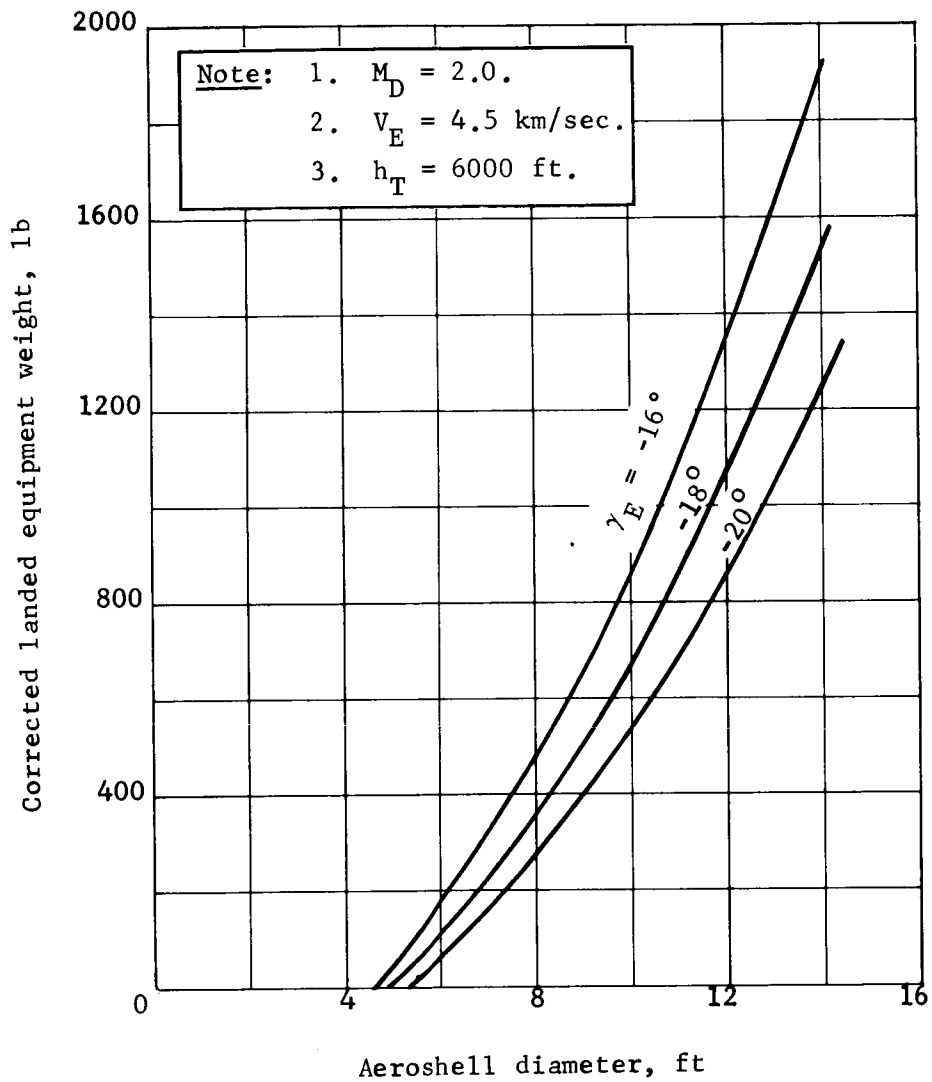


Figure 35.- Maximum  $W_{LE}$ , 10% Margin

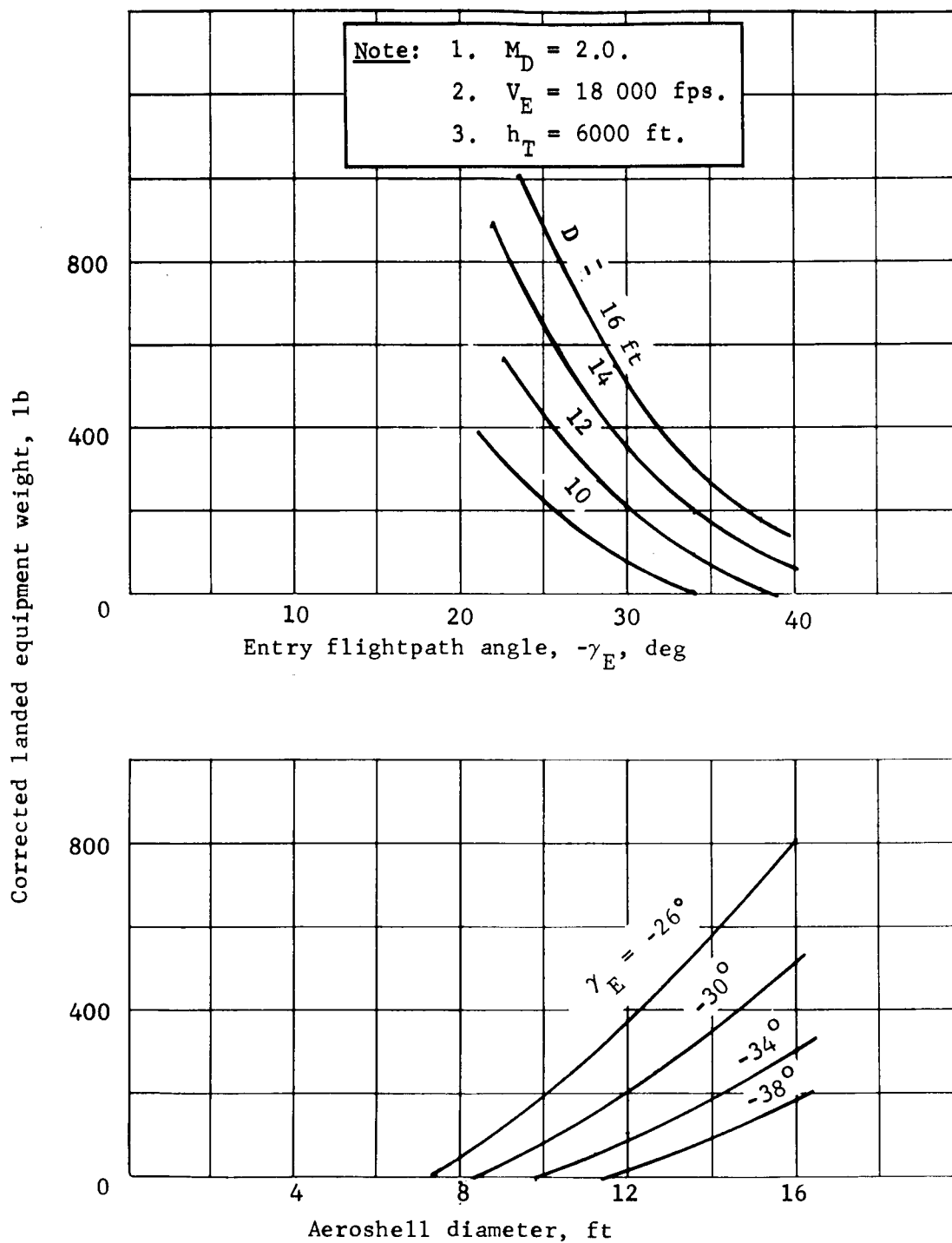


Figure 36.- Maximum  $W_{LE}$ , 10% Margin

Aerothermodynamics analysis. - This analysis is limited to a definition of the pressure and heating loads that the aeroshell must be designed for. The study was based on the 70° half-angle cone for both modes. Sufficient comparisons were made between the 60 and 70° cones to show that a valid mission mode study can be based on the 70° cone configuration.

The normalized pressure distribution over the aeroshell is independent of all the parameters involved in this study. The design airloads then are only functions of the maximum dynamic pressures given in Appendix B.

The aerodynamic heating rates and loads are functions of entry parameters,  $V_E$  and  $\gamma_E$  and configuration parameters  $B_E$  and diameter. In addition, the atmosphere effect is felt through both scale height and chemical composition. The specific combinations of all parameters tabulated were studied for each mode. Complete data are presented in Appendix C, section 1.

Mode	$V_E$ , fps	$\gamma_E$ , deg	$B_E$ , slugs/ft <sup>2</sup>	Atmosphere
Orbit	14 000	2 $\sigma$ above skipout	0.1	VM-7
	15 000	-17	0.3	VM-8
	16 000	-20	0.6	
Direct	18 000	2 $\sigma$ above skipout	0.1	VM-7
	21 000	-28	0.3	VM-4
	24 000	-38	0.6	

Diameter was considered as a variable in cases where the significant factors cannot be scaled on the basis of size.

The aerodynamic heating for the orbit mode is entirely due to convection. Turbulent flow and its associated increase in heating is experienced for a limited range of conditions in VM-8, i.e., diameter greater than 12 ft,  $B_E = 0.6$  and  $\gamma_E = -17$  to  $-20^\circ$ .

However, the critical heating loads occur in VM-7 for all orbit mode cases. The effects of the entry corridor and configuration variables on maximum heating rate and total heating load are shown in figure 37. Both the maximum heating rate and total heating rate increase slowly with increasing velocity.



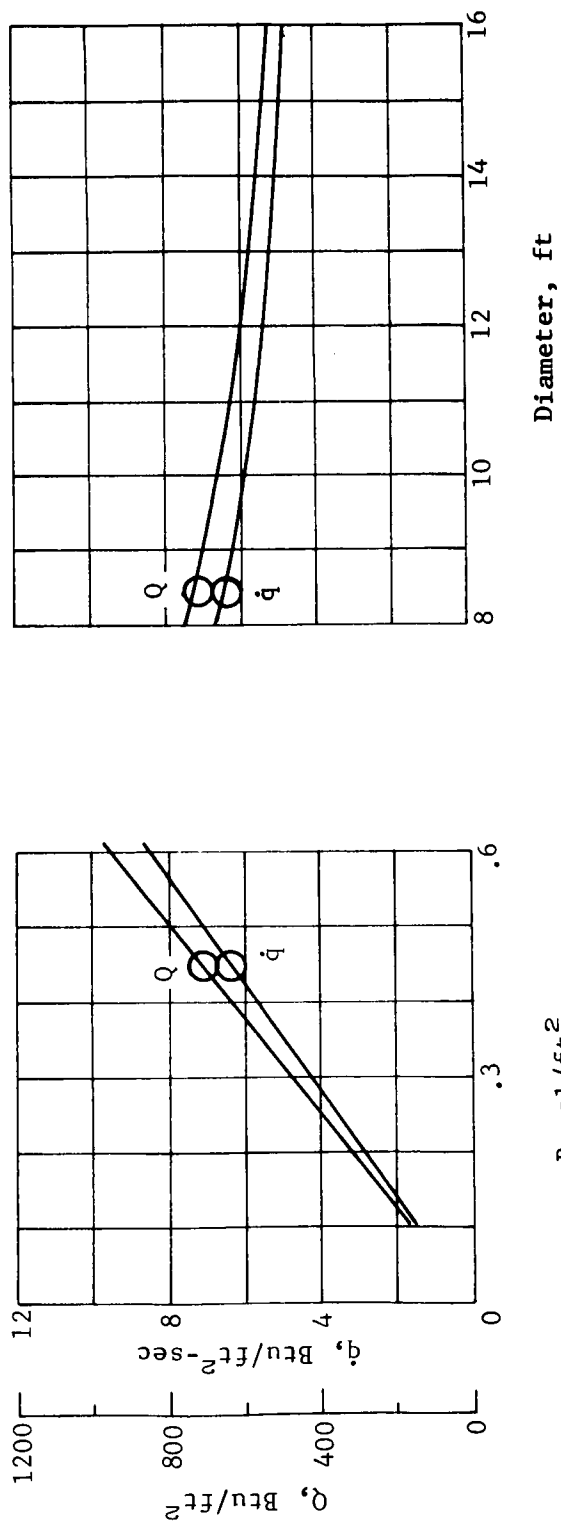
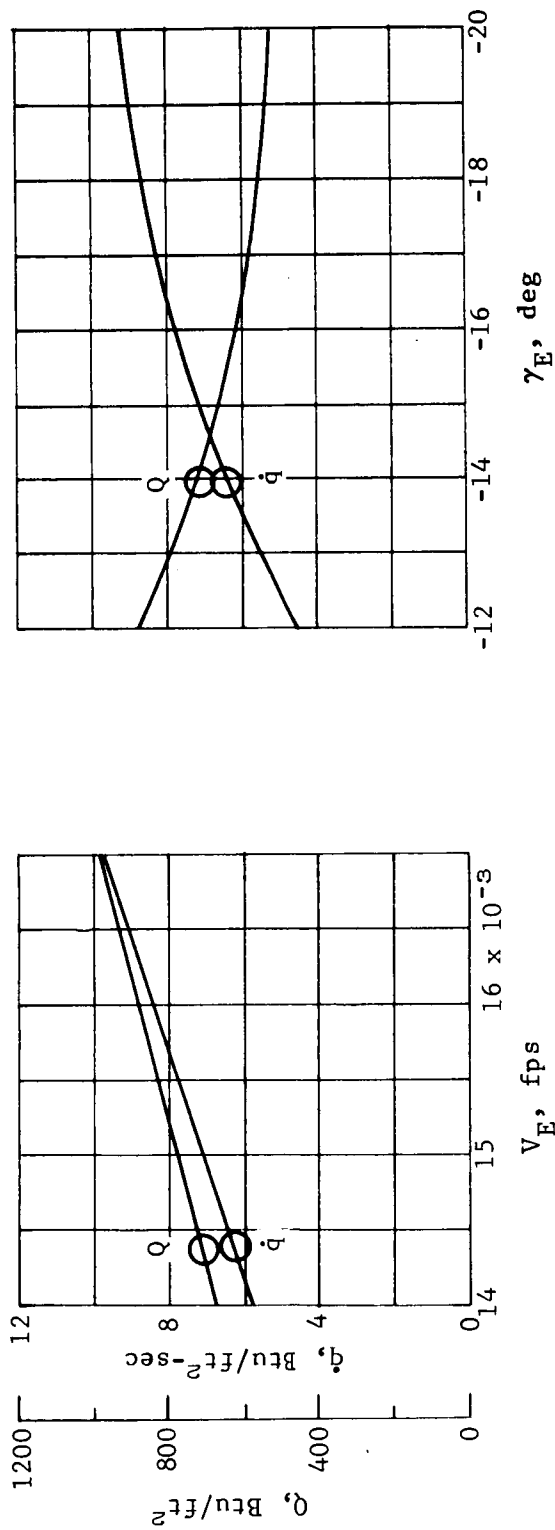


Figure 37.- Orbit Mode, Aeroheating Sensitivities, VM-7, Cone Edge

Total heating load decreases with more negative flightpath angles, while the maximum heating rate increases. Increases in ballistic coefficient cause increases in both heating rate and load, while increases in diameter result in a reduction of both parameters. The data of figure 37 show the effect of changing only one variable at a time and of course there are interactions. The entry flight condition and configuration effects can be considered independently. The orbit mode design condition for a given configuration occurs at the lowest entry angle. The configuration variables  $B_E$  and diameter are not independent;  $B_E$  decreases as diameter increases for a fixed system weight. The heating load must decrease (according to fig. 37) as the diameter increases for fixed entry weight and entry corridor. Thus, the ablator thickness must decrease. However, the total ablator weight increases due to the increasing aeroshell surface area.

Both radiative and turbulent convective heating become significant for the direct mode. Turbulent heating occurs only for extreme combinations of variables in VM-7, similar to the VM-8 case for orbital entry. Thus, turbulence is not of concern in VM-7 for realistic conditions. However, turbulence exists for a wide range of conditions in VM-4 and may be critical for design.

The VM-7 sensitivity of heating to  $V_E$ ,  $\gamma_E$ ,  $B_E$  and diameter is shown in figure 38. The trends of convective heating are like those for the orbital mode. Radiative heating increases rapidly with velocity and can become dominant at the higher velocities.

Heating sensitivity data for VM-4 are shown in figure 39. The effect of velocity on heating is similar to that shown in VM-7. However, each of the other parameters reflects the effect of transition to turbulent flow. In each case the lowest value of the variable shown results in laminar heating and transition to turbulence results as the variable increases. Turbulence can be critical to heat shield design in two ways: (1) if the heating rate is greater than 100 Btu/ft<sup>2</sup>-sec, a more dense ablator must be used (Appendix C, section 2), and (2) the heating load may become great enough to define the ablator thickness required. Transition to turbulence is sensitive to  $\gamma_E$ ,  $B_E$  and diameter. It is unlikely that both the entry corridor and configuration can be so constrained that turbulent heating can be avoided. However, it may be possible to constrain these parameters so turbulence is not critical to design.

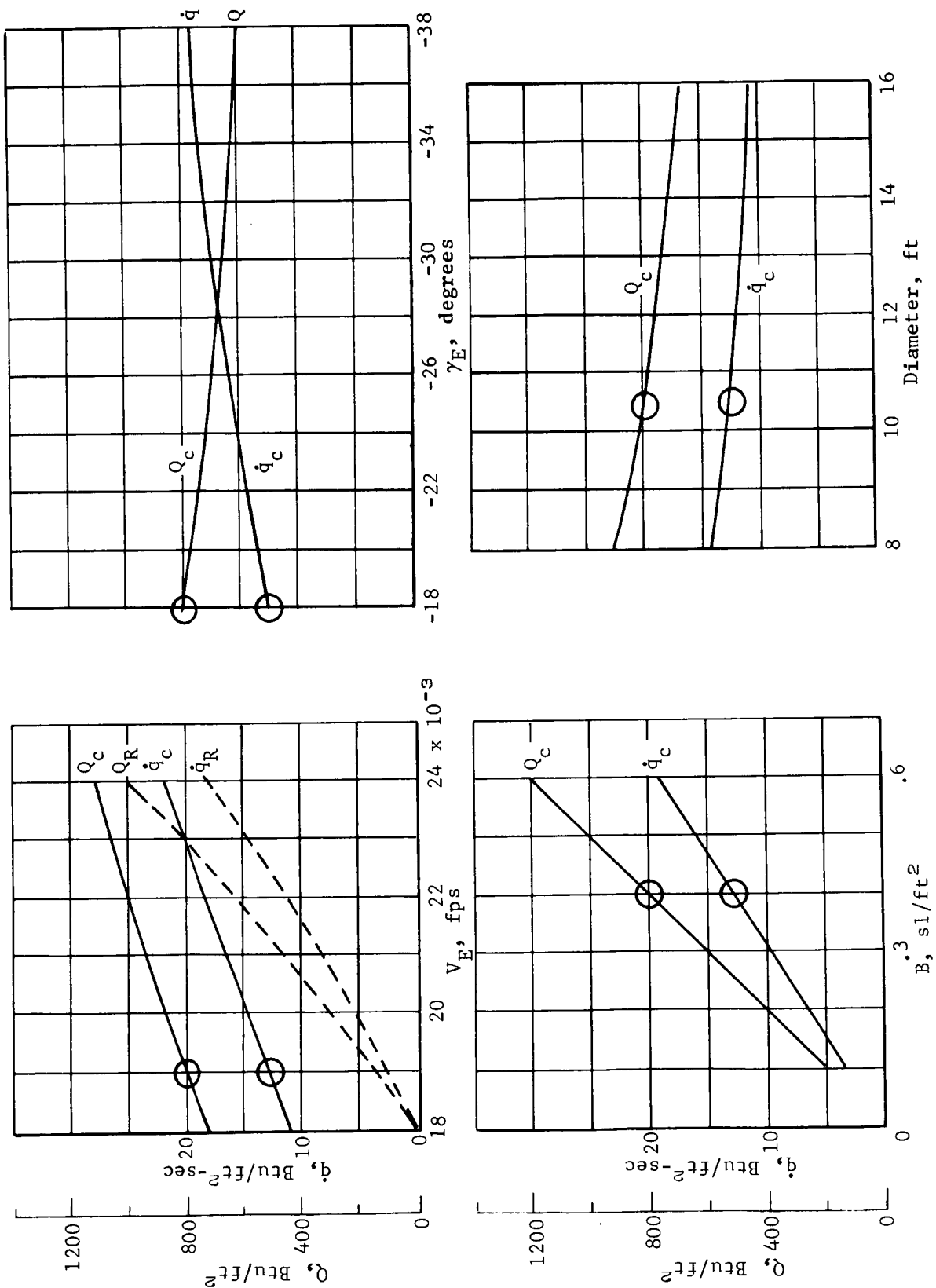


Figure 38.- Direct Mode, Aeroheating Sensitivities, VM-7, Cone Edge

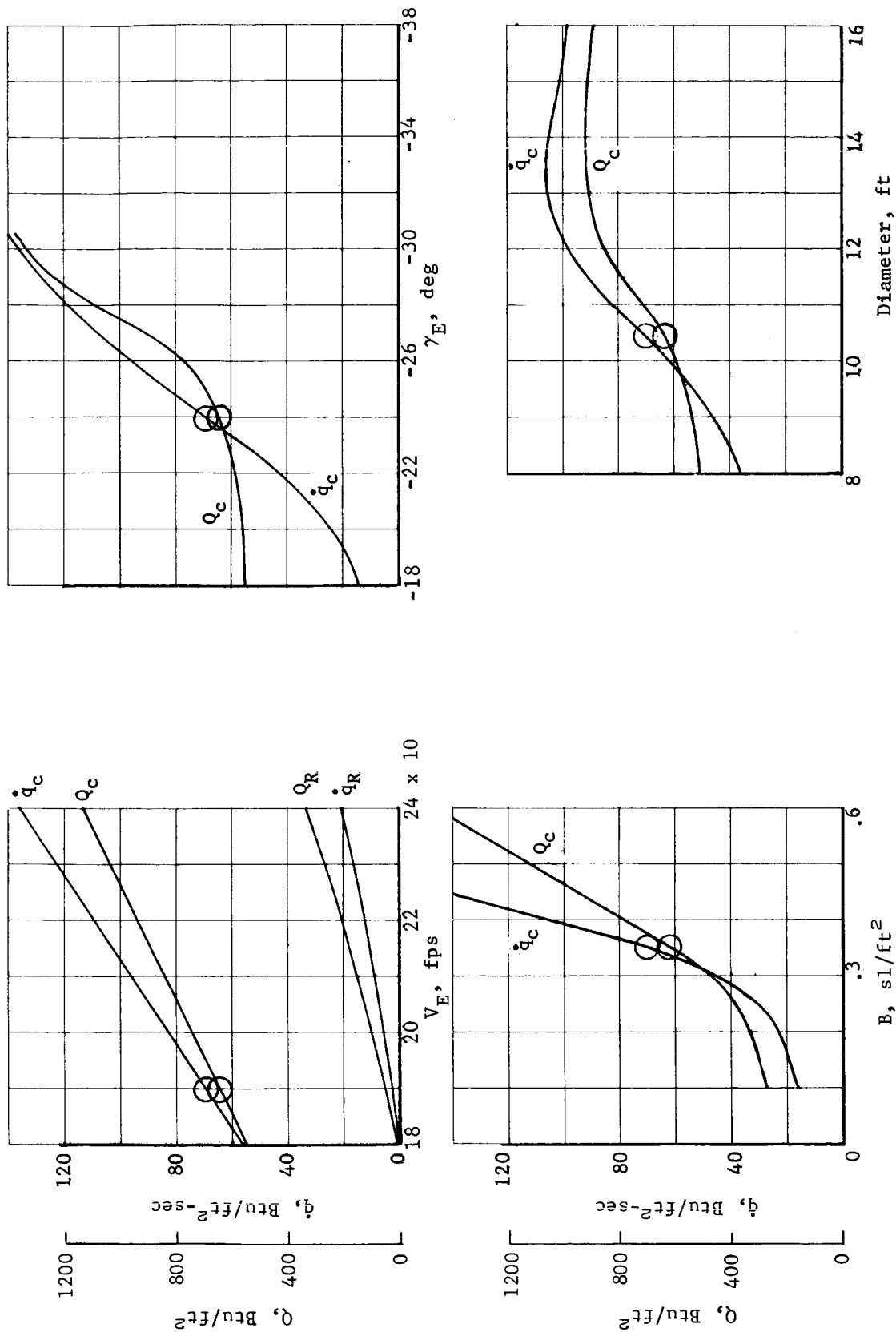


Figure 39.- Direct Mode, Aeroheating Sensitivities, VM-4, Cone Edge

There are significant uncertainties associated with both radiative and turbulent convective heating that will require extensive experimentation to resolve. Radiation intensities are poorly known for the atmosphere compositions of interest and large uncertainties are associated with current predictions of radiative heating. Flow transition criteria are rather nebulous. This can result in large variations in predicted convective heating for specific conditions.

Entry velocity is the primary difference between modes and is used to illustrate the effects of mission mode on aeroheating in figures 40 and 41. Figures 40 and 41 are based on specific conditions from the parametric study and are intended only to illustrate trends. The conditions are  $B_E = 0.30$ ,  $D = 15$  ft,  $\gamma = -17^\circ$  for orbital mode and  $-28^\circ$  for direct mode. Heating data for minimum entry angles ( $2\sigma$  above skipout) are also shown in figure 41.

Maximum heating rate data in figure 40 show significantly more laminar heating for the direct mode than for the orbital mode. However, the striking difference is the turbulent heating in VM-4. Radiative heating is again shown to be of major importance at high direct mode entry velocities. Total heating loads are shown in figure 41. The critical cases are VM-7 laminar at minimum  $\gamma_E$  for the orbital mode. For the direct mode, either VM-7 (laminar flow) or VM-4 (turbulent flow) might be the design condition. Turbulent flow does not dominate the heating load picture in the same way it does for heating rate. This is because the flow is not turbulent throughout the entire trajectory. In fact when the time of heating and the radiative heating are considered, VM-7 is probably most critical. Thus, VM-4 heating rates may define the ablator material but VM-7 will probably define the ablator thickness. The influence of both turbulent convective and radiative heating can be minimized if the entry velocity is kept low.

Heating of the vehicle base is roughly proportional to forebody heating. The differences in base heating magnitude between the orbital and direct entry modes may require different forms of base heat protection. The direct mode heat protection requirements for the entry vehicle may be much greater than those for the orbit mode; in any case a more extensive experimental program will be required to adequately define the aeroheating.

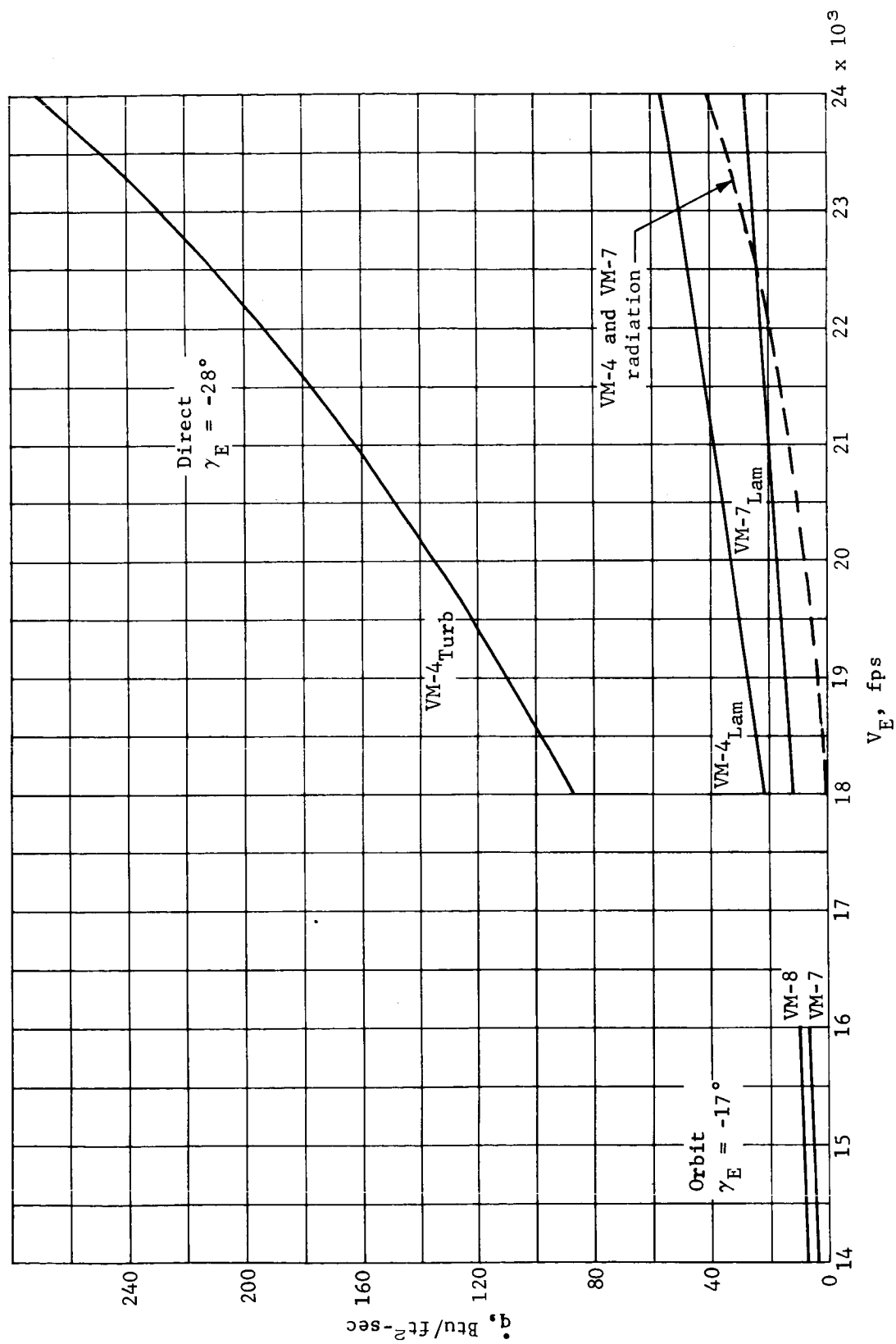


Figure 40.- Maximum Heating Rate Comparison,  $B = 0.30$ , Diameter = 15 ft, Cone Edge

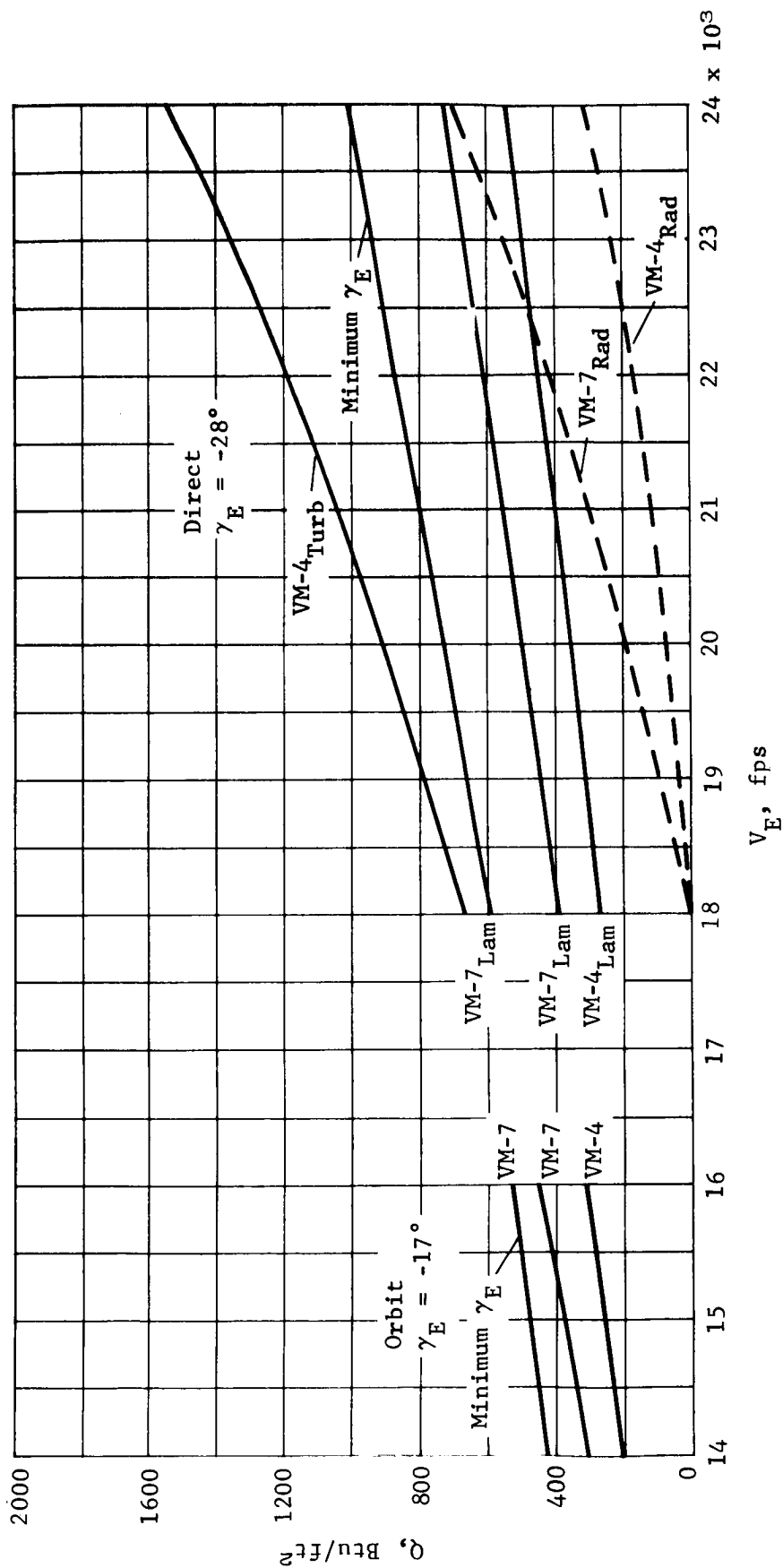


Figure 41.- Total Heating Load Comparison,  $B = 0.30$ , Diameter = 15 ft, Cone Edge

### Mission Profile Mode Comparison

The comparison of mission modes presented here is based only on the results of the parametric studies reported in the foregoing subsection. The implications of subsystem design characteristics are factored into the total mission mode comparison later in this report.

The basic elements of comparison in this subsection are the targeting capability, landing footprint size, terminal phase system performance, and required launch vehicles. The following comparison groups the targeting and error analyses into one category and the terminal phase system and launch vehicle performance into a second.

The targeting and error analysis mission mode comparison is summarized in figures 13, 15, and 16. Both mission modes have very nearly the same targeting capability when compared only from a flight profile analysis point of view. The direct mode requires a somewhat smaller  $\Delta V$ , but the orbit mode has a slightly greater targeting coverage and some degree of flexibility late in the mission (i.e., prior to deorbit). The differences between the two modes begin showing when the total mission requirements are considered. Any restrictions on DSN requirements during the encounter phase of the mission will reduce the targeting capability of the direct mode in terms of landing site longitudes. Longitude control is obtained by encounter timing with the direct mode, but time enters DSN schedules as well. A second consideration is the additional degree of freedom inherent in the combination of  $\Delta\beta$  capability and orbit shift with the orbit mode. This combination allows selection of more desirable orbits from an orbiting science mission viewpoint without compromising the landing site selection in a preflight mission planning sense. This argument can be negated if the assumption is made that the orbiter, while using the direct mode, can make a significant plane change after capsule landing. However, this will require 50% more propellant than is required for orbit insertion. Finally, the orbit mode allows inspection of the landing area prior to deorbit with orbiter TV pictures. This survey is, for the most part, a weather survey rather than a detailed site survey, which presumably came from the earlier orbiting missions. If weather patterns indicate activity near the primary site, a secondary site can be targeted to. The direct mode does not have this flexibility because the landing site is nominally committed at liftoff. Major changes can be made at the first or second midcourse corrections, but this is highly unlikely from either an operational viewpoint or from the probability that new information dictating such a decision would become available that early in the mission.



The accuracy analysis summarized in figures 15 and 16 show more favorable characteristics for the orbit mode. Not only are the entry dispersions smaller, but the effect of dispersions on landed payload margin is smaller for the orbit mode. The landing footprints are smaller for the orbit mode and can be made smaller yet by small increases in nominal entry angle without strongly affecting the landed payload margin.

The maximum performance characteristics of the various terminal phase systems and launch vehicles are compared for fixed aeroshell diameters of 8.5 and 15.0 ft, fixed landed equipment weight of  $W_{LE} = 600$  lb, and fixed entry weight of  $W_E = 1500$  lb.

The 8.5-ft-diameter condition is summarized in figure 42. These data show the range of total capsule system weight as a function of  $\gamma_E$  (highest values on bars correspond to shallowest  $\gamma_E$ ). The corresponding  $W_{LE}$  are also shown on the bars for reference. The scale up the middle of the chart shows the performance capability of the various launch vehicles. It is clear from figure 42 that all of the orbit mode cases require the Titan IIIC/Centaur launch vehicle but with a considerable launch vehicle margin. The high deployment Mach no. aerodecelerator has the most  $W_{LE}$  performance capability. The direct mode performance requirements fall into the Titan IIIF/Stretched Transtage capability, but have a negligible landed weight capability in all cases.

Similar data for the 15-ft-diameter aeroshell are shown in figure 43. The orbit mode  $W_{LE}$  are large, but unfortunately the total capsule system weight exceeds even the Titan IIIF/Centaur capability.

The direct mode performance requirements clearly fall within the Titan IIIC/Centaur range, with the corresponding  $W_{LE}$  comparable to that obtained with the 8.5-ft-diameter orbit mode. Again, the Titan IIIC/Centaur is the launch vehicle on this basis and, again, with a large launch vehicle margin. For the direct mode, the all-retro terminal phase system is the best performer.

The next comparison shown in figure 44 is made on the basis of a fixed landed equipment weight of 600 lb. In this case, the highest capsule system weight corresponds to the steepest entry flightpath angle. The data show lowest total system weight for the orbit mode with the  $M_D = 2$  parachute the best of the terminal phase systems. The diameters for these cases are given in figure 32.

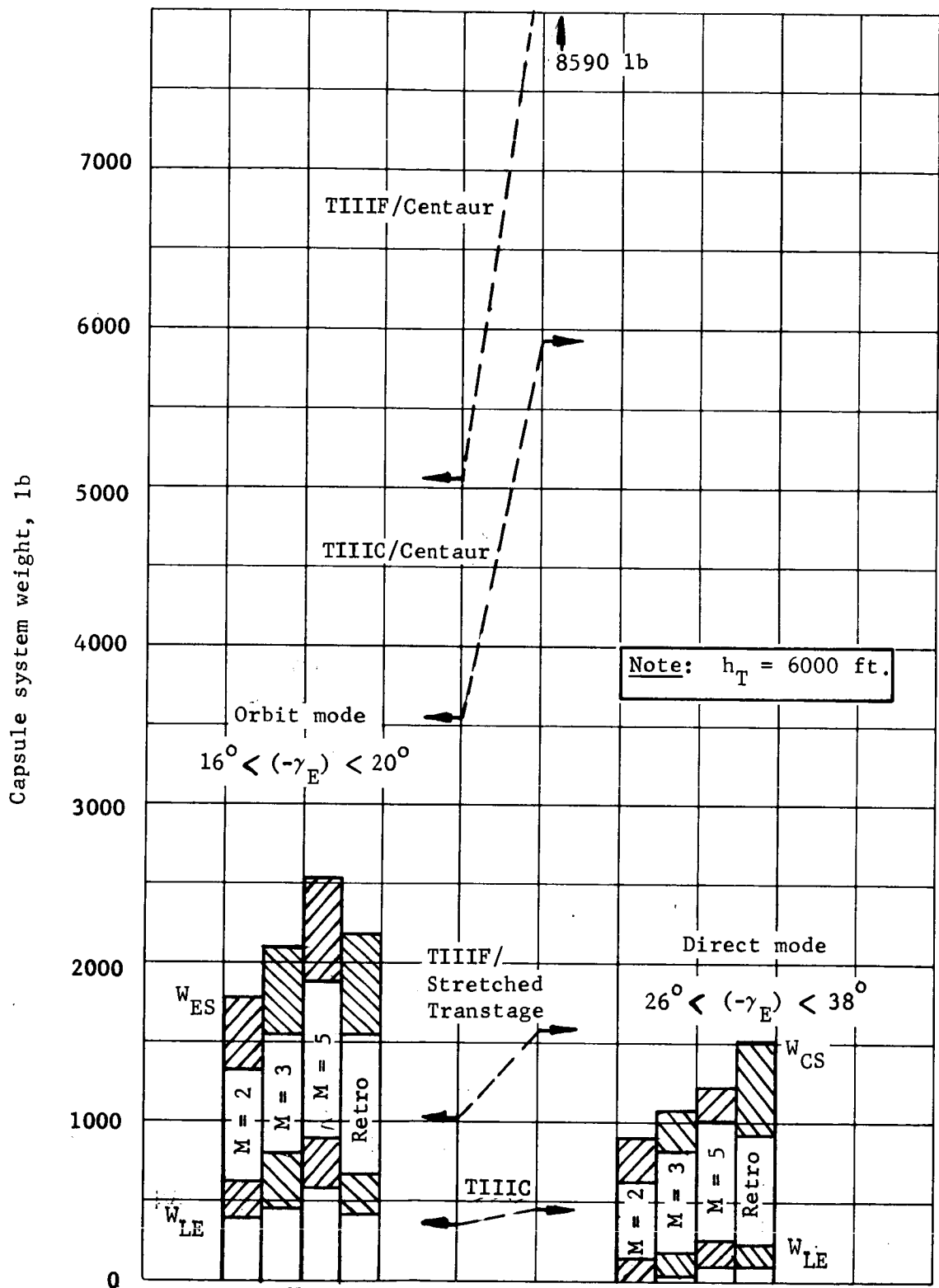


Figure 42.- Performance Summary, Aeroshell Diameter = 8.5 ft

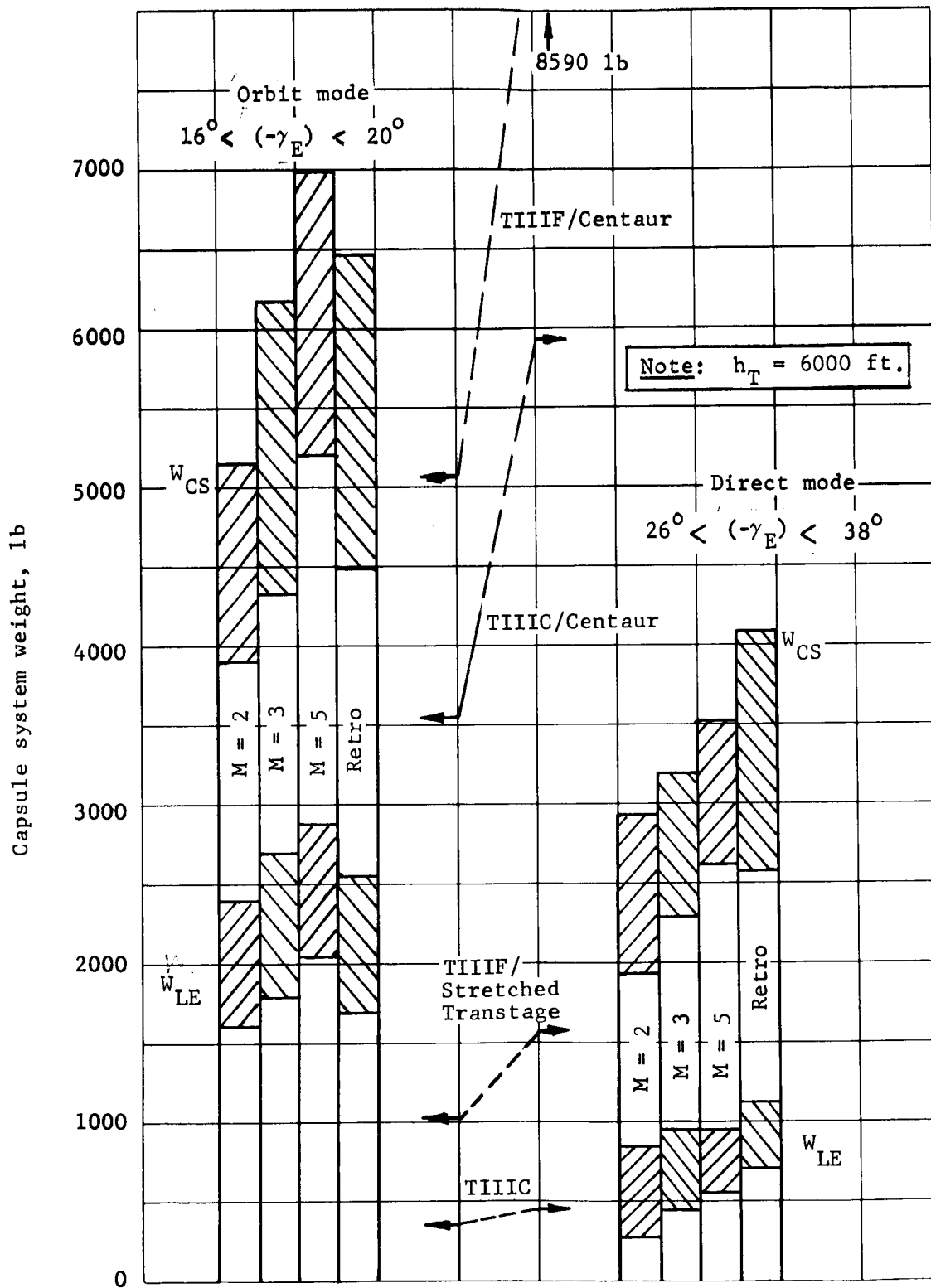


Figure 43.- Performance Summary, Aeroshell Diameter = 15 ft

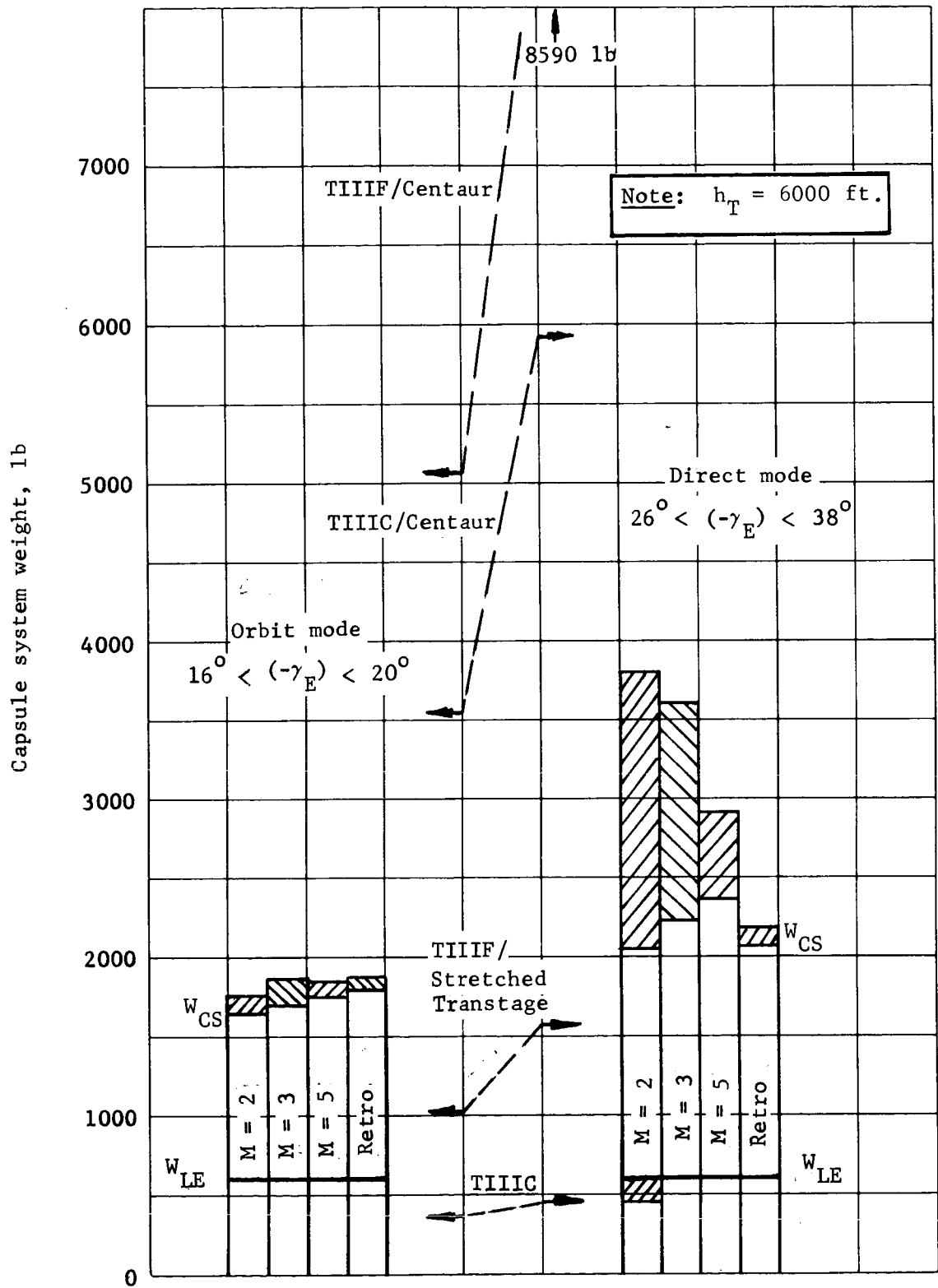


Figure 44.- Performance Summary,  $W_{LE} = 600$  lb

The performance requirements for all of the systems and for both modes fall into the Titan IIIC/Centaur capability with large launch vehicle margins.

The final comparison, shown in figure 45, is on the basis of a fixed entry weight of 1500 lb. On this basis, the total system weights are generally comparable with the  $M_D = 2$  parachute and landed equipment weight for the orbit mode. The most competitive configuration for the direct mode is the all-retro system. The diameters are shown in figure 34.

It is clear from these comparisons and the data in Appendix B, section 2, that the tradeoff between aeroshell diameter, landed equipment weight, and total capsule system weight can be made in many ways. However, the following generalizations can be made:

- 1) Orbit mode - The  $M_D = 2$  parachute is most efficient from a weight viewpoint, while the ballutes are favored from an aeroshell diameter viewpoint;
- 2) Direct mode - The same generalization relative to aerodecelerators is true here, but the all-retro system is competitive. The all-retro system is sensitive to thrust-to-weight ratios (throttling requirements go up). Relative to ballute vs  $M_D = 2$  parachutes, the latter are generally preferred on the basis of more straightforward packaging and release considerations;
- 3) Direct vs orbit mode - Both modes require the Titan IIIC/Centaur launch vehicle. On this basis, the greater inherent flexibility and adaptability of the orbit mode make it the more desirable.

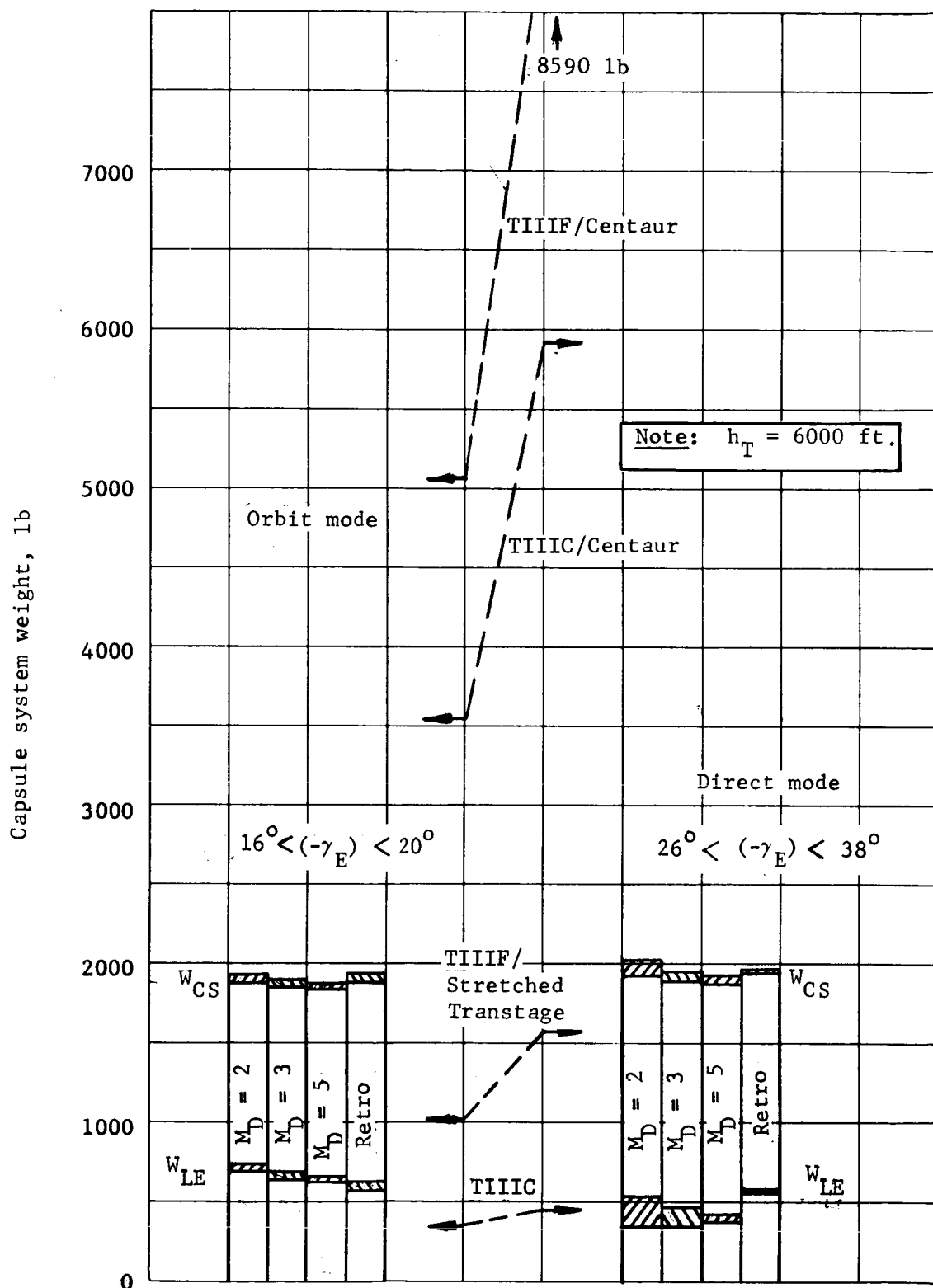


Figure 45.- Performance Summary,  $W_E = 1500$  lb

This page intentionally left blank.

## 2. SUBSYSTEM STUDIES

### Science

The flight capsule mission objectives and the science requirements to meet them, shown in table 4(a) were given by Langley Research Center. The measurements selected to provide the data needed to meet these requirements are listed in table 4(b).

The need for special studies evolved in four areas:

- 1) Entry science error analysis;
- 2) Meteorology measurements;
- 3) Requirements for a tape recorder;
- 4) 1975-1977 science.

Entry science error analysis. - It is necessary to confirm that the entry measurements will provide the data needed to define the atmosphere structure profiles, and that the necessary error limits and sampling rates do not impose severe restraints on instrument and data handling equipment.

The problem in atmosphere reconstruction is to transform from the time base in which the measurements are taken and to express the parameters as a function of altitude above the planetary surface. A wide variety of measurements are involved in determining the atmospheric parameters and the entry flightpath, and such a large quantity of data are produced that a statistical procedure is required to process them. The Kalman-Bucy minimum-variance technique developed by the Martin Marietta Research Institute for Advanced Studies (RIAS) has been most useful, as demonstrated in the Martin Marietta USAF PRIME program.

The Kalman-Bucy technique has been modified into a Mars entry atmospheric determination error analysis program. This program is now operating and is the first step in the development of a complete atmosphere determination program for planetary entry. This program has been used in the mission mode work to compare direct and orbital modes of entry for their accuracy in determining the atmosphere structure profiles. It has also been used to study various combinations of sensors to determine the relative importance of different types of data and the sensitivity of structure determinations to instrument accuracies. The detailed results of this work are given in Appendix D, section 6. Typical results are shown in figure 46 and table 5.



TABLE 4.- FLIGHT CAPSULE MISSION OBJECTIVES, SCIENCE REQUIREMENTS, AND SCIENCE MEASUREMENTS  
(a) Capsule Mission Objectives and Science Requirements, 1973

		Requirements		Life
Objectives		Parameters	2σ accuracy	
Entry	Atmospheric composition and vertical structure	Pressure below 60 km	±5% of value at known altitude but no closer than 0.5 mb	During descent only
		Temperature below 60 km	±2% of value at known altitude but no closer than 3°K	
		Density below 60 km	±5% of value at known altitude	
		Composition below 50 km	±5% for >50% species	
		10-60 AMU (CO <sub>2</sub> , N <sub>2</sub> , A, H <sub>2</sub> O)	±10% for <50% species	
Surface	Imagery	Low resolution	Resolution: 0.1°/line, 4 scenes at right angles, 25° azimuth x 70° elevation	Minimum 1 diurnal cycle  Goal: 90 Mars days
		High resolution	Resolution: 0.01°/line, 4 scenes at right angles, 5° x 5°	
	Meteorology	Pressure variation with time	±5% of value at known time but no closer than 0.5 mb	
		Temperature, °K	±2% of value at known time but no closer than 3°K	
		Wind velocity	±5% of value at known time but no closer than 5 m/sec	
		Wind direction	±10° at known time	
	Soil composition	Specific humidity	Dew/frostpoint of ±2°K	
		Surface soil inorganic composition	Same as Surveyor	
			α-scatter spectrometer	



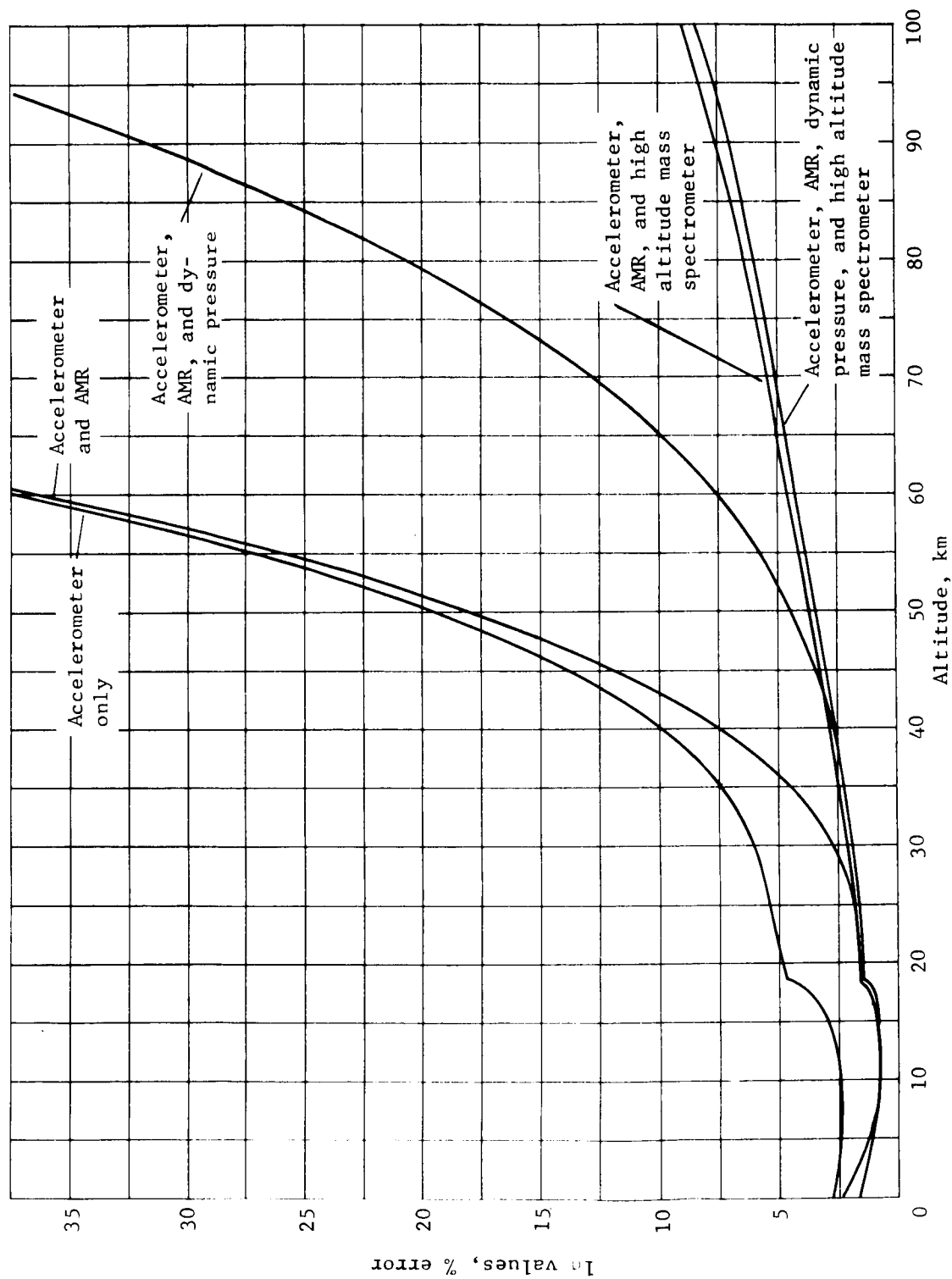


Figure 46.- Results of Entry Science Error Analysis for Three Groups of Sensors

TABLE 5.- MEASUREMENT ACCURACIES AND SAMPLING RATES

Measurement	Accuracy, %	Sampling rate, sec	Availability
Accelerometer triad	3	1	60 km to surface
Altitude marking radar	2	1	60 km to 8 km
Dynamic pressure	2	1	60 km to 8 km
High-altitude mass spectrometer	10	1	140 km to 70 km

Figure 46 compares two combinations of sensors on the basis of error in value of density at known altitudes. In one combination, the accelerometer triad and the stagnation pressure instrument are used in combination with a radar altimeter that operates below 200 km. In the second combination, the open ion source mass spectrometer is included, adding a direct measurement of density from 140 km down to 70 km. Table 5 lists the instrument accuracies used in this analysis.

Three conclusions are possible from the error analysis: (1) the mode of entry (direct or orbital) does not significantly affect the accuracy of atmosphere structure determination; (2) direct measurement of density at high altitude with the open ion source mass spectrometer is necessary to get within the specified error bands at altitudes below 60 km; (3) state-of-the-art accuracies for the entry instruments are marginally adequate to determine structure profiles to the specified accuracy.

Meteorology measurements. - In regard to surface science, the meteorology measurements were believed to require special consideration for purposes of this study. The reason for this is that of all the landed instruments, the meteorology group is the least advanced in development. By comparison, the facsimile camera and the alpha scatter spectrometer are well advanced. Since the humidity and the wind instruments are items that will control in procurement of meteorology equipment, a detailed discussion giving the reasoning behind their selection is presented in Appendix D, section 9. The conclusions reached there, and reflected in the instrument payload described in Part II, are that the aluminum oxide hygrometer and the sonic anemometer instruments are preferred.

Three primary factors influenced the selection of these instruments. First, they are mechanically simple; no moving parts are involved. This is a significant advantage considering the importance of inherent ruggedness and ability to withstand unexpected environmental extremes. Second, the sensor materials are stable at dry heat sterilization temperatures and exposure times. Thus, no serious problems in meeting sterilization requirements are expected. Third, there is an adequate base of technology from which qualified hardware can be projected for the Mars '73 mission.

Figure 47 shows frostpoint as a function of specific humidity for the two extremes of surface atmospheric pressure given in the monograph models. The range of present predictions was obtained from the Handbook of the Physical Properties of the Planet Mars (NASA SP-3030). Frostpoint temperatures over this range are equivalent to those found in the Earth's atmosphere from balloon sonde measurements (near 100 000 ft). The aluminum oxide hygrometer has a record of successful performance in this application. Significant points from this figure are discussed in more detail in Appendix D, section 9.

Requirements for a tape recorder. - A third area requiring special consideration is the question of need for a tape recorder in the data handling system. Under favorable conditions of landing and orbiting, it is possible to accomplish the '73 mission objectives and meet the science requirements without the capability for bulk storage of imaging data. However, this approach to mission design leaves little margin for recovery from an unplanned event that would place the landing site in a position of darkness relative to the relay communication link. The need is established on the loss of flexibility in mission planning and operations imposed by the constraint of real-time transmission of imaging data. A tape recorder has been included in the science subsystem concept and the supporting analysis for this decision is given in Appendix D, section 5.

1975-1977 science. - The fourth special study was made in connection with additional science equipment selected for '75 and '77 mission payloads. As shown in table 6, the added instruments are primarily for the purpose of extended capability in the area of exobiology. Although no specific life detection experiment has been identified for early Mars missions, a number of possible candidates are in various stages of development. The one thing common to these experiments is that they all examine for life or signs of life that may exist in the soil on the microbial level. This establishes a common requirement for soil sample acquisition and identifies an area where some useful analysis can be carried out for purposes of this study.

$$q = \frac{m_v}{m_v + m_a}$$

q = specific humidity

m<sub>v</sub> = mass of water vapor

m<sub>a</sub> = mass of air containing m<sub>v</sub>

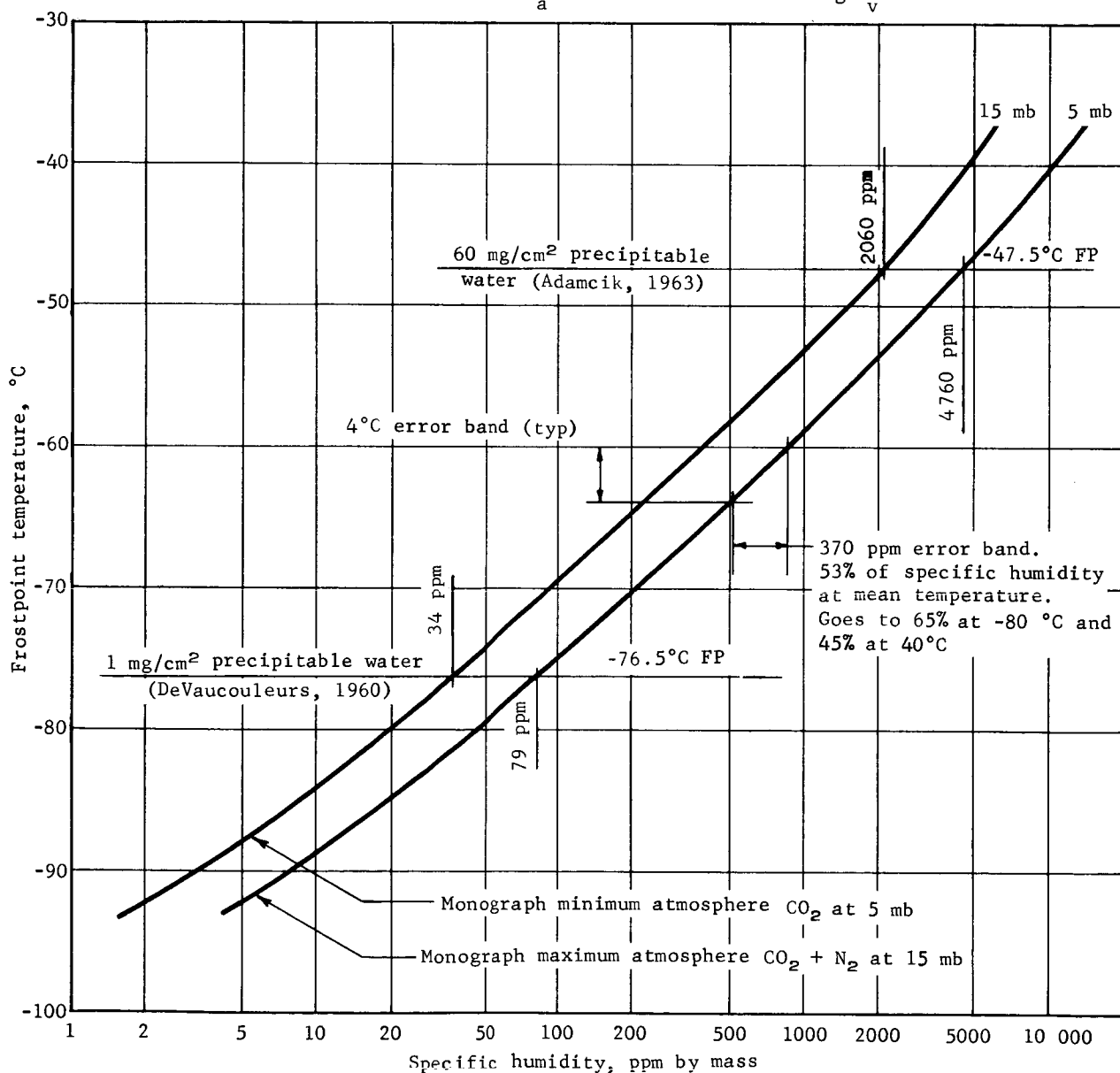
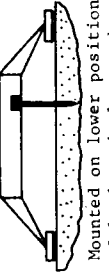
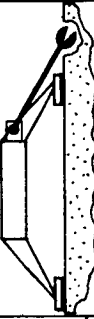


Figure 47.- Specific Humidity versus Frostpoint at the Martian Surface  
Showing Range of Present Estimates

TABLE 6.- SUMMARY OF EXTENSION TO '73 SCIENCE EQUIPMENT FOR 1975 AND 1977 MISSIONS

Objective	Parameter	Instrument	Mounting requirement	Sampling Rate	Data bits/sample	Weight lb	Volume in. <sup>3</sup>	Power W
Soil subsurface environment	Soil temperature	Soil probe carrying temperature and moisture sensors <sup>a, b</sup>	 <p>Mounted on lower position of lander, deploys and penetrates into the soil subsurface</p>	1 per diurnal cycle (10 repeat averaging signals)	80	5	50	1
	Soil moisture			1 per diurnal cycle (10 repeat averaging signals)	80			2
Soil composition	Soil organic composition	Soil sample acquisition <sup>c</sup> thru <sup>e</sup>	 <p>Clamshell scoop on the end of an extendable boom, mounted on side of lander. Scoop deploys, acquires a soil sample and deposits sample in soil processor</p>	One sample	$1 \times 10^3$	18	175	15
		Ultraviolet spectrophotometer <sup>f, g</sup>		One sample examined 50 times	$1 \times 10^3$ per examination	20	520	10

**Note:** 1. This extension instrument summary is in addition to the Science Instrument Summary for 1973 shown in table III.  
 2. The atmospheric composition measurement capability is extended to make measurements at the surface.  
 3. The meteorology package has an extended life capability.  
 4. The life objective is 2 diurnal cycles minimum with a goal of 90 Mars days.

<sup>a</sup>Lull, H. W.; and Reinhart, K. G.: Soil Moisture Measurement. Occasional Paper 140, Southern Forest Experiment Station, Forest Service, U.S. Department of Agriculture, 1955.  
<sup>b</sup>Colman, E. A.: Soil Moisture Meter and Cells. MC-300A, California Forest and Range Experiment Station, 1964.  
<sup>c</sup>Engstrom, J.: Selection of Sample Acquisition and Processing Equipment, Landed Science Subsystem. ED-22-6-111, Martin Marietta Corporation, Denver, Colorado, Sep. 1967.  
<sup>d</sup>Rouze, E. R.; Clary, M. C.; LeCroissette, D. H.; Porter, C. D.; and Fortenberry, J. W.: Surveyor Surface Sampler Instrument. Technical Report 32-1223, Jet Propulsion Laboratory, Feb. 1968.  
<sup>e</sup>Scott, R. F.: Mars Surface Sample Acquisition. Appendix D, section 10 of this report.  
<sup>f</sup>Ridgway, M.: Selection of Instruments for Life Detection Experiments, Landed Science Subsystems. ED-22-6-109, Martin Marietta Corporation, Denver, Colorado, Sep. 1967.  
<sup>g</sup>Anon.: Research on Detection of Extraterrestrial Life by Ultraviolet Spectrophotometry, Final Report, Melpar, Inc., 1964.

Based on the belief that the soil sampling function will strongly influence design of landers for missions in '75 and '77, a special study was conducted to develop an approach for design of a sampling device. Dr. Ronald F. Scott of the California Institute of Technology conducted the study on a consulting arrangement with Martin Marietta. Dr. Scott was the Principal Investigator responsible for the lunar soil mechanics experiments conducted with the scoop device carried by Surveyor spacecraft.

In the soil sampling study reported in Appendix D, section 10, the conclusion is reached that the surface existing at a Martian equatorial landing site has a high probability of consisting of fine-grained cohesionless mineral particles. With a soil of this nature, a sampling device does not need a rock-coring, scouring, or grinding capability.

It is further concluded that a semiautomatic approach is preferred. The surface sampling device would be preprogramed to obtain a soil sample and deposit it in an analytical experiment, but the operation could be interrupted on Earth command to permit certain simple decisions to be made. The sampler could be programed to acquire soil from a number of positions within the viewing area of a surface imager.

A conceptual sketch, figure 48, is included showing essential features of the sampling function and the method of acquiring samples.

#### Structures and Mechanisms

Three parametric studies of structures and mechanisms were conducted in support of the Mars Mission Mode study. The first was a study of methods for extending the aeroshell beyond the 15-ft-diameter limit imposed by the shroud. The second optimized aeroshell frame spacing and payload frame radius. The third involved a study of the entry heat shield. Detailed analyses of these studies are presented in Appendix C, section 2 and Appendix C, section 3.



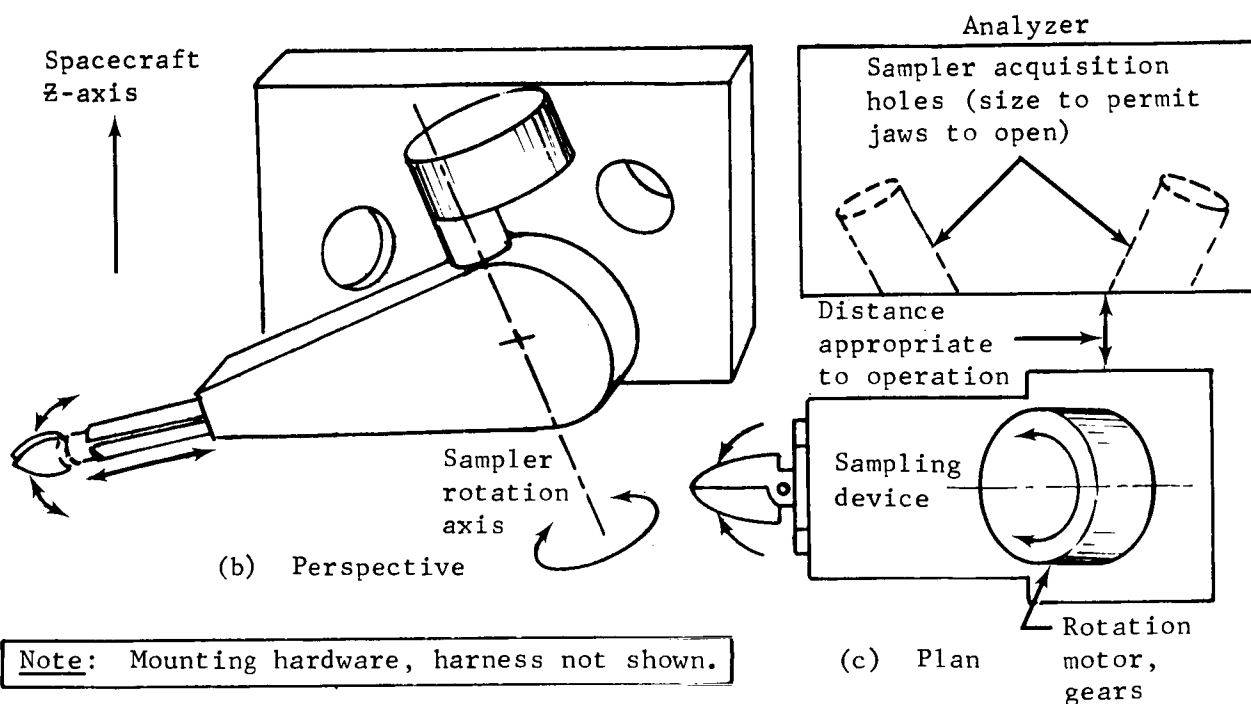
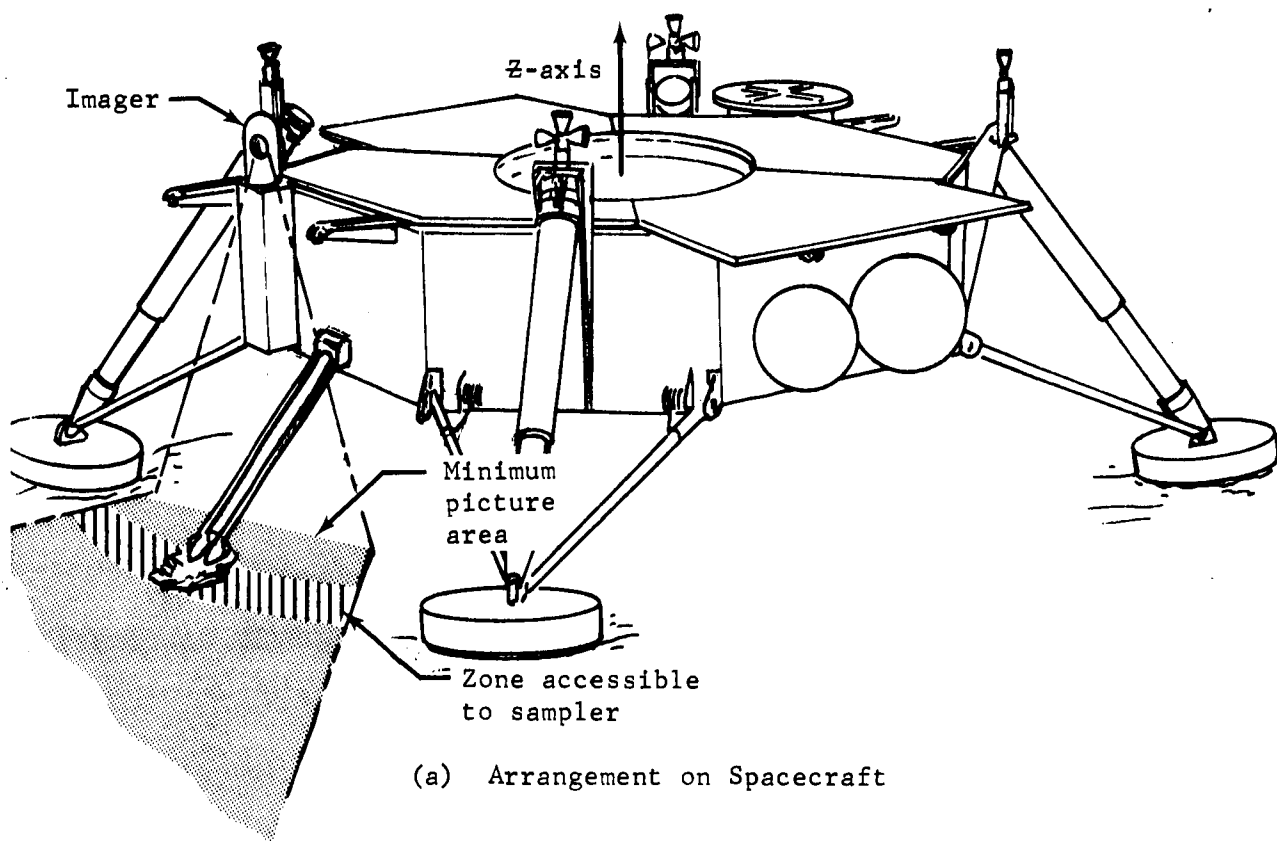


Figure 48.- Sampler and Analyzer Arrangement

Extendible aeroshell. - Two concepts for extending the effective diameter of the aeroshell were investigated. One used deployable panels (flaps) and the other consisted of a continuous inflatable "airmat" extension. Both would be deployed to the entry configuration prior to capsule atmospheric entry. Figure 49 presents a comparison of structural weights for an aeroshell with flaps, an aeroshell with an inflatable airmat, and a solid aeroshell, for an entry weight of 3000 lb and various ballistic coefficients.

Flaps: The configuration using deployable flaps is presented in figure 50. The flaps are hinged at the edge of the aeroshell and are stowed in a vertical position by a restraining cable. At deployment, the restraining cable is severed pyrotechnically and torsion springs rotate the flaps into the entry position where they are locked by a latch mechanism. The flap and extension mechanism shown in figure 50 utilizes an aluminum honeycomb, ablator-covered panel supported by two full-span spars spaced to produce equal bending moment in the honeycomb. The spars are attached to the aeroshell through hinges located in a structural ring at the periphery of the solid aeroshell cone, and through a toggle linkage used to deploy the panel and to react the loads near the outboard end of the panel. The linkage includes a planar truss at the inboard end and two ball-ended links that support the spars at the outboard end.

Several flap geometries were investigated, including variation of the number, size, and shape of the flaps. An earlier study considered flaps that, after deployment, would form a solid, conical surface as an extension to the fixed aeroshell. It was found that stowing these shapes presented significant problems in that relatively complex mounting and deployment schemes were required to avoid mechanical interference between adjacent sections. It was also determined that more than 8 flaps contributed a progressively smaller increment to the total drag area for a given fixed aeroshell diameter (15 ft) and variable extensions ranging from 2.5 to 7.5 ft for a total aeroshell reference diameter of 20 to 30 ft (fig. 51). Figure 51 also indicates the relationship in area for various diameters of both solid and flapped aeroshell.

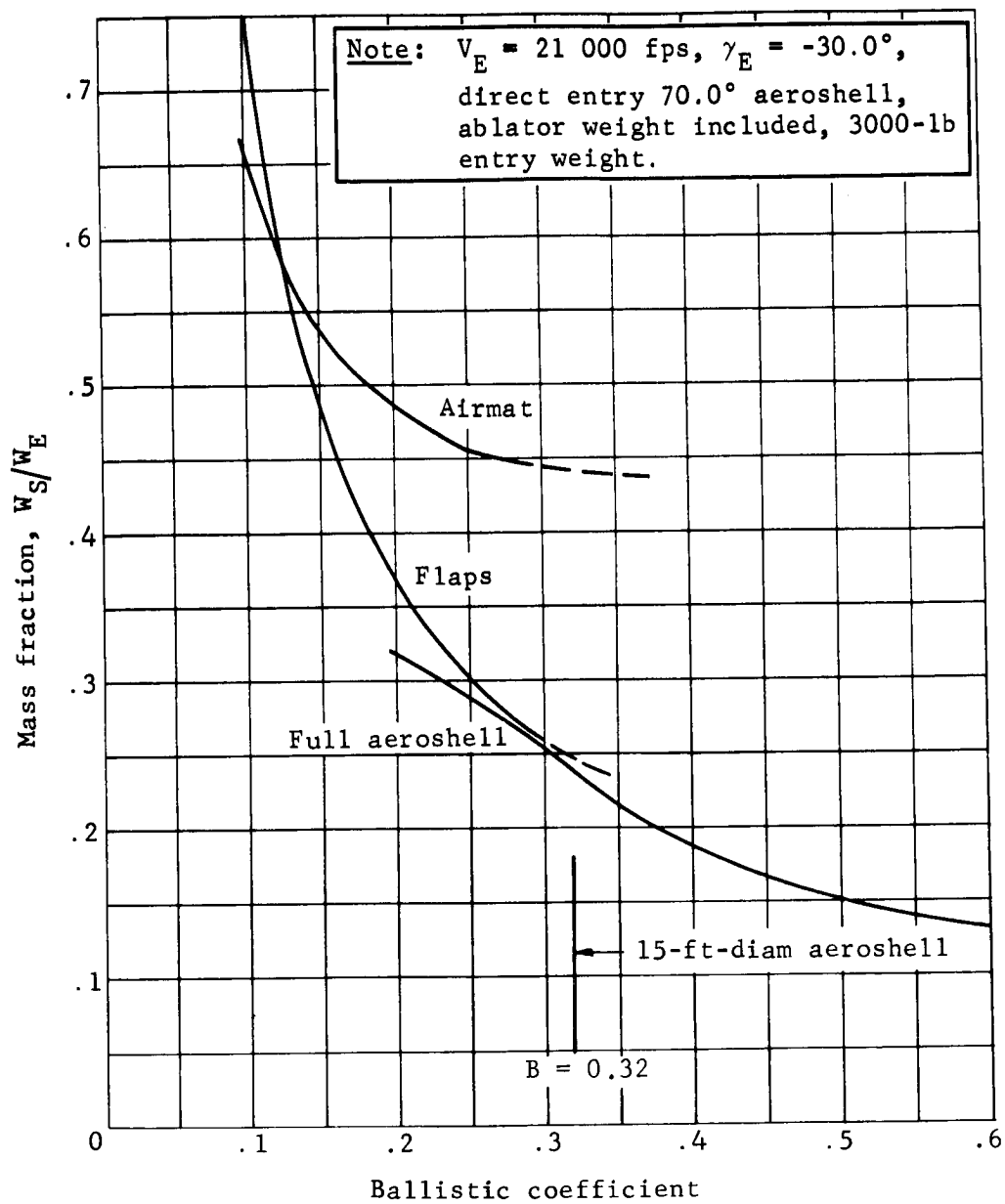


Figure 49.- Aeroshell Structural Weight Comparison

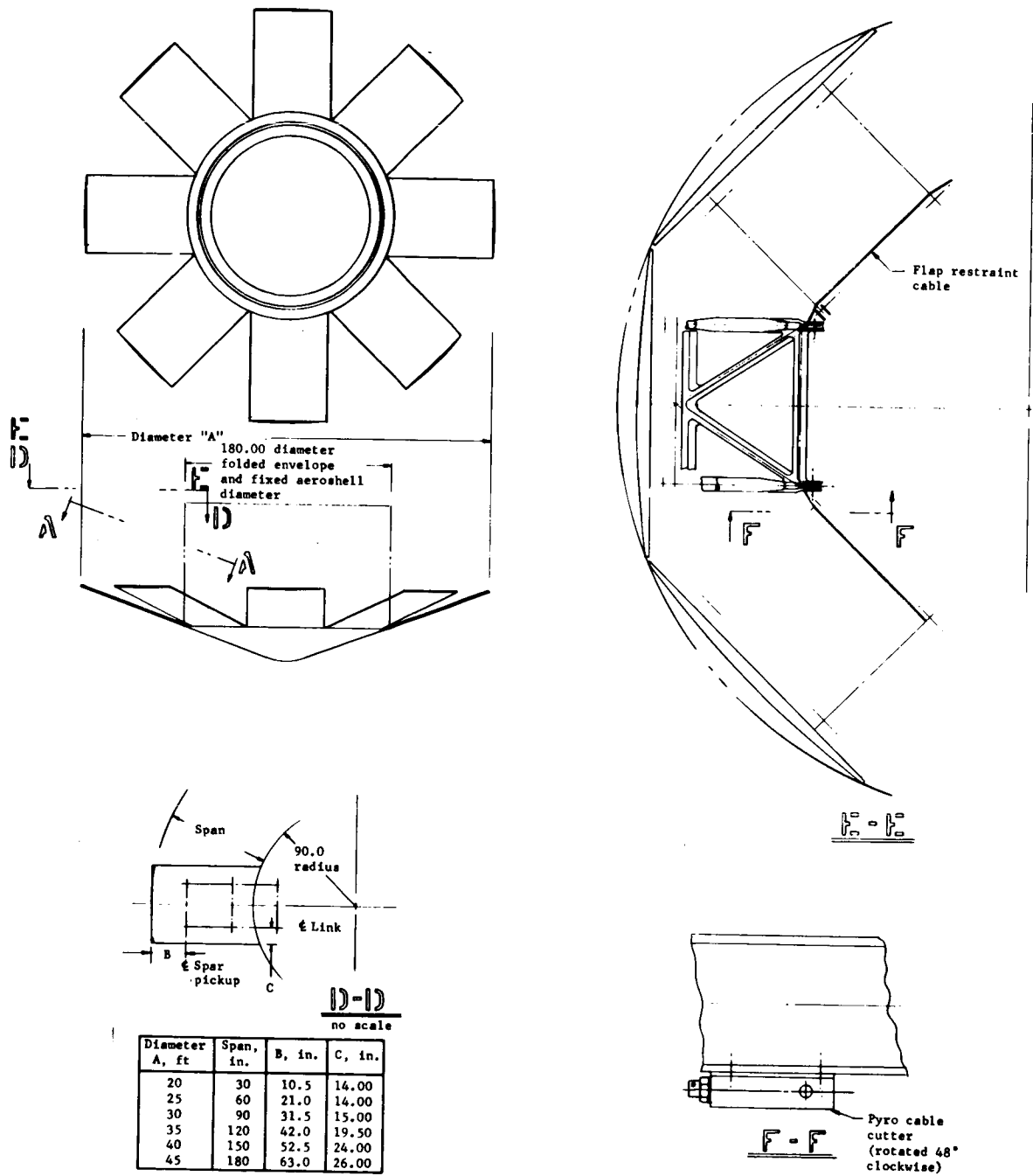


Figure 50.- Parametric Layout Study, 15-ft Diameter Fixed Aeroshell with Flaps

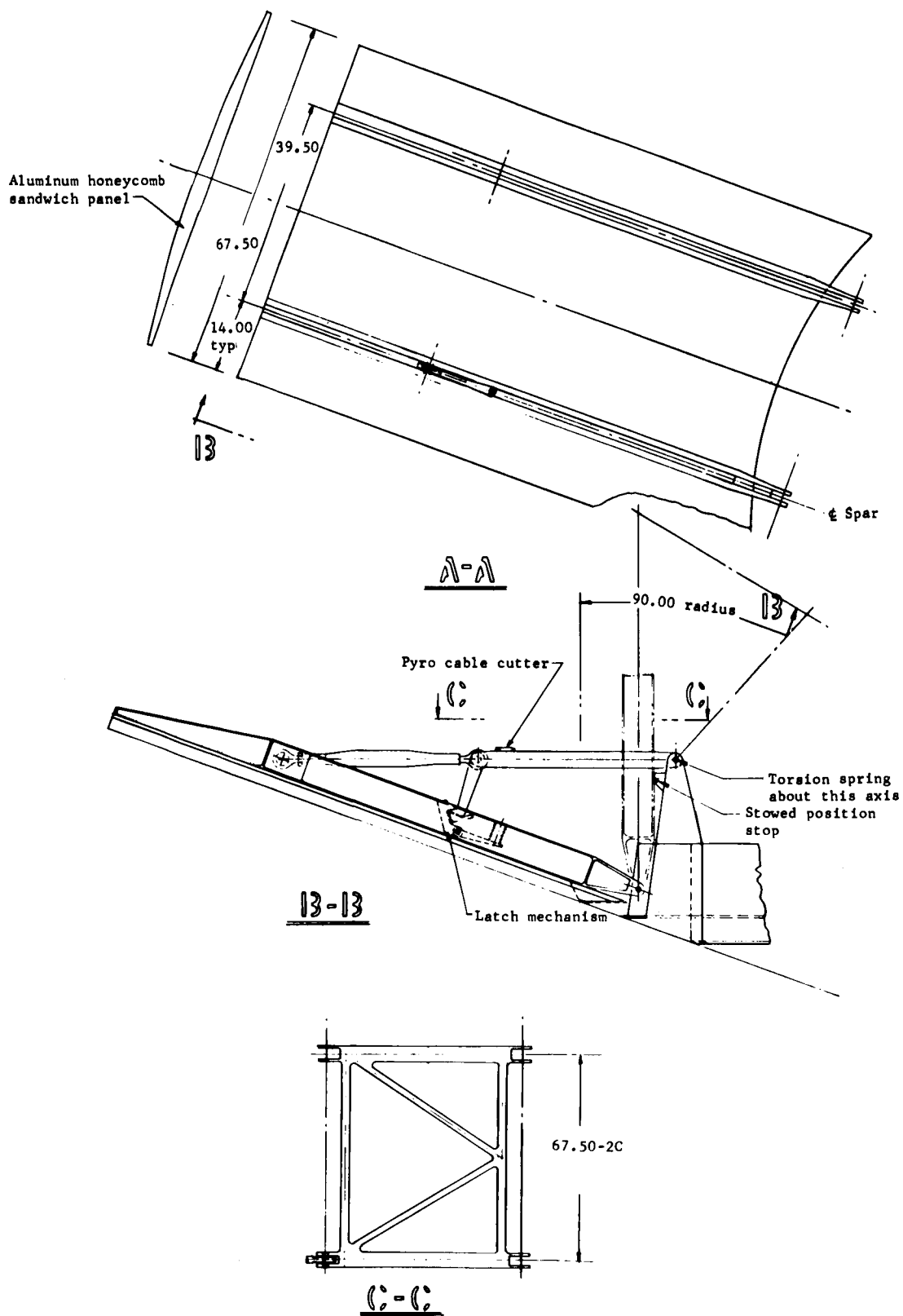


Figure 50.- Concluded

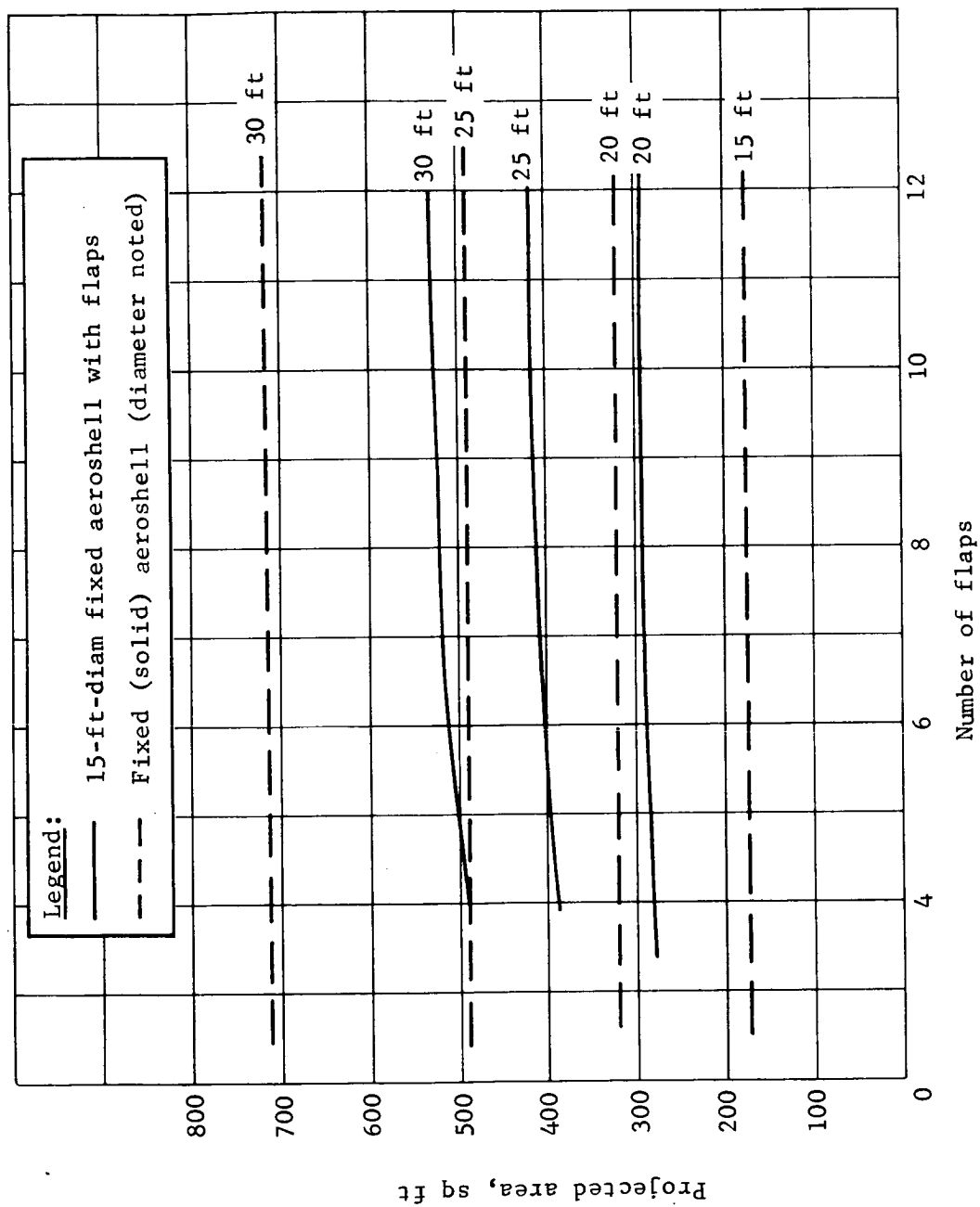


Figure 51.- Projected Area versus Number of Simple Flaps on a 15-ft Fixed Cone

Airmat: Figure 52 presents the pneumatically deployed airmat cone configuration. "Airmat" is a textile product (Goodyear Aerospace Corporation) in which two plain cloth surfaces are joined in a special loom process by "drop threads" to form a structural shape (cross section) that may have rectangular, trapezoidal, or single/double curved boundaries (upper and lower surfaces). As configured for aeroshell extensions, a number of "airmat" sections can be joined to form the desired conical shape when sealants and an internal pressurization system are applied to ensure pressure and geometrical integrity at the appropriate time and conditions in the entry phase.

The system consists of the inflatable cone, the gas, storage, and plumbing system, and the stowage, release, and separation devices. The cone is folded and secured in an annulus by retention lines at the periphery of the aeroshell during interplanetary cruise. After capsule separation and prior to atmospheric entry, a pyrotechnic cutter severs a bridle, which releases the retention devices and allows the cone to be inflated by the stored gas. The "airmat" is protected during entry by a flexible ablator.

Ablative materials can be applied to the surfaces requiring protection from the aerodynamic heating during entry. The required thickness and the inherent rigidity of candidate materials will have a significant impact on the packageability of the airmat extension. It is anticipated that an intensive development program will be required if this approach is selected, particularly when the requirements for heat sterilization and high packing densities are considered.

Aeroshell: A parametric study of direct entry aeroshell airloads was conducted to determine the aeroshell optimum frame spacing and the optimum radius of the payload frame. Results were similar to the Voyager Capsule Phase B study, which indicated stabilization frame spacing should be small -- around 2 in. -- and that the payload frame radius should coincide with the tangency between the aeroshell conical section and the nose cap. Details of this study are included in Appendix C, section 3.

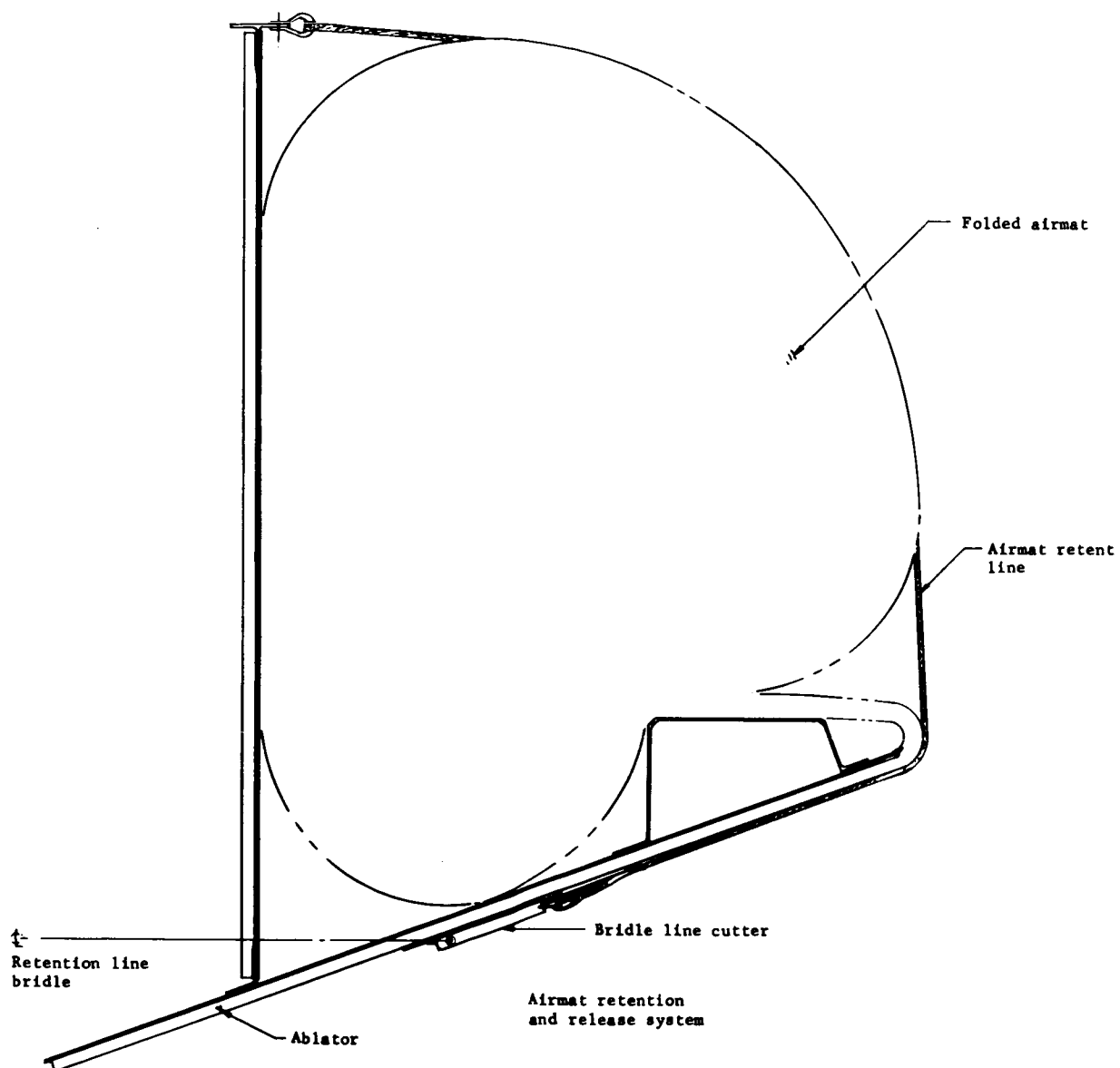


Figure 52.- Parametric Layout Study, 15-ft Diameter Fixed Aeroshell with Airmat Extension



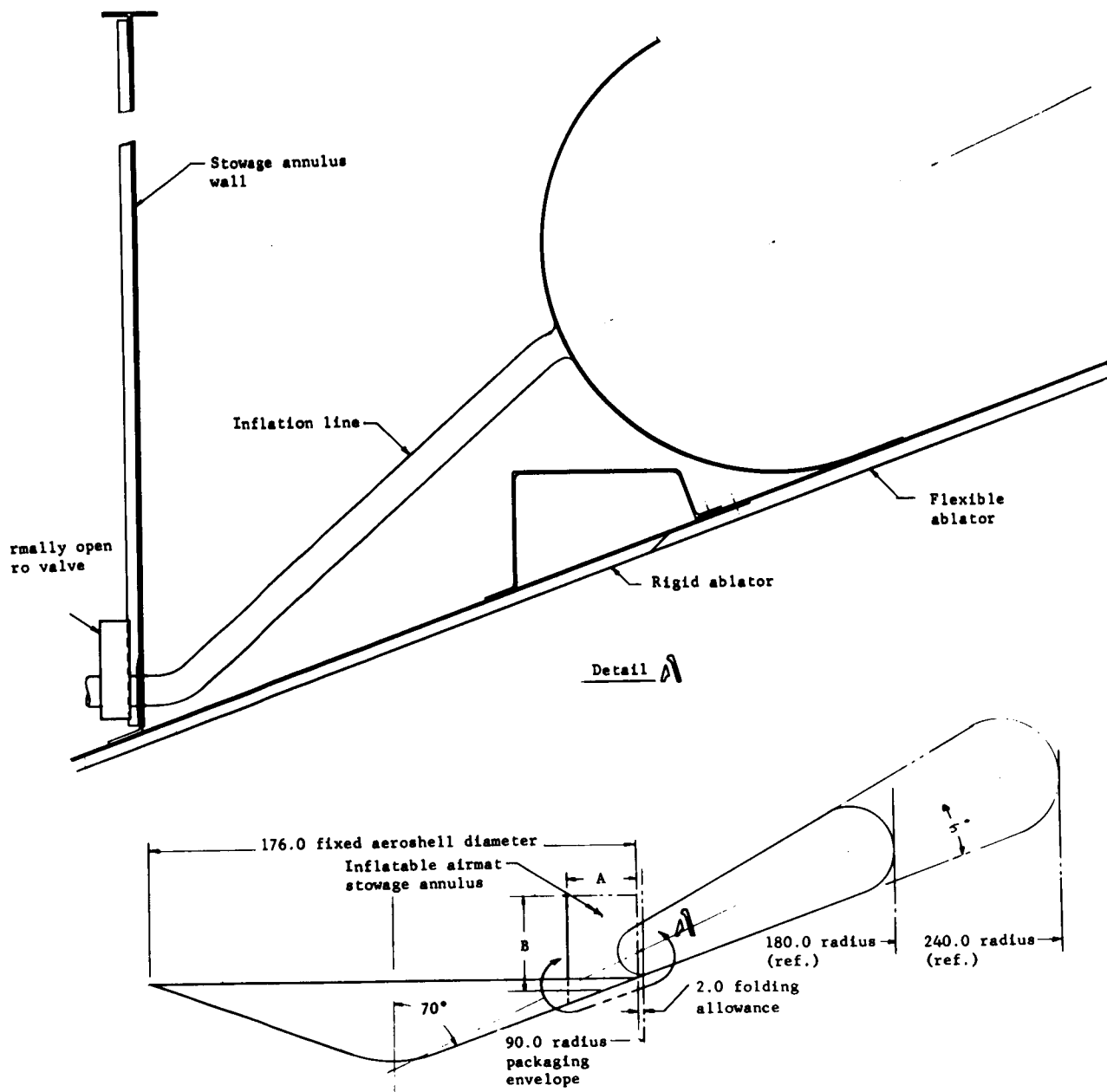


Figure 50.- Concluded

**Heat shield:** A heat shield parametric study was made and several point design ablators were identified for the Mars entry, both from orbit and direct. The study was conducted to determine heat shield requirements for entry vehicles with a range of ballistic coefficients from 0.10 to 0.60 and for both direct and out-of-orbit entry conditions. Total heat shield weights were determined from analyses conducted for the stagnation region, the aft edge of the aeroshell, and flaps or afterbody extensions, when applicable. The primary ablative material considered was SLA-561 -- a cork and filled silicone material specifically developed by Martin Marietta for the out-of-orbit Mars mission. For the heating rate cases above 100 Btu/ft<sup>2</sup>-sec, that result from the turbulent flow regions for the direct entry mode, ESA 5500M, a carbon fabric with filled silicone, was considered. For the inflatable airmat heat shield, PPA 1078, a foamed silicone material, was used. This material was developed during the initial Mars direct entry studies prior to the more recent out-of-orbit design studies. It was selected because it is representative of materials that must be highly elastic and flexible to allow folding and stowage of the inflatable afterbody. Substituting the ESA 5500M and PPA 1078 for the lower density SLA-561 increases the heat shield weight by approximately a factor of three.

In general, the Mars entry environment is relatively mild and requires a good insulating heat shield material. For the out-of-orbit case, the heating is predominantly convective and very low, with the maximum rate in the range of 20 Btu/ft<sup>2</sup>-sec. For the direct entry cases, radiant heating becomes significant with peaks up to 6 Btu/ft<sup>2</sup>-sec. The convective peaks increase up to 70 Btu/ft<sup>2</sup>-sec in the laminar regions and to 90 Btu/ft<sup>2</sup>-sec for the turbulent regions. Although the heating rates increase to values that cause significant surface recession in the low-density materials, the viscous shear forces are less than 2 psf so the recession is essentially thermochemical. The Mars direct entry missions border on heating rates that would result in significant surface combustion in the CO<sub>2</sub> atmosphere. If necessary, this can be avoided by using melting- rather than burning-type ablators. The other potential problem area is the effect of radiant heating. Again for the direct entry missions, this effect just approaches significance. Therefore, the heat shield technology problems for Mars entry are minimal and the design problem is one of selecting the material with the best combination of surface recession characteristics and thermal efficiency, with the emphasis on thermal efficiency.

## Propulsion

Propulsion subsystem parametric data of weight as a function of total impulse were derived for deorbit, deflection, retro, vernier, and attitude control systems; these data are applicable for the required range of capsule weight and velocity increments. Qualified engine systems -- Lunar Orbiter, Mariner '69, LM Descent, LM Ascent -- were also considered in the parametric data in an attempt to apply one of these systems to the capsule designs and eliminate an engine development program. The results of the parametric data analyses are presented in Appendix D, section 3.

The types of main systems included in the study were monopropellant ( $N_2H_4$ ), bipropellant ( $N_2O_4/MMH$ ), and solid propellant. The attitude control systems considered are monopropellant ( $N_2H_4$ ) and gaseous nitrogen.

Entry mode selection has only a small effect on the weight of the propulsion subsystem (3 to 12%) and does not affect the basic design of either the landing system or deflection system.

Monopropellant and solid motor deorbit (out of orbit) and deflection (direct) systems were compared. Monopropellant systems employ a landing engine while the solid systems employ an aluminized-propellant solid motor to perform the deorbit or deflection burn. Weight calculations were based on the same initial capsule system weight in both cases with results reflecting the differential in useful landed weight as a function of the deorbit or deflection propulsion subsystem configuration. Useful landed weight was defined as science and the equipment required to support it after landing. The solid motor systems have a useful landed weight advantage of approximately 45 lb (~8%) for the configurations compared. This weight gain is offset by the additional cost and risk associated with development of a sterilizable solid motor.

Regulated and blowdown pressurization subsystems were compared as shown in figure 53.

Propulsion systems using blowdown pressurization are lighter than regulated systems when the blowdown ratio is greater than 2:1. A blowdown ratio of 4:1 is optimum; however, a ratio of 3:1 was selected to reduce the engine throttle ratio. Blowdown pressurization was selected because of the weight advantage and elimination of regulator failure modes.

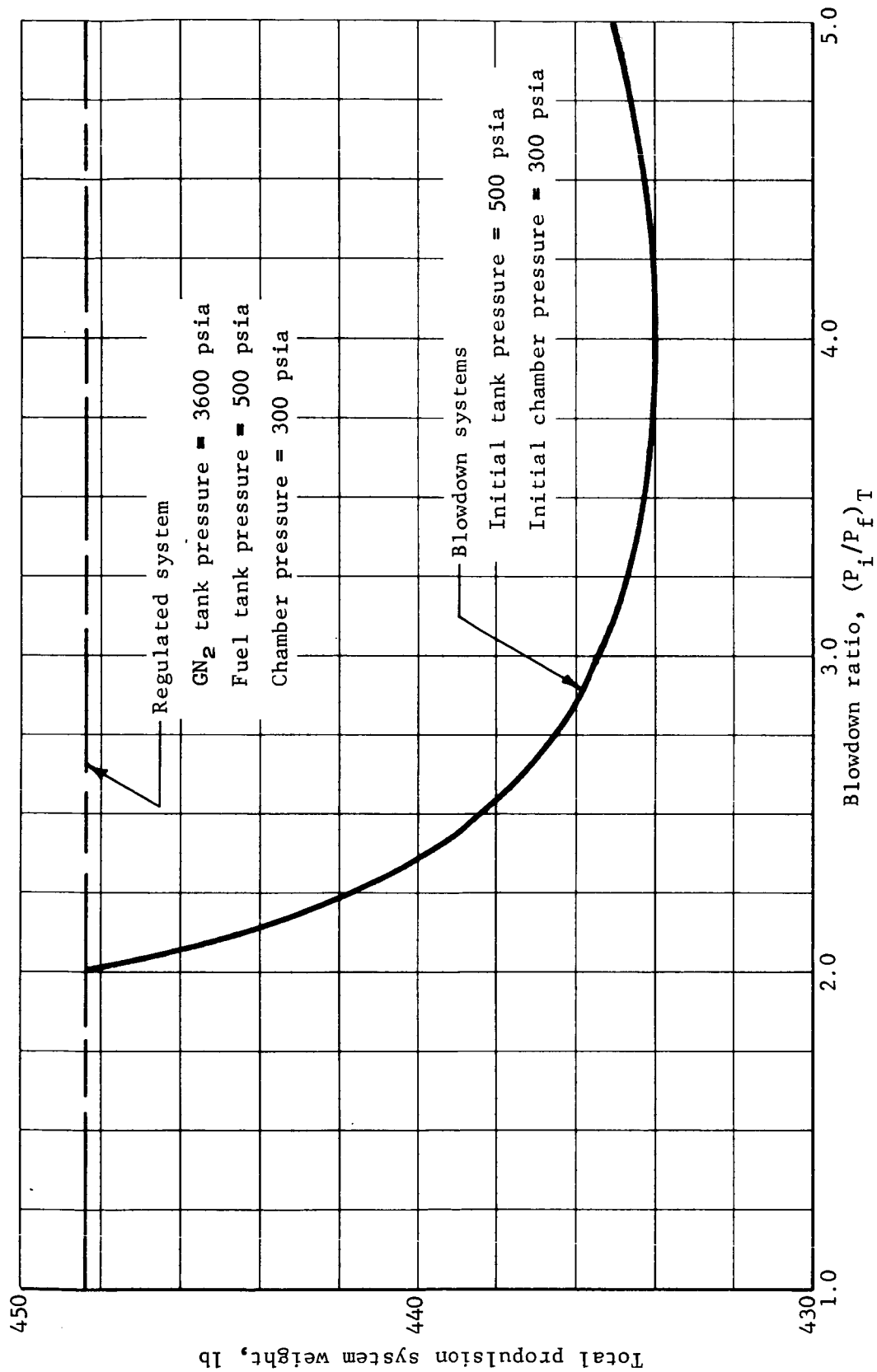


Figure 53.- Comparison of Regulated and Blowdown Pressurization Subsystems

The type of attitude control system for the Mars mission mode point designs was determined. Systems considered in this analysis were monopropellant ( $\text{N}_2\text{H}_4$ ) with blowdown (1.5:1) pressurization and cold gas (regulated  $\text{GN}_2$ ). As shown in Appendix D, section 3, the monopropellant attitude control system has a weight advantage of approximately 23 lb; however, the cold gas system has lower cost and higher reliability.

The low-weight configuration is essential to Configuration 1A because of weight restrictions imposed by the  $8\frac{1}{2}$ -ft aeroshell; therefore, a monopropellant attitude control system was selected. To keep the configurations comparable, the same system is used in Configuration 1B.

### Guidance and Control Subsystem

The basic guidance and control subsystem functions for all missions considered in this study are:

- 1) Provide attitude control for all mission phases from separation from the orbiter to lander;
- 2) Provide velocity control for deorbit maneuver;
- 3) Provide velocity and position control during the vernier landing phase;
- 4) Provide capsule system sequencing and science sequencing.

The equipment required to perform these functions is described in Part II for both mission modes. The size and performance of this equipment were not considered as parameters in this study because the functions required are essentially the same for either mission mode.

Exceptions to this statement are modifications to the G&C equipment for an autonomous capsule configuration and for spacecraft or capsule configurations with planetary approach guidance.\* The autonomous capsule modifications are described in Part II. The approach guidance study results are summarized below and in more detail in Appendix D, section 4.

---

\*Planetary approach guidance as used herein is the guidance function as the spacecraft approaches the planet, prior to and during the final velocity correction. This is the same as the "terminal guidance" defined in the contract work statement.

In support of the capsule efficiency parametric studies described elsewhere in this report, parametric attitude control system impulse equations were generated. Also, vernier phase propellant and initiation altitude data were generated as shown in Appendix D, section 4. These data were condensed and used in the terminal phase parametric analysis reported earlier in this report.

#### Planetary approach guidance. -

Problem definition: As the spacecraft approaches Mars on the interplanetary trajectory, the knowledge of the exact trajectory with respect to the planet will be inaccurate because of errors in DSN tracking, planet ephemeris error, and errors in the physical constants of the equations of motion. These errors result in entry errors for the capsule and orbit ephemeris errors for the orbiter. Figure 54 shows an estimate of these errors as proposed for this study. The upper curve represents the present DSN capability. The lower curve represents projected improvements in DSN capability by 1973. The curves represent position error normal to the approach asymptote. Velocity errors are small (about 0.02 m/sec), enough to be neglected with respect to position error and maneuver execution errors.

Figure 54 also shows how position error propagates to produce a capsule entry angle error. This curve was obtained from the more general data shown in the targeting and error analysis section of this report. As shown, the present DSN capability of about 100 km will result in entry angle dispersions of about  $2^\circ$  ( $1\sigma$ ). If the vehicle is targeted  $5\sigma$  above skipout ( $16^\circ$ ), with a  $+3\sigma$  error the maximum entry angle is  $32^\circ$ . If the navigation error can be reduced to 25 km, the entry angle error is about  $\frac{1}{2}^\circ$ , which results in a maximum entry angle of under  $24^\circ$ , a considerable improvement in the weight growth capability for direct mode entries. The improvement diminishes with a reduction of the navigation error below 25 km ( $\frac{1}{2}^\circ$  entry angle error) because maneuver uncertainty to correct the trajectory results in entry angle errors of about  $\frac{1}{2}^\circ$  for typical guidance system accuracy.

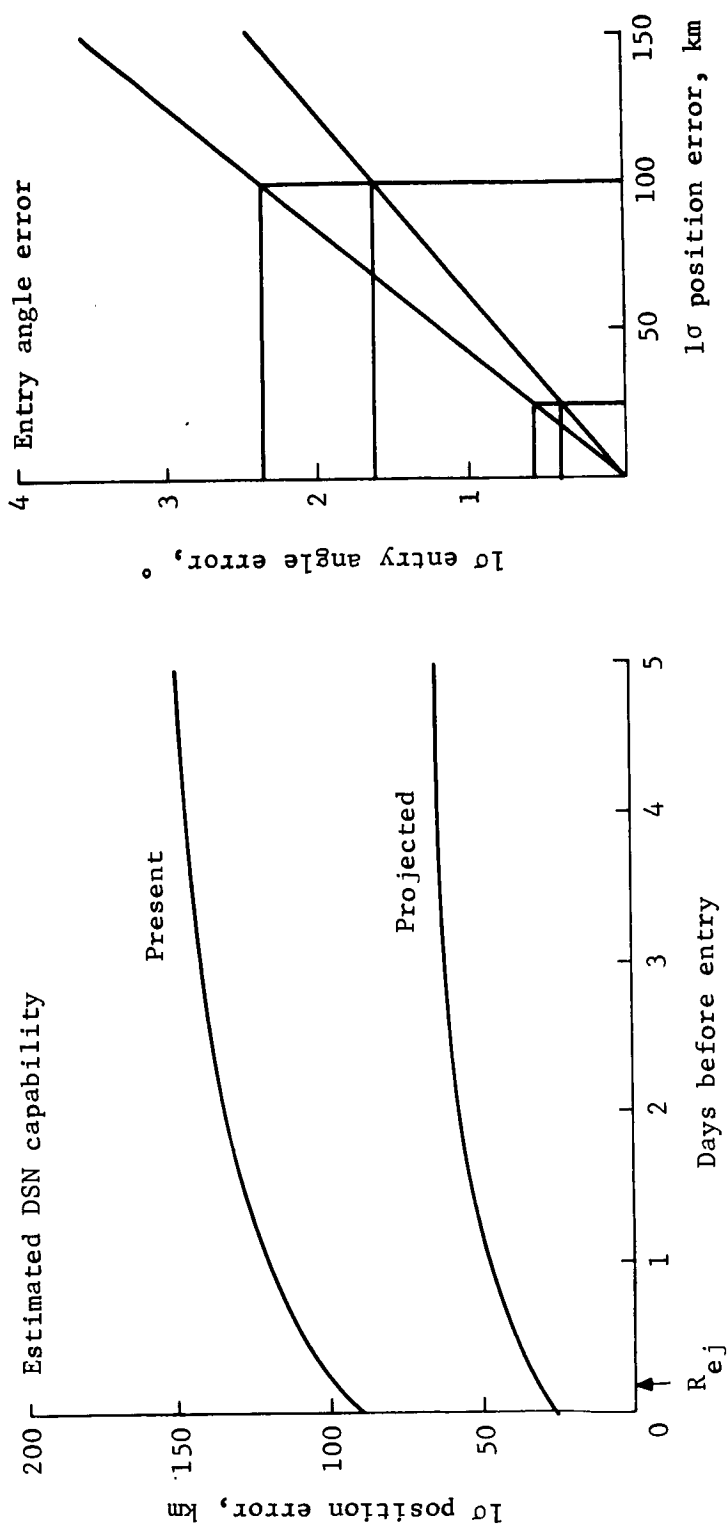


Figure 54. - Navigation Accuracy Effect on Entry Angle

Study approach: A study to assess the feasibility of improving navigation accuracy through the use of spacecraft measurements has been conducted. The objectives of the study were to:

- 1) Postulate and analyze potential planetary approach guidance mechanizations to define required sensor accuracy;
- 2) Survey the present and projected availability of the required type of sensors;
- 3) Recommend a preferred approach.

For the purpose of this study, the onboard measurements were assumed to be processed independently of DSN data. DSN data were used to initialize the calculations. This assumption simplifies the analysis and simulation problem and provides conservative estimates of the sensor accuracy requirements.

The measurements to be considered were quickly reduced to passive optical techniques. Active ranging devices are expensive in terms of weight and power at the ranges under consideration. Celestial objects available are the sun, stars, Mars, the Martian moons, and other planets. Of these, the system selected for study consisted of a sun tracker, a star tracker, and a Mars tracker providing line-of-sight directions to these bodies. In addition, the Mars tracker would provide a disc measurement of the planet image from which range could be computed. Simplified geometry of these measurements is shown in figure 55. The three angles  $A_{PS}$ ,  $A_{PC}$  and  $\alpha$  shown in the figure are sufficient to define the position of the spacecraft with respect to the planet.

A simulation program that simulates the measurement geometry, sensor noise, the nominal approach trajectory, a perturbed trajectory, and data processing by a Kalman filter was constructed. Parametric data were obtained for sensor accuracy (both random and bias terms) as summarized below.

Summary and conclusions: The most useful simulation results are summarized in table 7. Plots of the time histories of these cases are given in Appendix D, section 4. Cases 1 thru 4 show the sensitivity of the navigation process to the disc angle accuracy. Downrange position (X) is affected strongly, while in-plane normal (Y) and crossrange (Z) are not appreciably affected. Comparing Cases 3 and 4 shows that a disc angle error of 90 arc-sec is only slightly better than no disc measurement at all.



### Measurements

- Sun sensor - LOS to sun
- Star sensor - LOS to Canopus
- Planet tracker - LOS to planet
- Plus angle subtended by planet ( $\alpha$ )

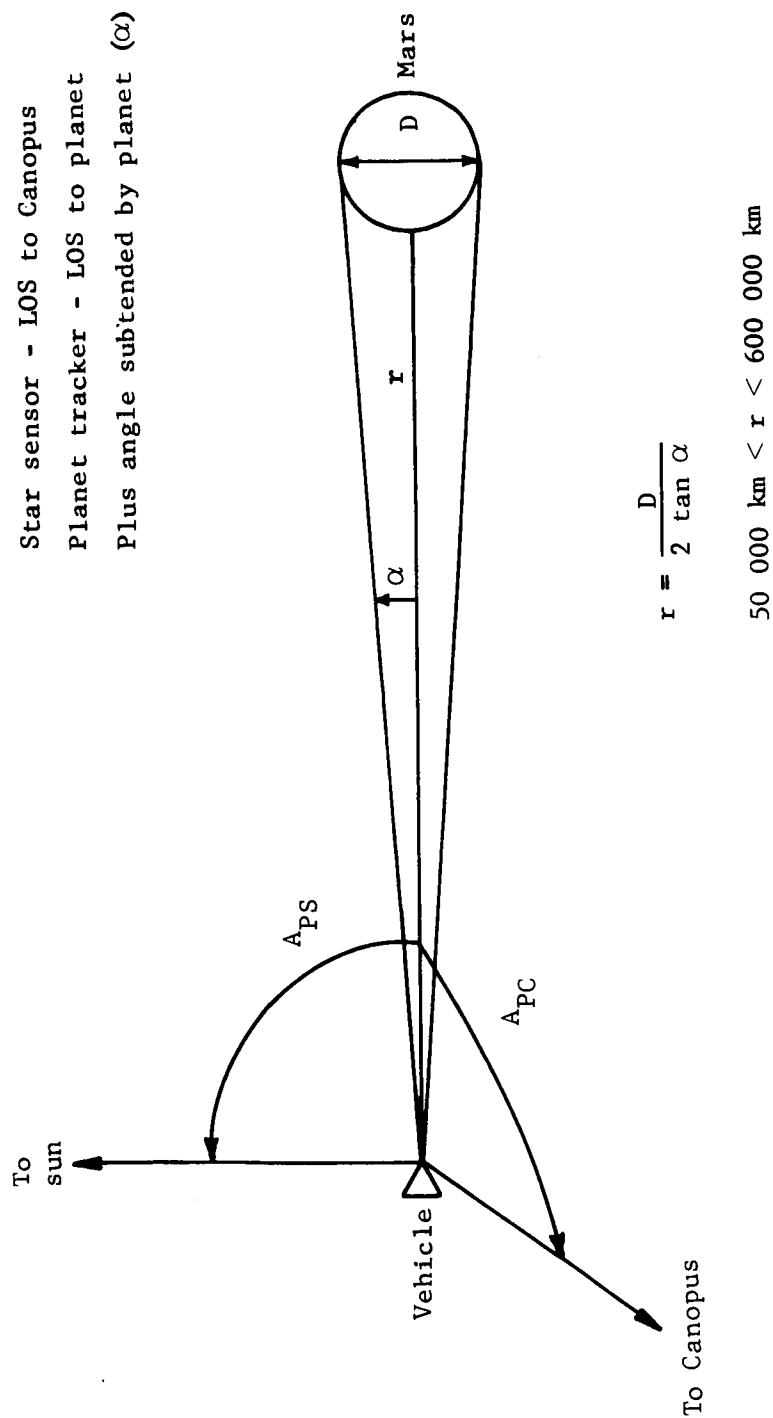


Figure 55.- Planetary Approach Guidance Geometry

TABLE 7.- PLANETARY APPROACH GUIDANCE SUMMARY OF RESULTS<sup>a</sup>

Case	Sensor accuracy, arc-sec (1 $\sigma$ ) <sup>(b)</sup>			Position error, km (1 $\sigma$ ) <sup>(c)</sup>			Bias
	Sun	Star	Planet	Disc	X	Y	Z
1	20	20	16	5	7.	2.1	2.1
2	20	20	16	30	38.	3.1	2.1
3	20	20	16	90	71.	4.8	2.1
4	20	20	16	None	73.	5.2	2.1
5	20	20	16	None	128.	14.5	5.5
6	20	20	16	None	136.	15.9	5.7
e <sub>7</sub>	20	20	16	None	95.	6.2	1.9
8	120	20	16	None	150.	15.4	2.1
9	20	120	16	None	86.	5.6	12.5
10	20	20	120	None	150.	15.5	12.6
11	20	20	120	None	153.	36.6	33.0
12	20	20	120	90	119.	35.2	33.0

<sup>a</sup>All results taken after 20 hr of measurements taken at 15-minute intervals starting at range of 300 000 km.

<sup>b</sup>Sensor accuracy represents random error on sun LOS, star LOS, planet LOS, and planet disc angle, respectively; no biases included.

<sup>c</sup>X is direction along velocity vector, Y is trajectory plane normal to X, Z is normal to plane.

<sup>d</sup>Small bias represents 20, 20, 16, 5 arc-sec bias added to the four measurements. Large bias is 20, 20 200, 50 arc-sec.

<sup>e</sup>Case 7 is identical to Case 4 except arbitrary star directions were assumed rather than Sun-Canopus.

In these runs, the sun was assumed to be near the trajectory plane and Canopus about  $60^\circ$  below the plane. As shown in Case 8, a sun sensor accuracy degradation affects the in-plane errors X and Y. Case 9 shows that the Canopus error affects only the cross-plane error Z. The planet line-of-sight angle affects both the angles  $A_{PC}$  and  $A_{PS}$  shown in figure 55. Thus, as Case 10 shows, all three position errors are affected by this measurement accuracy. The effects of biases in the measurements are shown in Cases 5, 6, 11, and 12. In these cases, the Kalman filter is mechanized to estimate the biases and remove them from the measurements. As seen, the convergence is not as good as the cases without biases. Since these runs were taken with a fixed number of measurements, taking more frequent measurements will probably further reduce the effect of biases.

Interpreting these results in terms of the capsule entry is simplified because the entry angle error is sensitive only to the Y direction error. The X direction error produces only a time of arrival error at the arbitrarily specified entry altitude. The Z direction error produces negligible entry angle error. Scanning the results of table 7 shows that the Y direction error is less than 25 km for all cases except the large bias cases 11 and 12. This is true even though some cases do not mechanize the disc angle measurement. The large bias Case 11 is small enough to believe that a slightly more frequent measurement interval would reduce the error below 25 km.

The use of planetary approach guidance to improve the orbiter ephemeris accuracy was not considered in this study. It is obvious, however, that some improvement could be achieved over the case with DSN tracking alone. For the orbit injection case, the disc angle error is probably more important.

The recommended use of this guidance approach is as follows. The sun-Canopus and planet tracker should be mounted on the orbiter. In a direct approach mode, measurements could begin as far out as 600 000 km for the purpose of partially removing sensor bias. However, the most useful data occur within 300 000 km as the error sensitivity becomes smaller. These measurements would be processed in conjunction with DSN tracking on Earth to define the actual approach trajectory to within the accuracy described. Allowing 3 hr for communication link and ground data processing, 20 hr of useful data can be obtained from 300 000 km to 50 000 km. The capsule deflection impulse could be applied at 50 000 km with the required velocity based on the improved trajectory estimate. Use of a longer link time than 3 hr causes the measurements to be required at greater ranges, resulting in less accuracy.

An alternative mechanization that places the sensors on the capsule has several disadvantages:

- 1) A duplication of the sun-Canopus sensor function already on the orbiter is required;
- 2) The capsule would have to be separated from the spacecraft at about 300 000 km to allow adequate error convergence time;
- 3) If the capsule were separated closer in, say 50 000 km, only about 4 hr remains to entry so onboard data processing is required;
- 4) The sensor data may not be available for the orbiter in applying the orbit insertion maneuver.

In conclusion, it appears that significant improvement in the capsule entry angle over what can presently be achieved with DSN tracking alone is possible. The sensor accuracy required is 1 to 2 arc-minutes on the sun, Canopus, and planet tracker. The disc angle measurement is not required. Bias up to 2 arc-minutes in the measurements can be tolerated by proper mechanization of the recursive data processing. Sun and star trackers of this quality are currently available. The planet tracker originally considered for Mariner '69 is in the accuracy range required and should be considered as a potential spacecraft sensor for direct mode missions.

#### Telecommunications

Parametric weight and performance data for the S-band Mars/Earth communications and the uhf relay link were developed in Part I of this study. These data were developed in consort with technical guidelines derived from mission and system requirements and constraints. The parametric studies conducted are described in detail in Appendix D, section 7.

Direct-link S-band parametric studies. - These studies must be applicable for all mission opportunities in the 1973-1977 period. For a range of effective radiated power (ERP), transmitter power output, and transmitter antenna gain product, the influence of mission opportunity is that of performance capability with the mission opportunity-dependent Earth/Mars communication geometry. As discussed in Appendix D, bounds on the geometrical parameters can be obtained from a consideration of the 1973 mission opportunity.

A requirement to accommodate both Type I and Type II heliocentric transfer trajectories established the direct link range capability for short-term mission durations of a few days as  $1.68 \times 10^8$  km as a minimum, to  $3.60 \times 10^8$  km as a maximum. Mission durations of six months or longer require a transmission capability out to the maximum Earth/Mars separation distance of  $3.96 \times 10^8$  km. Thus, for the typical data used in Appendix D, section 7, a requirement for a long-duration mission imposes an increase in range capability for the communication subsystem of only 10%, or 0.8 dB.

Nonsteerable, low-gain antennas with wide angular coverage requirements have been considered for a number of applications. The capability of receiving Earth-generated commands independent of landed system orientation is a requirement for any class of lander system weight. The beamwidth requirements for this type of antenna are derived from the elevation angle of Earth at the earliest possible arrival date and the latitude of the landing site, uncertainty in latitude, and predicted surface slopes. On the basis of data presented in Appendix D, section 7, the beamwidth and gain requirements for a nonsteerable, low-gain antenna are  $140^\circ$  and 5 dB for landing latitudes within  $10^\circ$  of the Martian equator.

For articulated, directive antennas, the size of the antenna must be consistent with the daily data volume requirements for a given transmitter output power level and must be compatible with the pointing requirements. From the discussion in Appendix D, a 2.5-ft-diam antenna allows an initial data link to be established with Earth by self-contained, automatic techniques with a 5-dB antenna pointing loss. Fine orientation through ground command, after initial data transfer, can reduce the pointing loss to 1 dB. With a reduction in uncertainties, the later missions will allow the antenna size to increase to 6 or 7 ft while still maintaining an initial downlink capability with 5 dB of pointing loss.

Past space programs and design studies were surveyed to obtain parametric weight data as a function of parabolic antenna diameter. Nonrectable, solid configurations only were considered. Curve fitting of the data points resulted in the equation

$$W = 1.25 \times D^{1.47}, \text{ lb}$$

where  $D$  is diameter in ft.

Modulation techniques were determined for different antenna designs. For a low-gain antenna of the type discussed above, the effective radiated power is on the order of 48 dBm for 20 W of transmitter output power. Even with 53 dBm of ERP, there is not enough signal strength at the ground receiver at maximum range to lock up the carrier tracking loop. Nonbinary implementations of noncoherent modulation techniques must be used for low ERP configurations to obtain a coding power gain. The modulation choice was noncoherent multiple frequency shift keying (MFSK).

Directive apertures result in ERP levels of 63 dBm or greater. At these power levels, sufficient signal strength exists at the ground receiver to satisfy the carrier loop tracking requirements and allocate power to a data channel. The modulation choice for these concepts was single-channel PSK/PM with sync combined with the data stream. The rationale for this selection is presented in Appendix D.

The direct-link performance capability of noncoherent MFSK and single-channel coherent PSK/PM for ERP levels from 40 to 75 dBm was derived in the parametric studies. Transmission rate capability with 85- and 210-ft DSIF antennas was determined over the range of ERPs for a nominal communication range of  $2.6 \times 10^3$  km and a maximum range of  $3.96 \times 10^3$  km. The data rate capability for single-channel coherent PSK/PM with coding techniques was also derived. Performance capability of single-channel PSK/PM and noncoherent MFSK for appropriate ERP levels is given in table 8.

TABLE 8.- COMPARISON OF DIRECT-LINK PERFORMANCE

Noncoherent MFSK: Transmitter - 20-W output		
Antenna - +5.0 dB, body-fixed, 3-dB pointing loss		
ERP - +48 dBm		
<u>DSIF antenna, ft</u>	<u>Range, km</u>	<u>Data rate,<sup>a</sup> bps</u>
210	2.6 x 10 <sup>8</sup>	2.5
	3.96	1.0
85	2.6	0.3
	3.96	0.14

Single-channel PSK/PM: Transmitter - 20-W output			
Antenna - 2.5-ft dish (1 dB pointing loss)			
ERP - +64.8 dBm			
<u>DSIF antenna, ft</u>	<u>Range, km</u>	<u>Uncoded channel, bps</u>	<u>Coded channel, bps</u>
210	2.6 x 10 <sup>8</sup>	230	550
	3.96	115	275
85	2.6	37	74
	3.96	11	22

<sup>a</sup>Data rate includes 20% allocation for sync.

UHF relay link parametric studies. - The radio relay link via an orbiter provides a real-time transmission capability to maximize the probability of data return. Past studies have shown that direct communications to Earth from the flight capsule during entry are not possible because of occultation during the latter part of the descent trajectory for a number of flight capsule trajectories. With a relay link used for separation to landing phases of the mission, the communication geometry is independent of mission mode because both modes studied are identically constrained by line-of-sight requirements and multipath considerations.

Analysis of orbiter surface traces for the specified orbits for this study shows that an adequate number of periapsis contacts occur over the first few days to satisfy the data volume requirement of  $10^7$  bits total. Since these contacts occur at ranges under 5000 km, bit rates in excess of 3000 bps can be supported for transmitter output levels of 30 W.

Parameters considered in these studies were frequency selection, modulation technique, and antennas. An operating frequency of 400 MHz was selected on the basis of ease of antenna integration into the flight capsule system and the orbiter. Other considerations relative to frequency selection are given in the appendix. Noncoherent FSK was used for the modulation in evolving the parametric data because of its insensitivity to time-varying multipath conditions and ease of recovery from entry communication blackout. This selection has been justified in previous tradeoff studies of modulation techniques. The flight capsule antenna was constrained to meet gain and coverage requirements with a fixed, body-mounted antenna. Of all alternative antenna configurations, a cavity-backed crossed-slot antenna, which provides a gain of 5 dB on axis and a gain of 0 dB or better over  $160^\circ$ , was selected because of its greater power handling capability in conjunction with its greater pattern coverage.

The data rate capability for the entry and postlanding phases as a function of transmitter output level for various communication ranges was developed and the data are presented in the appendix. These data were derived on worst-case design points and thus represent lower bounds on actual link performance capability. For the entry phase, a 10-W output transmitter is required to provide a data rate of 3000 bps at communication ranges out to 2500 km under worst-case conditions. To provide postlanding data at a rate of 10 000 bps requires 25 W of output power for the same conditions.

#### Power and Pyrotechnic

Parametric weight and performance data were developed during the first part of this study. These data were developed within the technical guidelines derived from mission and system requirements and constraints. The parametric studies conducted are described in detail in Appendix D, section 8. These studies are summarized in the following paragraphs.



Power subsystem. - Energy density vs A-h rating curves have been developed for typical sealed, sterilizable, silver-zinc (Ag-Zn) and nickel-cadmium (Ni-Cd) batteries. These curves are based on the latest data obtained from government and industry programs.

For a short-term mission of a few hours, batteries may be used to provide the required energy; however, for missions of several days to several months, other energy sources must be used with a battery providing power for nighttime and peak power periods. Two systems capable of providing long-term operation at reasonable system weights are the radioisotope thermoelectric generator (RTG)/battery and the solar array/battery system.

Equations defining the relationship of the RTG power output and the battery energy requirements to the generalized power profile were developed. Curves based on these equations provide a rapid method of determining the RTG and battery minimum size.

Similar equations were developed to define the relationship of the solar array average power and the battery energy requirements to the generalized power profile. These equations, and curves defining the equations to be used, provide a means of determining the average power required from the solar array and the battery size necessary to meet the power profile. A computer program was developed to assess solar array panel characteristics for arbitrarily oriented flat panels. Curves resulting from the output of this program show the solar array energy/day/ft<sup>2</sup> vs the landing site latitude, the surface slope, the panel orientations, and the date (fig. 56).

For the preferred configuration, a solar array/battery system is recommended for extending the life of the lander, with an all-battery system provided to assure operation for at least two days.

Pyrotechnic subsystem. - Curves were developed for determining the weight of a pyrotechnic subsystem. The reference configuration for these curves uses capacitors for energy storage with solid-state switching for the safe/arm switches and the squib-firing circuits. Details of the system and circuits used in determining the subsystem weights are given in Appendix D.

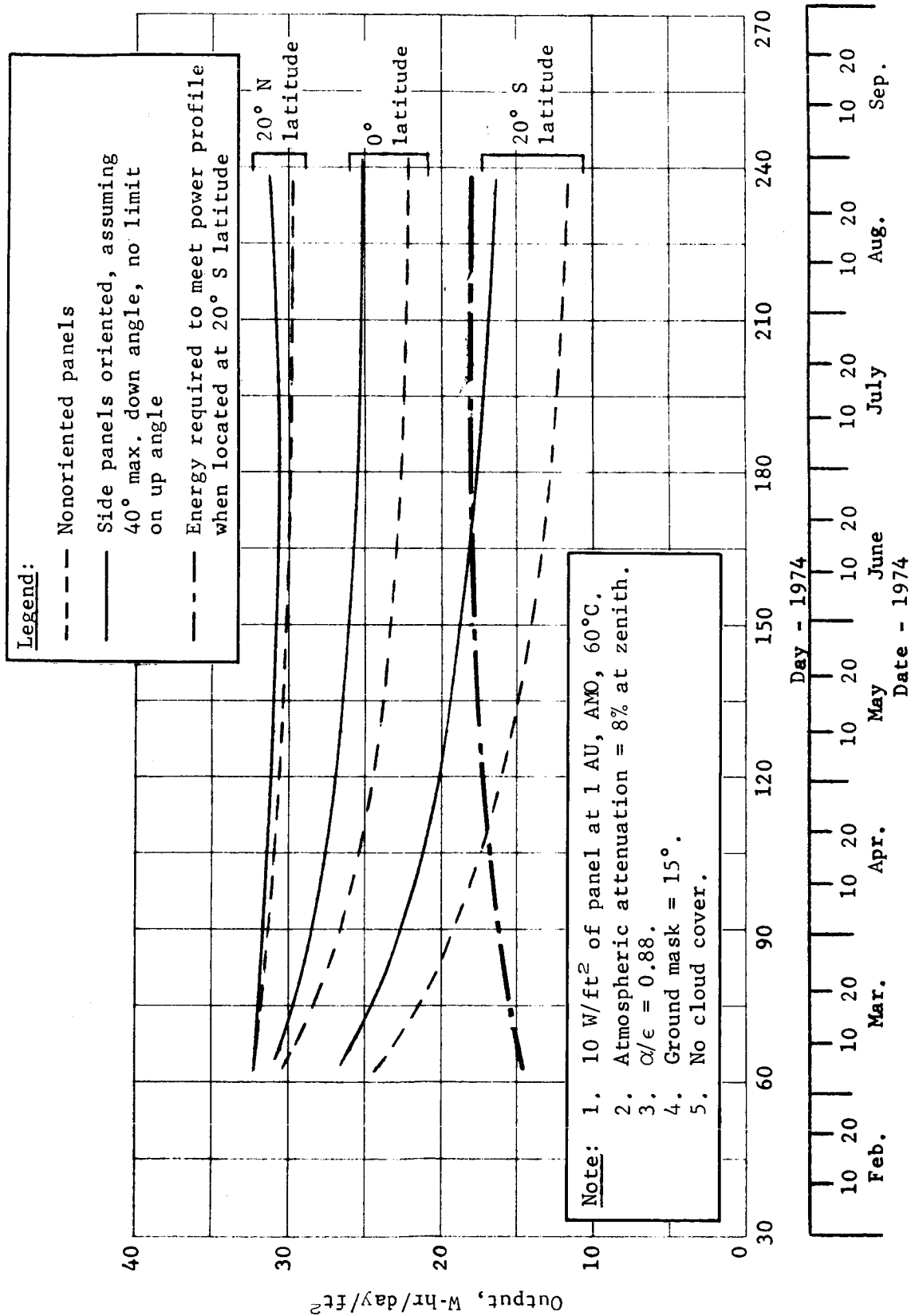


Figure 56.- Mars Lander Solar Array Output, 17° S Slope

## Thermal Control

Three compatible thermal control systems are required for the flight capsule: (1) cruise mode, (2) descent mode, and (3) Mars surface. The first two of these are well understood; therefore, primary emphasis was placed on the Mars surface system where a large number of parameters are involved and many options can be considered.

Mars surface thermal control. - All of the parameters that have a significant effect on the thermal control system are listed in table.9, in addition to a nominal value and expected range of each.

Surface environment: The environments defined for the surface correlations are a cold extreme environment at a temperature of  $-190^{\circ}\text{F}$ , an intermediate environment with a solar constant of  $160 \text{ Btu/hr-ft}^2$  and atmospheric transmissivity of 50%, a clear day environment with a solar flux of  $180 \text{ Btu/hr-ft}^2$  and atmospheric transmissivity of 100%, and a hot extreme environment with a solar constant of  $232 \text{ Btu/hr-ft}^2$  on the longest day and 100% atmospheric transmissivity. Daily cycles of surface and atmospheric temperature for each of these environments are included.

Insulation: A particular insulation consisting of radiation shields separated by 1 in. of low-density fiberglass ( $0.53 \text{ lb/ft}^3$ ) mounted between aluminum skins which are separated by epoxy-fiberglass standoffs was analyzed. Insulation conductivity was calculated as a function of temperature for Mars atmospheres of  $\text{N}_2$  and  $\text{CO}_2$ . This analysis shows that an insulation conductivity in the range from 0.007 to  $0.025 \text{ Btu/hr-ft-}^{\circ}\text{F}$  can be achieved.

TABLE 9.- THERMAL CONTROL PARAMETERS

Parameter	Range		
Life	2 days to years		
Size (volume of survivable equipment)	10 to 100 ft <sup>3</sup>		
Environment (Appendix D, section 2)	Clear day, cold & hot extreme, intermediate		
	Nominal	Range	
Insulation performance			
Conductivity, Btu/hr-ft-°F	0.0125	0.007	0.025
Density, lb/ft <sup>3</sup>	1	0.5	4
Thermal control energy source			
Specific weights			
Batteries, lb/Btu	Function of output (Appendix D, section 2)		
Chemical, lb/Btu	Function of output and type (Appendix D, section 2)		
Radioisotope, lb-hr/Btu	0.044	0.035	0.088
Solar cell with phase change, lb-day/Btu <sup>a</sup>	0.022	0.01	0.04
Solar cell with battery, lb-day/Btu <sup>a</sup>	0.050	0.03	0.08
Capillary pumped loop for RTG, lb-hr/Btu	0.01 (+ 3 lb)	0.005 (+ 2 lb)	0.02 (+ 6 lb)
Energy storage - phase change material, lb/Btu	0.0125	0.01	0.015
Energy rejection device			
Temperature-controlled heat pipe, lb/W <sub>(Rej)</sub>	0.17 (+ 5 lb)	0.10 (+ 3 lb)	0.25 (+ 7 lb)
Equipment power dissipation			
Average, W	60	15	130
Daytime peak, W-h	300	25	750
Penetration losses, W (40 to -190°F)	15	5	60
<sup>a</sup> Based on a clear day environment. For the intermediate environment add 0.01 to the nominal and minimum and 0.015 to the maximum. These systems are not applicable in the cold extreme environment.			

Energy sources: Implementation approaches and parametric weight estimates were calculated for the following energy sources:

- 1) Batteries;
- 2) Chemical reactors;
  - a) Solid - solid reactants,
  - b) Solid - liquid reactants;
- 3) Solar cells,
  - a) Battery storage,
  - b) Phase change storage;
- 4) Radioisotopes;
- 5) Capillary pumped fluid loop from RTGs.

Energy rejection: A concept for controlled heat rejection consisting of a heat pipe with temperature control valves and dual radiators is described and a parametric weight equation is given.

Procedure for estimating system weight: The daily and peak heat rejection rates were computed as a function of lander size, environment, insulation thickness, and conductivity. These data are used in conjunction with the parametric data developed for thermal control components to estimate system weights for any combinations of parameters desired. The procedure was used to develop a series of parametric weight curves. Figures 57 and 58 are examples of these weight curves.

Cruise and Descent Modes. - Cruise mode thermal control for capsules without RTGs is accomplished by multilayer insulation on the outside of the sterilization canister and thermostatically controlled heaters powered from the orbiter solar cells. The key weight element in the design is the multilayer insulation. Parametric weight equations were developed based on full-scale cruise mode tests conducted by Martin Marietta on our Voyager Phase B configuration.

Cruise mode thermal control for capsules with RTGs is based on passive cooling. This concept was analyzed in detail in our Voyager Phase B studies. Feasibility of this approach was proved in full-scale tests conducted by Martin Marietta with RTGs with up to a 13 600-W thermal output (500-W electrical).

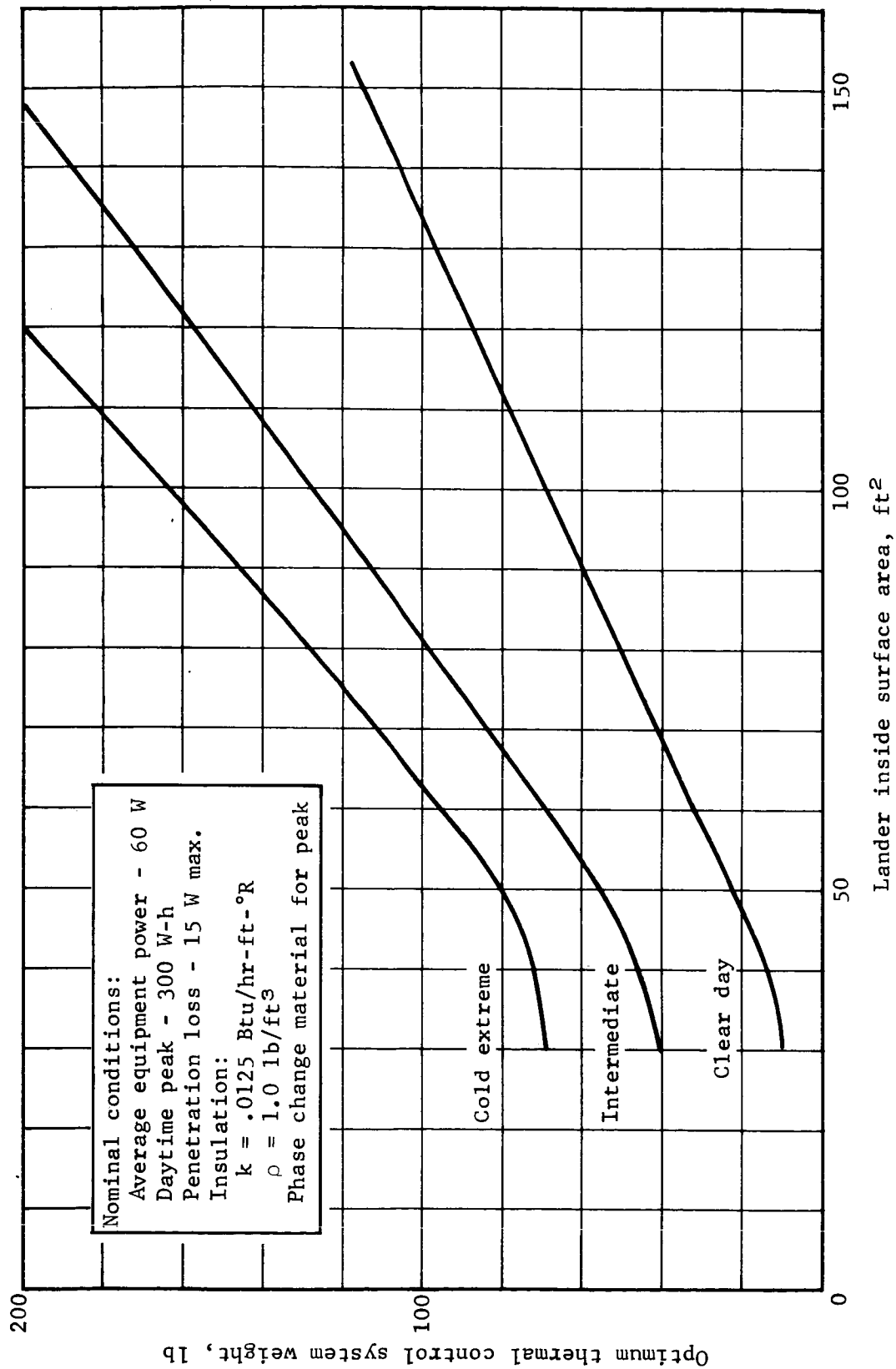


Figure 57.- Thermal Control System Weight versus Lander Size (2-Day Life), Solid Chemical Energy Source

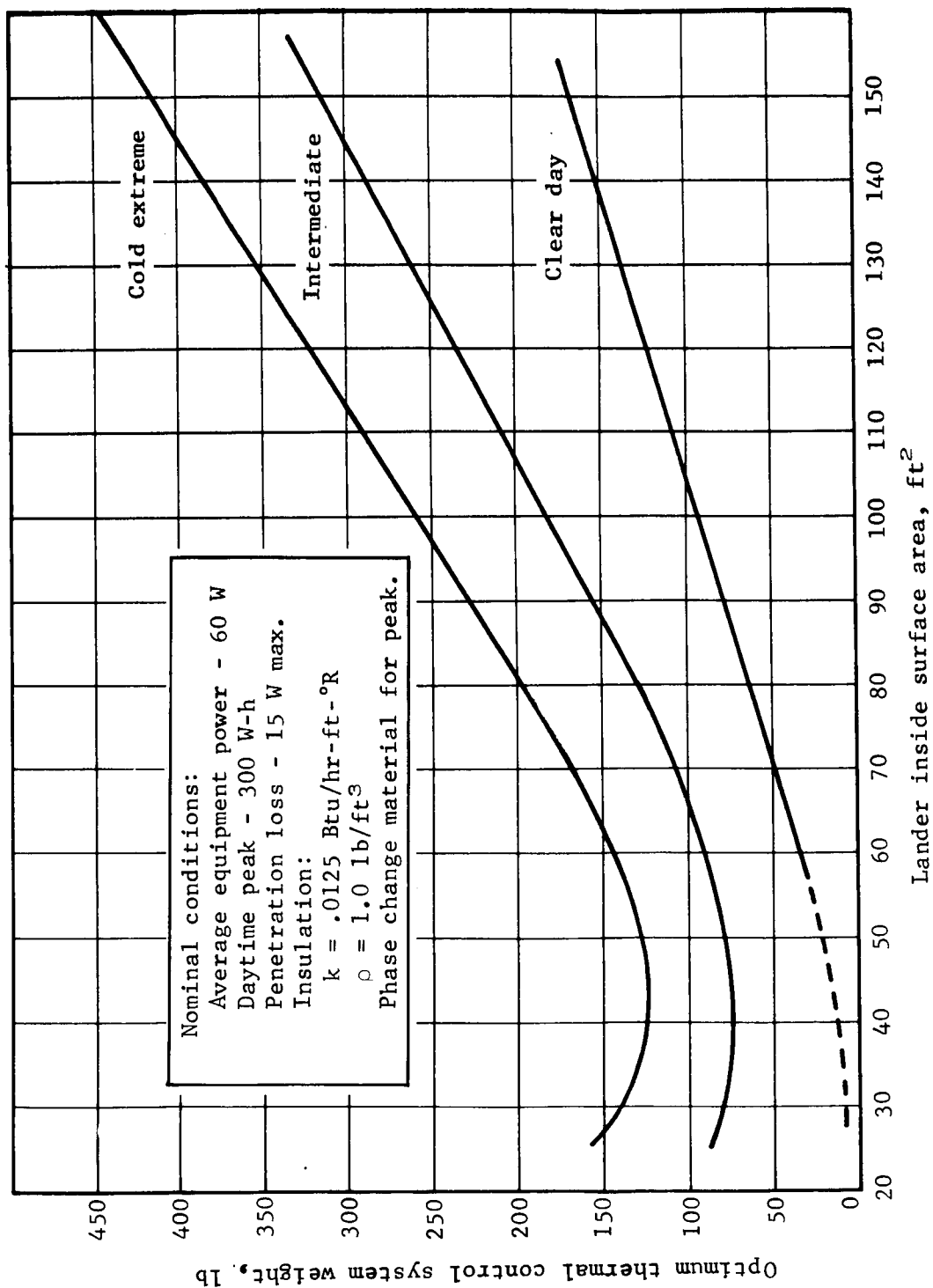


Figure 58. - Thermal Control System Weight versus Lander Size  
 (2-Day Life), Battery Heat Source

The descent mode thermal control is passive and weight estimates are based on the detail design developed during our Voyager Phase B studies. The only exception to this approach is that an entry aerodynamic base heating shield is added for the direct entry capsule.

### Weights

The parametric weight equations generated were used in the terminal phase computer program. These equations and their derivation are shown in detail in Appendix D, section 1. In all cases it was necessary to construct the equations so they were a function of parameters that were inputs to the computer program or could be derived therein. Entry weight, ballistic coefficient, and aeroshell diameter were selected as the input variables to the program, and equations were established to go from these up to flight capsule weight or down to landed equipment weight.

The propulsion subsystem equations are dependent on engine thrust and propellant weight. The parachute equation is a function of parachute diameter and the deployment  $q$ .

The output parameter of landed equipment weight consists of all weights that are independent of the vehicle size and entry mode. This weight was then available to be apportioned to the necessary function to support the surface mission of the vehicle. A detail definition is found in Appendix D, section 1.

The parametric weight data and computer program was used to maximize the landed equipment weight for both direct and orbital entry. From these data, several point designs were recommended to Langley Research Center to be used in Part II. The resulting point designs have been reexamined and detail weight estimates developed.

Some new information and design concept changes incorporated in the point designs result in weights that do not completely agree with the parametric weight equations. These changes consist of new estimates of parachute weight based on work done by LRC and Martin Marietta. These new parachute data are included in Appendix D, section 1. The propulsion systems have been changed to incorporate sterile insertion of propellant, and the weight of engines has been changed to reflect spherical combustion chambers. The parametric equation for the attitude control system, of necessity, had to be simplified to be dependent on available input parameters; in the point designs these systems have



been examined in detail and the weight of ACS propellant and systems vary slightly from results obtained from the parametric equation. Of all these changes, only the change in parachute weight will affect the system optimization, and this only when the parachute diameter is greater than 50 ft.

A final change from the parametric data is found in the weight of the canister. This results from a change in the method of mounting the spacecraft within the booster. The parametric data assumed that the flight capsule would be mounted atop the orbiter. Under the new concept, the canister is supported on the booster adapter and the orbiter is supported on the canister with the aeroshell supported to the canister by its aft frame. Thus the section previously referred to as the adapter becomes the canister interface frame.

Longerons to support the orbiter have been added to the aft canister and separation bolts have been added between the canister and the aeroshell aft frame.

## PART II

### FINAL ANALYSES AND CONCEPTUAL DESIGNS

## 1. CONFIGURATION 1A DESCRIPTION, OUT-OF-ORBIT

### Requirements and Constraints

This subsection list the major requirements and constraints that controlled the Configuration 1A system concept.

Mission. - The mission requirements and constraints are:

- 1) Launch: 30-day launch period, 2-hr daily launch window;
- 2) Trans-Mars trajectory: Type I; 75 mps midcourse  $\Delta V$ ;
- 3) Entry mode: from orbit;
- 4) Orbit period: 1000 x 33 000 km (synchronous period compatible with 1000 x 15 000 km);
- 5) Deorbit  $\Delta V$ : 120 mps maximum;
- 6) Deorbit coast time: 8.0 hr maximum;
- 7) Entry angle ( $\gamma_E$ ):  
Nominal  $\gamma_E = 16.5^\circ$ ,  $5\sigma$  above skipout,  
Entry corridor,  $14^\circ \leq \gamma_E \leq 18^\circ$ ;
- 8) Landing site:  
Elevation - mean surface level,  
Latitude -  $\pm 20^\circ$  from equator,  
Longitude -  $30^\circ$  on daylight side of evening terminator;
- 9) Surface life:  
All experiments - 2 days, battery powered,  
Weather station - 1 year (goal), Solar array/battery.

System and Subsystem. - The system and subsystem requirements and constraints are:

- 1) General:  
No consumables that limit surface life,  
Minimum cost,  
Mariner '71 orbiter with minimum modification;
- 2) Aeroshell:  $140^\circ$  cone, 8.5-ft diam, conventional aluminum construction;

- 3) Propulsion: three vernier engines and one deorbit engine with common design to vernier;
- 4) Aerodecelerator: Mach 2 parachute;
- 5) Landing system: four legs;
- 6) Attitude control: Active, three axis;
- 7) Power:
  - Separation through first two days, batteries,
  - Long-term operation, solar array/battery;
- 8) Thermal Control: electrical heater or radioisotope heat sources;
- 9) Communication:
  - Separation thru first two days, relay link,
  - Long-term operation, low-gain direct link,
  - Direct link command system,
  - Total data return,  $> 10^7$  bits;
- 10) Science:
  - Entry - temperature, density, pressure, humidity and composition,
  - Landed - imaging, soil composition, atmospheric temperature, pressure and humidity, wind velocity.

## Performance Summary

Table 10 presents pertinent launch to landing performance parameters.

TABLE 10.- CONFIGURATION 1A PERFORMANCE PARAMETERS

Launch vehicle . . . . .	Titan IIIC/Centaur
Launch date . . . . .	July 13, 1973
$C_3$ , $\text{km}^2/\text{sec}^2$ . . . . .	16.3
Arrival date . . . . .	February 2, 1974
$V_{HE}$ , $\text{km/sec}$ . . . . .	3.15
Injected payload capability, lb . . . . .	8555
Spacecraft weight, lb . . . . .	5298
Space vehicle margin, lb . . . . .	3257
$\Delta V_{M/C}$ , $\text{mps}$ . . . . .	75
Encounter weight minus ACS gas, lb . . . . .	5133
$\Delta V_{O/I}$ , $\text{mps}$ . . . . .	1350
Orbit characteristics (reference)	
$h_p$ , $\text{km}$ . . . . .	1000
$h_a$ , $\text{km}$ . . . . .	33 070
$P$ , $\text{hr}$ . . . . .	24.62
Spacecraft weight in orbit (minus propulsion), lb . .	2790
Flight capsule weight, lb . . . . .	1723
$\Delta V_{D O}$ , $\text{mps}$ . . . . .	120
$\gamma_e$ , $\text{deg (max.)}$ . . . . .	-18
$V_e$ , $\text{fps (max.)}$ . . . . .	16 000
$B_e$ (8.5-diam aeroshell), $\text{sl/ft}^2$ . . . . .	0.466
Entry weight, lb . . . . .	1383
Parachute deployment altitude, $\text{ft}$ , $h_T = 0$ . . . . .	13 000
$B_{DEC}$ (65-ft-diam chute), $\text{sl/ft}^2$ . . . . .	0.021
Vernier ignition altitude, $\text{ft}$ . . . . .	4000
$W_{LE}$ , lb . . . . .	570

## System Definition

Configuration 1A enters from orbit, uses a Mach 2 parachute intermediate decelerator and a propulsive final descent to a soft landing. The system functional schematic is shown in figure 59. Landed equipment weight required to meet mission requirements is 570 lb, which results in a flight capsule weight of 1723 lb.

The major system elements and characteristics are described in this subsection.

Science. - The science subsystem comprises instruments for obtaining science data and a data automation system (DAS) for special science data conditioning, formatting, encoding, storage, and instrument sequencing.

Instruments included are an accelerometer triad, two stagnation pressure sensors, a total temperature sensor and an open ion source mass spectrometer for obtaining data during the ballistic entry phase. From parachute deployment to landing, ambient pressure and temperature sensors, a hygrometer, and a double focusing mass spectrometer obtain atmospheric data. Landed experiments are a facsimile camera for panoramic and site survey imaging, an alpha scatter spectrometer for soil analysis and a meteorology package containing pressure, temperature, humidity, and wind velocity sensors.

The DAS consists of digital multiplexers, and instrument sequencer, data compression and processing element, and a magnetic tape recorder.

Structures and mechanisms. - Flight capsule structure consists of the following major elements: sterilization canister, deorbit module, aeroshell, aerodecelerator, lander, and landing system.

The sterilization canister lid is of titanium skin construction. **The body structure is titanium.**

The deorbit module structure employs mounting provisions for the deorbit propulsion engine, fuel and pressurization tanks.

The aeroshell is an 8 1/2-ft-diameter, 70° half-angle cone employing an SLA-561 ablator material heat shield. Nose-to-base radius is 0.5. The primary structure is conventional ring-stiffened aluminum construction.

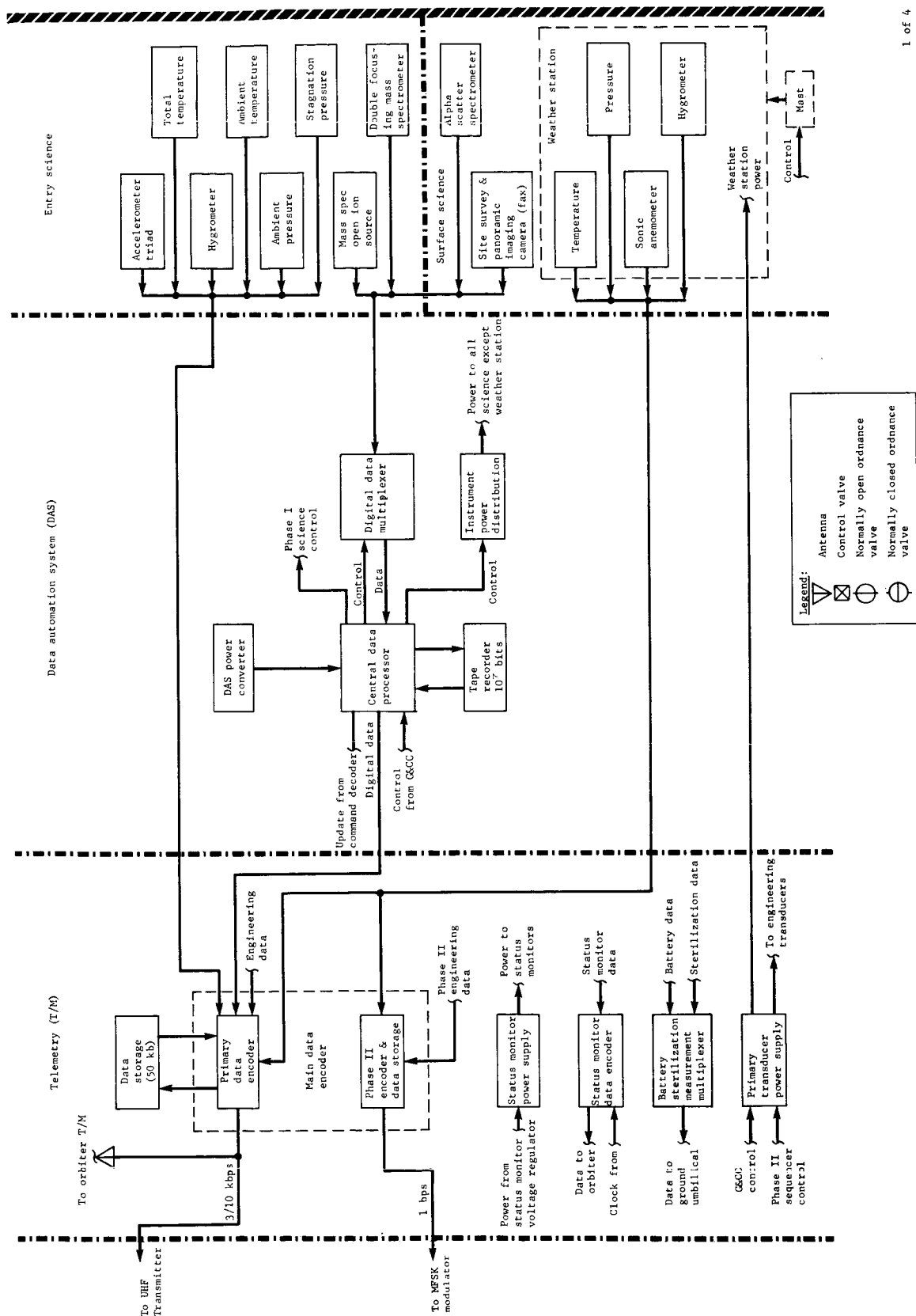


Figure 59.- System Block Diagram, Configurations 1A, 1B, and 2A

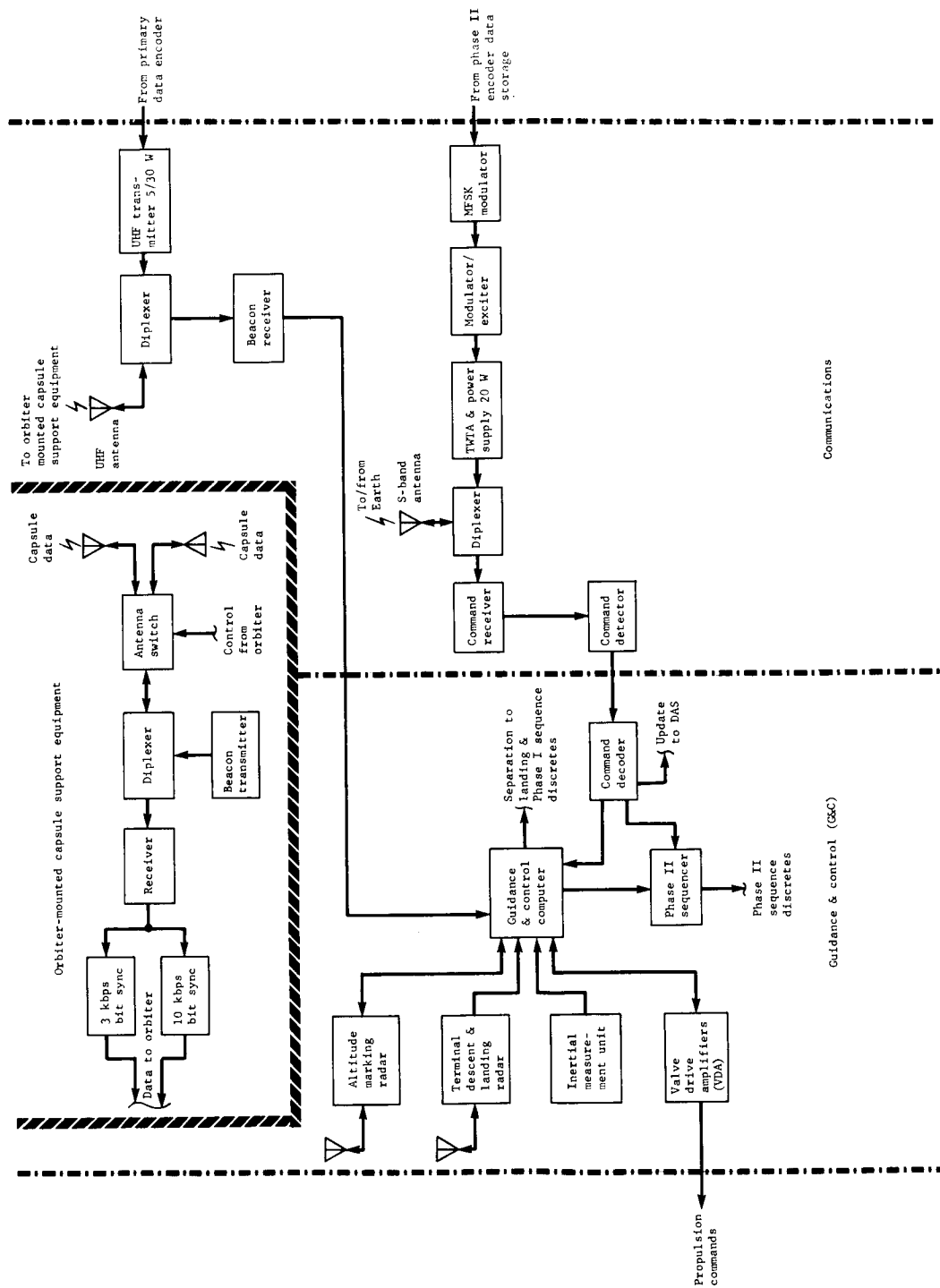


Figure 59.- Continued



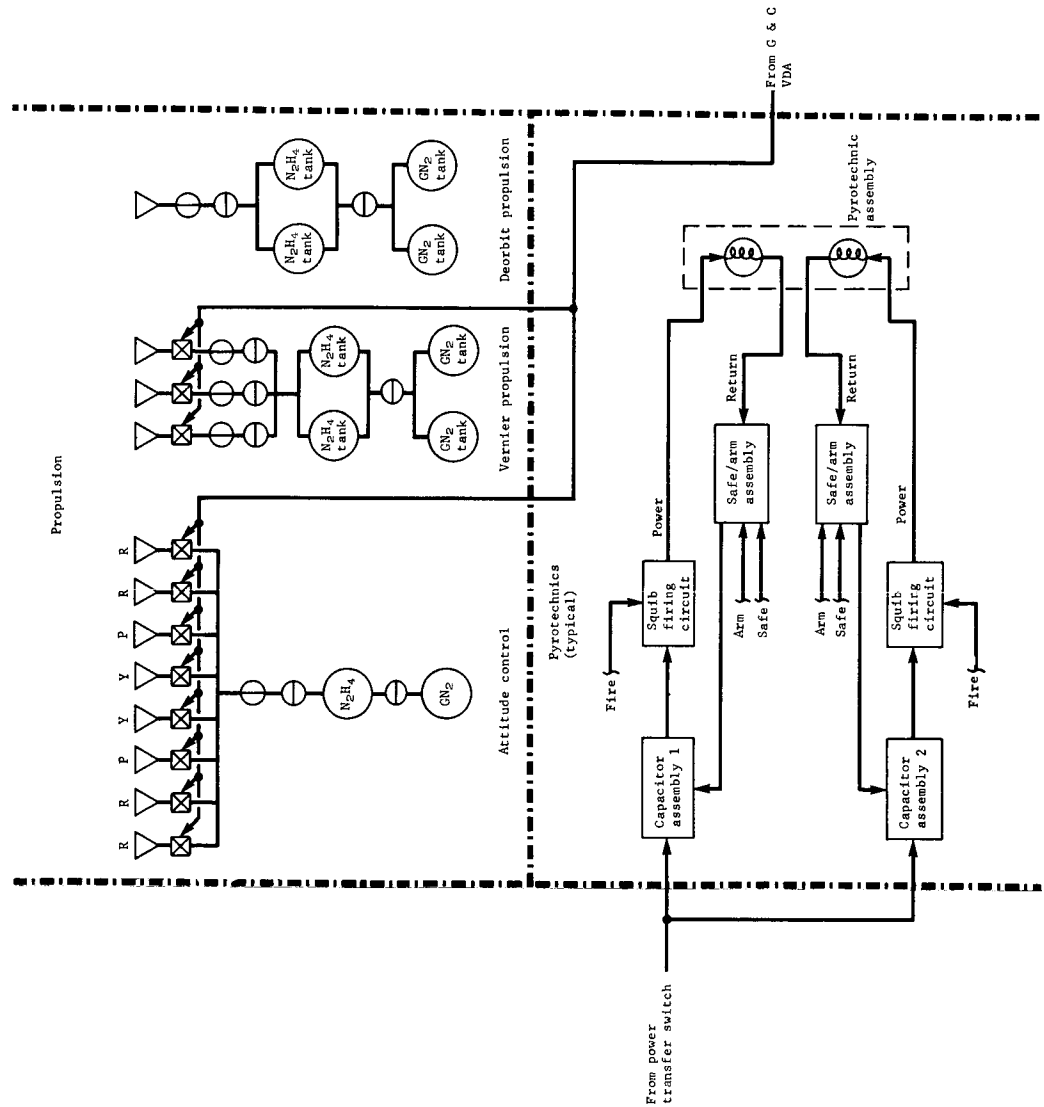
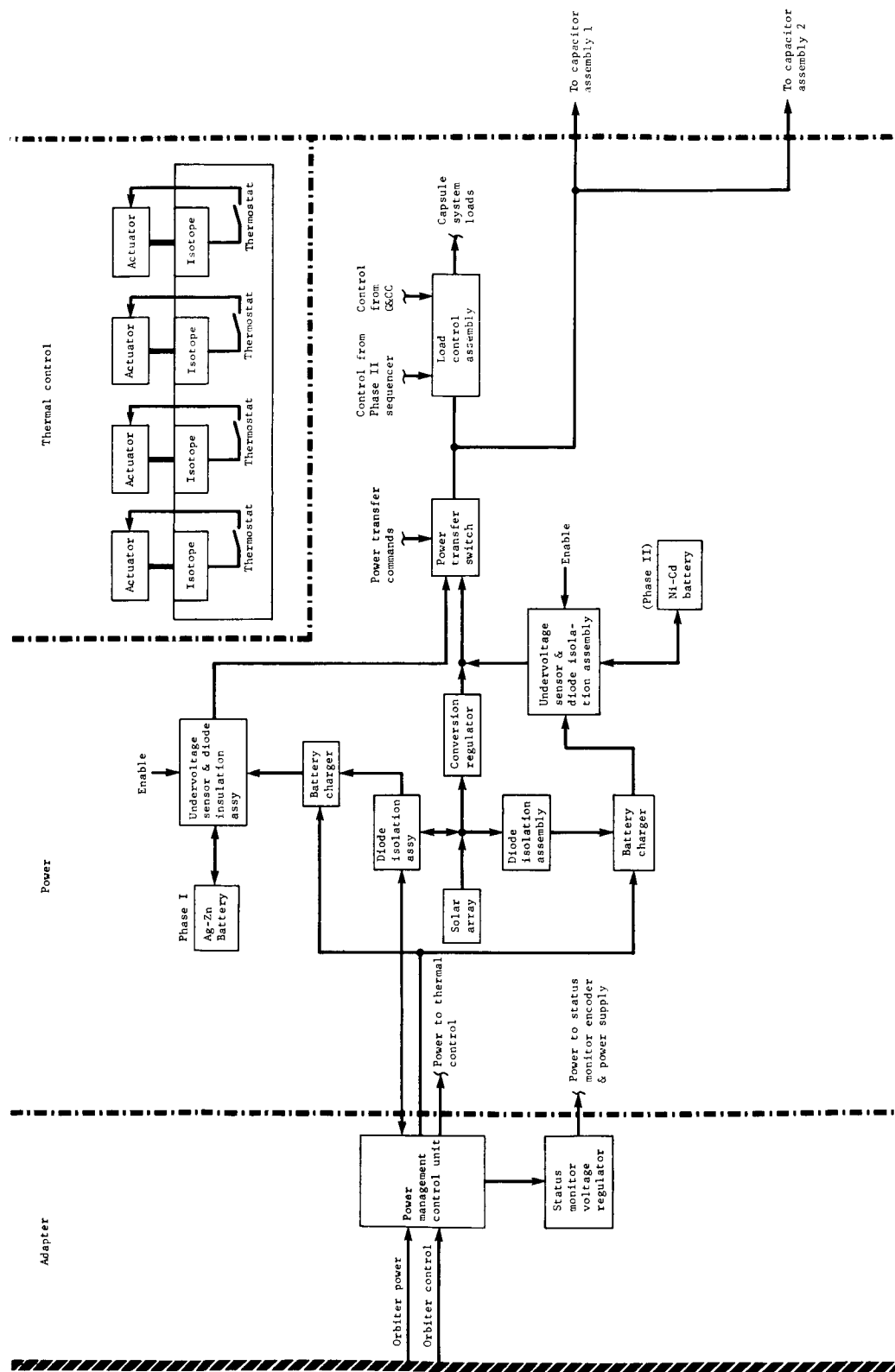


Figure 59.- Continued



4 of 4

Figure 59.- Concluded

The aerodecelerator is a subsonic-type parachute which is deployed at Mach 2. The chute is deployed by a mortar fired on an altitude mark command from the guidance and control system. The lander is suspended on a four-link bridle attached through a swivel to the riser.

Lander structure is conventional aluminum truss with provision for equipment mounting, landing gear, and parachute attachment.

The landing system consists of four equally spaced legs with crushable foot pads and Surveyor-type main struts.

Propulsion. - The propulsion subsystem comprises deorbit propulsion and vernier propulsion modules and an attitude control system (ACS).

The vernier propulsion uses three throttleable monopropellant engines; pitch and yaw attitude control is maintained by differential throttling and roll control is supplied by the ACS roll engines. Deorbit propulsion uses a single monopropellant engine identical to the vernier engines, except that the throttle valve is removed. Pitch, yaw, and roll attitude control is provided by the ACS. Two pitch, two yaw, and four roll monopropellant engines in the ACS provide attitude control from separation to landing.

Blowdown pressurization, with gaseous nitrogen, is used throughout. Positive propellant orientation is provided by screens for the deorbit propulsion and by bladders for the ACS.

Guidance and control. - The guidance and control system consists of an inertial measurement unit (IMU), general purpose digital computer and valve drive amplifiers, a five-beam doppler radar (TDLR), an altitude measuring radar (AMR), and a Phase II sequencer.

The IMU utilizes three 2-axis strapped-down gyros for attitude reference and three off-axis mounted accelerometers for axial acceleration sensing. This gyro and accelerometer configuration provides the capability to function nominally with the loss of one gyro and accelerometer.

The 4000-word general purpose computer provides preseparation to landing and Phase I mission sequences and accomplishes all attitude and control computations required. In addition, the computer functions as a command decoder for Phase I mission operations.

The five-beam Bessel sideband doppler radar furnishes velocity and range data required for terminal descent and landing and has the functional capability to operate with the loss of any two beams.

The AMR operates nominally from 200 000 ft altitude to aeroshell separation and supplies information to correlate entry science data and to deploy the parachute. The antenna is flush mounted in the aeroshell.

The Phase II sequencer employs a fixed sequence for extended mission operations with command update in the clock.

Telecommunications. - Two primary communications systems are used. A uhf (400 MHz) transmitter and crossed-slot antenna provide relay communications at 3 kbps from separation to landing and 10 kbps after landing. A uhf beacon receiver initiates subsequent relay communications. An S-band transmitter and receiver provide direct link communication and command capability after landing.

The telemetry subsystem has a primary data encoder with outputs of 3 kbps, 10 kbps, and 1 bps, and a static (core) storage capability of 50 kbps. It provides data storage, signal conditioning, and data formatting.

Power and Pyro. - The power subsystem uses silver-zinc batteries for primary power from separation to landing plus 50.3 hr (Phase I). Phase II power is furnished by a semi-oriented solar array and a nickel-cadmium battery. The outboard elements of the array can be oriented (single degree of freedom) on command, to maximize the array output as a function of landing site, slope, and sun declination.

Pyrotechnic functions are initiated by capacitor stored energy. All pyrotechnic devices have two squibs per function and one bridgewire per squib. Solid-state safe/arm and fire switches are used.

Thermal Control. - Thermal energy for the primary equipment module is supplied by radioisotope heaters with an output of 200 thermal W. Control is maintained by moving the heater into or out of the lander by actuators. Electric heaters are provided for peripheral components as necessary. Phase change material, insulation, and surface coatings comprise the remainder of the thermal control system.

## Functional Sequence

The flight capsule is in a nonoperating mode from launch to orbiter separation -1:00 hr. Pertinent flight capsule status measurements are obtained during this mission phase and transmitted to Earth by the orbiter. Orbiter solar power is used for thermal management, status monitoring, and battery charging.

The flight capsule mission active phase begins at separation -1:00 hr. The flight capsule equipment is turned on and warmed up on command from the orbiter. Canister separation occurs at orbiter separation -30 min with a relative velocity of 1 fps imparted by springs. Flight capsule/orbiter separation is accomplished following verification of systems status and updating of stored commands by the Space Flight Operations Facility (SFOF). Active attitude control and relay communications (in the low-power mode) are started at separation +1 sec.

Deorbit attitude is attained during a 30-min coast to the deorbit impulse position. The 30-min coast is required to achieve an 1800-ft separation from the spacecraft before firing the deorbit motor. Deorbit impulse is initiated and terminated and the deorbit coast attitude is established on command from the guidance and control system. The deorbit propulsion module is jettisoned following deorbit impulse. Deorbit coast time is 8 hr, maximum.

At 30 min before reaching 800 000 ft (preprogramed), capsule entry attitude is established and the entry science subsystem instruments are turned on. Altitude measuring radar (AMR) operations commence at 200 000 ft. Parachute deployment is commanded on receipt of the deployment altitude mark from the AMR and the terminal descent sequence is initiated. Aeroshell separation occurs 6 sec after parachute deployment.

The terminal descent and landing radar (TDLR), which is activated at aeroshell separation, commands vernier engine ignition at minimum thrust at 4000 ft -2 sec. Engine ignition and reliable operation are verified by the guidance system and parachute release commanded at 4000 ft above the surface, followed by vernier descent under closed-loop TDLR control and a subsequent soft landing. Following touchdown, Phase I sequence is initiated. The mission phase extends for a maximum period of 51.3 hr.

Before orbiter set at touchdown +6 min, the facsimile camera, meteorology package, and solar array are erected and verified operational, and the alpha-scatter spectrometer is deployed and

initiated. In addition, one low-resolution image from the facsimile camera and approximately 100 samples from each of the meteorology instruments are obtained and transmitted via the uhf relay link.

During the first diurnal cycle of Phase I mission operations, three low-resolution and two high-resolution pictures are obtained and the meteorology instruments are sampled once per hour. Data are obtained continuously from the alpha scatter experiment for the first 12 hr. Data are stored for subsequent uhf transmission at touchdown +24.5 hr (30.5 hr for the 1000 x 15 000-km orbit).

The low-resolution and three high-resolution pictures are obtained and meteorology sampling continued once per hour during the second diurnal cycle.

The final Phase I uhf transmission occurs 49.2 hr after touchdown (51.3 hr for the 1000 x 15 000-km orbit).

Phase II, or weather station mode, is initiated following orbiter set on the second day. This phase uses available solar energy for a total landed mission lifetime of approximately one year. Meteorology instruments are sampled once per 4 hr and data stored for subsequent transmission. Data are transmitted for 2 hr/day via the low gain M'ary FSK direct link at 1 bps.

Phase I mission operations can be reestablished on command, solar energy and relay link availability permitting.

#### Sequential Weight Statement

Table 11 is a summary sequential weight statement of Configuration 1A. A detail flight capsule weight summary is given in Section 1 of Appendix D. The weight of landed equipment for this configuration is 570 lb of which 84.8 lb are landed science. In addition there are 18 lb of entry science in the aeroshell, giving a total science weight of 102.8 lb.

TABLE 11.- CONFIGURATION 1A SEQUENTIAL WEIGHT STATEMENT

Titan IIIC Centaur capability	(9295)	
Fairing and/or beefup penalty	290	
Adapter	450	
Margin	3257	
Spacecraft weight		
Orbiter expendables	(5298)	
(includes 43 lb of N <sub>2</sub> gas)	1988	
In-orbit weight	(3310)	
Orbiter propulsion system	520	
Useful inorbit weight	(2790)	
Useful inorbit orbiter weight	990	
Capsule adapter	77	
Flight capsule weight	(1723)	
Canister	165	
Aft section, body	102	
Forward section, lid	45	
Electrical in canister	18	
Separated capsule weight	(1558)	
Deorbit structure	30	
Deorbit propulsion system	61	
Deorbit propellant	81.5	
ACS propellant	2.5	
Entry weight ( $B_E = 0.466$ )	(1383)	
Aeroshell	126.5	
Science in aeroshell	18.0	
ACS propellant	1.5	
Decelerator load	(1237)	
Chute weight (65 ft)	169	
Verniered weight	(1068)	
Vernier propellant	108	
ACS propellant	1.0	
Landed weight	(959.0)	
Propulsion system	113.7	
Useful landed weight	(845.3)	$W_{LE}$
Structure	156	
Attitude control system	32.6	
Power system	211.0	211
Guidance and control	131.0	131
Telecommunication	93.4	76.4
Thermal control	87.0	67
Pyrotechnic control	49.5	
Science	84.8	84.8
Landed equipment weight, $W_{LE} = 570.2$		

## Space Vehicle Integration

Figure 60 illustrates integration of space vehicle systems comprised of an 8½-ft-diameter flight capsule, 950-lb (useful) Mariner '71 orbiter modified to include the additional propulsion capability for flight capsule orbit insertion, Surveyor shroud, and Titan IIIC/Centaur launch vehicle.

The standard 10-ft-diameter (i.d.) Surveyor shroud is used as the space vehicle nose fairing and mates through a modified adapter barrel section to the Centaur stage. The adapter also functions as the spacecraft/launch vehicle interface. The shroud is separated by release of explosive clamps with lateral rotation supplied by redundant cold gas thrusters mounted in the nose.

Spacecraft/launch vehicle separation occurs following trans-Mars injection by the Centaur stage on release of explosive actuated nuts. Separation energy is provided by several separation spring assemblies.

The sterilization canister body performs the following functions:

- 1) Provides the spacecraft structural interface with the launch vehicle at the shroud adapter;
- 2) Provides the sterilization canister aft closure;
- 3) Provides the capsule structural interface with the Mariner '71 orbiter at the orbiter/flight capsule adapter.

## Science Subsystems

Functional description. - A functional description of the science subsystem in Part I tabulated the measurements selected to meet the mission objectives.

Provision for meeting the science entry requirements for atmosphere measurements, surface meteorology, and soil composition analysis are discussed in **this subsection.**



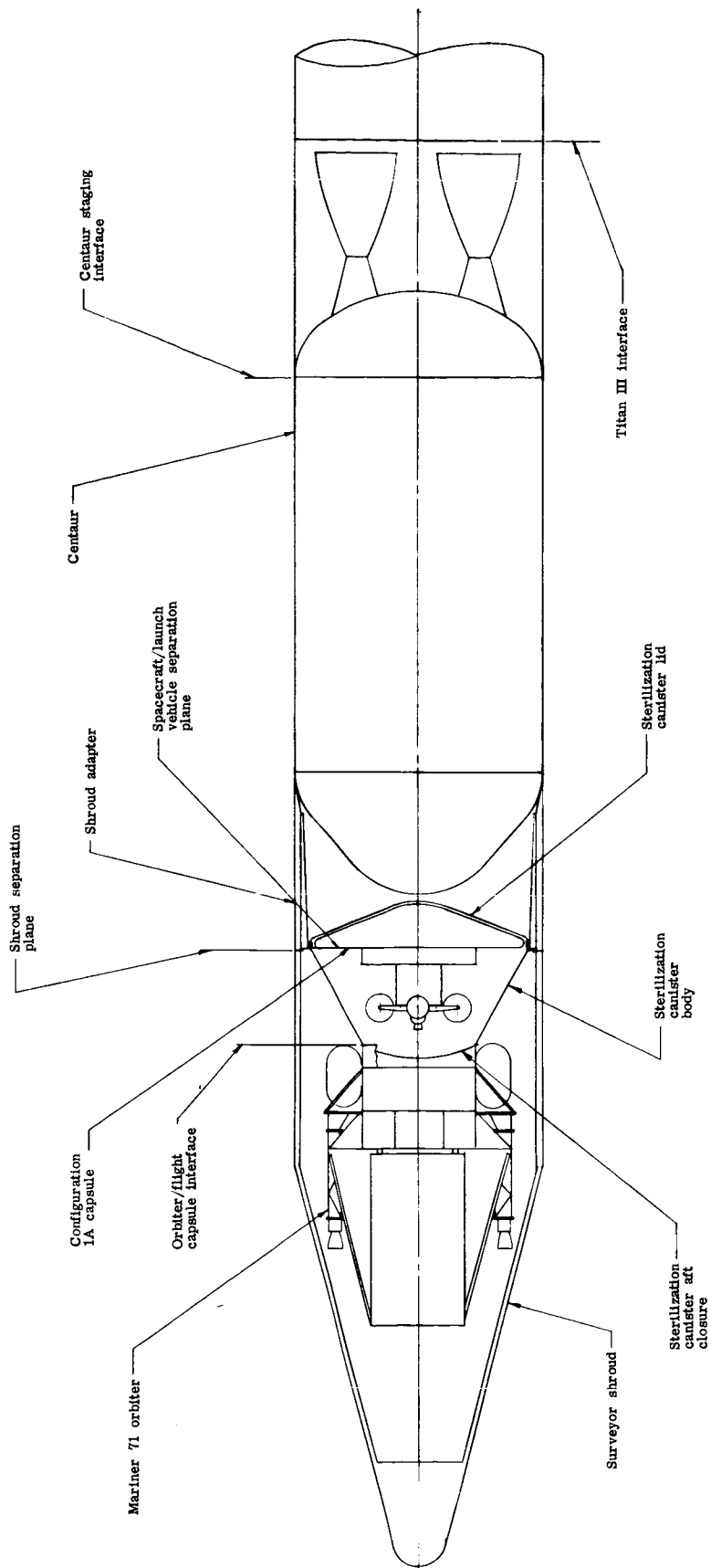


Figure 60. - Space Vehicle Integration, Configuration 1A

Entry atmospheric measurements: The entry science requirements are depicted in figure 61 using current estimates of the Martian atmosphere (ref. 1). These new monograph models have been developed to update those given in NASA SP-3016. Both maximum and minimum estimates are plotted. Figure 61 is also used to show how the science measurements provide the basic data for computing the four structure quantities,  $\rho$ ,  $T$ ,  $p$ , and composition. Instruments selected for the entry science payload are also shown in the figure.

To get into the required accuracy band for density below 60 km, a sequence of direct measurements of density are made at altitudes above the specified range of interest. In the case of the minimum atmosphere, the region covered extends from about 140 km downward to 70 km. The open ion source mass spectrometer is used here. This is the only place during entry where it is possible to make a direct measurement of any atmosphere structure parameter. As shown in Section 6 of appendix D, this capability makes a major contribution toward reducing uncertainties in all structure quantities deduced from entry measurements.

Ambient temperature cannot be measured directly during the ballistic entry phase. This parameter must be inferred from the density and composition measurements by integrating the density profile, and from total temperature measurements at velocities below Mach 3. Calculation of ambient temperature from total temperature measurements below Mach 3 uses the familiar adiabatic relationship shown in the figure.

As is the case of temperature, it is not possible to sense ambient pressure from the entry vehicle. Pressure must be computed from density and temperature profiles, together with composition measurements. Below Mach 3 the adiabatic relationship for stagnation pressure is also used.

One of the most significant things present in these new model atmospheres is recognition of the reduction in mean molecular weights in the upper altitudes due to ultraviolet dissociation. Along the composition profiles above the region of turbulent mixing (constant molecular weight) atomic oxygen is a major constituent. For this reason, the open ion source instrument is a requirement for accurate composition analysis. Figure 62 (ref. 2) demonstrates this point. The figure shows that atomic oxygen in the upper atmosphere as indicated by the open ion source instrument is nearly 30 times as abundant as shown in previous measurements made by instruments receiving a sample through a length of tubing. These results show the need for an open source to measure a reactive component such as atomic oxygen.

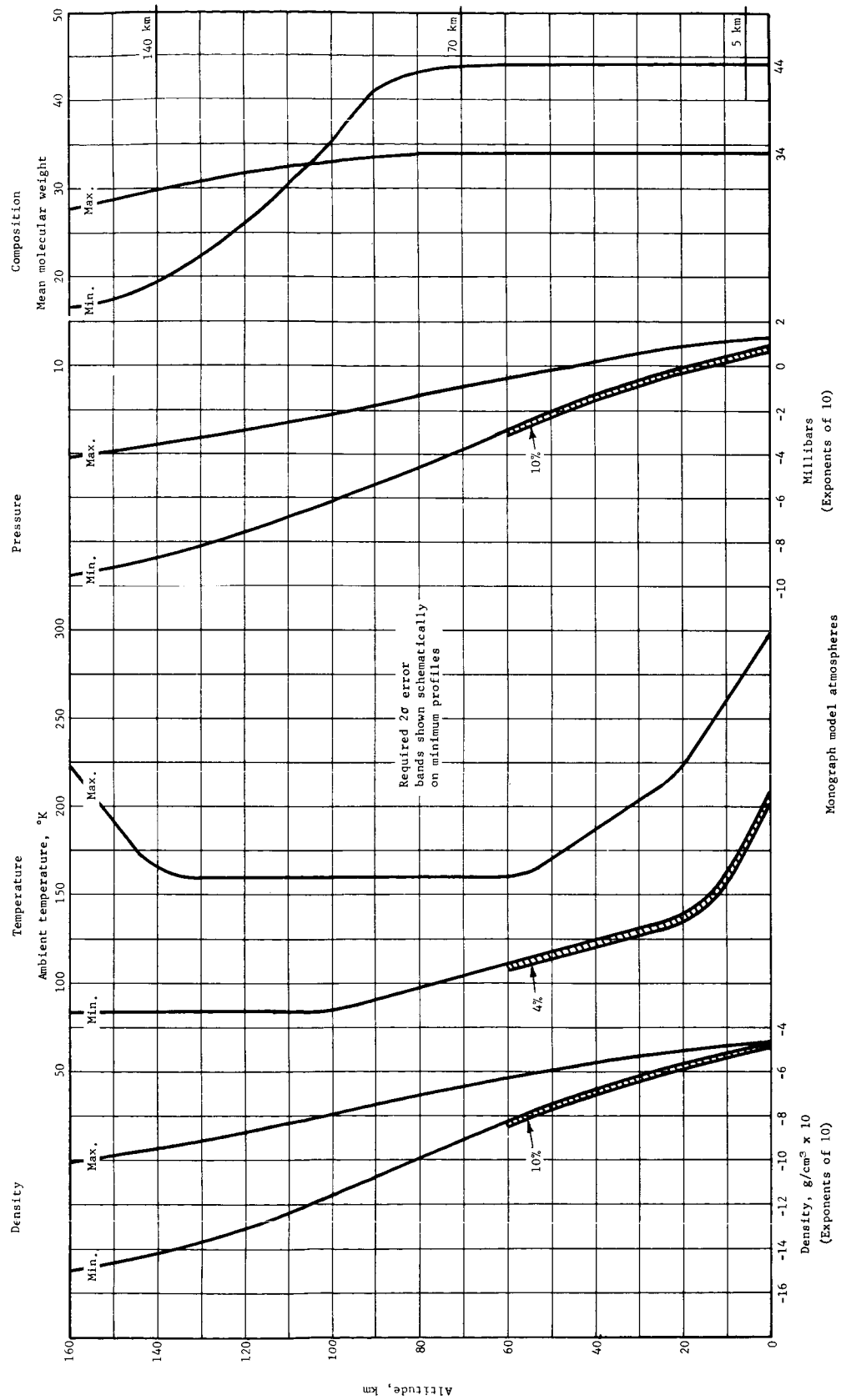
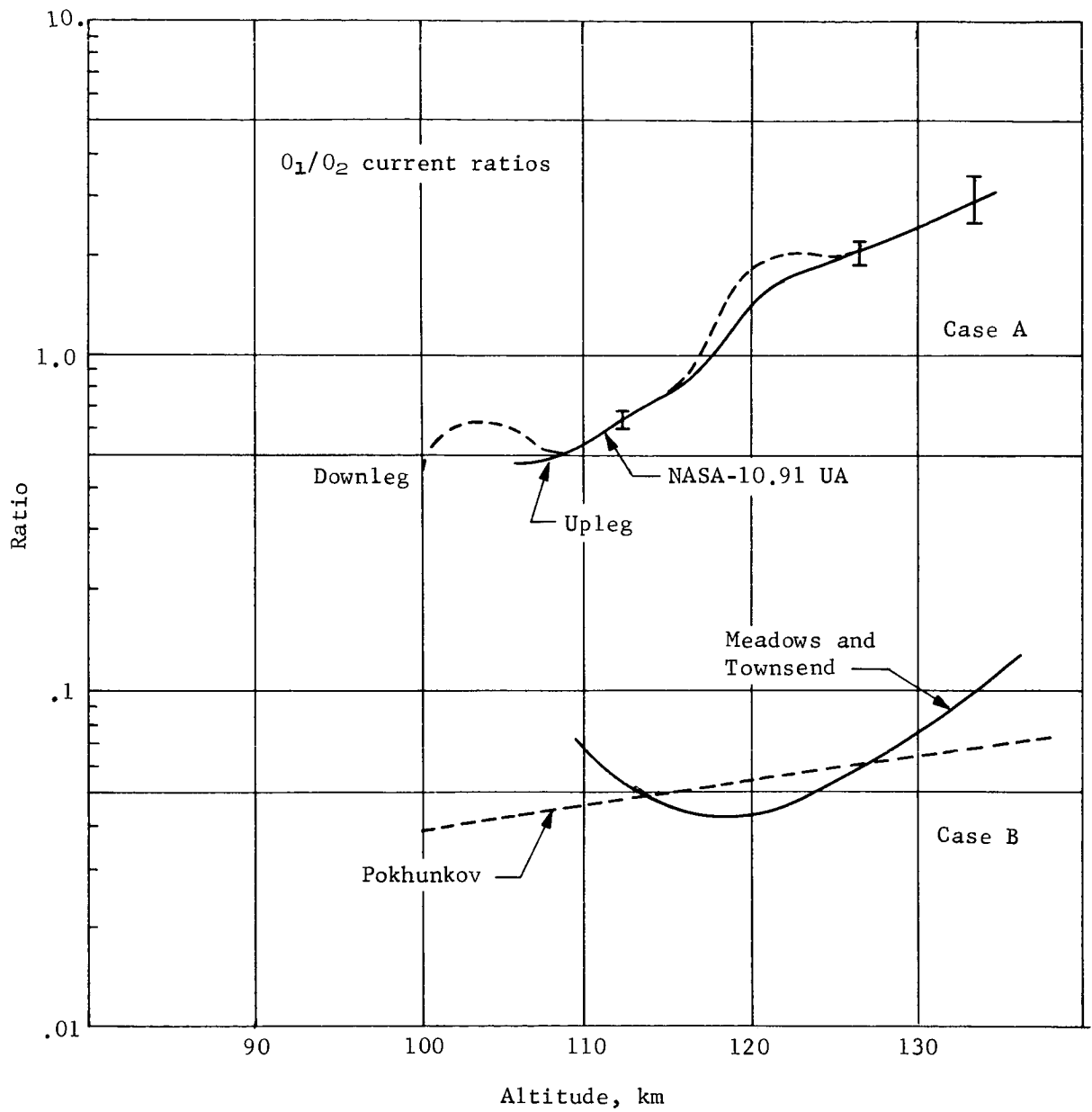


Figure 61.- Atmosphere Structure Quantities from Entry Science Measurements

Working relationships			Experimental quantities	Instruments
Density	Temperature	Pressure		
Sensitivity threshold for OIS mass spectrometer $\rho_k = \frac{n_k m_k}{A v}$ $\rho = \sum_k \rho_k$	$T = \frac{\int_0^Z -\rho g dz}{\rho_0 R/\bar{m}} + \frac{\rho_0}{\rho} T_0$ $T = \frac{g/R}{\frac{d}{dz} \ln \frac{n_1}{n_2}} (m_2 - m_1)$	$P = \frac{\rho}{\rho_0} T$	Number density of ambient neutral particles	<ul style="list-style-type: none"> <li>Open ion source mass spectrometer</li> </ul>
Sensitivity threshold for accelerometers and stagnation pressure sensor $\rho = \frac{2m a_x}{C_D A v^2}$ $\rho = C_F^{-1} \frac{P}{g} \frac{g}{v^2}$	$T = \frac{\int_0^Z -\rho g dz}{\rho_0 R/\bar{m}} + \frac{\rho_0}{\rho} T_0$ $T = \frac{T_0}{1 + \frac{\gamma - 1}{2} M^2}$	$P = \frac{\rho}{\rho_0} T$ $P = \frac{P_0}{\left(1 + \frac{\gamma - 1}{2} M^2\right)^{\frac{\gamma}{\gamma - 1}}}$	Drag acceleration Stagnation pressure Stagnation temperature	<ul style="list-style-type: none"> <li>Accelerometer triad</li> <li>Stagnation pressure sensor</li> <li>Stagnation temperature sensor</li> </ul>
Begin direct sensing during terminal descent phase $\rho = \frac{P}{R T}$	Direct measurement	Direct measurement	Ambient: Temperature Pressure Composition Humidity	<ul style="list-style-type: none"> <li>Temperature sensor</li> <li>Pressure sensor</li> <li>Double focusing mass spectrometer</li> <li>Hygrometer</li> </ul>

<b>Nomenclature:</b> $\rho_k$ = mass density for $k^{\text{th}}$ species $n_k$ = number density for $k^{\text{th}}$ species $m_k$ = mass number of $k^{\text{th}}$ species $A v$ = Avogadro's number, $6.02 \times 10^{23}$ molecules/g mol $m$ = total mass of entry vehicle $a_x$ = acceleration along flightpath	$v$ = speed along flightpath $C_D$ = drag coefficient $C_F$ = pressure coefficient $A$ = frontal area $P$ = ambient pressure $R$ = universal gas constant, $8.3 \times 10^7$ erg/mol °K $\bar{m}$ = mean molecular weight	$T$ = ambient temperature $\gamma$ = ratio of specific heats $M$ = Mach number $T_s$ = stagnation temperature $P_s$ = stagnation pressure $g$ = gravitation acceleration
--	---	---

Figure 61.- Concluded



Case A: Sampling by open ion source  
 Case B: Sampling by inlet tube leading  
 to an internal cavity

Figure 62.- Ratio of O<sub>1</sub>/O<sub>2</sub> Ion Currents from Mass Spectrometer Measurements

Water content will be measured during the ballistic period of entry by a mass spectrometer. A quantitative water vapor analysis is possible with the open ion source instrument because it can sample directly from the undisturbed ambient environment. At lower altitudes, however, quantitative analysis with the double focusing instrument will be difficult because of the necessity for sampling through a leak device. Without special precautions, such as heating the inlet system, water vapor will condense on the inlet plumbing.

The entry science instruments are mounted as a group at the apex of the aeroshell. This interface is simple consisting of a bolted structural joint and a single electrical connector. This approach is advantageous because it permits development, qualification, and integration of science equipment to proceed on a relatively independent basis.

Surface imagery: Figure 63 is a sketch of the lander showing the viewing geometry, area coverage, and resolutions specified. A tabulation on the figure shows the total data bits produced by one set of imaging scenes consisting of four low-resolution wedges each containing one high-resolution square. The required total of  $10^7$  bits of imaging data are contained in one such set. As discussed later, the point designs are capable of returning imagery data in excess of this minimum amount.

For purposes of this study, a facsimile camera was selected as the imaging instrument. This device is in an advanced stage of development due to NASA work carried out over the past seven years (ref. 3). The most significant advantages of a facsimile camera over a vidicon instrument for Mars surface imaging are the following: (1) small size, lightweight, low power and inherent ruggedness due to an optical system that looks at only one resolution element at a time and a small solid state sensor; (2) no distortion of the image near extremes of the format since optical geometry is identical for each resolution element; (3) no field of view restriction, making it possible to reproduce a panoramic scene without the need for mosaic overlay of adjacent images; and (4) the instrument is not damaged by direct viewing of sunlight.

A recent design for a variable parameter facsimile camera is shown in figure 64, along with a tabulation of some of its major characteristics.



Parameter ranges	
Image point, deg . . . . .	0.01 to 0.6
Frame, deg . . . . .	10x10 through 90x360
Threshold, ft-L . . . . .	0.5
Dynamic range . . . . .	10 000:1 (80 dB)
Frame time . . . . .	1 sec to 50 hr
Depth of field, ft . . . . .	3 to infinity
Spectra . . . . .	.4 to 1.2 microns B&W and 3 "color" bonds
Characteristics	
Size, in. . . . .	3 diam by 18 long
Weight, lb . . . . .	6.5
Voltage, Vdc . . . . .	28
Power, W . . . . .	15
Bandwidth, kbps . . . . .	Up to 50

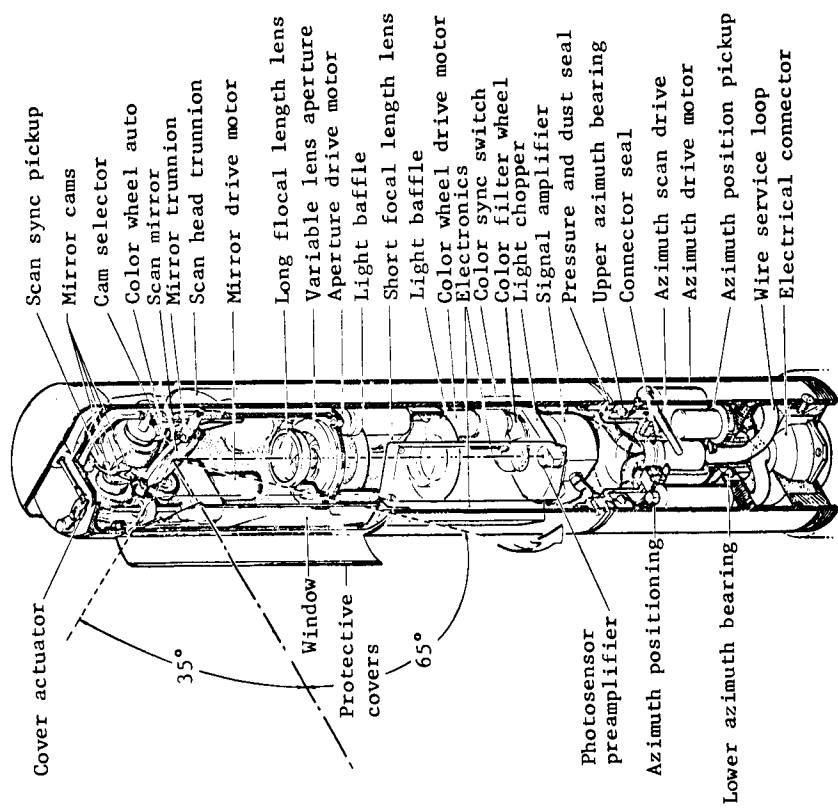


Figure 64.- Proposed Variable Parameter Facsimile Camera



Figure 65 shows examples of photography from Surveyor taken from reference 4. These are included to give an idea of the type of imaging resulting from resolutions near those specified.

**Meteorology:** Figure 66 shows the packaging concept for meteorology instruments. Sensors for atmosphere temperature, pressure, humidity, and wind vector are located on an extendable boom. The instruments are deployed permanently after landing. This concept is similar to AFCRL development of a droppable package of weather instruments for remote measurements of temperature, pressure, humidity, and wind.

Selection of a sonic anemometer and an aluminum oxide hygrometer for the meteorology package is discussed in Section 9 of appendix D. A pressure sensor similar to one of the 830 series of the Rosemount Engineering Company is the preferred choice. For the temperature measurement a sensor similar to the Rosemount Model 152T is recommended, with modifications to reduce radiative effects. Requirements for special housings for the temperature, pressure, and humidity sensors will be determined by environmental testing under simulated Mars surface atmospheric conditions.

**Soil composition:** As specified in the science requirements, the Surveyor alpha scatter spectrometer experiment was assumed for purposes of study. Figure 67 gives two views of this instrument. Specific information on the instrument is reported in tables 12 and 13.

Subsystem characteristics. - Figure 69 shows the power profile for the science subsystem. The power demand levels are shown for the first 50 hr after landing. The total energy requirement is 205 W-h.

Table 12 is a summary of the science instruments, identifying measurement parameters against science mission objectives and corresponding instruments. Other instrument parameters identified include period of operation, special mounting requirements, sampling rate, data bits per sample, power, weight, and volume.

Table 15 is a detailed weight statement for the science subsystem. Locations are given for the instruments and deployment considerations. Total science equipment weight is 102.8 lb.



FOV 25.4°  
8.2 lines/degree

Example of Imaging at a Resolution  
Approximating 0.1°/TV Line



FOV 6.4°  
94 lines/degree

Example of Imaging at a Resolution  
Approximating 0.01°/TV Line

Figure 65.- Examples of Surveyor I Photography for Visualizing Imaging Resolution Requirements

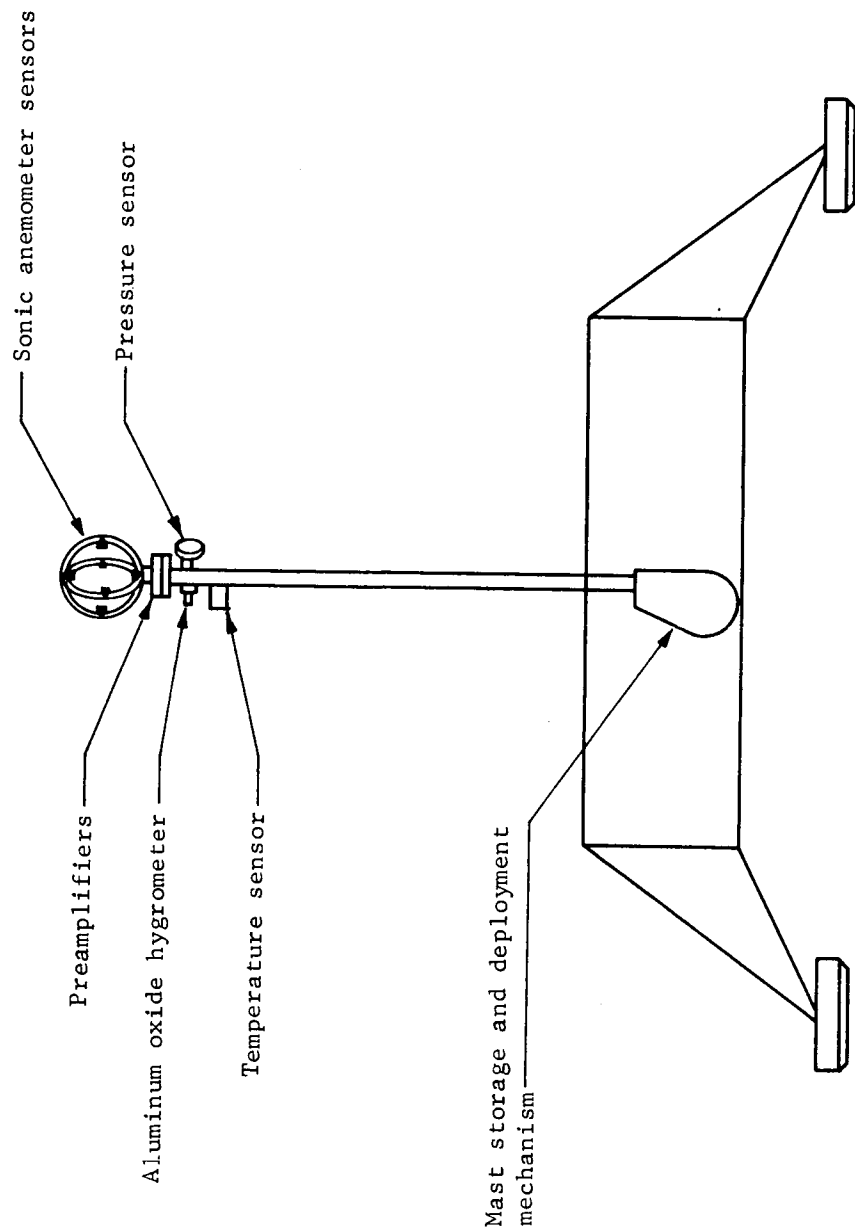
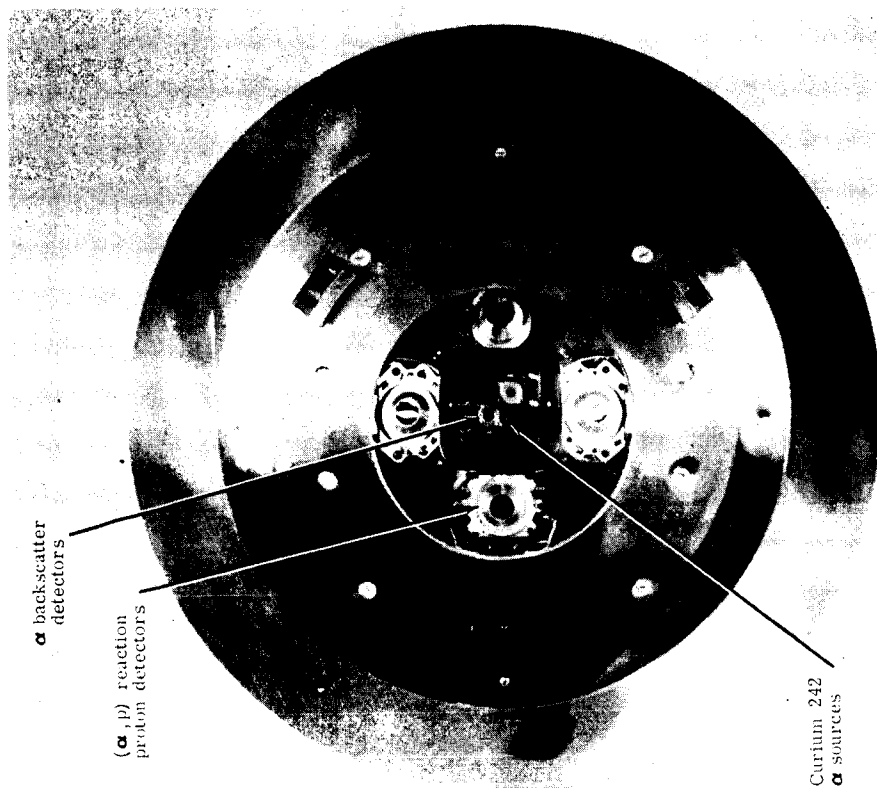


Figure 66.- Meteorology Package Concept



"Mars Eye" View of the Array of Sources and Detectors

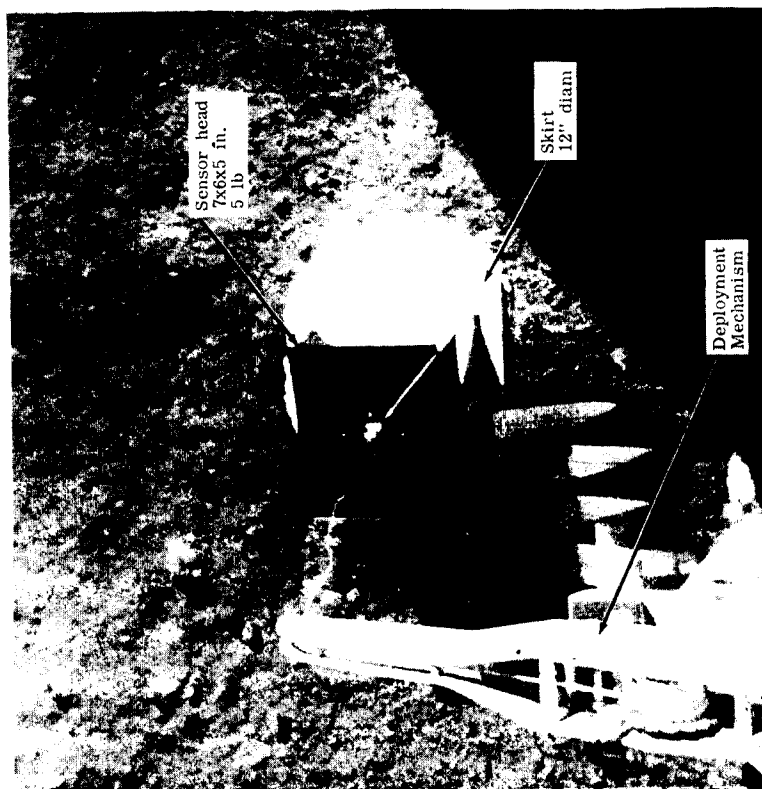


Image of the  $\alpha$ -Scatter Spectrometer in Operating Position on the Lunar Surface

Figure 67.- Surveyor V Alpha Scattering Instrument

TABLE 12.- SCIENCE INSTRUMENT SUMMARY, 1973

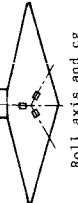

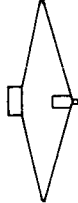

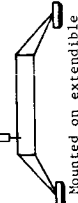


Objective	Parameter	Instrument	Mounting requirement	Period of operation	Sampling Rate	Data bits/sample	Weight, lb	Volume, in. <sup>3</sup>	Power, w
Atmospheric composition and vertical structure	Density from drag deceleration	Accelerometer triad <sup>a</sup>	 Roll axis and cg	From start of entry to parachute deployment	5 per sec	24	1.5	18	3.0
	Density from stagnation point pressure	Stagnation pressure transducer <sup>a</sup>	 In nose of aeroshell with sensor exposure to environment	Transition flow thru release of aeroshell	5 per sec	16	2.0	23	3.0
	Temperature	Total temperature sensor <sup>a</sup>		At velocities below M3	5 per sec	8	1.4	15	1.0
	Composition and density	Open ion source mass spectrometer <sup>b,c</sup>	 Located in nose of aeroshell with ion source exposed ahead of aeroshell	During molecular flow and pressure range 10 <sup>-5</sup> thru 5 x 10 <sup>-4</sup> mb	1 per sec	9.0 x 10 <sup>2</sup>	6.8	360	10.0
	Pressure	Ambient pressure transducer <sup>a</sup>	 Low-altitude, low-velocity descent atmospheric instrument mounted on a lander with forward-facing exposed probes	During terminal descent (below 5 kw)	5 per sec	8	1.0	12	3.0
	Temperature	Ambient temperature transducer <sup>a</sup>			5 per sec	8	1.2	14	1.0
	Humidity	Aluminum oxide hygrometer <sup>a,d,e</sup>			1 per sec	8	1.2	16	2.0
	Composition	Double focusing mass spectrometer <sup>b</sup>			1 per 3 sec	1.0 x 10 <sup>3</sup>	8.0	320	8.0
	Surface imagery	Facsimile camera <sup>f</sup> thru j	 Mounted on extendible boom		4 low-resolution pictures 25°x70° 4 high-resolution pictures 5°x5°	1.02 x 10 <sup>7</sup>	10.0	340	15.0
	Pressure variation with time	Stretched-diaphragm transducer <sup>a</sup>	 Mounted on extendible boom	On the surface	1 per hr (10 repeat signals)	80	1.5	16	1.5
Meteorology	Temperature variation with time	Platinum resistance transducer <sup>a</sup>			1 per hr (10 repeat signals)	80	1.2	14	1.0
	Humidity	Aluminum oxide hygrometer <sup>a,d,e,k</sup>	Meteorology instruments mounted as a package on an extendible boom		1 per hr (10 repeat signals)	80	1.2	16	2.0
	Wind	Sonic anemometer <sup>k</sup> thru m			1 per hr	1 x 10 <sup>2</sup>	3.0	370	2.0
	Soil composition	Alpha back-scatter spectrometer <sup>n</sup>	 Mounted below and deployed to the surface		1 sample	1 x 10 <sup>5</sup>	13.0	250	2.5

TABLE 12.- SCIENCE INSTRUMENT SUMMARY - Concluded

- <sup>a</sup>Wolfert, L. G.: Selection of Instruments for Measurement of Atmospheric Structures of the Martian Atmosphere. ED-22-6-102, Martin Marietta Corporation, Denver, Colorado, June 1967.
- <sup>b</sup>Wolfert, L. G.: Selection of Instruments for Measurement of Composition of the Martian Atmosphere. ED-22-6-103, Martin Marietta Corporation, Denver, Colorado, Sep. 1967.
- <sup>c</sup>Anon: Determining Composition of a Planetary Atmosphere at High Altitude Using an Open Ion Source Mass Spectrometer on an Entry Vehicle. PR-22-10-88, Martin Marietta Corporation, Denver, Colorado, Sep. 1967.
- <sup>d</sup>DelPico, J.; and Brousaides, F.: Performance of Thin Film Humidity Sensors, AFCRL-67-0543, Air Force Cambridge Research Laboratories, Oct. 1967.
- <sup>e</sup>Hilsenrath, E.: Private communication, Goddard Space Flight Center, May 1968.
- <sup>f</sup>Swale, J. F.; and D'Arcy, J.: Analysis of Selection of Preferred Design of Television Subsystems. PR-22-10-45, Martin Marietta Corporation, Denver, Colorado, Aug. 1967.
- <sup>g</sup>Swale, J. F.; D'Arcy, J.; and Demers, R.: Preliminary Design of Television Subsystems-Entry Television. PR-22-10-47, Martin Marietta Corporation, Denver, Colorado, Sep. 1967.
- <sup>h</sup>Champney, R.: Selection of Visual Imaging Instruments, Landed Science Subsystem. ED-22-6-105B, Martin Marietta Corporation, Denver, Colorado, Sep. 1967.
- <sup>i</sup>Tomkins, D. N.: The Mars Facsimile Camera. Presented to Society of Motion Picture and Television Engineers, Los Angeles, California, Oct. 1966.
- <sup>j</sup>Tomkins, D. N.: The Lunar Facsimile Camera. Presented to Institute of Electrical and Electronics Engineers, Boston, Massachusetts, May 1966.
- <sup>k</sup>Magee, R.: Selection of Instruments for Atmospheric Measurements. ED-22-6-106, Martin Marietta Corporation, Denver, Colorado, Sep. 1967.
- <sup>l</sup>Peirce, R. M.; and Bisberg, A.: Application of Pulse Techniques to Sonic Anemometry. Given at the ISA Conference in Boston, Massachusetts, June 3, 1968, to be published in the transactions, (Peirce, Air Force Cambridge Research Laboratories, Bisberg, Cambridge Systems, Inc.), Jan. 1968.
- <sup>m</sup>Bisberg, A.; et al.: The Sonic Anemometer, A New Instrument for Wind Measurement. Technical Report, Cambridge Systems, Inc., Aug. 1967.
- <sup>n</sup>Ridgeway, M. M.: Selection of Instruments for Surface Composition and Atmospheric Composition Measurements. ED-22-6-107-a, Martin Marietta Corporation, Denver, Colorado, Sep. 1967.

TABLE 13.- EQUIPMENT STATUS

Equipment item	Present status			Major problem areas in qualification
	Feasibility demonstrated	Development in progress	Modification of developed equipment	
Accelerometer triad		X	Bell Aerosystems model VII preferred. More than 500 units flown satisfactorily in missiles and satellites. Tests after 8-hr exposure to 135°C showed no serious degradation.	Complete present work of qualifying for the sterilization environment.
Stagnation pressure transducer		X	Rosemount Engineering Co. model 830BA, or equivalent.	Modification of present models to resist sterilization. Present sensitivity ranges are adequate.
Total temperature sensor		X	Rosemount model series 103, or equivalent.	Modification of present models to increase sensitivity, provide redundant sensing elements, and change radiation shields.
Open ion source mass spectrometer	X Use of the repelling potential analyzer for particle mass discrimination demonstrated on Explorer satellite. Use of a calibrated ion source for relating the sample to the undisturbed ambient atmosphere proven by rocket <i>sonde</i> experiments in Earth's atmosphere.			Optimizing the design of the ion source geometry and voltage control circuitry for sensitivity and resolution in analysis of neutral number densities.
Ambient pressure transducer		X	Rosemount model 830BA, or equivalent.	Modification of present model to increase sensitivity.
Ambient temperature transducer		X	Rosemount model series 103, or equivalent.	Modification to increase sensitivity of thermocouples and change radiation shields.
Hygrometer	X Aluminum oxide sensor approach preferred. See section 9 of Appendix D for discussion of this choice.			Development of a sensor having characteristics that are stable with time and insensitive to the range of atmospheric environment expected during terminal descent.
Double focusing mass spectrometer		X Development now in progress at JPL on a low-altitude mass spectrometer for determining atmosphere composition.		Design of an inlet system for sampling from the ambient atmosphere.

TABLE 13.- EQUIPMENT STATUS - Concluded

Equipment item	Present status			Major problem areas in qualification
	Feasibility demonstrated	Development in progress	Modification of developed equipment	
Facsimile camera		X Performance demonstrated for a fixed parameter instrument. Development of a variable parameter instrument being planned		Qualification of variable parameter instrument for the sterilization environment.
Meteorology package: Pressure transducer			X Rosemount model 830BA, or equivalent.	Modification of present model to increase sensitivity.
Temperature transducer			X Rosemount model 152T, or equivalent.	Modification of present model to reduce radiative heating or cooling effects on the sensor.
Hygrometer	X Aluminum oxide sensor. Same as for terminal descent instrument.			Same as listed above for the terminal descent instrument.
Anemometer	X Sonic anemometer preferred. See section 9 of Appendix D for discussion of this choice.			Redesign of present transducers to improve energy coupling with atmosphere gas at Mars surface pressures.
Alpha scatter spectrometer			X Surveyor instrument assumed. Modification of this instrument to include X-ray detectors and associated electronic channels is being planned.	Sterilization of lithium drifted silicon detectors. Development of new alpha particle sources with longer half life than Cm 242. Modification of present mechanical and electronic design to include X-ray detector channels.
Tape recorder				Magnetic bead wear from use of sterilizable metal tape. Tape transport drives. Lubrication.
Data storage	X See section 5 of Appendix D for discussion of state of the art for sterilizable tape recorders.			



Table 13 assesses instrument status. This information is based on a literature study together with visits to a number of universities, National Bureau of Standards, Naval Research Laboratory, Air Force Cambridge Laboratories, Jet Propulsion Laboratory, Goddard Space Flight Center, Langley Research Center, and the leading instrument vendors. Instruments requiring major development are identified, by indicating the long lead time items. Instruments that have not demonstrated feasibility were excluded from serious consideration.

Functional block diagram. - The science subsystem block diagram is shown in figure 68. Major elements of the science subsystem are: entry science - ballistic phase; entry science - terminal descent phase; surface science; and the data automation system (DAS), including a magnetic tape recorder.

All data from instruments having 0 to 5 V analog output are routed to the telemetry subsystem main data encoder. This includes data from most of the instruments (excepting the two mass spectrometers) in the entry science subsystem and the data from the meteorology package in the surface science subsystem. Those instruments that require sequencing commands, clock pulses, data conditioning, or other specialized signal interfaces are routed to the DAS and are either put into storage in the magnetic tape recorder or may be routed directly to the main data encoder.

The DAS performs the functions of instrument sequencing, digital data multiplexing, data formatting, identification and coding, and data sequencing into tape storage and from tape storage. The DAS provides power distribution (power ON, power OFF) to the science instruments from which it sequences data. The DAS central data processor compresses the alpha scatter spectrometer data. The instrument sequencer in the DAS generates and provides basic clock pulses required by the science instruments for data scanning and digitizing. The sequencer is basically a fixed program sequencer in terms of the majority of routines and sequencing commands; however, a certain amount of updating capability is possible to select optional camera pointing angles.

Data output from the science instruments are 8-bit binary coded words except for imaging data which are 6-bit coded words.

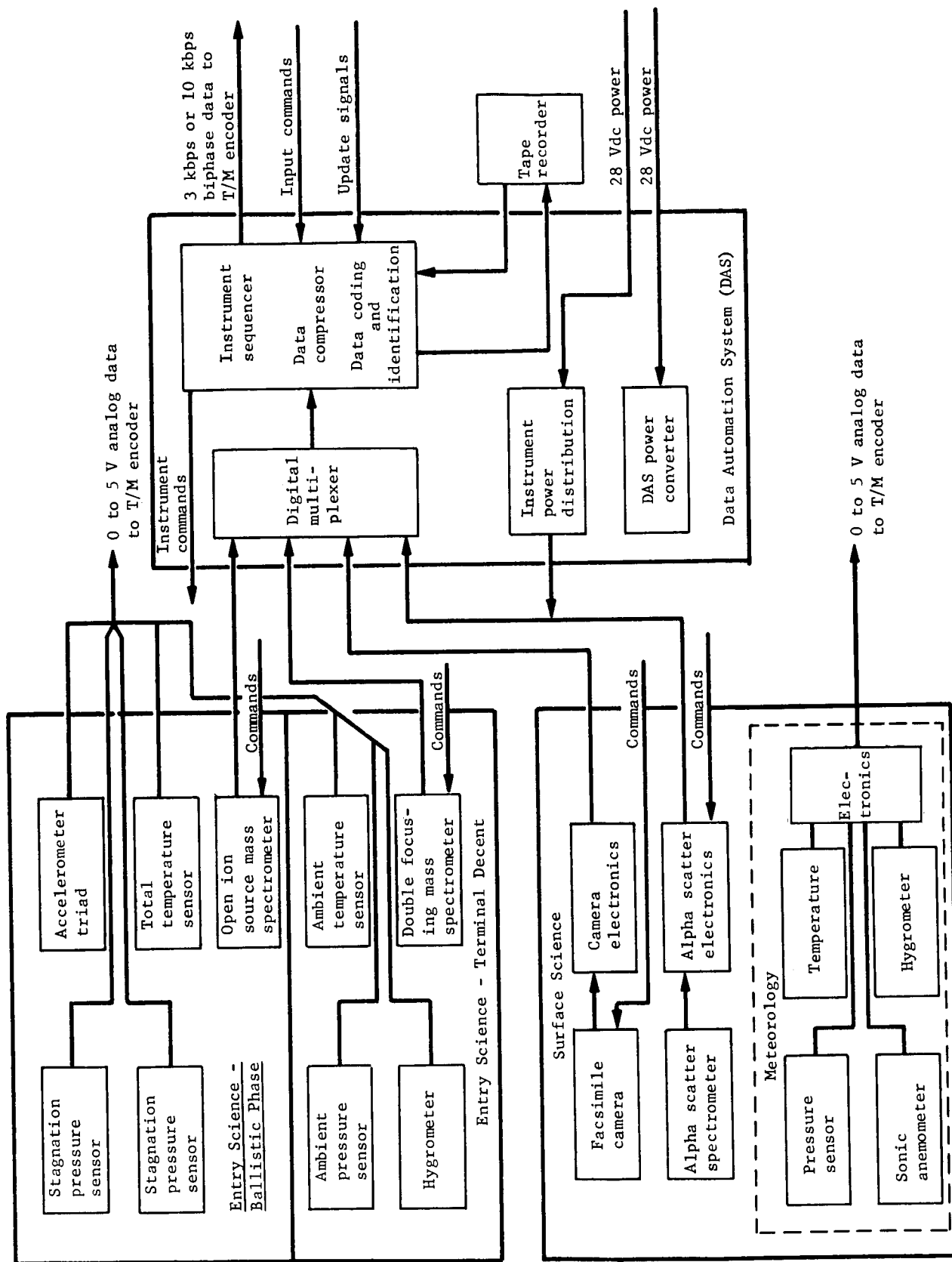
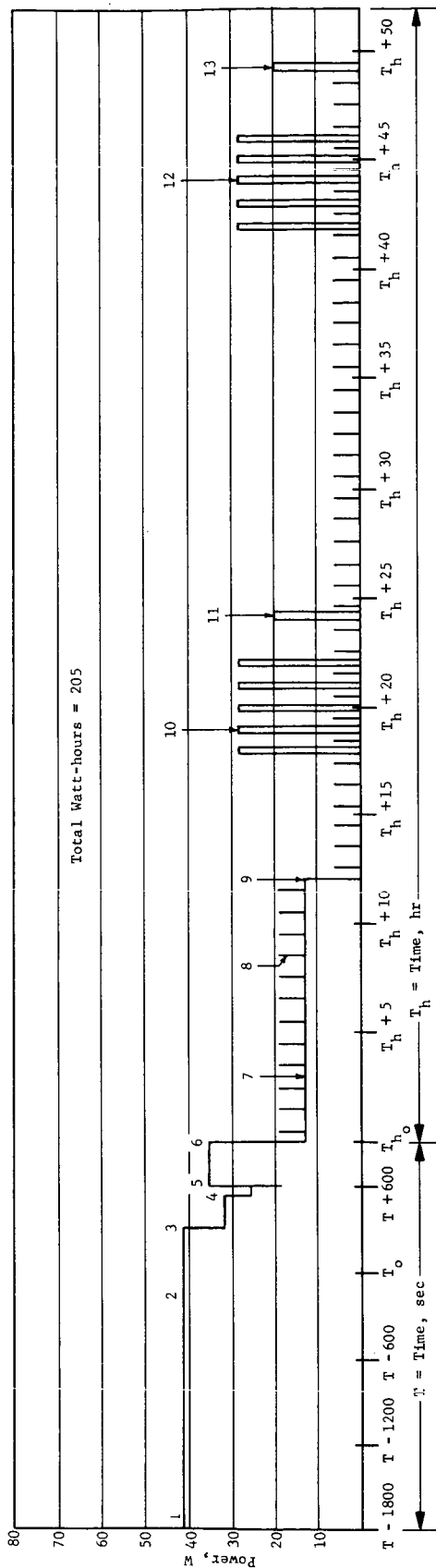


Figure 68.- Science Subsystem Functional Block Diagram



- Note: 1. All entry science instruments are turned on for warmup. Following warmup, engineering and calibration data are taken. Instruments remain turned on and OIS mass spectrometer measurement data start at a pressure of  $10^{-13}$  mb.
2.  $T_o$  = altitude at  $800 \times 10^3$  ft.
3. Ambient pressure = approximately  $5 \times 10^{-4}$  mb, a shock wave has begun to form and the OIS mass spectrometer has been saturated and its function has been completed.
4. At 16,000 ft altitude the parachute is deployed, the aeroshell including the high-altitude science instruments is ejected and terminal descent data are taken, including operation of the double focusing mass spectrometer.
5. Landing has been completed, the double focusing mass spectrometer is turned off, the landed science instruments (imaging, meteorology, and alpha backscattering) are deployed and operating. One set of data is also taken from the lander-mounted entry instruments (temperature, pressure, and humidity) as a redundancy and as a calibration reference.
6. At the end of the transmission opportunity all science instruments are turned off except the alpha backscatter instrument. All data generated up to this point have been transmitted to the orbiter. The science data automation system is left on, and preprogrammed periodic meteorology and photographic sequence is initiated.
7. The alpha backscattering instrument is generating data for a preprogrammed 12-hr period. These data are collected in a solid core buffer storage and periodically recorded on the on-board tape recorder.
8. Meteorology data are taken once every hour according to a preprogrammed schedule. This continues for 49 hr.
9. The alpha backscattering experiment has been completed and the science data automation system is turned off.
10. Five preprogrammed photographs are taken during optimum lighting conditions and stored in the tape recorder.
11. All data generated after (6) are transmitted to the orbiter during this second transmission opportunity.
12. Five preprogrammed photographs are taken during optimum lighting conditions and stored in the tape recorder.
13. All data generated after (11) are transmitted to the orbiter during this third transmission opportunity.

Figure 69.- Power Profile and Sequence Description

Data output from the DAS to the telemetry subsystem is biphase level coded data taken from the DAS at the rate of 3000 bps during the immediate postlanded phase and 10 000 bps during subsequent relay link transmission opportunities.

The DAS interfaces with the guidance control computer, receiving the necessary discrete commands to initiate the different data gathering events and to receive update commands transmitted from earth.

Sequence of events: Table 14 presents the science sequence of events covering the entry phase and surface science over the first two diurnal cycles. The science sequences are broken up into five phases: capsule entry; initial postlanding; first diurnal cycle; second diurnal cycle; and extended operation. This breakdown is predicated by data transmission opportunities over the relay link. The number of imaging scenes is based on a minimum time period for data transmission for each opportunity and the rate of data transmission.

For extended operation beyond two days, only the meteorology package remains operative.

TABLE 14.- SCIENCE SEQUENCE OF EVENTS

I. Capsule entry phase			
Event	Capsule altitude, ft	Flight capsule event	Remarks
Turn on entry science for instrument warmup			Entry minus 30 minutes.
Initiate instrument calibration sequence			Entry minus 15 minutes.
Start entry science data collection, ballistic phase	800 000	Entry	Aeroshell mounted instruments plus c.g. mounted accelerometer.
Altitude data starts	200 000		Altitude marking radar data starts.
Total temperature measurement starts	100 000		Total temperature probe deployed, below Mach 3.
Start entry science data collection, terminal descent and landing phase	16 000	Parachute deployed and aeroshell separated	Data from lander mounted entry instruments during terminal descent.
Terminate entry science data collection	0	Touchdown	Lander on surface.
II. Posttouchdown phase - first 10-minute period			
Event	Data		Remarks
Initiate posttouchdown surface science sequences: Deploy facsimile camera Deploy meteorology package Apply power to instruments			Posttouchdown sequence commences immediately on landing to use fully the relay link transmission with the spacecraft.
Initiate facsimile camera data sequencing One set of data is taken from the lander-mounted entry instruments (pressure temperature humidity) for redundancy and as a calibration check.	One, 25° azimuth x 70° elevation scene resulting in $1.05 \times 10^6$ bits of data		Relay link data transmitted during this phase is $1.08 \times 10^6$ bits, based upon 6 minutes of transmission time at 3 kbs rate.

TABLE 14.- SCIENCE SEQUENCE OF EVENTS - Continued

Event	Data	Remarks
Meteorology package data; pressure, temperature, moisture, and anemometer data.	Approximately 100 samples of each instrument will be obtained and transmitted for a total of 4000 bits.	These data are transmitted over the relay link with the imaging data.
Deploy alpha scatter spectrometer detector to the surface.	Approximately $1 \times 10^6$ bits of data gathered over a 12-hr period and put into storage.	No alpha scatter data (other than engineering data) transmitted during this mission phase. Data are gathered and stored for transmission during the next relay link opportunity.
III. Landed phase - first 24-hr period		
Event	Data	Remarks
Meteorology package data gathering continues on a periodic basis throughout this phase.	Data sampled once per hour throughout the day and night resulting in $10^3$ bits of data over a 24-hr period.	Data are gathered and stored; data is transmitted at the next relay link opportunity, touchdown plus 24.6 hr at 10 kbs rate; total data link capability during this period is about $7.2 \times 10^6$ bits.
Facsimile camera image sequencing (first day after landing) scenes are spread throughout daylight period for maximum contrast variation.	Three $25^\circ$ azimuth x $70^\circ$ elevation scenes, and two $5^\circ$ x $5^\circ$ scenes are taken at intervals spread throughout the morning and afternoon period; total data: $6.15 \times 10^6$ bits.	Imaging data are gathered and stored in the magnetic tape recorder. Data are transmitted over the relay link at touchdown plus 24.6 hr at 10 kbs rate.
Alpha scatter spectrometer operation and data gathering continues on an uninterrupted basis for 12 hr after touchdown.	$10^6$ bits of alpha and proton data taken over a 12-hr period are compressed to $10^5$ bits of data.	Soil composition data are stored in the magnetic tape recorder for transmission over the relay link along with meteorology and imaging data.

TABLE 14.- SCIENCE SEQUENCE OF EVENTS - Concluded

Event	Data	Remarks
Engineering data are sequenced from the science instruments at periods determined by the telemetry subsystem and the science instrument operation period.	50x10 <sup>3</sup> bits of data over the 24-hr period.	
IV. Landed phase - second 24-hr period		
Event	Data	Remarks
Meteorology package data. (Same as 1st 24-hr period)		
Facsimile camera image sequencing (second day after landing); scenes are spread throughout the daylight period for maximum contrast variation.	Two 25° azimuth x 70° elevation scenes and three 5° x 5° scenes are taken at intervals spread throughout the morning and afternoon period; total data: 6.6x10 <sup>6</sup> bits.	Imaging data are gathered and stored in the magnetic tape recorder. Data are transmitted over the relay link at 10 kbs rate; total data link capability in this period is about 7.2x10 <sup>6</sup> bits.
Engineering data are sequenced from the science instruments at periods determined by the telemetry subsystem and the science instrument operation.	50x10 <sup>3</sup> bits of data over the 24-hr period.	Engineering data are multiplexed with the science data for relay transmission.

TABLE 15.- DETAILED WEIGHT STATEMENT

Instrument	Quantity	Weight, lb	Location
<u>Entry science - ballistic phase</u>			
<u>Aeroshell-mounted</u>			
Stagnation pressure transducer	2	2.0	These instruments are located on a mounting plate at the apex of the aeroshell
Total temperature sensor and electronics	1	1.4	
Open ion source mass spectrometer	1	6.8	
Housing, baseplate, and cover	1	4.0	
Pressure inlet port	1	0.8	
Total temperature cover and tube	1	0.8	
Cabling, connectors, and brackets		<u>2.2</u>	Center of gravity of capsule system
Total in aeroshell		18.0	
<u>Lander-mounted</u>			
Accelerometer triad	1	1.5	
Accelerometers mounting bracket		0.5	
Quick disconnect and cables to lander		<u>1.1</u>	
Total in lander		3.1	These instruments are mounted on the lander
Total entry science - ballistic phase		21.1	
<u>Entry science - terminal descent &amp; landing phase</u>			
Ambient pressure transducer	1	1.0	
Ambient temperature transducer	1	1.2	
Hygrometer, sensor, and electronics	1	1.2	
Double focusing mass spectrometer	1	8.0	These instruments are mounted on the lander with the camera extended upward on a telescoping mast.
Instrument seals or covers		1.5	
Instrument mounting brackets	1	1.5	
Instrument cabling and connectors		<u>1.4</u>	
Total		15.8	
<u>Landed science</u>			
<u>Imagery</u>			
Facsimile camera	1	6.0	These instruments are mounted on the lander with the camera extended upward on a telescoping mast.
Camera electronics	1	3.0	
Camera deployment mast	1	6.0	
Cabling and brackets		<u>1.5</u>	
Total		16.5	



TABLE 15.- DETAILED WEIGHT STATEMENT - Concluded

Instrument	Quantity	Weight, lb	Location
Meteorology			
Meteorology package	1	1.0	These instruments are mounted on the lander and deployed upward on an extendable mast.
Pressure transducer	1	1.5	
Temperature transducer	1	1.2	
Hygrometer, sensor, and electronics	1	1.2	
Sonic anemometer and electronics	1	3.0	
Deployment mast	1	3.0	These instruments are located on the lander with the spectrometer detector head deployed to the surface of the planet.
Cablings and brackets	1	1.8	
Total		<u>12.7</u>	
Soil composition			
Alpha scatter spectrometer	1	6.0	
Deployable head	1	2.0	The data automation system is located on the lander in the thermally controlled science equipment compartment.
Lander interface module	1	3.5	
Deployment mechanism	1	1.0	
Cables and brackets		<u>12.5</u>	
Total			
Data automation system			
Data automation package			
Digital multiplexers		0.5	The data automation system is located on the lander in the thermally controlled science equipment compartment.
Instrument sequencer		1.0	
Data compressor		5.0	
Identification code generator		0.5	
DAS power converter		1.0	
Instrument power distribution		1.0	
Package		2.2	
Internal cable		.8	
Total		<u>12.0</u>	
Magnetic tape recorder		11.0	
Cablings and supports		1.2	
Total		<u>24.2</u>	
Total Science Weight		102.8	

## Structures and Mechanisms

Functional description. - The structure and mechanisms subsystem consists of the sterilization canister, 8.5-ft diameter aeroshell, deorbit module, aerodynamic decelerator, lander structure, and related mechanisms. These major components are shown in figure 70, sheets 1 and 2.

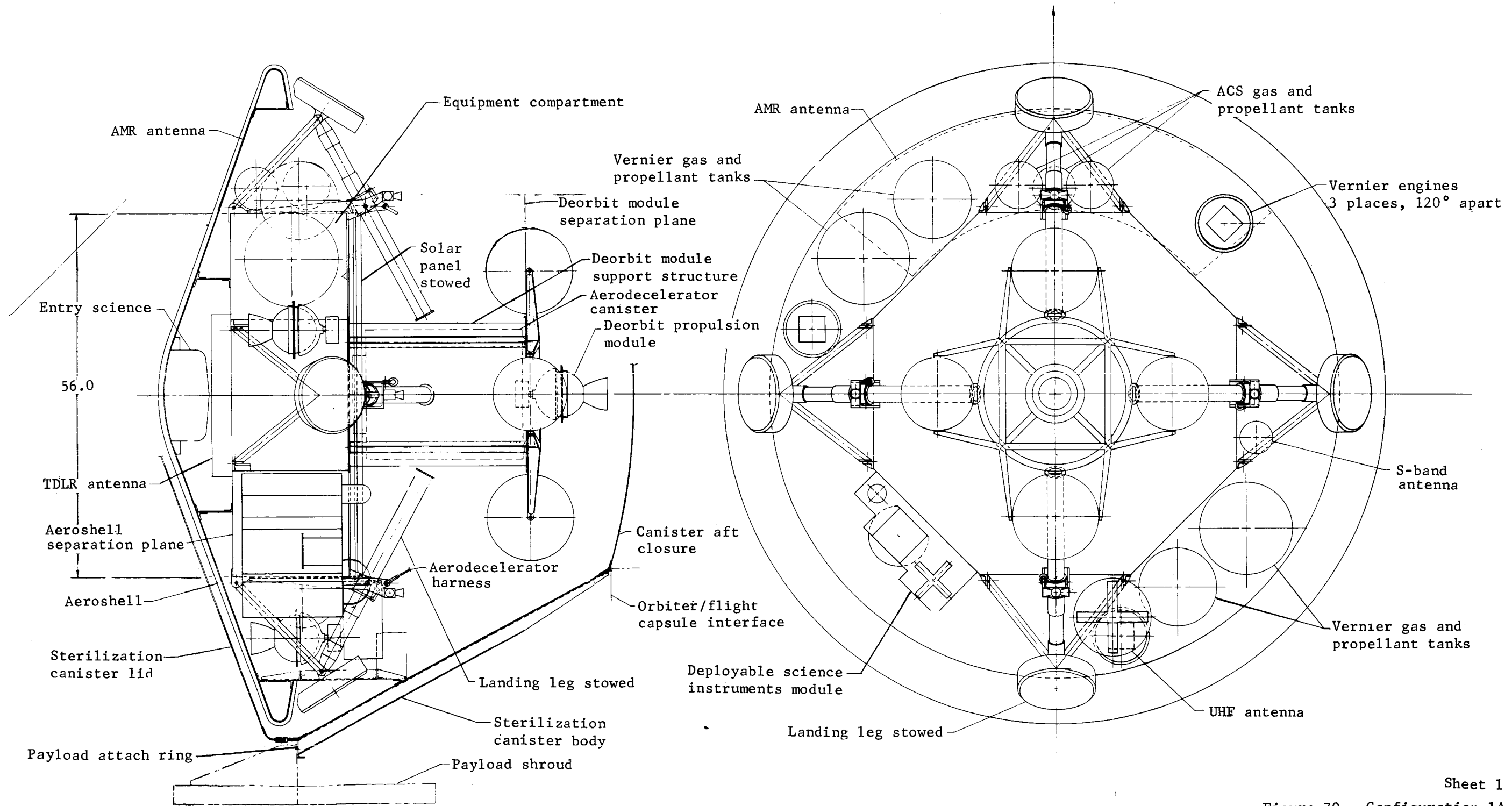
Sterilization canister (fig. 70, sheet 1): The sterilization canister is composed of three parts:

- 1) A pressuretight, conical body;
- 2) A pressuretight titanium aft closure attached to the canister body at the field splice to the orbiter adapter;
- 3) A pressuretight lid constructed of 0.005 titanium covers the capsule aeroshell, and attaches to the canister body near the spacecraft/launch vehicle separation plane.

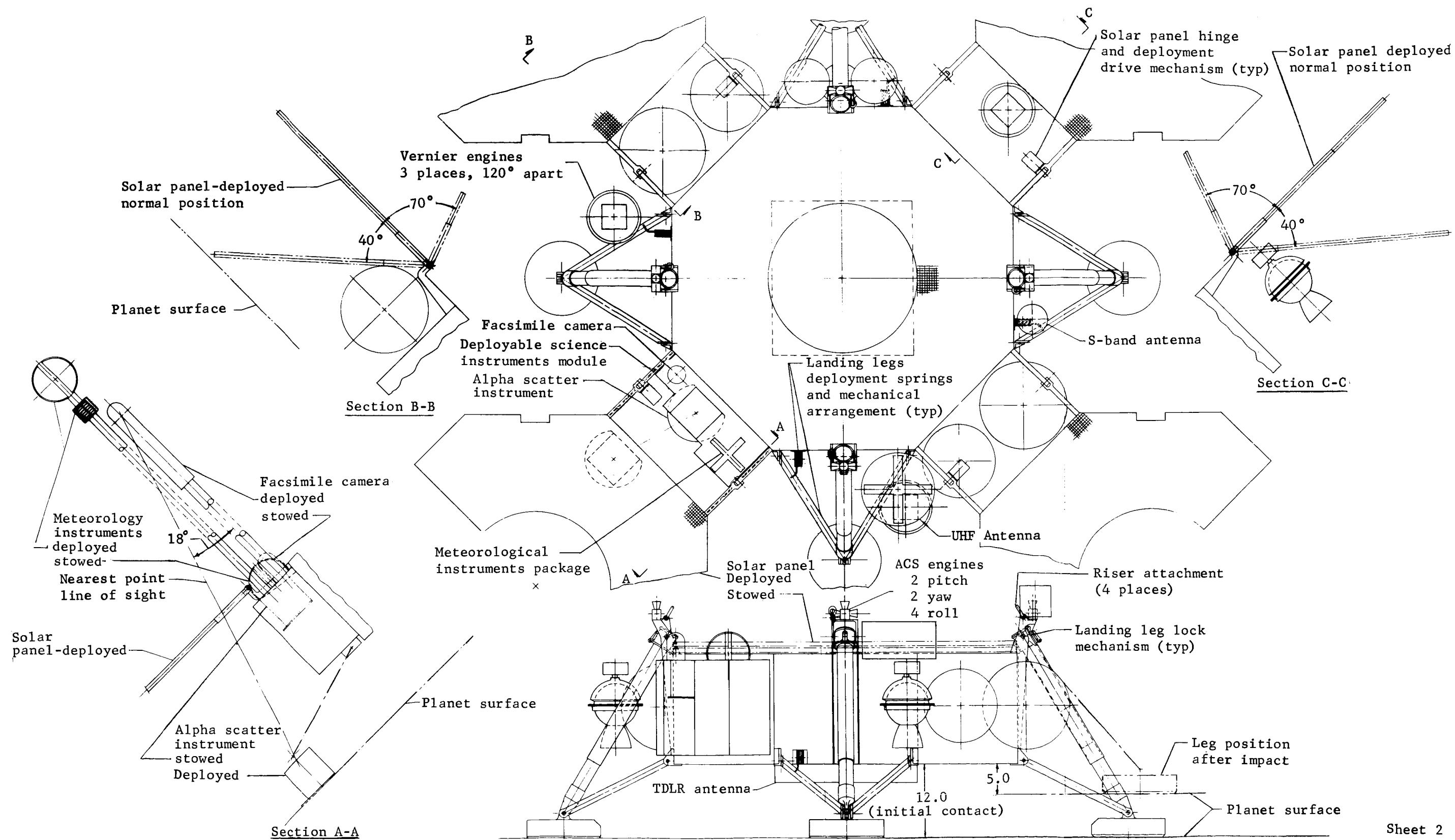
The canister body is an all-aluminum, longitudinally stiffened, truncated cone that supports the flight capsule and orbiter in the launch vehicle. The orbiter is supported on the canister body through a cylindrical adapter. The flight capsule is supported by the canister body at a ring-frame located near the spacecraft/launch vehicle separation plane, with an inflight separation interface.

Aeroshell (fig. 70, sheet 1): The aeroshell is an all-aluminum frame stabilized semimonocoque 8.5-ft base diameter, 70° half angle cone. Previous studies showed a beryllium skin with aluminum frames to be 35% lighter than an all-aluminum structure. However, because of cost and current technology considerations, aluminum is selected.

Protection against entry heating is provided by SLA 561 ablator. A large ring-frame is used to attach the lander structure to the aeroshell. The aeroshell/lander separation system consists of pyrotechnic devices at this ring-frame that are fired after the capsule has reached subsonic velocity following parachute deployment. The higher ballistic coefficient of the released aeroshell, as compared with that of the lander on the parachute, will separate the aeroshell from the lander.



Sheet 1  
Figure 70.- Configuration 1A



Sheet 2  
Figure 70.- Concluded

A second large ring-frame near the outer edge of the aeroshell supports the entry vehicle on the capsule adapter. An entry science package is located at the apex of the aeroshell cone. The AMR antenna is located between the aeroshell skin structure and the ablator.

Deorbit module (fig. 70, sheet 1): The deorbit module structure consists of a magnesium forged beam assembly on which the deorbit motor, titanium propellant and gas tanks, and other components of the deorbit propulsion system are symmetrically mounted about the vehicle roll axis. A forging was selected because of the many structural attachments required for the propellant and pressurant tanks and the engine. The module is attached at four points to an aluminum structural cylinder that also houses the aerodynamic decelerator system. The deorbit module is jettisoned after the deorbit velocity increment has been achieved. The spent module is staged by pyrotechnic release devices and separation spring assemblies.

Aerodynamic decelerator (fig. 70, sheet 1): The 65-ft-diameter aerodecelerator and deployment mortar are housed in an aluminum cylindrical container inside the deorbit module support structure. A ring of shock attenuating crushable honeycomb material installed between the mortar and the lander structure reduces the mortar reaction loads on the lander structure.

A harness assembly is used to attach the aerodecelerator to the lander structure. Four straps attach to the lander at the main strut support fittings at the upper edges of the octagonal lander body. From these points, the straps run radially inboard into the mortar housing where they terminate at a common ring. This ring, located beneath the packed aerodecelerator, is also the common attachment point for the aerodecelerator risers. Auxiliary harness straps, attached to the four main harness straps, tie to the deorbit module support structure. When the aerodecelerator is separated from the lander, by release of the harness at the four attachment points, the deorbit module support and spent mortar are also separated from the lander and carried away with aerodecelerator.

Lander structure and related mechanisms (fig. 70, sheets 1 and 2): The lander body is an all-aluminum octagonal welded truss structure designed to support and protect the various deorbit, entry, deceleration, and landing subsystems, as well as the landed science subsystem. Four leg assemblies attenuate the landing shock loads and support the lander during surface operations. The

octagonal structural shape provides a simple geometrical interface with the four legs of the lander. The lander body is sized to provide a reasonable packaging density for landed equipment and at the same time keep the landed c.g. height low with respect to landing leg radius for landing impact stability. A preliminary analysis indicates that this configuration will land stably on slopes to  $32^\circ$ , assuming combinations of landing velocities to 25 fps vertical and 10 fps horizontal, and initial contact of at least two of the four landing legs on the surface. The aluminum truss structure was selected to provide a lightweight, easily assemblable system. A previous study indicates that a welded magnesium or titanium truss could save up to 30% of the lander structural weight. Further studies on lander truss materials should be made before the final selection.

The octagonal lander body houses the science, telemetry, power and pyrotechnics, and guidance and control subsystem components not externally located. Equipment that must function after landing is enclosed within a 3-in. insulation blanket and is thermally conditioned by isotope heaters. These heaters are located on the sides of the octagon, and when extended, dissipate heat to the surrounding environment; when retracted they add heat to the surviving equipment compartment. The lander body has a gross volume of 27 cu ft and a net volume of approximately 18 cu ft after accounting for insulation and structure. The equipment packaging density is approximately 32 lb/cu ft.

The lander leg assemblies are aluminum tripod structures, incorporating two pivoted fixed length struts and a shock attenuating strut, held in the retracted position while the aeroshell is attached by latching the main strut at the pivoted guide bushing. After the aeroshell is jettisoned, the main strut is released, allowing torsion springs to rotate the secondary struts to extend the leg assembly into the landing position. The main strut is then again latched to the pivoted guide bushing. The attenuator in the main strut is a Surveyor-type fluid spring. This attenuator was selected because of its self-leveling features. With solar panels exposed to ground winds, all four legs should be in contact with the surface to stabilize the lander for imaging. The fluid spring system will need to be qualified for long-time exposure to vacuum conditions.

The disc-shaped lander foot is held in the retracted position by a latching device that is released by relative rotation between the main and secondary struts. A torsion spring then rotates the foot into the landing attitude. Due to the proximity

of the lander feet to the outside diameter of the aeroshell, ablative material applied to the bottom and side of the foot protects it against expected high heating rates during entry. The lander foot could be stowed inside the aeroshell by increasing the aeroshell diameter to  $10\frac{1}{2}$  ft or by designing a more complex leg folding mechanism.

A total of  $44.4 \text{ ft}^2$  of solar array area is provided on the lander. A fixed area of  $14.8 \text{ ft}^2$  is located on the top of the lander body, and the remaining  $29.6 \text{ ft}^2$  is provided on four identical deployable panels stowed in two layers above the lander body. They are rotated into position after landing by four reversible solenoid stepper motors with attached gearboxes. The panels may be driven to any position between  $70^\circ$  above and  $40^\circ$  below the lander horizontal plane to maximize solar cell output. Panel hinge lines are located outboard of the lander body to provide a space between the inboard edge of the deployed panels and the lander to allow deployment of several landed science experiments, and to increase the maximum permissible inclination angle of the panels to  $40^\circ$  below the horizontal.

Three vernier engines are located on supporting structures attached to the periphery of the octagon. To achieve  $120^\circ$  spacing of the engines, two engines are located relative to two lander leg assemblies so that thermal protection is required to keep the leg structure temperatures within design limits. The vernier engine propellant supply system, consisting of two propellant and two pressurization tanks and associated plumbing, is located on structure attached to the outside of the octagon.

The eight attitude control nozzles are mounted on extensions of the four fittings that support the main strut pivoted guide bushings. The ACS propellant supply system, consisting of one propellant and two gas tanks, is located outside the lander body adjacent to one of the lander leg assemblies.

The landed science module is located on one side of the octagon with all deployable devices located outside the lander body. Supporting equipment is located inside the body. The facsimile camera and weather station are erected through the gap between the solar panels and the lander body. This arrangement allows instrument mass deployment even though the solar panels fail to deploy. The alpha scatter spectrometer after being lowered to the surface is within view of the facsimile camera to verify proper sensor deployment (fig. 70, sheet 2).

The TDLR, uhf, and S-band antennas are mounted on the lander. The TDLR antenna is located on the underside of the lander body. Although it protrudes into the nominal 5-in. rock clearance space between the body and the planet surface, the antenna has a structure that will yield on contact with an obstruction. The uhf and S-band antennas are located to provide an unobstructed pattern.

### Propulsion

Landing. - The recommended landing propulsion subsystem, shown schematically in figure 71 is a pressure-fed monopropellant hydrazine system. The system is sized to provide the impulse required to remove the landing velocity increment and to provide pitch and yaw control during landing.

The three main engines have the capability of throttling over a 5:1 range to provide an initial thrust to weight (Mars) ratio of 3.9:1 and a final thrust to weight ratio of 0.8:1. Pitch and yaw control is obtained by differential throttling of the lander engines. Roll control is provided by the attitude control system. Parallel redundant throttle valves are included in each engine, and the mission can be successfully completed with one valve failure per engine.

With the failure of an engine valve, there is an associated loss in engine thrust of 5% due to the reduction in propellant flow rate produced in the increase of valve pressure drop.

Engine thrust during the landing phase of the mission is controlled by the guidance and control subsystem by monitoring valve position through a position feedback indicator on each throttle valve.

Pressurization is accomplished without gas regulation by blowdown of gaseous nitrogen from 500 to 167 psia. Squib-operated valves isolate the propellant and pressurant supplies before system activation, and the system is resealed after landing by squib-operated valves. Welded or brazed construction is used throughout the propulsion subsystem to minimize leakage. Two fuel tanks and two pressurant tanks are symmetrically located about the roll axis for balance.



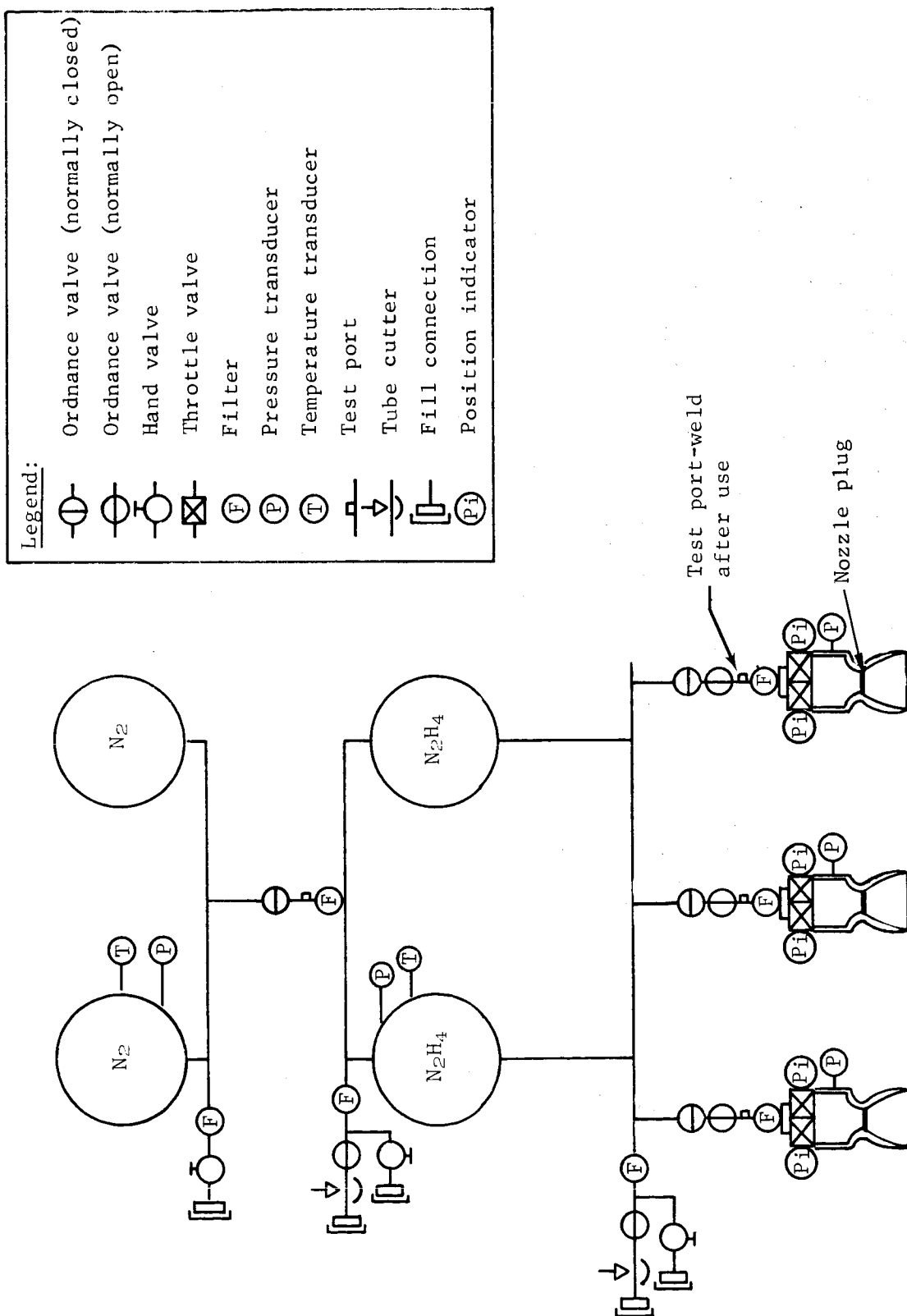


Figure 71.- Landing Propulsion System

The propellant load is sufficient to provide effective velocity increment of 690 fps to a vehicle with an initial landing phase weight of 1068 lb. Included in the propellant load is a 1% landing accuracy margin, a 1% contingency for minimum delivered specific impulse, and a 3% contingency for residual, or trapped propellant. Figure 72 is a schedule of propellant use.

Propellant tanks are sized to accommodate the propellant load and a 6% ullage volume to allow for propellant expansion due to temperature differentials. The tank material selected for the propellant and pressurant tanks is 6Al-4V titanium.

Hydrazine is assumed to be self-sterilizing. Thus, the propellant is loaded after the heat sterilization cycle to avoid unnecessary hazards during sterilization. Tube cutters are provided in the propellant fill and vent lines to allow separation from the sterilization canister. Separate unloading connections and valves are also provided to allow unloading in case of an abort. A filter is located at every penetration to the system to reduce the probability of contamination during fill operations. Filters are located downstream of all ordnance valves and upstream of the throttle valve inlets to prevent particulate contamination.

The sequence of events for the propulsion system is as follows:

- 1) The pressurant isolation valves are opened allowing  $\text{GN}_2$  to enter the propellant tanks;
- 2) While on the parachute, a signal is sent from the guidance and control system to the propellant isolation valves when the predetermined altitude and/or velocity have been achieved. Propellant is introduced to the engines with the throttle valves at minimum setting;
- 3) After engine operation has been verified and after 1.5 sec of operation on the parachute at minimum thrust, the lander is separated from the parachute and falls for approximately 3 sec at minimum thrust plus 10% operation until its flightpath intersects the terminal descent and landing trajectory;
- 4) Engine thrust command is then increased to 90% and the lander descends to near the planet surface;

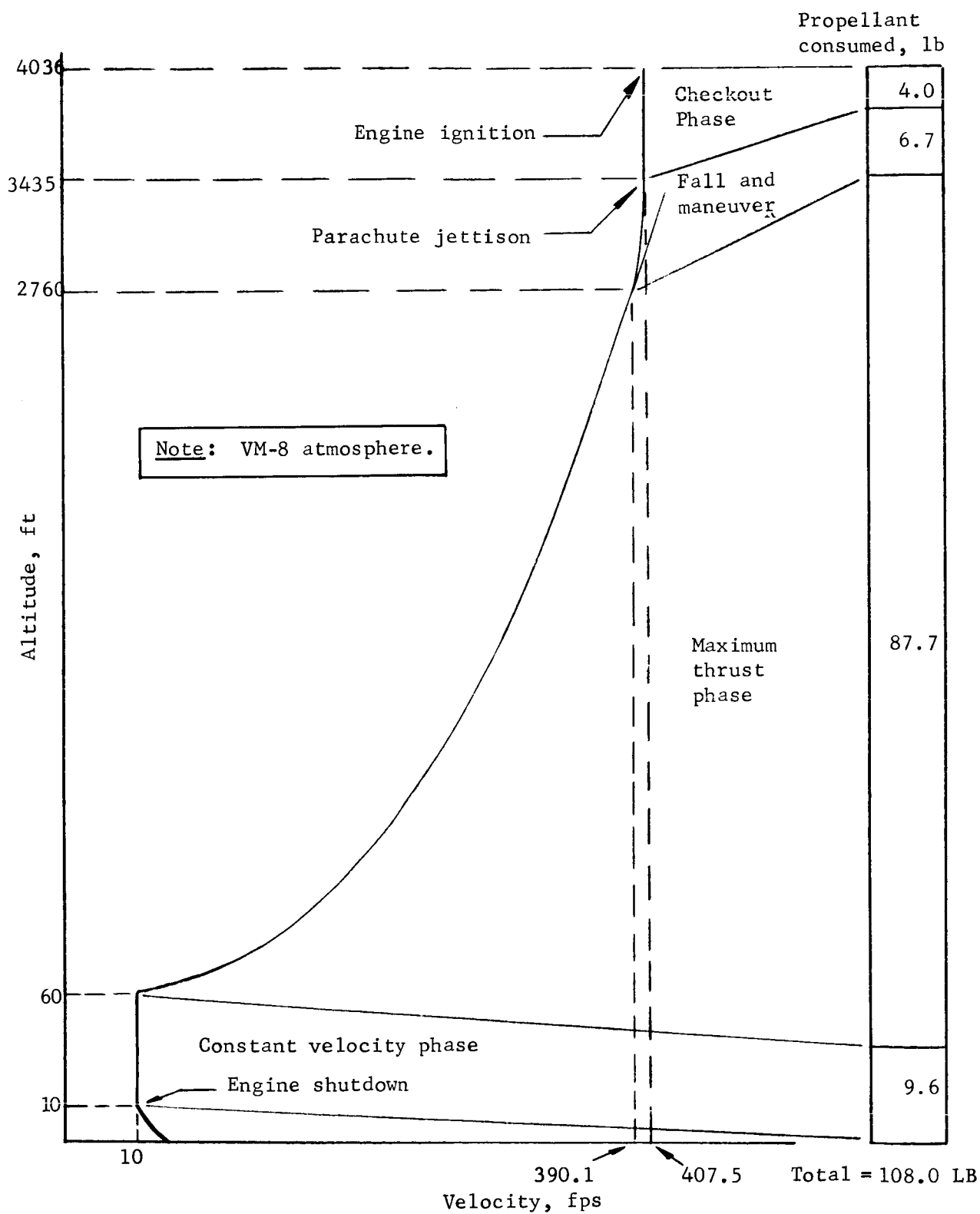


Figure 72.- Terminal Descent Profile and Propellant Utilization

- 5) At an altitude of 60 ft and a vertical velocity of 10 fps, the thrust is modulated to provide a constant velocity descent to an altitude of 10 ft;
- 6) At 10-ft altitude, the engines are shut down by closing the normally open ordnance valves located upstream of the throttle valves. This function seals the system and reduces the probability of surface contamination after landing.

Deorbit. - The deorbit propulsion subsystem is similar to the vernier system in that it is monopropellant and employs blowdown pressurization. The system is shown schematically in figure 73. The major differences between the deorbit and vernier systems are the following:

- 1) A single engine with no throttle valve provides deorbit thrust;
- 2) Control is accomplished by the attitude control system during the deorbit burn;
- 3) A propellant position control device is required for deorbit. This is a screen trap that uses surface tension forces to control propellant position before deorbit engine ignition.

The overall system characteristics are shown in table 16.

Attitude control system. - The attitude control system, shown in figure 74, is a monopropellant system that uses Shell 405 catalyst to decompose hydrazine to produce thrust. It has eight thrusters -- four in roll, two in pitch, and two in yaw. Pressurization is accomplished without gas regulation by blowdown of gaseous nitrogen at a blowdown ratio of 1.5:1.

Ordnance-operated valves isolate the propellant and pressurant supplies before system activation and reseal the system at vernier engine shutdown.

The attitude control system provides the thrust necessary to maintain capsule attitude, orient the capsule for the deorbit firing and atmospheric entry, damp aeroshell oscillations at entry, remove all disturbing torques produced by structural and thrust vector offsets during deorbit, and remove roll torques during vernier operation. Attitude control system characteristics and a schedule of propellant utilization are shown in table 17.

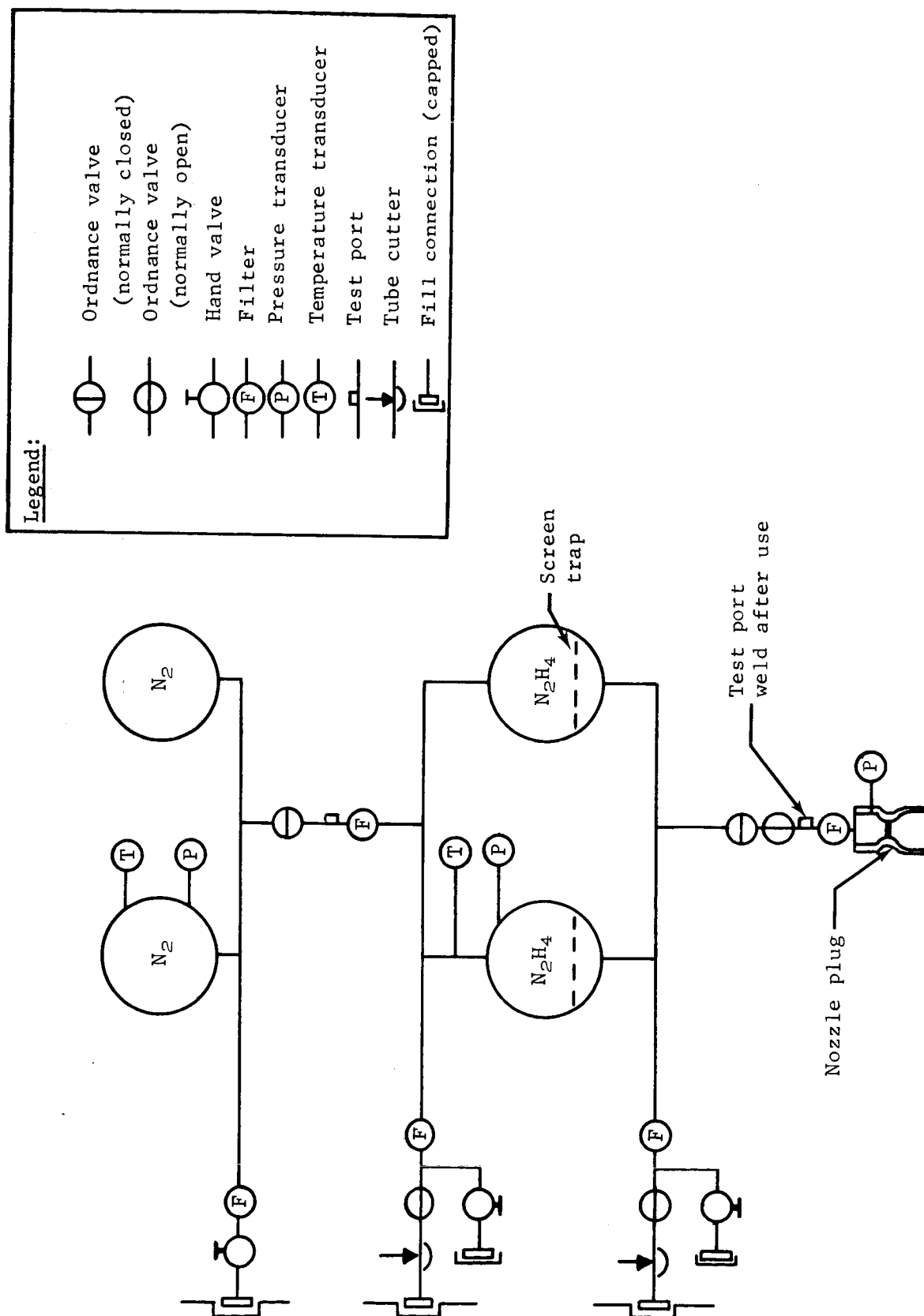


Figure 73.- Deorbit Propulsion System

TABLE 16.- PROPULSION SUBSYSTEM CHARACTERISTICS

Parameter	Deorbit	Landing
Total impulse available, lb-sec . . . . .	18,582	24,084
Maximum thrust per engine, lb . . . . .	510	510
Average delivered specific impulse, sec . . . . .	228	223
Maximum chamber pressure, psia . . . . .	300	300
Nozzle expansion ratio. . . . .	20:1	20:1
Throttling ratio. . . . .	----	5:1
Fuel weight, usable, lb . . . . .	81.5	108
Fuel weight, trapped, lb. . . . .	4.1	5.5
Pressurant weight, lb . . . . .	2.2	3.0
Engine weight, total, lb . . . . .	15.1	45.3
Fuel tank weight (2), total, lb . . . . .	4.8	5.8
Pressurant tank weight, (2), total, lb. . . . .	3.0	4.1
Component and line weight, lb . . . . .	13.0	18.3
Engine mount and tank support weight, lb. . . . .	16.7	27.7
Total weight, lb . . . . .	140.4	217.7
Volume per fuel tank, cu ft . . . . .	0.71	0.97
Outside diameter of fuel tank, in. . . . .	13.4	14.7
Volume per pressurant tank, cu ft . . . . .	0.43	0.58
Outside diameter of pressurant tank, in. . . . .	11.3	12.4
Engine exit diameter, in. . . . .	5.1	5.1
Operating temperature range, °F (min./max.) . . . . .	40/80	40/80
Storage temperature range, °F (min./max.) . . . . .	40/100	40/100
Fuel tank operating pressure range at 60°F (max./min.), psia . . . . .	500/167	500/167
Pressurant tank operating pressure range at 60°F (max./min.), psia . . . . .	505/167	505/167

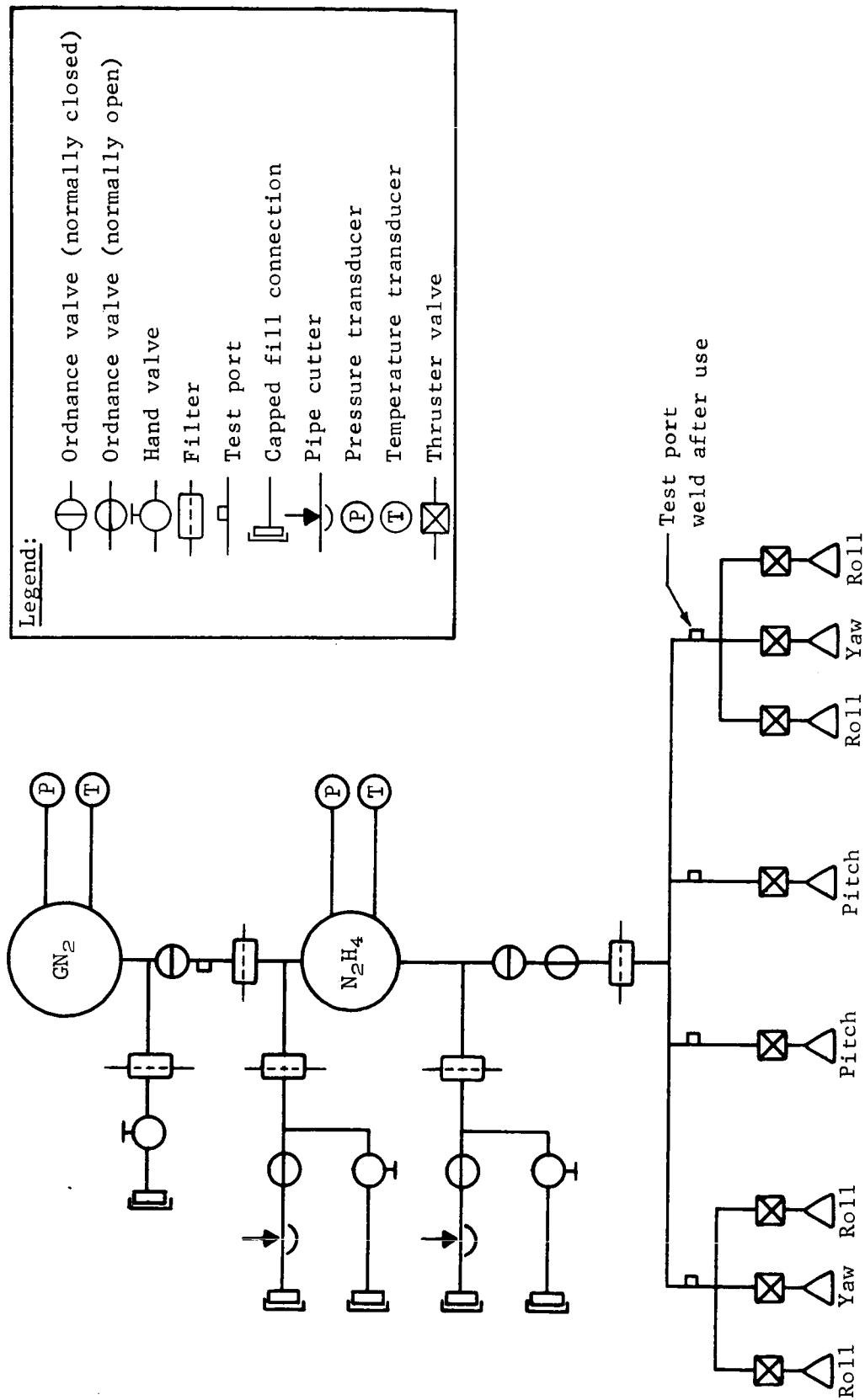


Figure 74.- Attitude Control System

TABLE 17.- ATTITUDE CONTROL SYSTEM

Characteristics		Propellant schedule	
Measurement	Thrust, lb <sub>f</sub>	Item	Propellant consumed, lb
Pitch and yaw Roll	3.7 to 2.8 2.2 to 1.7	Separate from spacecraft	.02
Measurement	Minimum impulse bit, lb-sec		
Pitch and yaw Roll	.056 .034		
Minimum pulse width	35 ms	Maneuver for deorbit thrust	.03
Measurement	Pressurization, psia	Deorbit thrust attitude hold	1.17
Initial GN <sub>2</sub> pressure	360	Coast, 8 hr	.07
Final GN <sub>2</sub> pressure	240		
Blowdown ratio	1.5:1	Maneuver for entry	.03
Items	Weight, lb	Coast, 4 min	.02
N <sub>2</sub> H <sub>4</sub>	5.10	Rate damping at entry	.61
Required	2.45		
Margin	2.45	Landing roll hold	.42
Trapped	0.20		
N <sub>2</sub> H <sub>4</sub> tank	0.6	Total required	2.45
GN <sub>2</sub>	.4		
GN <sub>2</sub> tank	1.0	Contingency (100%)	2.45
Thrusters	6.4		
Components, lines	13.0	Total loaded	4.90
Supports	8.7		
Total	35.2		



The data presented in figure 75 summarize the development status of the propulsion subsystems. The engine shows less development experience than any other component. However, throttling and a thrust level of 300 lb<sub>f</sub> have been demonstrated by 3 manufacturers, and technology funding for a throttlable monopropellant engine of a thrust level applicable to the mission mode designs will be available this year and engine development will proceed. Squibs have been successfully sterilized. However, development of a cartridge for the Mars '73 capsule is required.

### Guidance and Control

The guidance and control subsystem controls vehicle attitude, velocity, and sequencing from orbiter separation to landing on the Mars surface. After landing the subsystem continues its sequencing function. Attitude is controlled by sending steering signals to the attitude control thrusters or the terminal descent vernier engines, which provide control torques to orient the vehicle attitude in conformance with stored or computed information. Velocity is controlled during the terminal descent phase by controlling vernier engine thrust according to a stored range profile. At 10 ft above the planet surface the engines are shut down, allowing a free fall to the surface. Discrete sequencing is provided for all phases of flight. Timed discrettes are based on key inflight events such as separation, entry, and altitude marks, to initiate required sequences. In addition, surface science sequencing is provided by this subsystem. Information on sequencing and stored attitude can be updated through the command system before separation.

Secondary functions of the subsystem are to provide altitude and acceleration data to supplement entry science data.

The subsystem consists of the inertial measurement unit (IMU), guidance and control computer (GCC), altitude measuring radar (AMR), terminal descent and landing radar (TDLR), and the Phase II sequencer (fig. 76).

Inertial measurement unit. - The IMU measures changes in attitude and velocity with gyros and accelerometers operating in a strapdown mode. Three two-axis gyros provide parallel redundancy for angular measurements about the three vehicle axes. Failure detection logic is provided to remove a faulty gyro from the control loop. The gyros operate in a pulse rebalance mode to sense vehicle angular rates. The pulses, which represent incremental changes in attitude, are supplied to the GCC.

Requirement	Feasibility demonstrated	Development	Qualified	Flight	
Engine					ETO is only problem
Sterilizable catalyst	///				20:1 demonstrated
Throttling	///				IRC RFP
thrust level	///				2.5 lb <sub>f</sub> common
ACS thrusters	///	///			
Propellant feed and pressurization					
Blowdown	///	///	///	///	
Ordnance valves	///	///	///	///	
Filtration	///	///	///	///	
Screen trap	///	///	///	///	Titan III Transtage
Tankage	///	///	///	///	
Squibs (sterilizable)	///				Some sterilized by Martin Marietta under JPL contract 951709

Figure 75.-Development Status

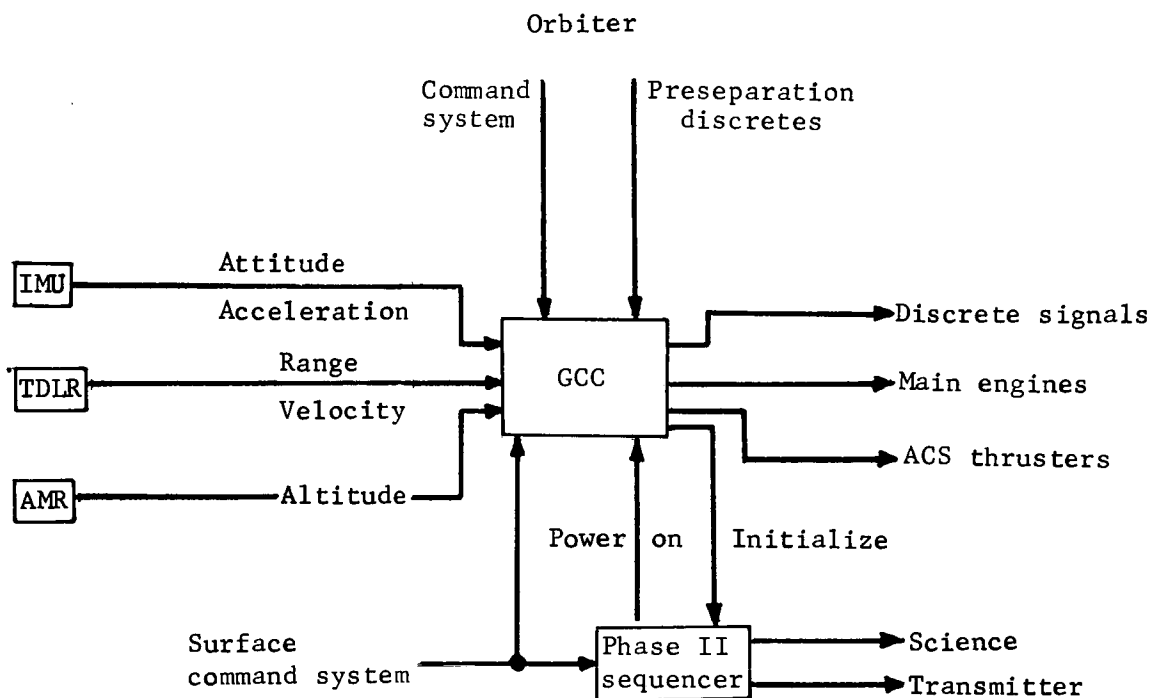


Figure 76.- Guidance and Control  
Subsystem Block Diagram

Three accelerometers are arranged so that the sensing axes are splayed symmetrically about the vehicle thrust axis. Analyses have shown that the longitudinal acceleration is at least an order of magnitude larger than lateral accelerations. Therefore, this arrangement will provide gross redundancy along the thrust axis in addition to the lateral measurements. Failure detection is accomplished in the GCC by software that will ignore the faulty signals, in addition to opening the lateral acceleration loops. Each accelerometer is a single-axis, force rebalance device with self-contained rebalance servo and digital output electronics.

The IMU is operated from orbiter separation to landing. Figure 77 shows the IMU block diagram.

Altitude measuring radar. - The AMR measures altitude with respect to the planet surface for entry science correlation and for initiation of such altitude-sensitive functions as parachute and aeroshell deployment. The operating range of the AMR is from 200 000 ft to aeroshell separation.

The AMR uses all-solid-state radar and time measuring circuits. Transmission frequency is 500 MHz. The associated antenna is a 2 x 6 element dipole array mounted on the aeroshell. It is designed with a microstrip circuit to conform to the aeroshell contour.

Terminal descent and landing radar. - The TDLR provides velocity and range information during the terminal descent phase of flight. Of the five beams provided, four are splayed symmetrically about the vehicle thrust axis and a single beam is directed along the thrust axis. Each beam supplies the required velocity and range information to the GCC. Valid information from three of the five beams is required for system operation. The GCC will detect and reject a faulty signal. Gross failure detection such as sensing the receiver AGC level will permit two failures of the TDLR.

The antenna is a five-beam planar array fabricated from thin-wall aluminum. An interleaved design permits full use of the total aperture by all of the beams to give a beamwidth of 3°. Crosstalk between beams is avoided by using separate transmitting frequencies.

The TDLR operating range is from 10 000 ft to 10 ft above the planet surface. A block diagram of the TDLR is illustrated in figure 78.

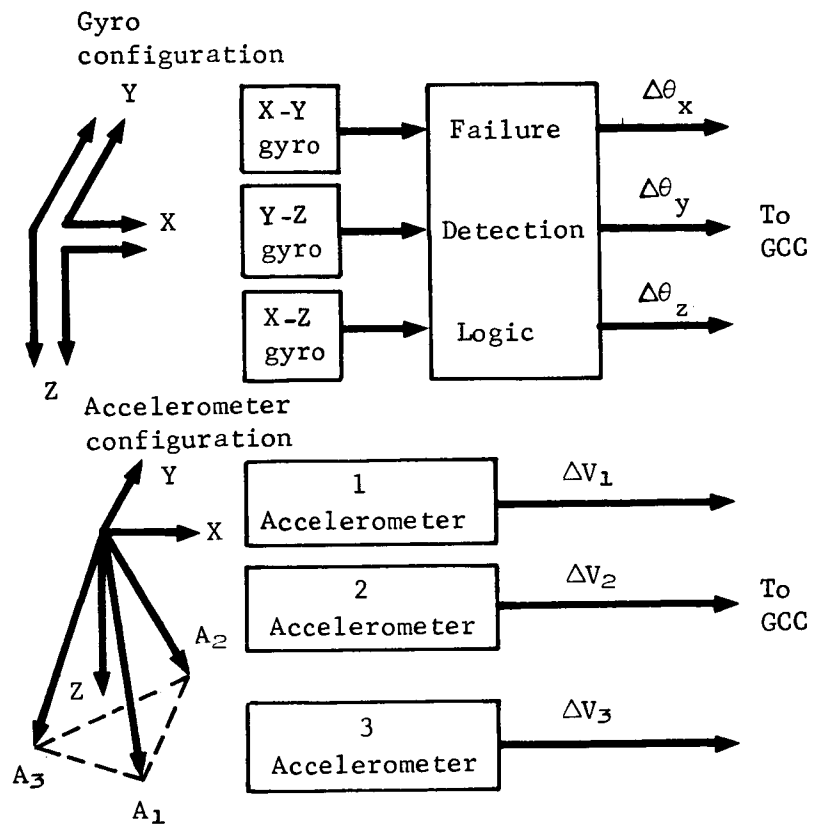


Figure 77.- Inertial Measurement Unit Block Diagram

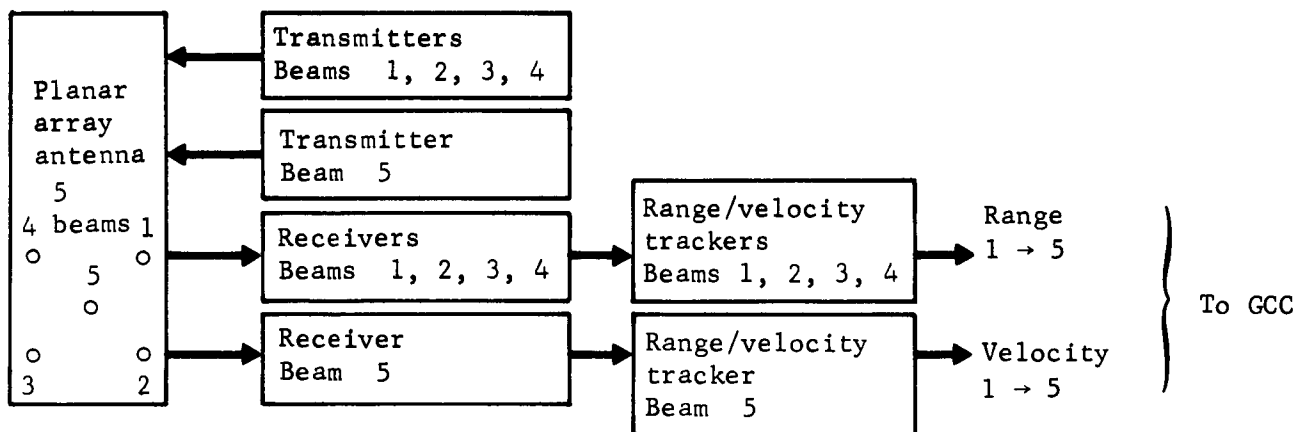


Figure 78.- Terminal Descent and Landing Radar Block Diagram

Guidance and control computer. - The GCC is a 4096 word, 18-bit-per-word general-purpose digital computer with an add time of 8  $\mu$ sec and a memory cycle time of 4  $\mu$ sec. Mission functional requirements and modes of operation are listed in table 18. In addition to its computation and sequencing functions, the GCC has the capability for command decoding required during the preseparation update and landed science sequencing update periods. The GCC mission extends from separation to the end of Phase I sequencing after landing. At this time the Phase II sequencer is initiated and the GCC is powered down.

TABLE 18.- GCC FUNCTIONAL REQUIREMENTS

1. Computational	3. Sequencing
Attitude hold	Inflight sequencing
Deorbit guidance	Landed science sequencing (Phase I)
Rate damp	
Terminal descent and landing	4. Checkout
Inertial navigation	Redundancy tests
2. Command decoding	
Preseparation update	
Phase I sequencing update	

Upon receiving discrete commands from earth via the Phase II sequencer, the GCC will power up, receive new landed science sequencing information, and issue the command sequence of events.

The GCC contains all the input/output circuitry required to interface with the subsystem components, the command subsystem, propulsion, telemetry, and the electrical power/pyro subsystem.

Phase II sequencer. - The Phase II sequencer controls the weather station operation and the transmission of this information through the issuance of timed discrete signals. Sequencing is initiated by the GCC when the Phase I sequence is complete. The sequencer block diagram is illustrated in figure 79. A command decoder is also provided to translate coded commands into discretes for resetting the sequencer, controlling power to the GCC, and reinitiating a Phase I sequence.

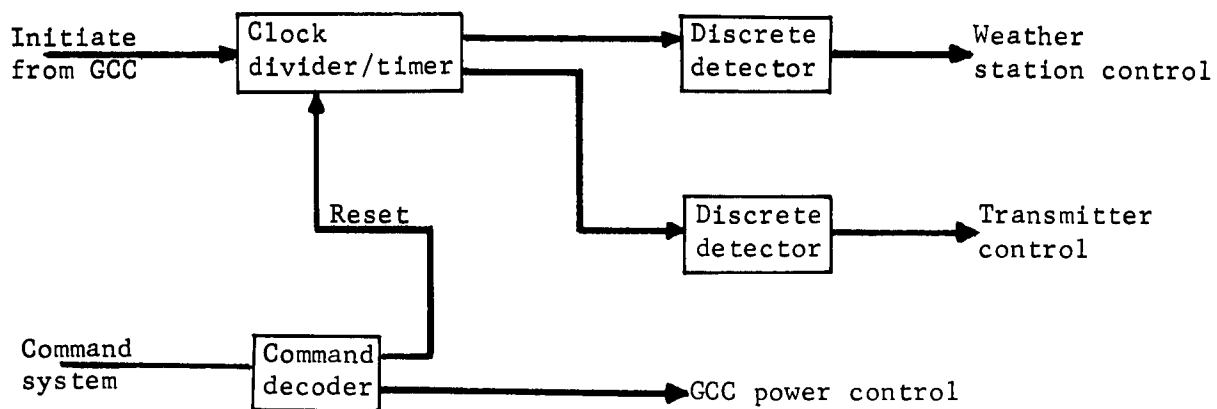


Figure 79.- Phase II Sequencer Block Diagram



Characteristics. - Physical characteristics of the guidance and control subsystem are summarized in table 19. A summary of subsystem performance is given in table 20. Corresponding component performance is summarized in table 21.

Development status. - Guidance and control system components are presently in a developmental status because of sterilization compatibility and mission-peculiar requirements. Sterilization affects the IMU more than the other components because of the electromechanical gyros and accelerometers in the IMU. Existing and contemplated JPL and NASA contracts promise to reduce uncertainty in the development of sterilizable inertial components. Sterilization appears to be a realizable design constraint for such electronic equipment as the digital computer, radar altimeter, landing radar, and Phase II sequencer. Some early development work may be needed on the radar altimeter antenna that is an integral part of the aeroshell. The preferred landing radar is a Bessel sideband configuration that requires development. A prototype development and aircraft flight test of a dual mode (Bessel/ICW) radar is under contract by LRC at the present time.

TABLE 19.- G&C WEIGHT, POWER, AND VOLUME<sup>a</sup>

Component	Weight, lb	Volume, cu in.	Power, W
IMU	22	1050	39
GCC w/I-O	42	1150	41
AMR w/antenna	12	556	7
TDLR w/antenna	33	2925	46
Phase II sequencer	3	300	3
<sup>a</sup> Does not include packaging, supports, and cabling. These items are tabulated in the sequential weight statement, Appendix D, section 1.			

TABLE 20.- SUBSYSTEM PERFORMANCE ( $3\sigma$ )

Flight phase	Errors, mrad		
	Roll	Pitch	Yaw
Preseparation	20	20	20
Separation and coast	6.2	6.3	2.8
Entry	37	37	37
Touchdown	Landing velocity, fps		
	Vertical	Horizontal	
	18 $\pm$ 5	0 $\pm$ 5	

TABLE 21.- COMPONENT PERFORMANCE

Component	Error source	Error ( $3\sigma$ )
Gyro	Alignment	2 mrad
	Gyro drift	0.22 deg/hr
	Torquer scale factor	0.17%
Accelerometer	Bias	$400 \times 10^{-6}$ Earth g
	Scale factor	0.2%
AMR	Alignment	0.34 mrad
	Altitude measurement	$\pm 120$ ft
TDLR	Range measurement	3% or 5 ft, whichever is greater
	Velocity measurement	4.5% or 3 fps, whichever is greater

## TELECOMMUNICATIONS

The telecommunications subsystem functional block diagram is shown in figure 80. This subsystem is composed of a telemetry subsystem and a communication subsystem plus the required support equipment installed on the orbiter.

Telemetry. - The telemetry subsystem provides the data management functions of processing all lander engineering data and analog science data and accepting serial digital data from the science data automation system. All data processed by the telemetry subsystem are sent to the communication subsystem as either a single serial digital data stream or a five-bit parallel data train. Elements of the telemetry subsystem are: main data encoder; 50 000-bit static storage; signal conditioner; status monitor data encoder; sterilization/battery measurement multiplexer, main transducer power supply; and status monitor power supply. The function of the power supplies within this subsystem is to provide regulated power at 5 Vdc to the transducers for all data modes. During interplanetary cruise, flight capsule data are processed by the status monitor data encoder and transmitted to the orbiter telemetry subsystem over hardwire. The sterilization/battery measurement multiplexer is used for ground checkout during terminal heat sterilization and during the subsequent formation charging of batteries. This element has a hardwire interface with flight capsule OSE. The static storage provides for delay and recovery of data collected through the communication blackout period and the storage of postland science and engineering data when real-time communication with the orbiter is not available. Flight capsule separation and entry data, and terminal descent and landing data are processed by the main data encoder. Signals not compatible with the data multiplexer input requirements are conditioned in the telemetry subsystem. Data rates and data modes are controlled by discrete logic inputs from the guidance and control computer.

The telemetry subsystem is capable of handling 120 analog, 70 discrete, and 10 digital channels for the entry phase of the mission, and 40 analog, 10 discrete, and 2 digital channels in the postland phase. It is designed using state-of-the art, space-proved technology. Predicted weight, power, and volume for the telemetry subsystem are shown in table 22. Packaging and internal cabling are not included in these estimates, but are included in the sequential weight statement.

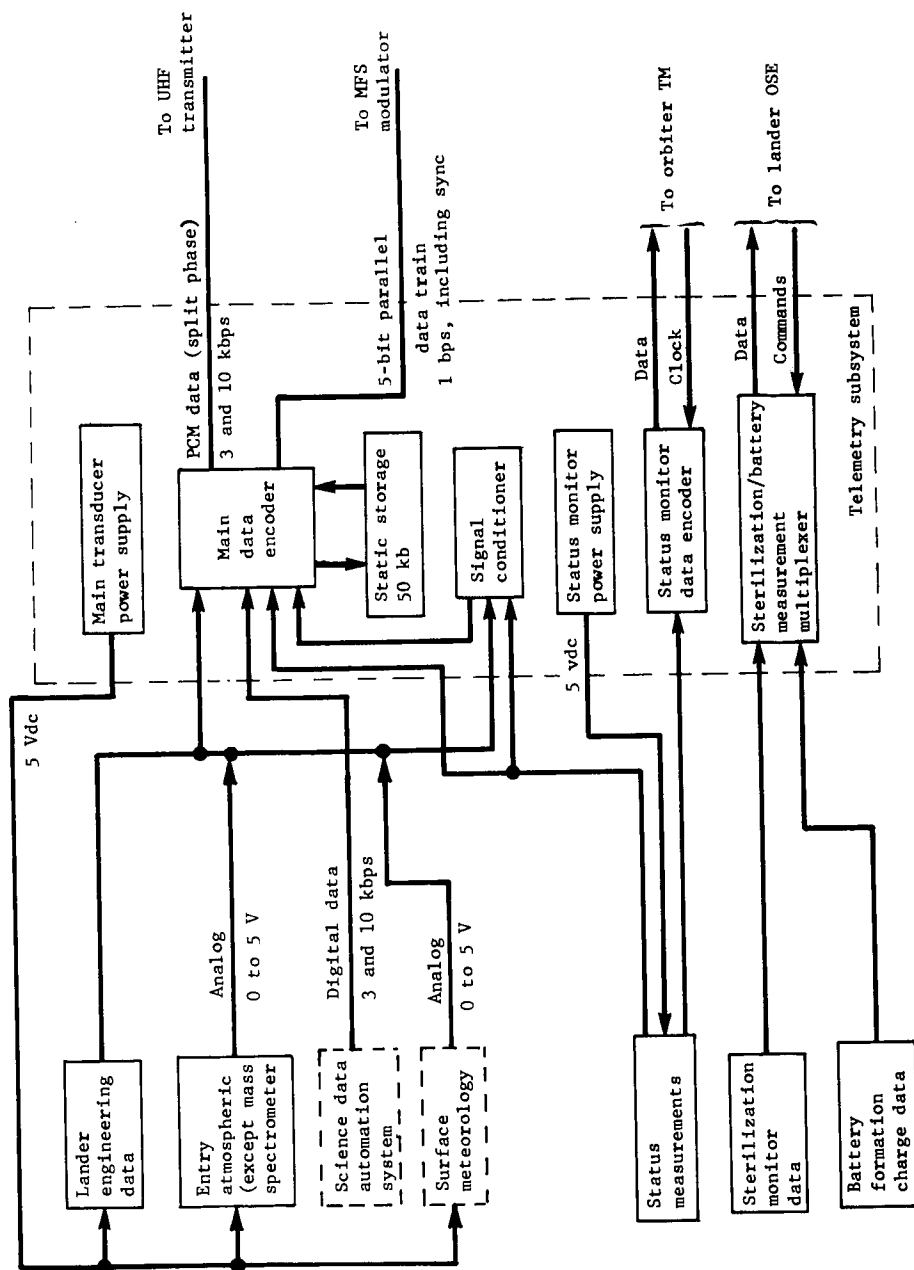


Figure 80.- Telecommunications Subsystem Configuration

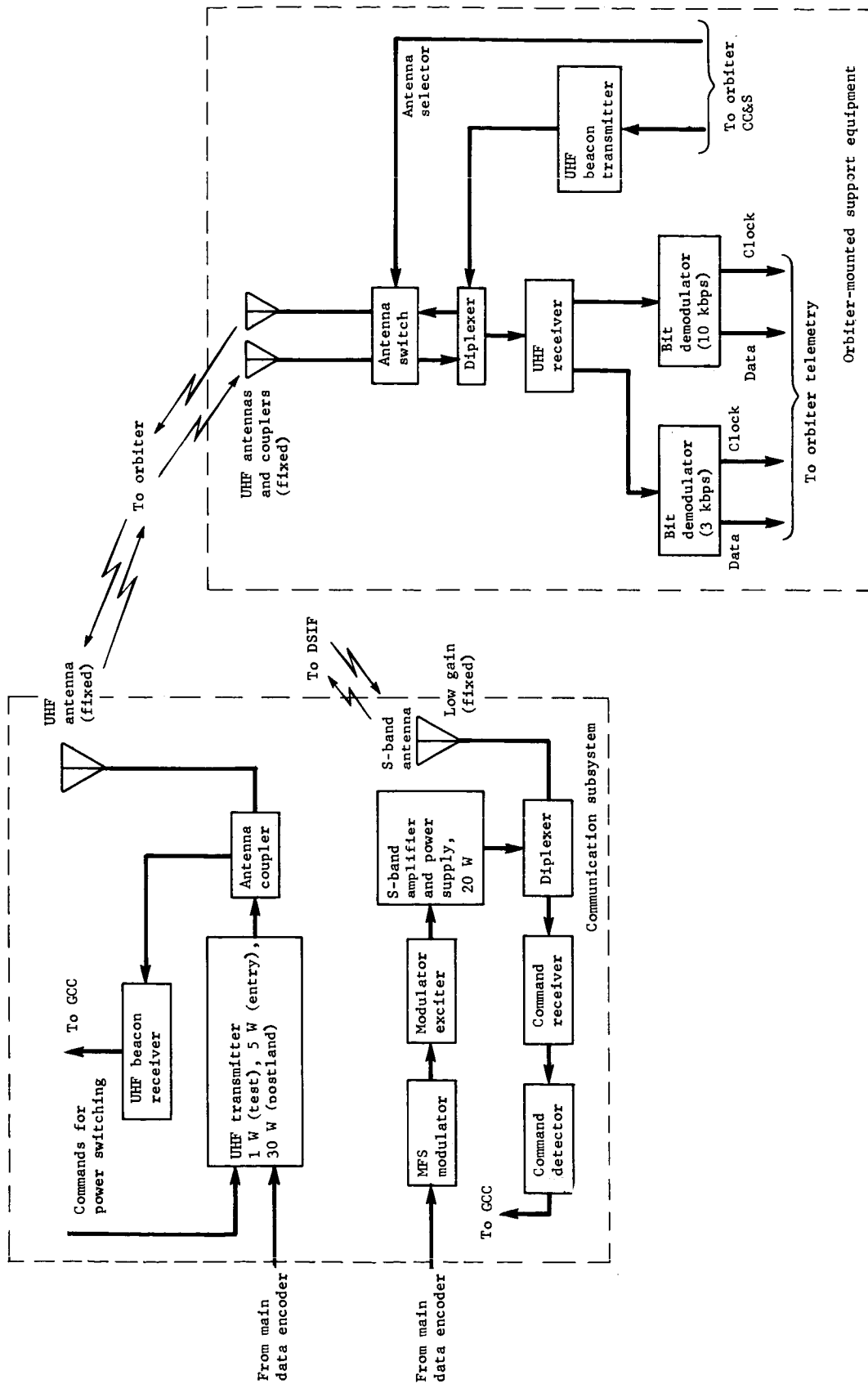


Figure 80.- Concluded

TABLE 22.- TELEMETRY SUBSYSTEM PREDICTED WEIGHT, POWER, AND VOLUME<sup>a</sup>

Component	Weight, lb	Nominal Power, W	Volume, in.		
			L	W	H
Main transducer power supply	0.7	2.0	3.5	3	1.5
Main data encoder	10.0	10.0	13	6	6
Static storage (50 kb)	4.0	1.0	6.5	6	6
Signal conditioner	1.5	----	2.5	6	6
Status monitor power supply	0.7	1.0	3.5	3	1.5
Status monitor data encoder	6.0	6.0	6.5	6	6
Sterilization/battery measurement multiplexer	4.0	----	3	6	6
<sup>a</sup> Does not include packaging, supports, and cabling. These items are tabulated in the sequential weight statement, Appendix D, section 1.					

Communications. - The communication subsystem consists of a uhf radio assembly with a uhf antenna and coupler assembly and an S-band radio assembly with an S-band antenna assembly.

Elements within the uhf assemblies are the transmitter, beacon receiver, and a antenna and antenna coupler. The transmitter consists of a voltage-controlled crystal oscillator, a frequency multiplier, an amplifier, and a circulator. Split-phase PCM telemetry data FSK modulates the voltage controlled oscillator. The transmitter is designed to operate at two power levels for the data transmission function, and a low-power level for test functions to limit the amount of power radiated inside the sealed sterilization canister. Direct-current switching will be used to vary the gains in the power amplifier stages. The transmitter operates at a nominal frequency of 400 MHz with a data transmission rate capability of 3000 bps at the 5 W output level for use up to landing and initial setting at the orbiter. For subsequent periapsis relay contacts, postland phase, the transmitter output level is increased to 30 W providing a data rate capability of 10,000 bps.

The uhf beacon receiver is an AM receiver operating in the 400 MHz band that detects the presence of an audio tone transmitted by the orbiter-mounted support equipment beacon transmitter. The dc output of this receiver is used during postland relay link contacts to initiate transmitter turn-on via the sequencer.

The uhf antenna and coupler combine diplexing and antenna functions into a single component. The design is a crossed-slot cavity-backed antenna capable of operation with orthogonal circular polarizations. The feed consists of a two-port, 3-dB coupler with matching circuitry at the coupler outputs to the slots. The on-axis gain is 5 dB with a 160° beamwidth at the 0 dB points.

Sample telecommunication design control Table 23 demonstrates the method of performance margin calculation. Table 24 is a telecommunication design control table for the reference orbit at 10 minutes after landing. This table is presented to show that a data transmission rate of 10,000 bps can be supported at the 5 W output level prior to initial orbiter setting. Thus, an option exists with the selected configuration to switch to the higher data rate on landing. This option would be exercised if a requirement for a higher data rate immediately after landing and prior to orbiter set were identified.

The uhf communication subsystem uses state-of-the-art, space-proved technology. Related design experience is available from past efforts in the design of solid-state S-band power drivers.

Predictions of weight, power, and volume for the elements of the uhf communication subsystem are shown in table 25. Packaging and internal cabling are not included in these estimates, but are included in the sequential weight statement.

Elements within the S-band assemblies are a multiple frequency shift (MFS) modulator, a modulator-exciter, an S-band traveling wave tube amplifier (TWTA) with an integrated power supply, a diplexer, a command receiver, a command detector, and an antenna. The MFS modulator includes the logic module to convert a five-bit binary word into one of 32 frequencies. A 33rd frequency for synchronization at the receiver is available from a clocked discrete input signal that is periodically inserted into the data stream. The 33 frequencies are generated in a frequency synthesizer module and multiplied up in frequency and amplified in another module. The output of the MFS modulator is fed to the modulator-exciter.

The S-band output of the modulator-exciter is derived from the input signal by frequency multiplication of the source signal in conjunction with amplification. This element also contains a filter-isolator and a power monitor in the output. The output power level is 60 mW as the drive signal for the TWTA.

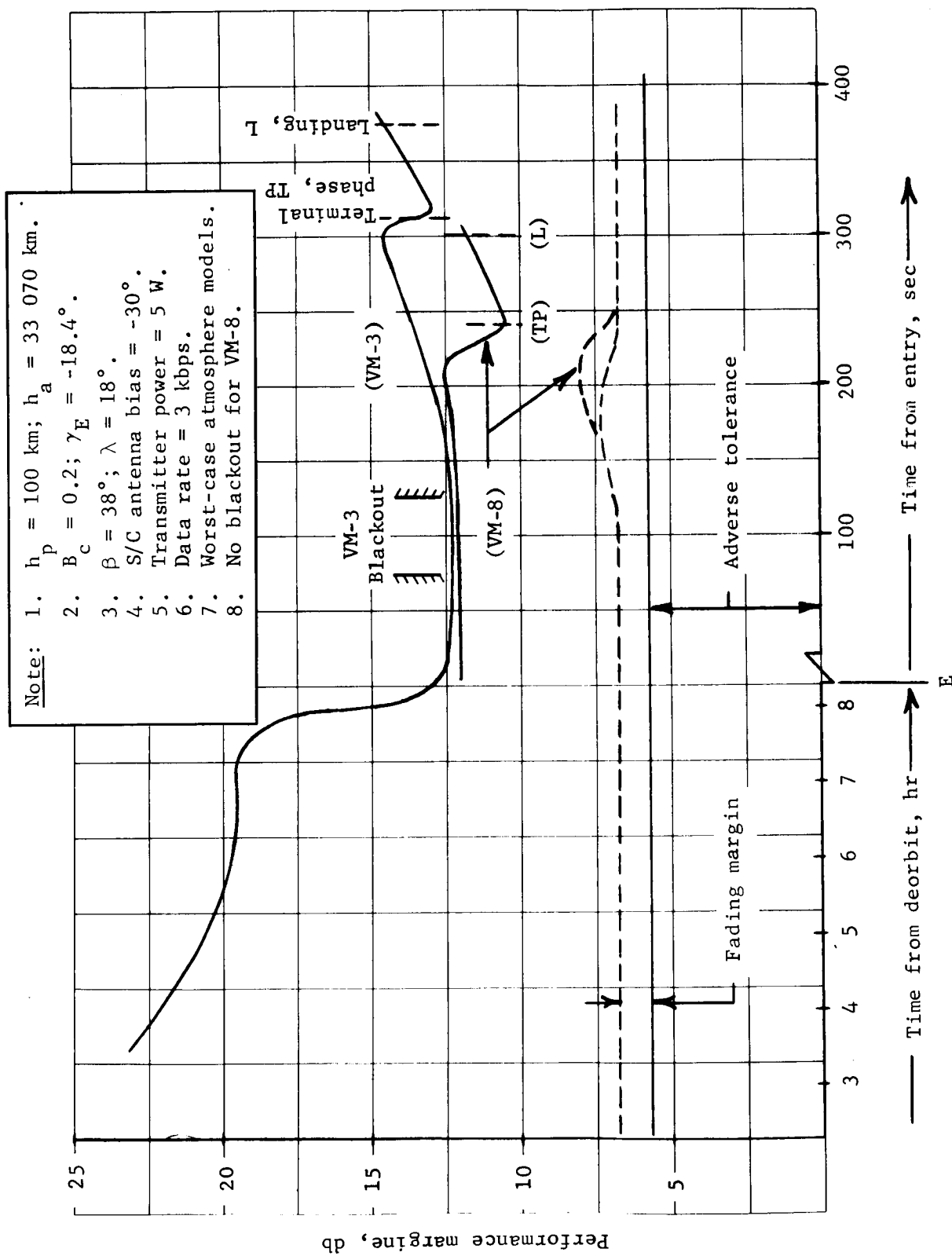


Figure 81 Communications Subsystem Performance, Reference Orbit



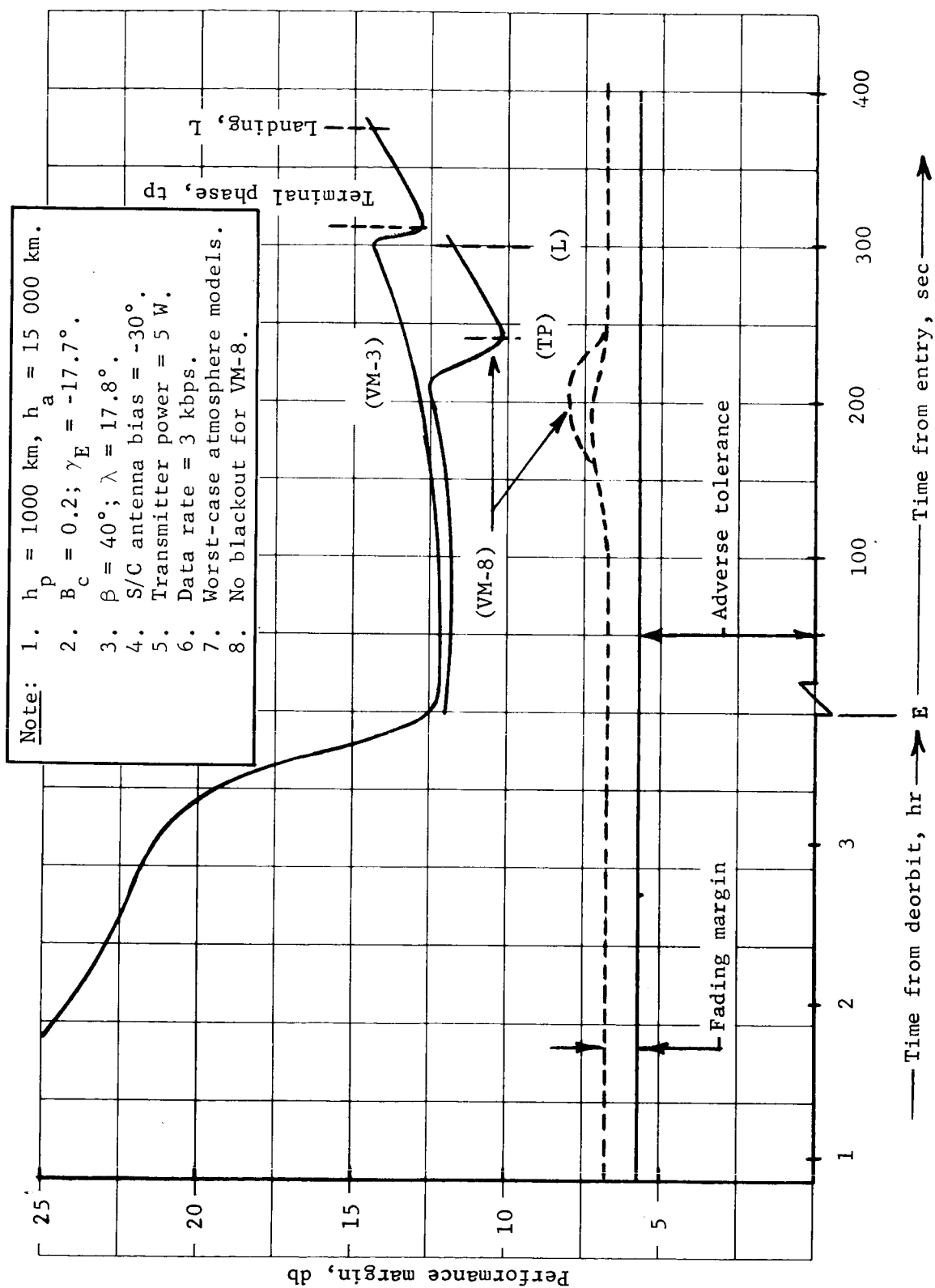


Figure 82.- Communications Subsystem Performance, Alternative Orbit

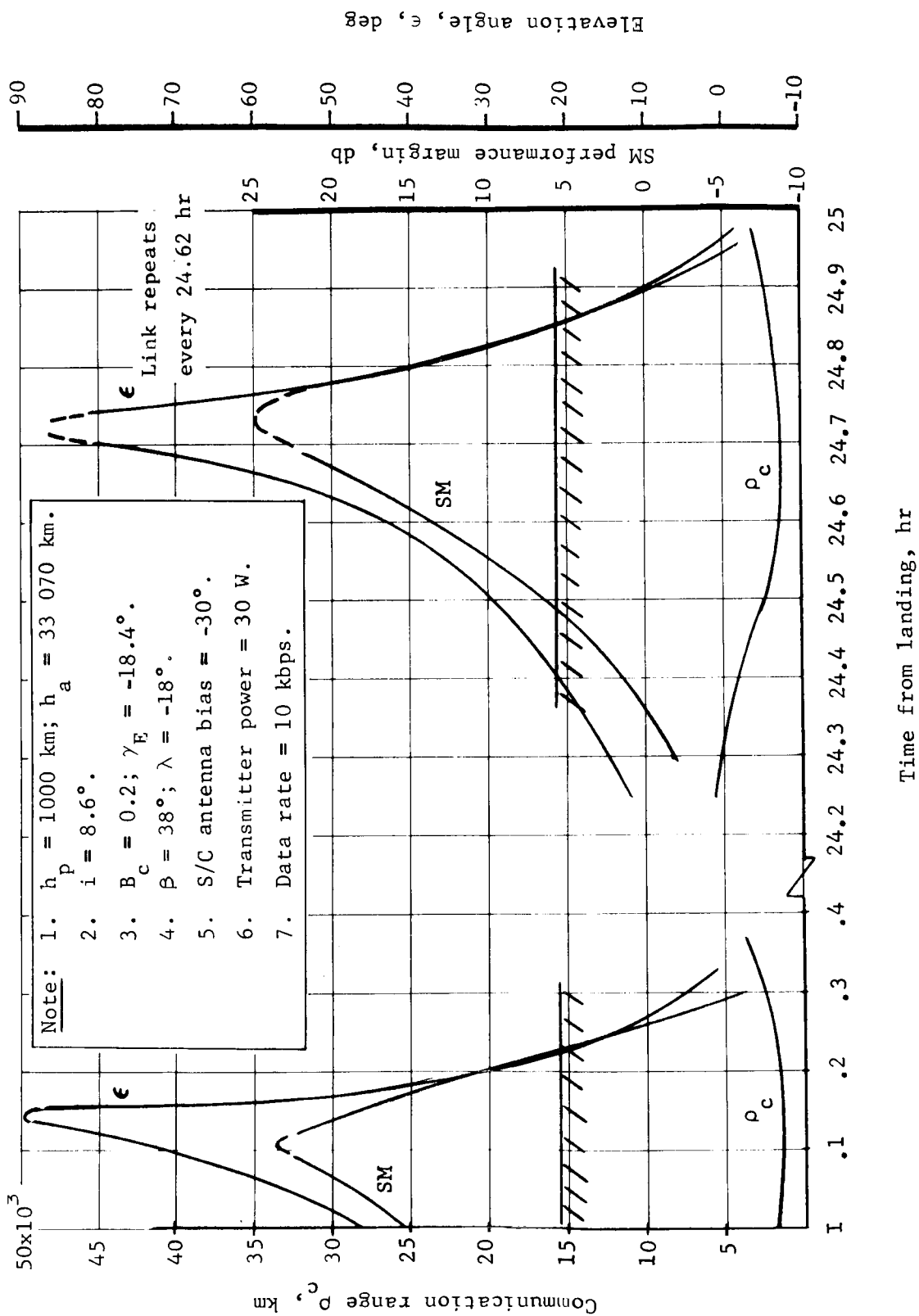


Figure 83.- Communications Subsystem Performance, Reference Orbit

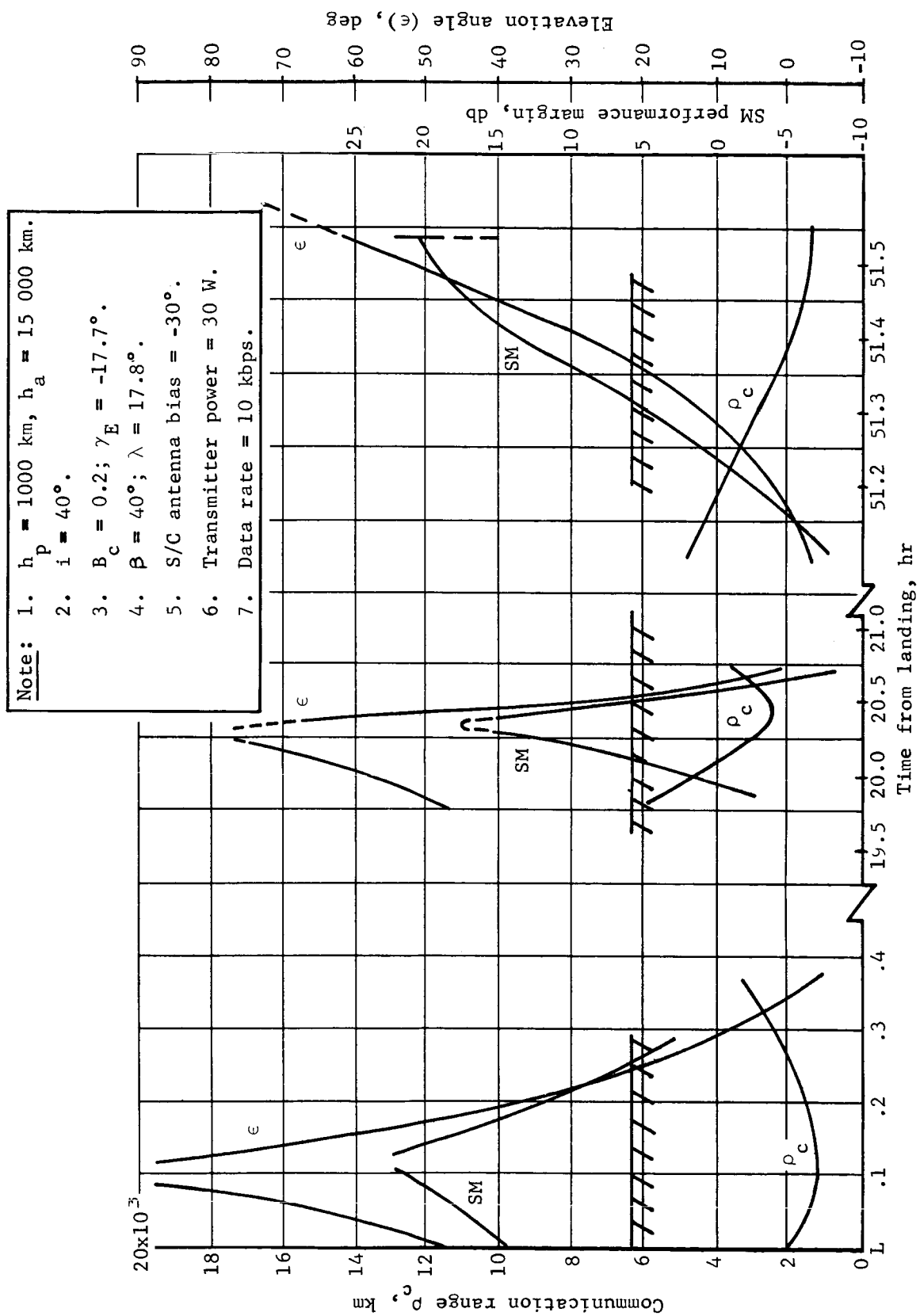


Figure 84.- Communications Subsystem Performance, Alternative Orbit

TABLE 23.- ENTRY LINK (Maximum  $\beta$  Case)

$$\beta = 44^\circ, \lambda = -17.5^\circ, \gamma_E = 17^\circ, B_c = 0.2, V_E = 14\ 400$$

No.	Parameter	Value	Tolerance		Notes
			(+)	(-)	
1	Transmitter power	+37.0 dBm	1.0	0.0	5 W
2	Transmitting circuit loss	-1.0 dB	0.0	0.5	
3	Transmitting antenna gain	+5.0 dB	0.5	0.5	
4	Transmitting antenna pointing loss	-1.5 dB			-45°
5	Space loss F = 400 MHz, R = 2240 km	-151.3 dB			
6	Polarization loss	-0.2 dB	0.2	0.3	
7	Receiving antenna gain	+5.0 dB	0.5	0.5	
8	Receiving antenna pointing loss	-4.2 dB			-65°
9	Receiving circuit loss	-1.0 dB	0.0	0.5	
10	Net circuit loss	-149.2 dB	1.2	2.3	
11	Received carrier power	-112.2 dBm	2.2	2.3	
12	Receiver noise spectral density T System = 630°K	-170.6 dBm/Hz	1.0	2.0	1000°K max.
13	Predetection noise bandwidth Bit rate = 3 kbps; $\Delta F = 21$ kHz	+44.8 dB/Hz	0.4	0.4	30 kHz $\pm 10\%$
14	Receiver noise power	-125.8 dBm	1.4	2.4	
15	Carrier-to-noise ratio	-13.6 dB	3.6	4.7	
16	Threshold carrier-to-noise ratio $P_e^b = 4 \times 10^{-3}$ , WT. = 10 dB	+3.5 dB	1.0	1.0	
17	Fading allowance	-1.0 dB		3.0	
18	Performance margin	+9.1 dB	4.6	8.7	
19	Worst-case margin	+0.4 dB	4.6		

TABLE 24.- INITIAL POSTLAND CONTACT (IMPACT +10 MIN)

No.	Parameter	Value	Tolerance		Notes
			(+)	(-)	
1	Transmitter power	+37.0 dBm	1.0	0.0	5 W
2	Transmitting circuit loss	-1.0 dB	0.0	0.5	
3	Transmitting antenna gain	+5.0 dB	0.5	0.5	
4	Transmitting antenna pointing loss	-0.6 dB			+30°
5	Space loss F = 400 MHz, R = 1240 km	-146.3 dB			
6	Polarization loss	-0.2 dB	0.2	0.3	
7	Receiving antenna gain	+5.0 dB	0.5	0.5	
8	Receiving antenna pointing loss	-0.4 dB			+24°
9	Receiving circuit loss	-1.0 dB	0.0	0.5	
10	Net circuit loss	-139.5 dB	1.2	2.3	
11	Received carrier power	-102.5 dB	2.2	2.3	
12	Receiver noise spectral density T system = 630°K	-170.6 dBm/Hz	1.0	2.0	1000°K max.
13	Predetection noise bandwidth Bit rate = 10 kbps; $\Delta F = 21$ kHz	+47.1 dB·Hz	0.4	0.4	51 kHz $\pm 10\%$
14	Receiver noise power	-123.5 dBm	1.4	2.4	
15	Carrier-to-noise ratio	+21.0 dB	3.6	4.7	
16	Threshold carrier-to-noise ratio $P_a^b = 4 \times 10^{-3}$ , WT. = 7.1 dB	+6.4 dB	1.0	1.0	
17	Lobing loss	-2.0 dB			
18	Performance margin	+12.6 dB	4.6	5.7	
19	Worst-case margin	+6.9 dB	4.6		

TABLE 25.- UHF COMMUNICATION SUBSYSTEM WEIGHT, POWER, AND VOLUME<sup>a</sup>

Component	Weight, lb	Nominal power, W	Volume, in.		
			L	W	H
UHF transmitter (1 W, 5 W, 30 W)	4.5	22.0 or 100.0	6	6	4
UHF beacon receiver	1.9	1.0	4	6	2
UHF antenna and antenna coupler	4.0	----	----	15.5 diam	7.5

<sup>a</sup>Does not include cabling and supports. These items are included in the sequential weight statement, Appendix D, section 1.

The TWTA amplifies the S-band signal from the modulation-exciter to a 20-W output level. The amplifier includes a TWT, a regulator and high-voltage dc power supply for the tube, a circuit to delay high-voltage application, telemetry monitors, and an rf power monitor and output filter. The TWTA power output is specified as the minimum output including insertion losses in the rf power monitor and output filter.

The command receiver is a multiple superheterodyne receiver using a narrow band phase-locked carrier tracking loop to derive the coherent local oscillator reference frequency. A synchronous detector is included in the receiver to demodulate the command subcarrier. The command subcarrier is provided to the command detector.

The command detector detects the digital command bits by demodulating the PN/PSK subcarrier from the output of the S-band receiver. The command detector includes the phase-lock loop and pseudo noise generator to generate bit sync, as well as the phase detector and integrate and dump circuits necessary to make bit decisions. The command detector will provide digital data at either 1 or 8-1/9 bps. An in-lock signal in addition to the command data and bit sync is supplied to the command decoder located in guidance and control subsystem.

The diplexer consists of a bandpass filter at the receiver and transmitter frequency and a susceptance annulling network at the common junction of these two filters to provide a constant impedance to the antenna. Isolation requirements are 80 dB, minimum, at both transmit and receive frequencies. The power handling capability will be 100 W.

The low-gain S-band antenna consists of a cavity-backed crossed-slot with a helical feed. This antenna provides right-hand circular polarization to a single port. The on-axis gain is 5 dB with a 160° beamwidth at the 0-dB points.

The S-band communication subsystem provides transmission of telemetry data for 2 hr/day at an information rate of 0.8 bps at maximum Earth-Mars separation distance with a 210-ft advanced antenna system at the ground station. Since 20% is required for sync, the data rate capability of the link is 1.0 bps. The subsystem provides 7200 bits of data, including synchronization, on each daily contact with Earth.

The S-band command subsystem provides for reception of command bits at either 1 or 8-1/9 bps. The high command data rate capability is employed for reprogramming of the GCC memory. Command transmission is supported for 2 hr/day after two-way lockup is achieved.

The S-band communication subsystem uses state-of-the-art, space-proved technology. The command receiver is similar to the receiver portion of the lunar orbiter transponder. The modulator-exciter will be similar to that module used in the lunar orbiter transponder. Mariner '69 technology will provide the design required for the command detector. The TWTA will use either a currently available 394H TWT or an updated version of the 394H or WJ-274.

Predicted weight, power, and volume for the elements of the S-band communication subsystem are shown in table 26. Packaging and internal cabling are not included in these estimates.

TABLE 26.- S-BAND COMMUNICATION SUBSYSTEM WEIGHT, POWER, AND VOLUME<sup>a</sup>

Component	Weight, lb	Nominal Power, W	Volume, in.		
			L	W	H
Command receiver	5.0	2.5	5	7	4.5
Command detector	4.0	1.5	5	6	1.5
MFS modulator	1.0	6.0	5	4	3
Modulator exciter	3.0	2.0	6	5	3
S-Band TWTA and power supply (20 W)	7.8	84.0	10	7	3
S-band diplexer	1.3	----	7	5	1.5
S-band antenna	0.6	----	---	4 diam	4
<sup>a</sup> Does not include packaging, supports, and cabling. These items are tabulated in the sequential weight statement, Appendix D, section 1.					

## Power and Pyrotechnic Subsystems

Power subsystem functional description. - The power subsystem is a 30 Vdc (nominal) system using solar cells and sterilizable nickel-cadmium and silver-zinc batteries to provide the energy required. Power from the orbiter is used during the cruise phase for battery charging, thermal control, and status monitoring. The power subsystem consists of equipment located in the capsule adapter and in the lander.

Figure 85 is a block diagram identifying the configuration of the power subsystem and the location of the equipment.

During cruise, power and control signals are supplied by the orbiter to support the lander. The power management control unit controls distribution of orbiter power as commanded from the orbiter. The status monitor voltage regulator provides a nominal 30 Vdc output to the telemetry subsystem. Power is also used for lander thermal control and battery charging. Battery chargers may be turned on or off by command. Isolation diodes are provided for all power from the capsule adapter to prevent loss of the power subsystem if a fault should occur in the wiring and connectors between the battery chargers and the capsule adapter. The power management control unit also responds to an orbiter command to operate the power transfer switch.

From power transfer through landing, a 76 A-h sealed, sterilizable silver-zinc battery provides operating power for the flight capsule. Figure 86 shows the power profile for this phase of the mission.

Surface operation for at least two diurnal cycles is assured by continuing to operate from the silver-zinc battery. Figure 87 shows the power profile for this phase of the mission based on the 1000x15 000 km alternative orbit. The profile for the 1000x33 000 km orbit is similar. Energy in the Ag-Zn battery is supplemented by the 17 A-h nickel-cadmium battery and the solar array. Thermal control uses radioisotope heaters.

The solar array becomes the primary energy source after the first two diurnal cycles of operation and is used to meet all continuous daytime load requirements, to recharge the Ni-Cd battery and when sufficient energy is available, to recharge the Ag-Zn battery permitting an extension of lander life during low light level periods. Use of the Ag-Zn battery for entry and the Ni-Cd battery for extended life resulted in the lightest power subsystem.



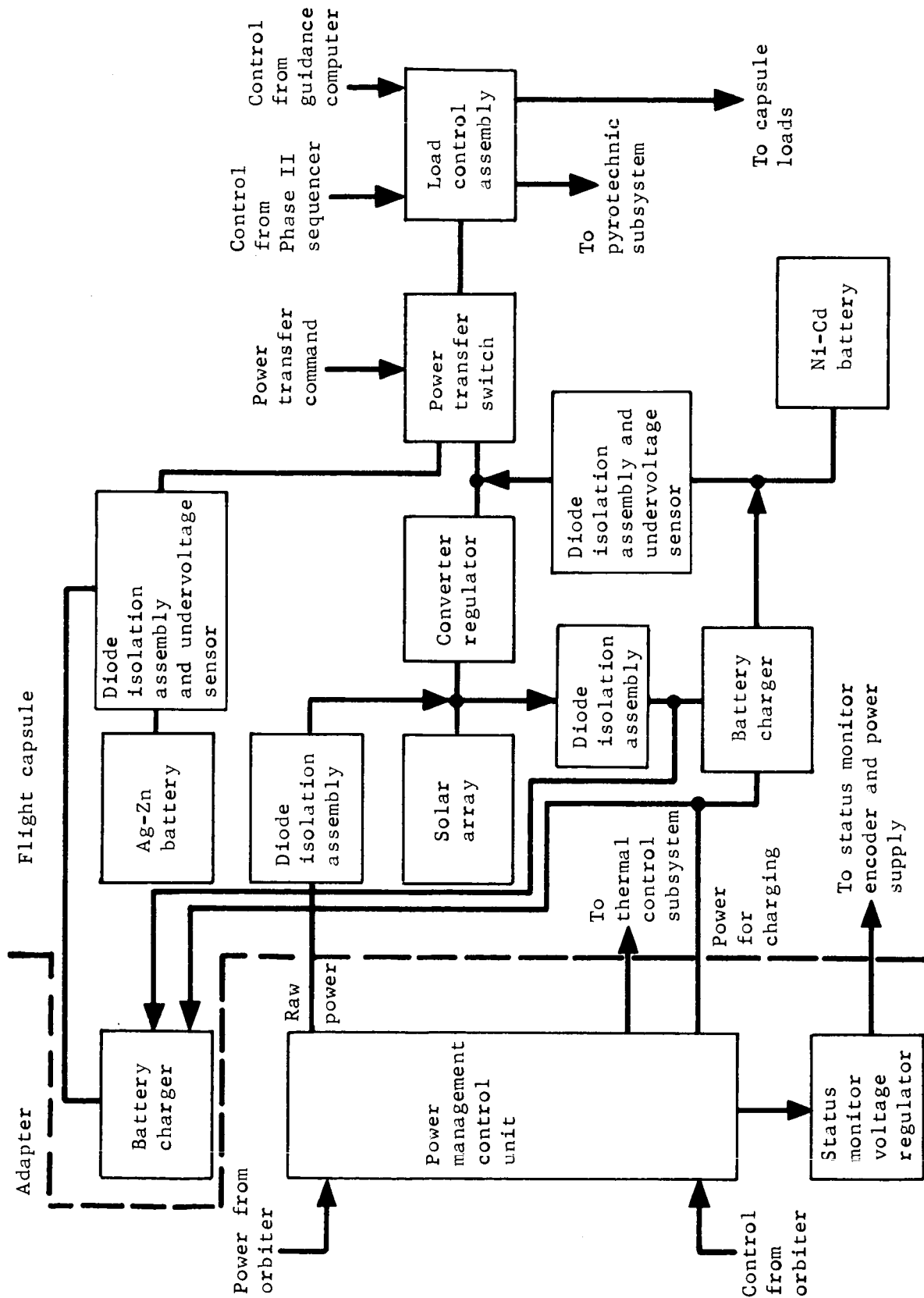


Figure 85.- Power Susystem Block Diagram

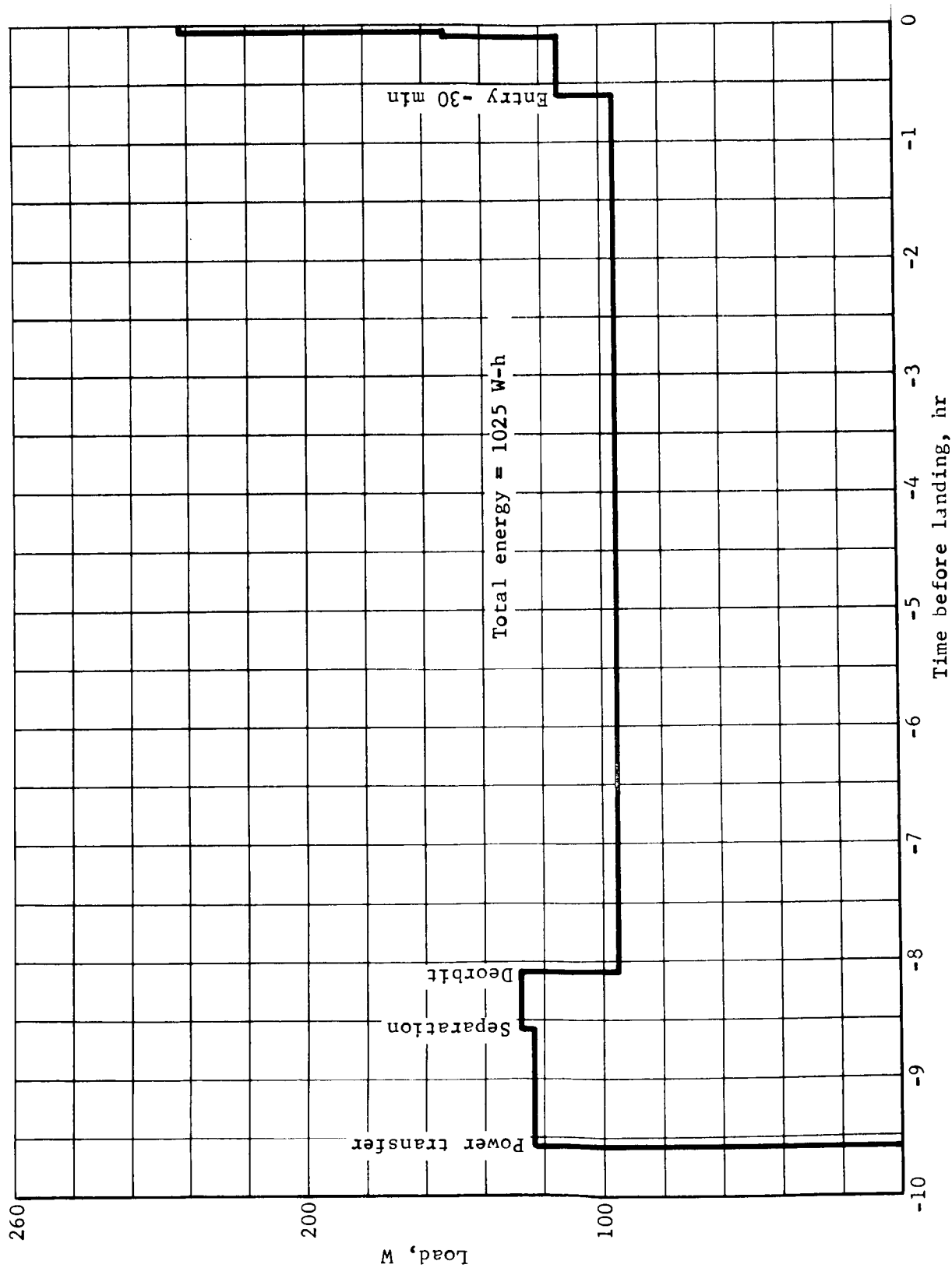


Figure 86.- Entry Load Profile

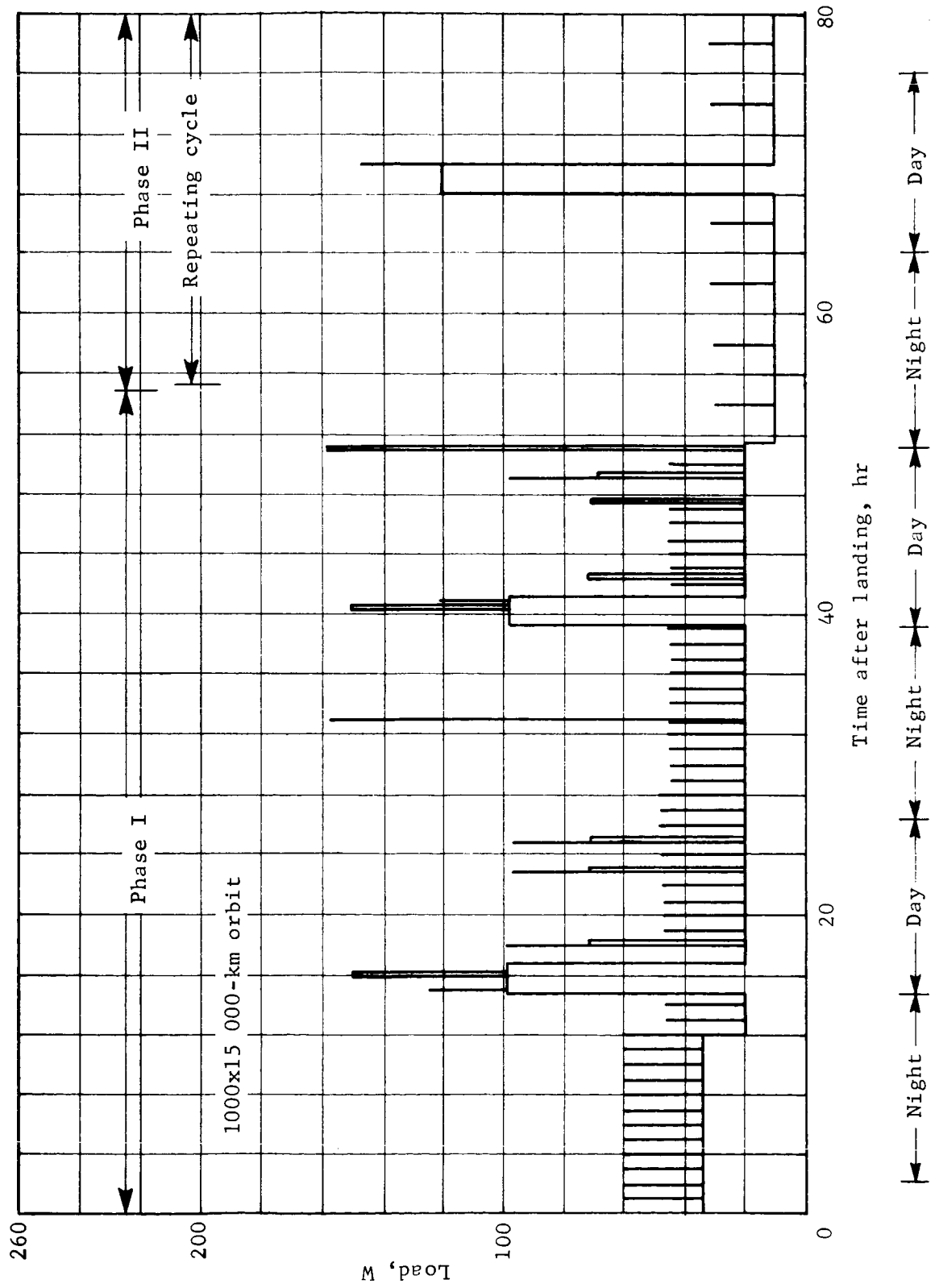


Figure 87.- Landed Operations Load Profile

The solar array configuration consists of a body-mounted array and four directed rectangular side panels. The side panels are not oriented in the usual sense, because they have but one degree of freedom and do not track the sun. Details of the panel structure and configuration may be found in the Structures section of this report.

The side panels are directed to provide sufficient power during missions at southern latitudes and under conditions of large adverse landing slopes. The advantages gained are clearly shown in figure 88 and Appendix D, section 8, where comparisons between the power outputs of directed and fixed horizontal arrays are shown. The directed side panel array supplies power required for the lander without the complexity, reliability, and weight disadvantages of a fully oriented array.

Side panel actuation is provided by reversible solenoid stepper motors as used on Surveyor and lunar orbiter. The gear drive ratio allows the panels to be stopped at the optimum power angle without the use of latches or mechanical stops. The optimum tilt angles for each panel will depend on the terrain conditions, landing latitude, and time of year, and will need periodic adjustment through command control during a long mission to correct for changes in the solar declination.

For the shortest daylight period at  $20^{\circ}$  S latitude the average power from the solar array must be approximately 18 W-h/ft<sup>2</sup>/day. Figure 88 shows that at  $20^{\circ}$  S latitude and a  $17^{\circ}$  S slope, 16.5 W-h/ft<sup>2</sup>/day are available. This means that during the period of minimum daylight a modified power profile must be used to reduce the average load if continued operation is desired.

The Ag-Zn battery is recharged when sufficient solar cell power is available, permitting at least 4 days operation of the lander during low light level periods.

The undervoltage sensor with an enable signal from the sequencer is used to keep either or both batteries isolated from loads when they are not required. Battery and solar array power is provided through the motor-driven power transfer switch to the pyrotechnic subsystem, and through the power transfer switch and the load control unit to the science, telecommunication, sequencing, and guidance subsystems. The load control assemblies contain one mag-latch relay for each load. This permits sequencer control of the loads with a minimum energy loss.

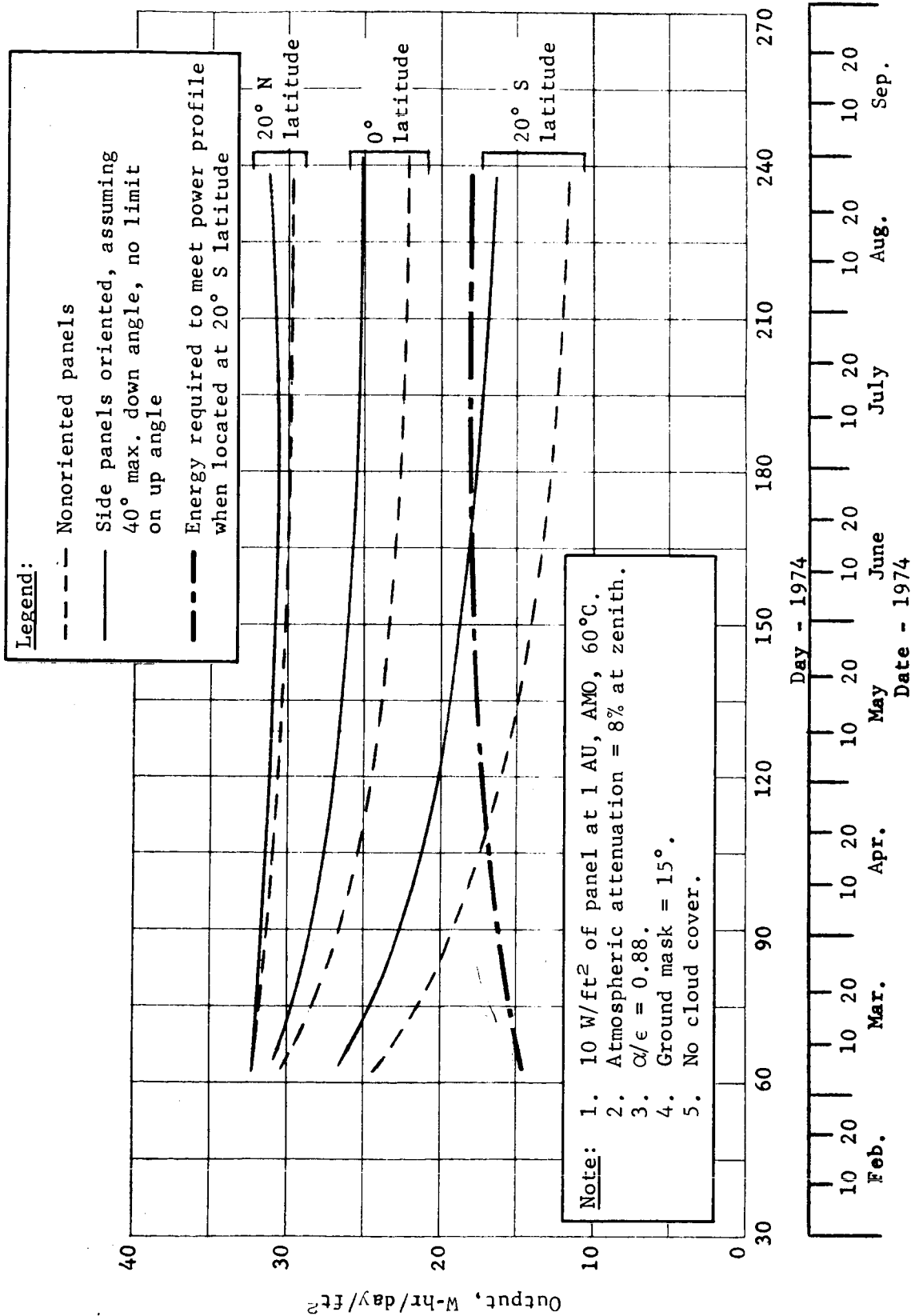


Figure 88.- Mars Lander Solar Array Output, 17° S Slope

The power management control unit provides direct current isolation between orbiter and lander grounds for control discretes. When raw power is used directly, the load is referenced to the orbiter. The grounding method used for the equipment bus is shown in figure 89. This method uses a ground bus for all insensitive equipment and a single-point ground for sensitive, critical loads, thus providing a system combining the advantages of the reduced weight of the ground bus with the low common impedance of the single-point ground. The reference to structure is through an isolation network, consisting of a resistor with an rf bypass capacitor. With this isolation a fault from a positive feeder to structure does not cause the loss of the power subsystem. The power subsystem weights are shown in table 27.

Pyrotechnic subsystem functional description. - The lander pyrotechnic subsystem consists of the equipment shown in the block diagram, figure 90. Power to the pyrotechnic subsystem is provided from the power subsystem, and control signals are received from the guidance and control computer.

Fourteen capacitor assemblies provide energy storage for firing the bridgewires at the prescribed time. Capacitor assembly charging is initiated at power transfer and within 12 sec the capacitors are ready for use. A minimum of 12 sec between subsequent events allows the capacitor assemblies to be recharged and used again. Each capacitor assembly provides the required energy to fire one bridgewire in a given event. The number of capacitor assemblies required is established by the maximum number of bridgewires required in an event.

Time-critical functions are grouped into events with sufficient time between events to allow the capacitor assemblies to be recharged.

The pyrotechnic subsystem size is based on a total of 88 bridgewires with a maximum of 14 bridgewires fired in a 12-sec period.

The use of a small capacitor assembly to fire each bridgewire instead of a larger capacitor bank to fire all bridgewires in a given event eliminates the need for current-limiting resistors in each bridgewire circuit and resultant larger capacitor bank to provide for resistor losses. A minimum firing energy of approximately 0.150 J per bridgewire is provided to ensure firing within an allowable time period.

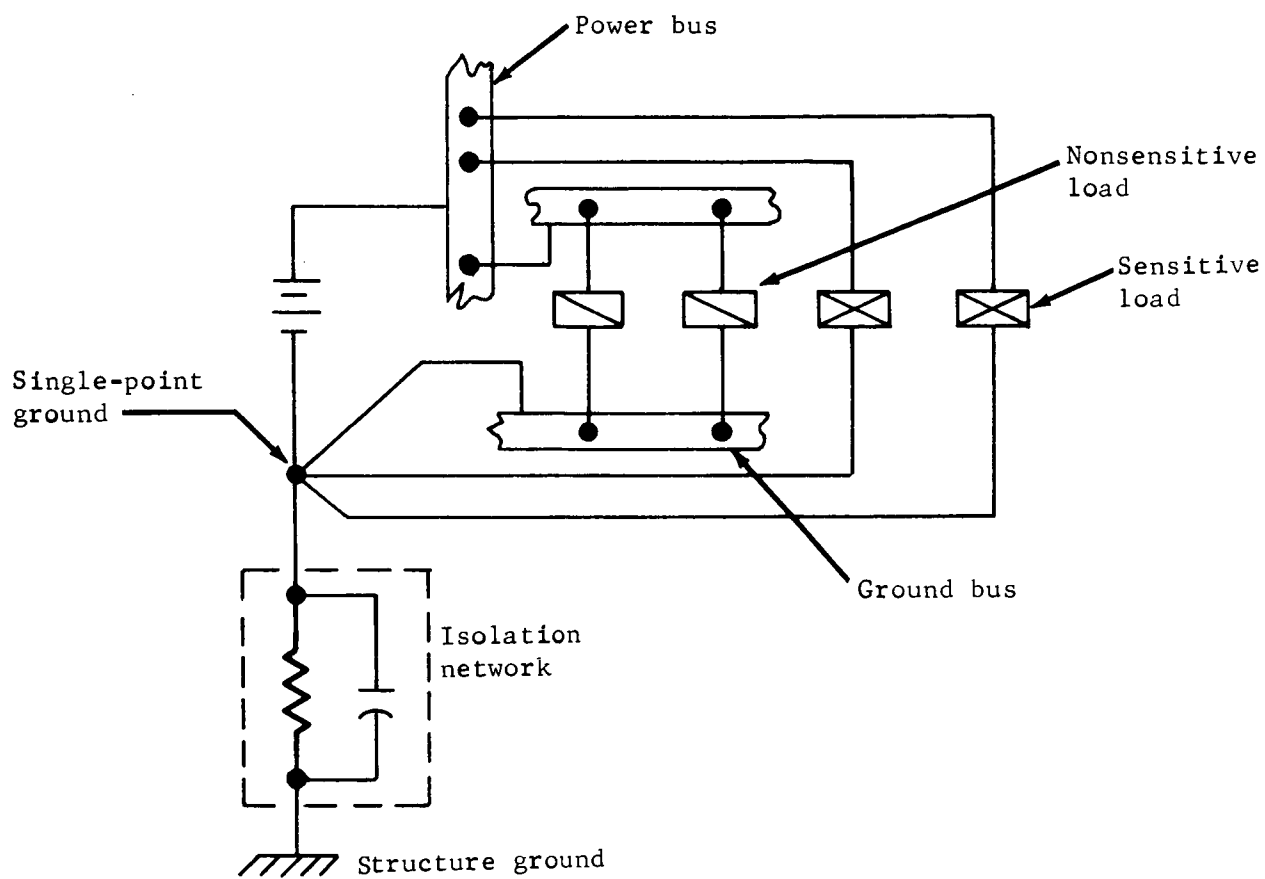


Figure 89.- Isolated Single-Point Ground

TABLE 27.- POWER SUBSYSTEM WEIGHTS<sup>a</sup>

Item	Quantity	Weight each, lb	Weight Total, lb
<u>Capsule adapter</u>			
Power management control unit	1	3.0	3.0
Status monitor voltage regulator	1	3.5	<u>3.5</u> 6.5
Internal cabling and connectors			7.5
Packaging and mounting			4.0
Capsule adapter, total			18.0
<u>Lander</u>			
Solar array			
Fixed panel, 20 sq ft	1	12.0	12 <sup>b</sup>
Side panels, 24 sq ft	4	6.0	24
Actuators	4	3.0	12.0
Ag-Zn battery, 76 Ah	1	60.0	60.0
Ni-Cd battery, 17 Ah	1	62.0	62.0
Ag-Zn battery charger	1	2.0	2.0
Ni-Cd battery charger	1	3.0	3.0
Converter regulator	1	7.0	7.0
Power transfer switch	1	2.5	2.5
Load control assembly	1	4.0	4.0
Shunts and isolation		1.5	1.5
Diode assembly	1	1.0	1.0
Undervoltage sensors	2	2.0	4.0
Internal cabling and connectors		3.0	3.0
Packaging		5.0	<u>5.0</u>
Lander, total			203.0

<sup>a</sup>Does not include external cabling and supports. These items are tabulated in the sequential weight statement, Appendix D, section 1.

<sup>b</sup>An additional 8.0 lb of substrate is charged to thermal control.



A safe/arm switch provides arming and safing of each pyrotechnic circuit. The events are arranged so that no function is armed more than one minute before firing. After all pyrotechnic functions in an event are fired, the switches are reset to the safe position thus opening the power circuit and removing any load caused by a bridgewire short.

The safe/arm switch contains a 100 000 ohm resistor connected from the negative bridgewire lead to structure. This provides a ground reference for the bridgewires to prevent a static charge build up before firing the bridgewire.

The final switch between the energy source and the squib is the solid-state squib firing circuit (SFC), which receives its fire control signal from the sequencing subsystem.

The squibs provide gas pressure to operate valves, cable cutter, and separation nuts or initiate linear-shaped charges for canister separation and nose cap ejection.

The block diagram, (fig. 90) shows the typical redundancy provided for each function. Parallel circuits are provided from the power subsystem through redundant capacitor assemblies, safe/arm switches, squib firing circuits and to one of two squibs in each pyrotechnic device. Two squibs with one bridgewire each are used for each function. With this design, the proper functioning of either circuit branch will fire all associated pyrotechnic devices.

Physical characteristics of the pyrotechnic subsystem are described in section 8 of Appendix D. The pyrotechnic subsystem weights are shown in table 28.

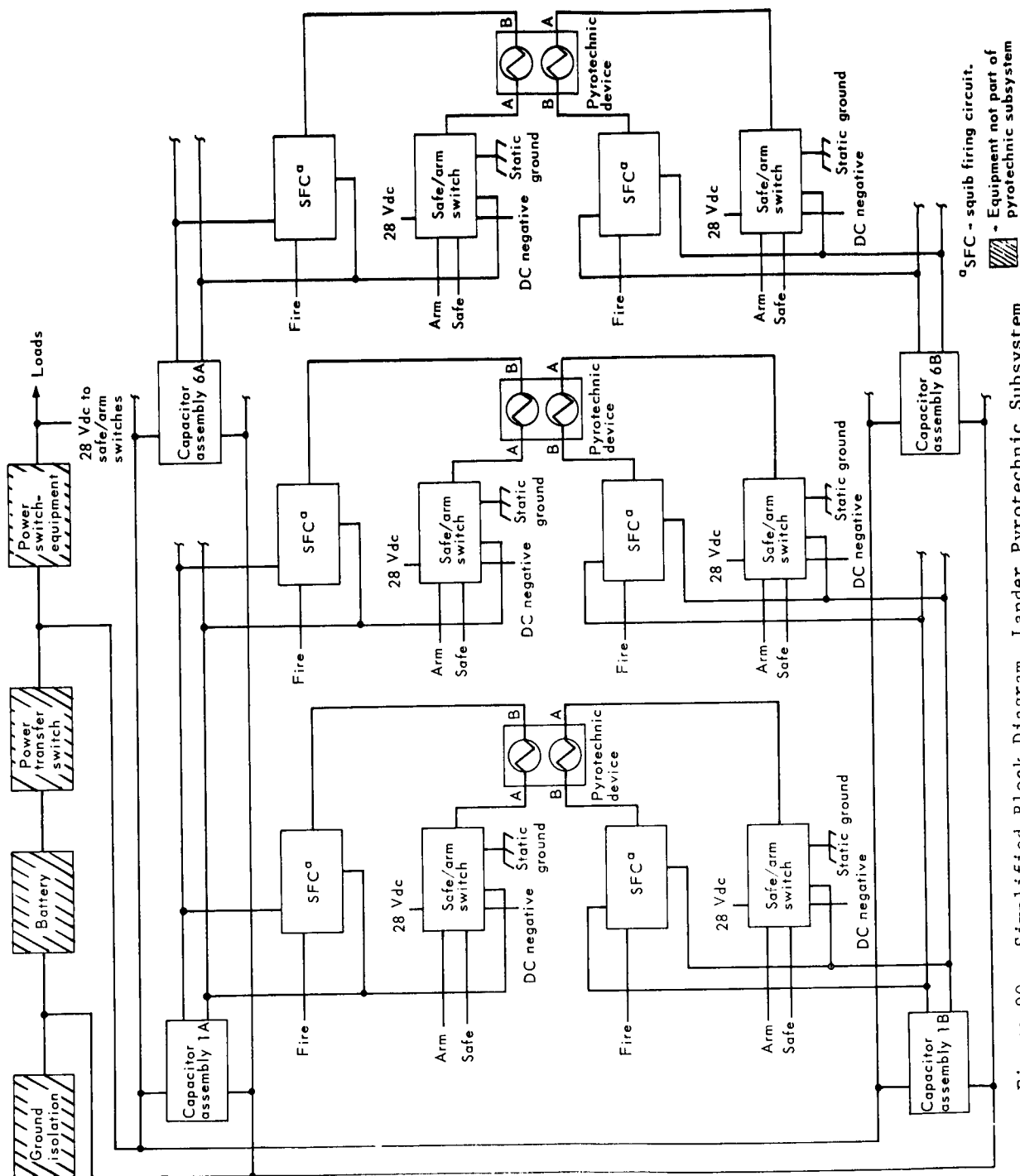


Figure 90.- Simplified Block Diagram, Lander Pyrotechnic Subsystem

TABLE 28.- PYROTECHNIC SUBSYSTEM WEIGHTS<sup>a</sup>

Item	Quantity	Weight each, lb	Total weight, lb
Capacitor assembly	14	0.16	2.2
Safe/arm switch	88	0.19	16.7
Squib fire switch	88	0.06	5.4
Subtotal			24.3
Internal cabling and connectors			.9
Packaging			5.3
Total			30.5

<sup>a</sup>Does not include external cabling and supports. These items are tabulated in the sequential weight statement, Appendix D, section 1.

## Thermal Control Subsystem

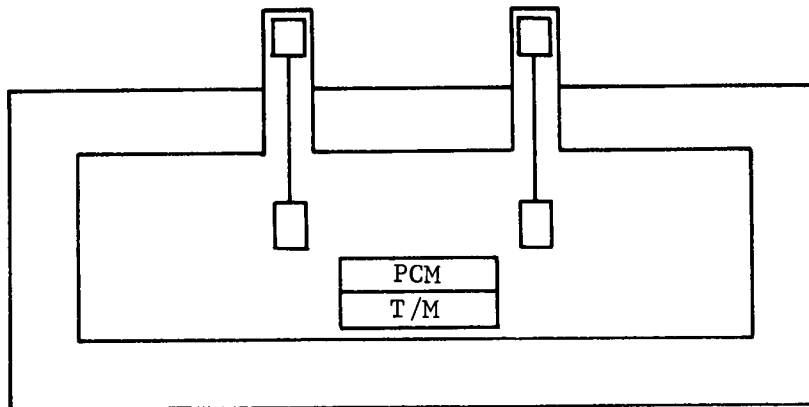
Mars surface. - A radioisotope heater system was selected for the point design because it is not life-limited and can be designed to survive extreme environments at an acceptable weight. The system is shown schematically in figure 91. It consists of 3 in. of insulation, isotope heaters controlled by moving them in and out of the lander by thermostatically controlled actuators, and phase change material on the S-band transmitter. Electrical heaters are used for the deployed science instruments.

The 370 lb of landed equipment to be thermally controlled is packaged in a 12-cu-ft volume. The power profile described in the power and pyrotechnic subsystem section, the hot and cold environments described in table 29, and the 40 to 100°F operating temperature limits are the other primary requirements influencing this design.

Radioisotope heaters. - The isotope heaters are assumed to be the same as the 25 W heaters proposed for the ALSEP program. A summary of the characteristics of these heaters is given in table 30. The total power required is approximately 200 W, which is provided by four heater assemblies, each of which contains two heaters. The installation concept and weight estimate are shown in figure 92. An electrical actuator with thermostat control is used.

**Note:** 370 lb of equipment in 12 cu ft lander with radioisotope heaters and 10W minimum equipment power.

4 assemblies of  
isotopes heaters with  
thermostatically controlled  
actuators



T/M - transmitter

PCM - phase change material

Item	Weight, lb
3 in. insulation, 1 lb/cu ft	12.6
200 W, radioisotope	28.8
Phase change material	5.4
Total subsystem	46.8

Figure 91.- Thermal Control Subsystem

TABLE 29.- THERMAL ENVIRONMENTS

Item No.	Environmental parameter	Cold extreme	Hot extreme
(1)	Solar flux at Mars, Btu/hr-ft <sup>2</sup>	----	232
(2)	Solar transmissivity of atmosphere	0	1.0
(3)	Solar absorptivity ( $\alpha$ ) of Martian surface	----	0.95
(4)	Emissivity ( $\epsilon$ ) of Martian surface	0.85	0.85
(5)	Martian surface thermal inertia, $\sqrt{k\rho c}$ , (Btu/ft <sup>2</sup> -°F-hr <sup>1/2</sup> )	----	0.97
(6)	Martian surface temperature °F	-190	Calculated using items (1) to (5)
(7)	Wind velocity, fps (continuous at 1 m elevation and 20 mb)	74	0
(8)	Atmospheric pressure, mb	20	5
(9)	Atmospheric temperature, °F	-190	Estimated based on Item (6)
(10)	Atmospheric composition	100% N <sub>2</sub>	100% CO <sub>2</sub>

TABLE 30.- 25 to 30 W ISOTOPE HEATER SUMMARY

<u>Materials</u>	
Fuel	Pu <sup>238</sup> O <sub>2</sub>
Structure	Ta-10 W
Fuel liner	TA-10 W
Clad	Hastelloy X
Ablator	80 AlF <sub>3</sub> -20 W
<u>Dimensions</u>	
Fuel volume, cu in. (50% void)	.935
Structure and liner thickness, in.	.150
Clad thickness, in.	.030
Minimum ablator thickness, in.	.600
Capsule diameter, in.	1.57
Ablator diameter, in.	2.77
<u>Weight, lb</u>	
Fuel	.170 (for 30 W)
Structure and liner	.564
Clad	.065
Total	.80
Ablator	1.84
Total	2.64

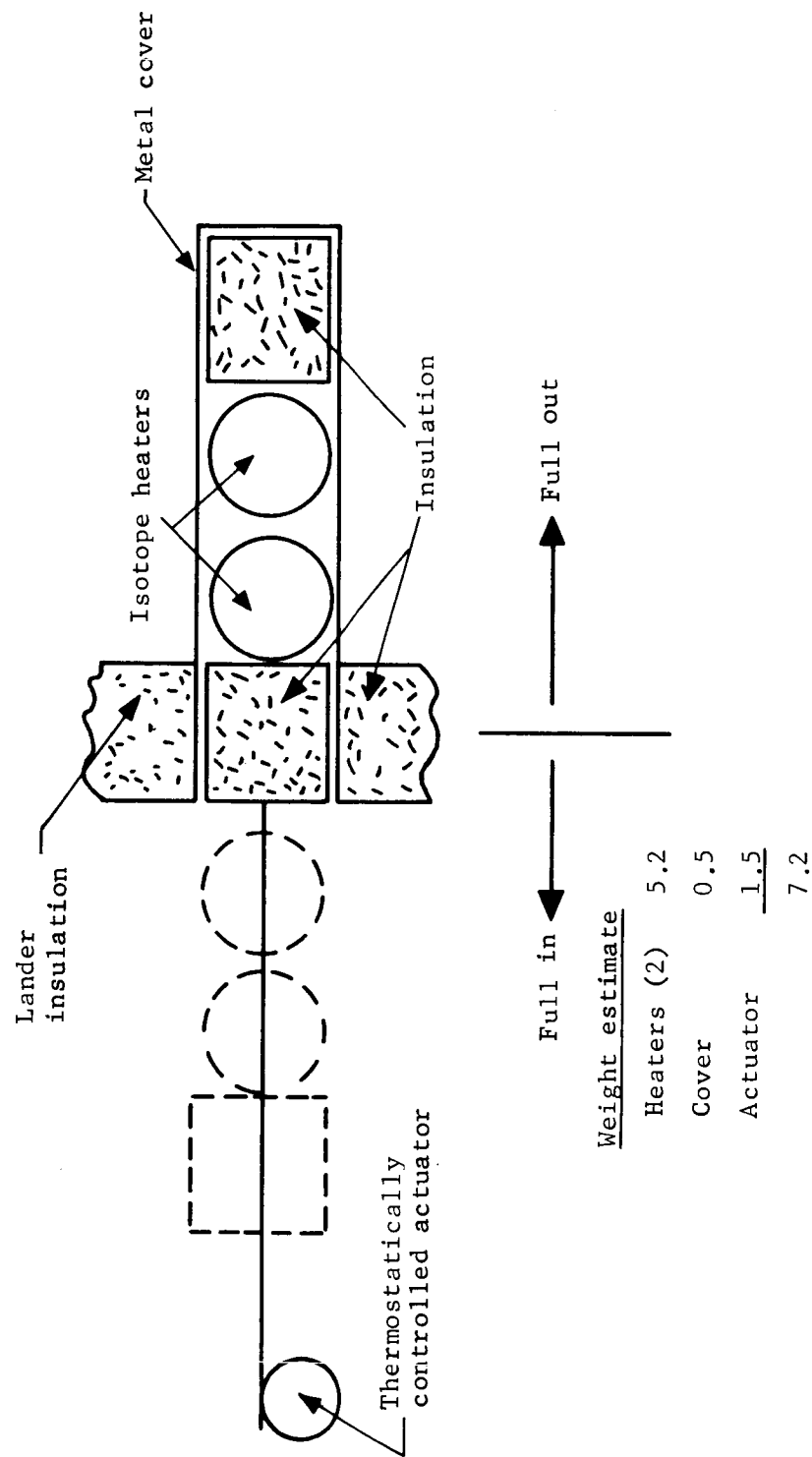


Figure 92.- Isotope Heater Control Concept

Insulation. - Candidate insulations include fibrous types, foams, multilayers and combinations of these materials. Thermal performance of these materials in the Mars environment has not been established. A contract to perform tests of candidate materials is scheduled to be let by JPL in June 1968 to acquire the necessary data.

The insulation design used in this point design consist of low density fiberglass ( $0.53 \text{ lb/ft}^3$ ) with radiation shields at 1-in. spacing. An analysis (section 2 of Appendix D) was done to estimate the performance of this insulation in the Mars environment, including effects of attachments. The performance of the insulation used, including the effects of penetrations is shown in figure 93.

Phase change material. - Eicosane is used to absorb the S-band transmitter heat peak. It has a melting point of  $98^\circ\text{F}$  and a heat of fusion of  $106 \text{ Btu/lb}$ . The packaging concept and weight estimate are given in figure 94.

System performance. - Results of an analysis using a transient computer program for the extreme cold and extreme hot environments defined in table 30 are shown in figures 95 and 96. Insulation conductivity for carbon dioxide was used for the hot case and conductivity for nitrogen was used for the cold case. The hot extreme environment used is based on a solar flux of  $232 \text{ Btu/hr-ft}^2$ , which is the highest possible at Mars. However, as shown on figure 95, the allowable equipment temperature limits are not exceeded even for this conservative environment. In the cold extreme environment, the equipment temperature rapidly drops to the minimum allowable ( $40^\circ\text{F}$ ) and 200 W of isotope power are required to hold this temperature.

Summary of component development status. - The status of insulation, radioisotope heaters, and phase change materials is listed in the following tabulation.



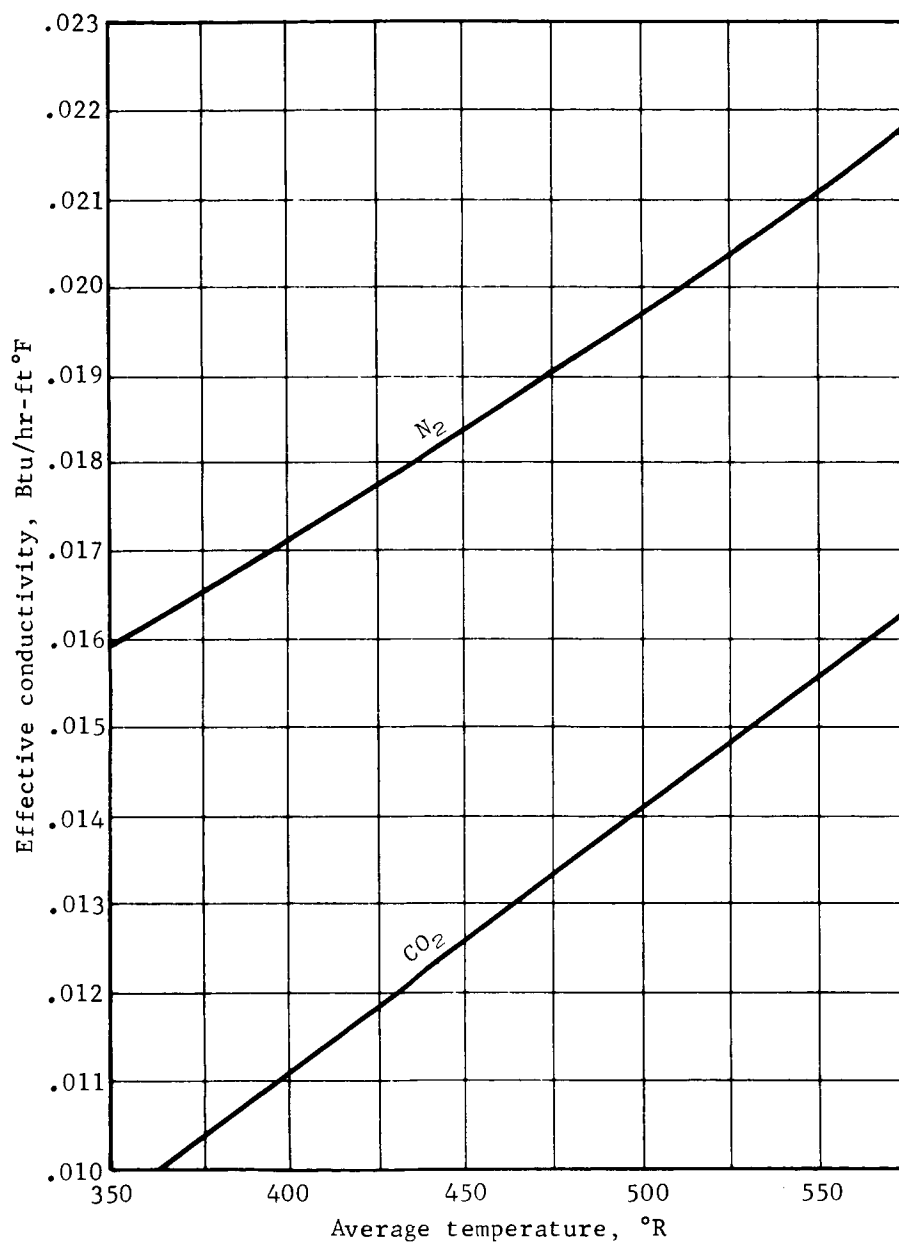
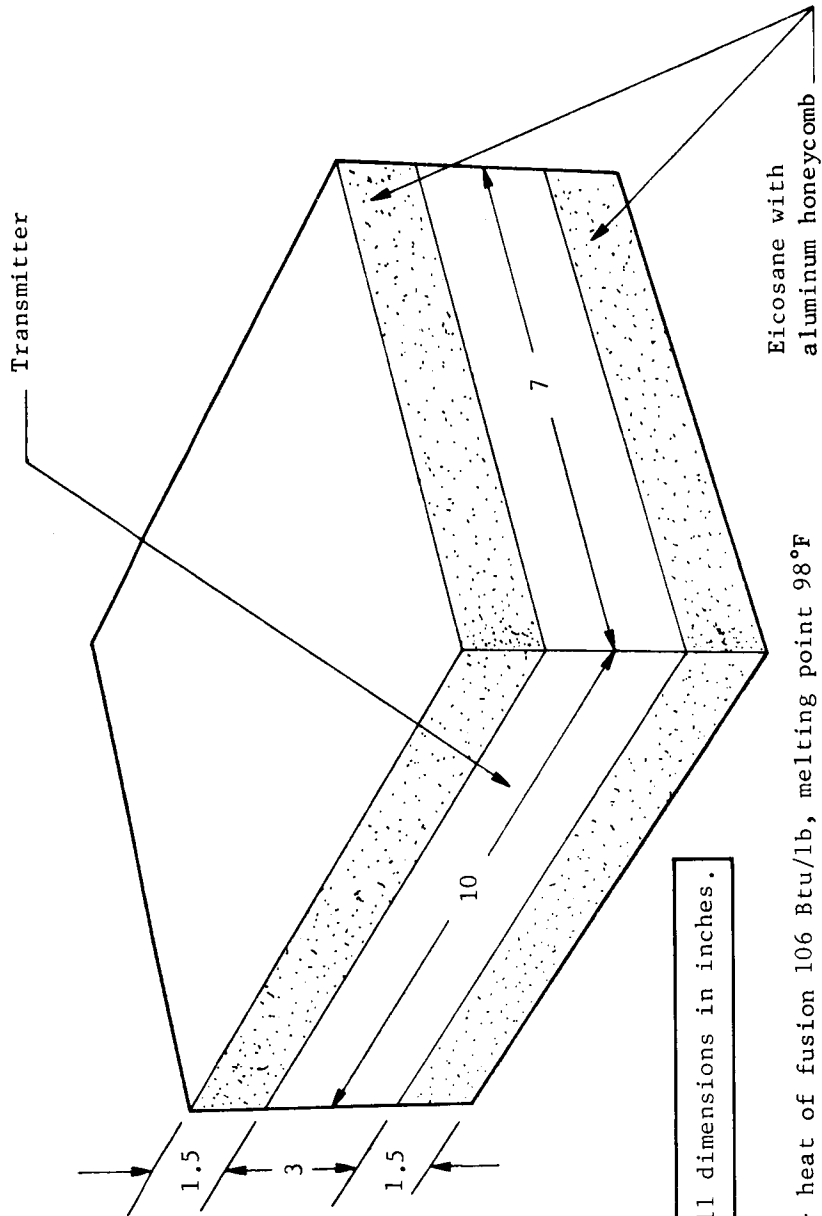


Figure 93.- Insulation Effective Conductivity



Note: All dimensions in inches.

Eicosane - heat of fusion 106 Btu/lb, melting point 98°F

Transmitter output - 72 W, 2 hr/day

Eicosane weight - 4.16 lb

Packaging weight =  $0.5 + 6.3/\Delta T$  (includes 0.020 walls plus honeycomb)

For  $\Delta T = 20^\circ\text{F}$ , total weight = 5.4 lb

Figure 94.- Phase Change Packaging Concept

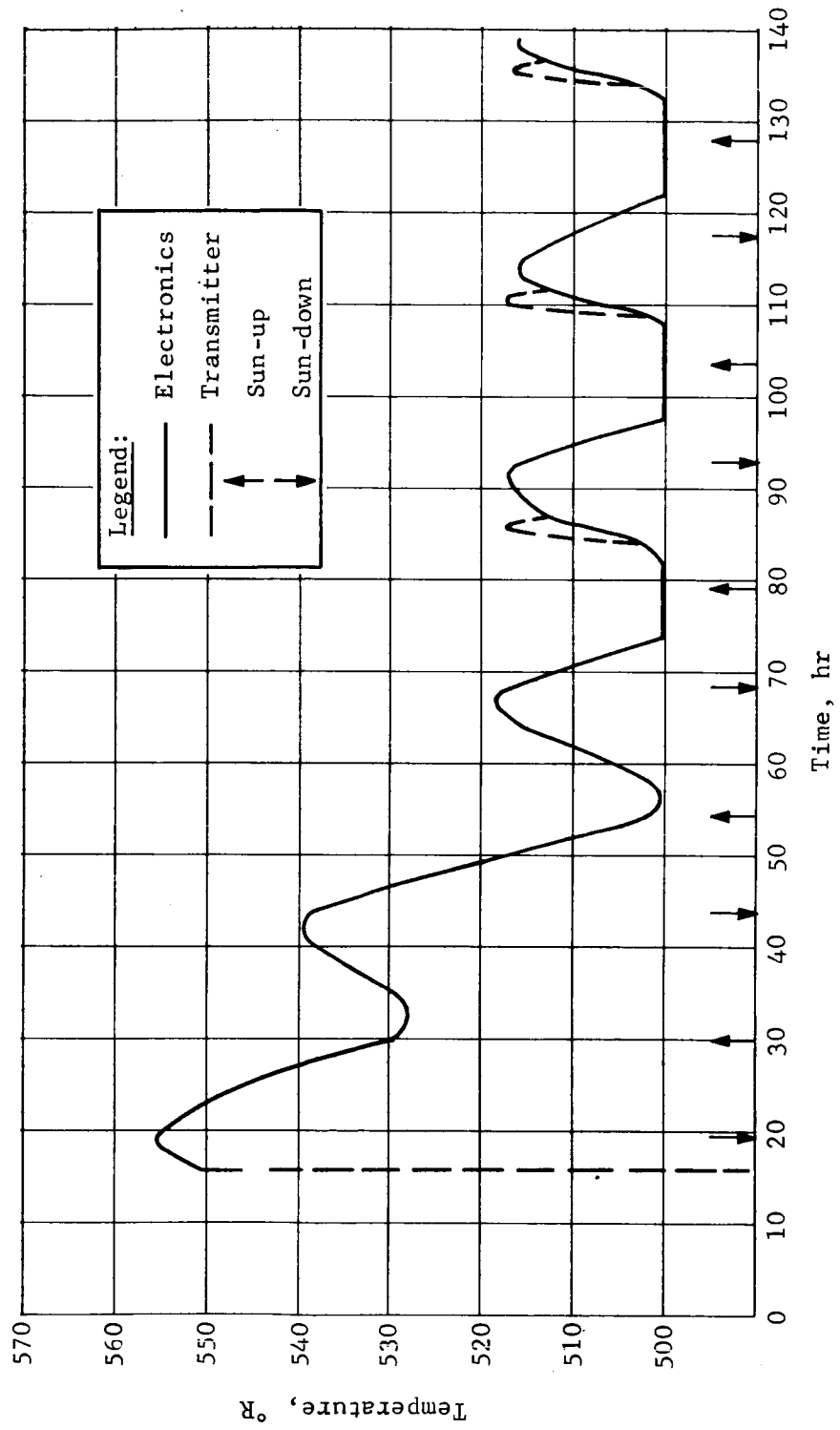


Figure 95.- Lander Temperature as a Function of Time, Hot Environment

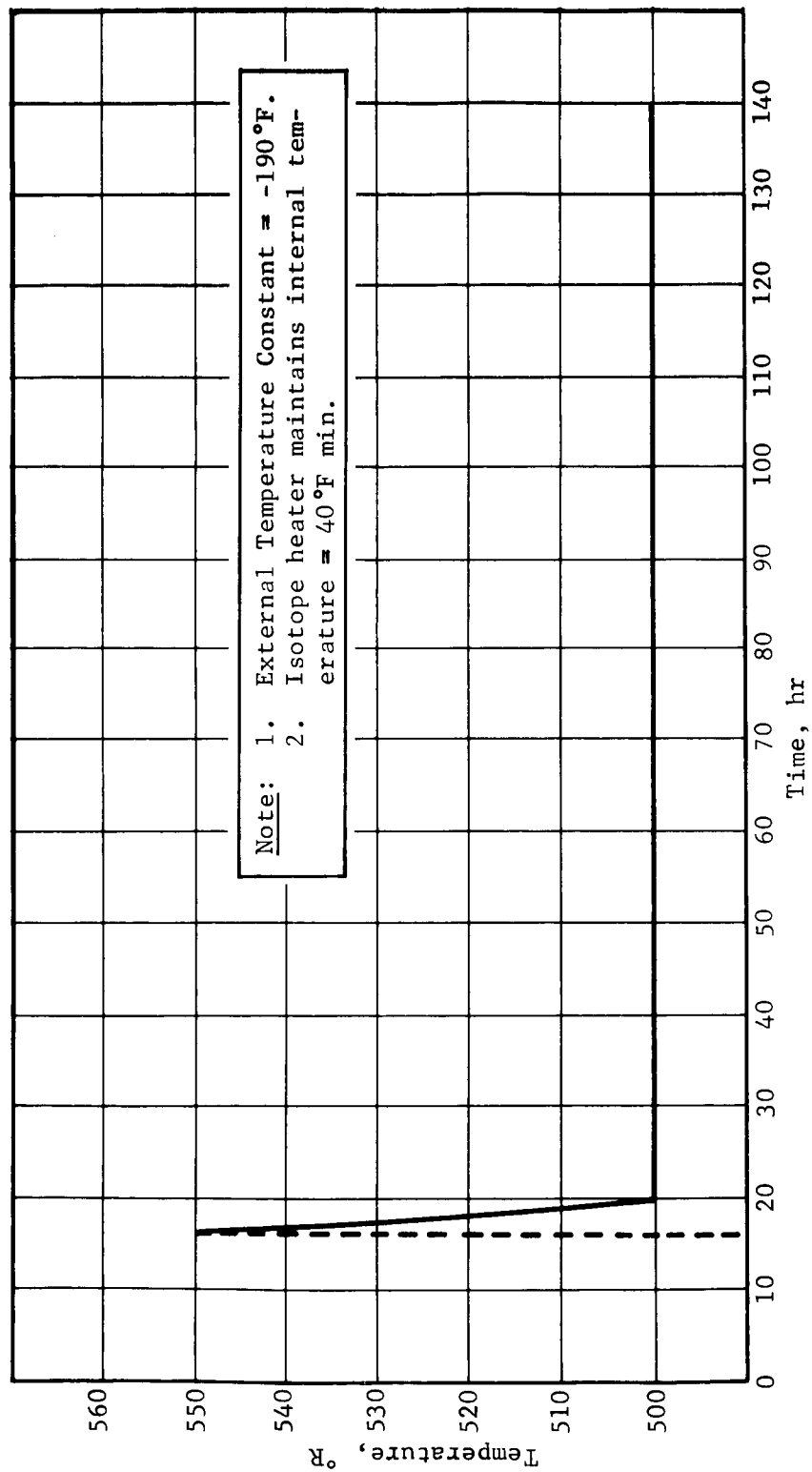


Figure 96.- Lander Temperature as a Function of Time, Cold Environment, 100%  $\text{N}_2$  Atmosphere

Component	Development Status
Insulation	<p>Little thermal conductivity data in simulated Mars environments available.</p> <p>No material compatibility data available.</p> <p>JPL is scheduled to let a contract in June 1968 to develop insulation materials and concepts.</p>
Radioisotope heaters	<p>2.5 W heaters were developed for Surveyor but were not flown (intact entry was not required).</p> <p>Four-month study for a 25 W heater for the ALSEP program completed by Atomics International. Decision by NASA to develop this heater expected by July 1968.</p>
Phase change materials	<p>Development work done for NASA by Northrup.</p>

Cruise and descent modes. - Cruise mode thermal control consists of multilayer insulation on the outside of the sterilization canister and thermostatically controlled electrical heaters powered from the orbiter solar panels. Descent mode thermal control is a passive system consisting of coatings, multilayer insulation, and bulk insulation on compartments and components as required to protect against aerodynamic heating. In addition, bulk insulation and heaters are used on the terminal descent rocket engines. This design approach was studied in detail during our Voyager Phase B studies. A method of estimating insulation weight is given in section 2 of Appendix D.

Development status. - The most critical component in the cruise and descent mode design is the multilayer insulation. Full-scale tests of a cruise mode insulation system were conducted by Martin Marietta Corporation. This insulation consisted of 10 layers of 1/4-mil Mylar aluminized on both sides with two layers of silk mesh between each shield. The following performance was achieved.

$$q/A = 0.40 \text{ Btu}/(\text{hr-ft}^2) \text{ at } 55^\circ\text{F}$$

$$\text{Weight (W/A)} = 0.078 \text{ lb}/\text{ft}^2 \text{ (with 2-mil Kapton cover)}$$

These data are in close agreement with the performance achieved by General Electric with a similar insulation design.

System performance. - During the cruise mode, the isotopes generate 200 W. Penetration losses are estimated to be 6 W, based on scaling from the Martin Marietta tests discussed above. Therefore, for this configuration (170 ft<sup>2</sup> canister), the allowable insulation heat loss during the cruise mode is 3.9 Btu/(hr-ft<sup>2</sup>), which is about a factor of ten larger than heat loss for the ten-layer insulation described above. The required heat flux for this configuration can therefore be obtained with a single layer plus cover and attachments.

## 2. CONFIGURATION 2A DESCRIPTION, DIRECT ENTRY

### Requirements and Constraints

The requirements and constraints imposed on Configuration 2A differ from those of Configuration 1A only as required to be compatible with the direct entry mode. Specific differences are discussed here.

Mission.- Mission differences are:

- 1) Direct entry;
- 2) Deflection  $\Delta V$ : 75 mps;
- 3) Entry angle,  $\gamma_E$ :

Nominal  $21^\circ$ ,  $5\sigma$  above skipout,  
Entry corridor,  $18^\circ \leq \gamma_E \leq 24^\circ$ ;

- 4) Landing site:

Latitude,  $\pm 20^\circ$  from equator  
longitude,  $30^\circ$  on daylight side of evening terminator.

System and subsystem.- The aeroshell diameter must be the minimum compatible with entry conditions and Mach 2 parachute usage.

### System Definition

Although this system enters direct from the approach trajectory rather than out of orbit, the functional schematic of figure 59 is still applicable. Major differences between this configuration and 1A are:

- 1) The aeroshell diameter is increased to 10.75 ft to be compatible with the parachute deployment conditions;
- 2) A thermal afterbody is added because of the higher base heating experienced during the high velocity direct entry;
- 3) A change in structural layout allowed by the larger aeroshell improving particularly the solar panel and vernier engine arrangements.

## Performance Summary

Table 31 presents pertinent launch-to-landing performance parameters.

TABLE 31.- CONFIGURATION 2A PERFORMANCE PARAMETERS

Launch vehicle . . . . .	Titan IIIC/Centaur
Launch date . . . . .	July 11, 1973
$C_3$ , (km/sec) <sup>2</sup> . . . . .	17.2
Arrival date . . . . .	January 30, 1974
$V_{HE}$ , km/sec . . . . .	3.21
Injected payload capability, lb . . . . .	8270
Spacecraft weight, lb . . . . .	4404
Space vehicle margin, lb . . . . .	(3866)
$\Delta V_{M/C}$ , mps . . . . .	75
Encounter weight, lb . . . . .	3776
$R_{EJ}$ , km . . . . .	100,000
$\Delta V_{O/I}$ , mps . . . . .	1375
Orbit characteristics (reference)	
$h_p$ , km . . . . .	1000
$h_a$ , km . . . . .	33 070
P, hr . . . . .	24.62
Spacecraft weight in orbit (minus propulsion), lb . . . . .	1067
Flight capsule weight, lb . . . . .	2077
$\Delta V_{EJ}$ , mps . . . . .	75
$\gamma_e$ , deg . . . . .	-24 (max.)
$\gamma_e$ , fps . . . . .	20 000 (max.)
$B_e$ , sl/ft <sup>2</sup> (10.75-ft-diam aeroshell) . . . . .	0.35
Entry weight, lb . . . . .	1700
Parachute deployment altitude, ft ( $h_T = 0$ ) . . . . .	11 000
$B_{DEC}$ , sl/ft <sup>2</sup> (71-ft-diam chute) . . . . .	0.020
Vernier ignition altitude, ft . . . . .	4000
$W_{LE}$ , lb . . . . .	570



The 570-lb landed equipment weight for this direct entry system results in a total flight capsule system weight of 2077 lb.

### Functional Sequence

The functional sequence for Configuration 2A is identical to Configuration 1A that the entry mode is direct and the aft heat shield separation occurs at parachute jettison.

### Sequential Weight Statement

Table 32 is a summary sequential weight statement of the 2A configuration. A detail flight capsule weight summary is given in section 1 of Appendix D. The weight of landed equipment for this configuration is 570 lb, of which 84.4 lb are landed science. In addition there are 18 lb of entry science in the aeroshell, giving a total science weight of 102.8 lb.

### Space Vehicle Integration

Figure 97 shows the spacecraft mounted inside the 12.0-ft-diameter bulbous shroud on the Titan IIIC/Centaur launch vehicle. Integration is functionally similar to Configuration 1A (fig. 60). The differences are those entailed by the larger capsule aeroshell diameter and deletion of the additional orbiter propulsion capability required by Configuration 1A.

### Science

The science subsystem is the same for this configuration as discussed under Configuration 1A.

### Structures and Mechanisms

Functional description.- The structure and mechanisms subsystem of the Configuration 2A capsule consists of the sterilization canister, aeroshell, orbit deflection module, aerodynamic decelerator, afterbody structure, lander structure, and related mechanisms. These major components are shown in figure 98, sheets 1 and 2.

TABLE 32.- CONFIGURATION 2A SEQUENTIAL WEIGHT STATEMENT

Titan IIIC/Centaur capability	(9240)	
Fairing and/or beefup penalty	470	
Adapter	500	
Margin	3866	
Spacecraft weight	(4404)	
Orbiter expendables	1035	
(including 25 lb N <sub>2</sub> gas)		
Inorbit weight <sup>a</sup>	(3369)	
Orbiter propulsion system	225	
(including residuals)		
Useful inorbit weight <sup>a</sup>	(3144)	
Useful inorbit orbiter weight	990	
Capsule adapter	77	
Flight capsule weight	(2077)	
Canister	224	
Aft section, body	142	
Forward section, lid	64	
Electrical in canister	18	
Separated capsule weight	(1853)	
Deflection module structure	33	
Deflection propulsion system	57.6	
Deflection propellant	61	
ACS propellant	1.8	
Entry weight (B <sub>E</sub> = 0.35)	(1699.6)	
Aeroshell	257.0	
Science in aeroshell	18.0	
ACS propellant	1.5	
Decelerator load	(1423.1)	
Chute weight	228	
Back face	47	
Verniered weight	(1148.1)	
Vernier propellant	116.0	
ACS propellant	.8	
Landed weight	(1031.3)	
Propulsion system	117.6	
Useful landed weight	(913.7)	W <sub>LE</sub>
Structure	222	
Attitude control system	32	
Power system	211	211
Guidance and control	131	131
Telecommunication	97.4	76.4
Thermal control	82	67
Pyrotechnic control	53.5	
Science	84.8	84.8
Landed equipment weight, W <sub>LE</sub> = 570.2		
<sup>a</sup> Because this is a direct entry case inorbit weight includes the flight capsule, which enters directly and the orbiter, which is put into orbit after separation.		

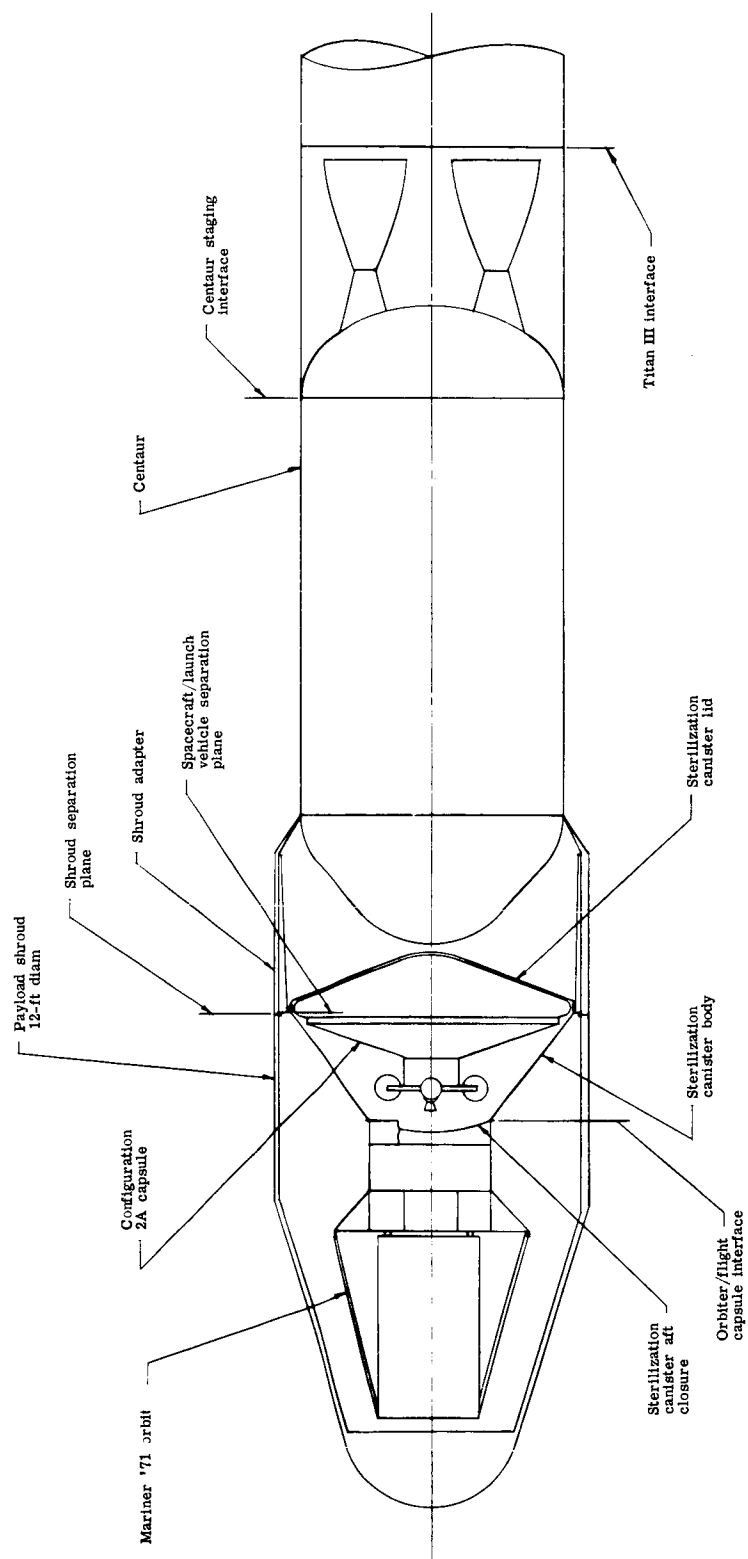


Figure 97. - Space Vehicle Integration, Configuration 2A

Sterilization canister: With the exception of the larger size of the components due to the 10.75-ft-diameter aeroshell required for Configuration 2A, all components are similar to those of Configuration 1A.

Aeroshell (fig. 98, sheet 1): The 10.75-ft-diameter aeroshell retains the same features used on the Configuration 1A 8.5-ft-diameter aeroshell design. In addition, the outboard ring-frame is extended to provide attachment structure for the outboard edge of the flexible position of the afterbody.

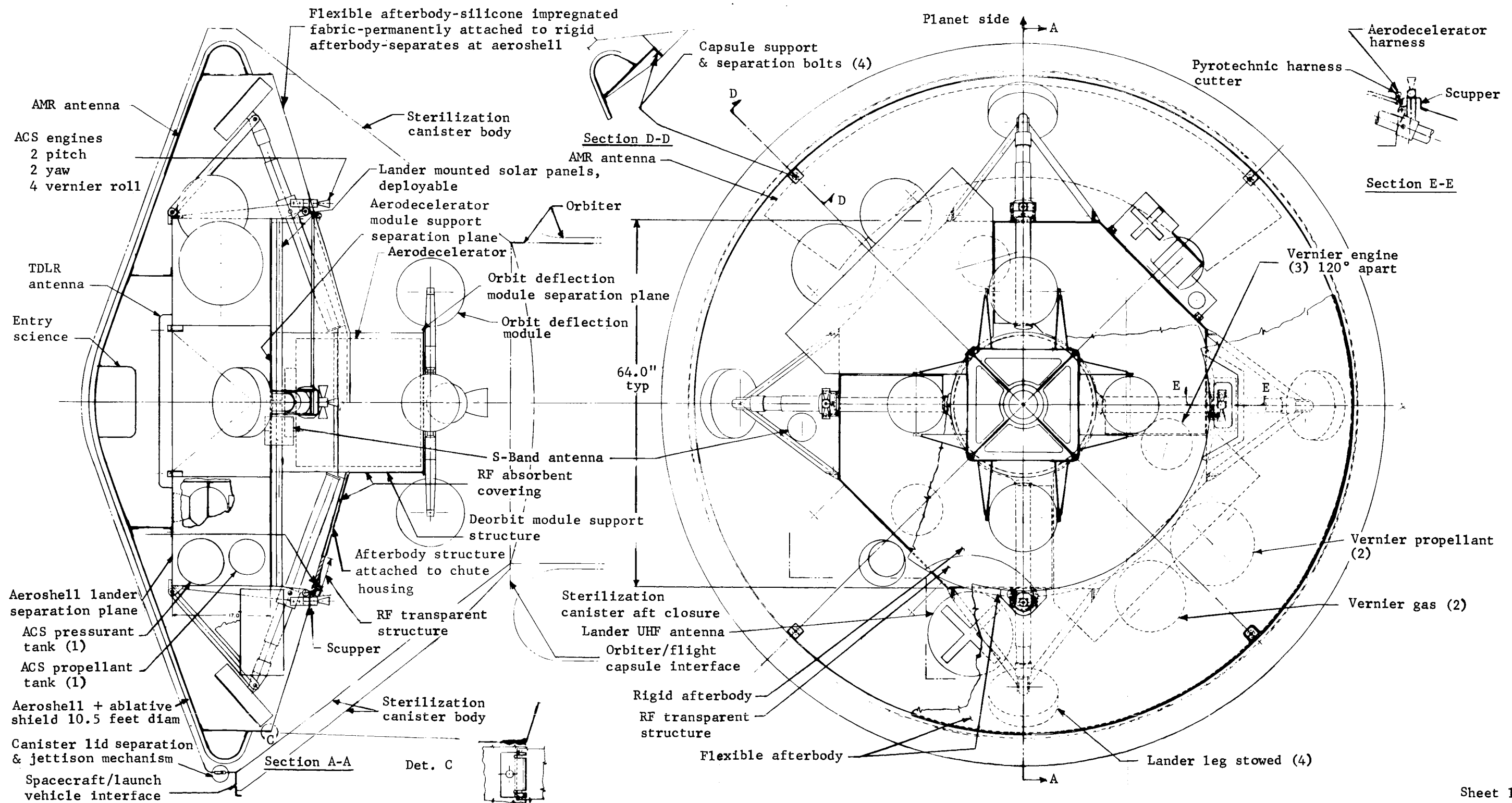
Deflection module (fig. 98, sheet 1): The deflection module of this configuration is similar in appearance and has the identical mounting and jettisoning features shown on the Configuration 1A deorbit module.

Aerodynamic decelerator (fig. 98, sheet 1): The Configuration 2A aerodynamic decelerator installation and operation is essentially the same as that of Configuration 1A. However, when the aerodecelerator is released from the lander, it carries with it not only the orbit deflection module support structure and spent mortar, but also the afterbody structure.

Afterbody structure (fig. 98, sheet 1): The Configuration 2A capsule incorporates a protective afterbody because of the anticipated higher heating rate during direct entry.

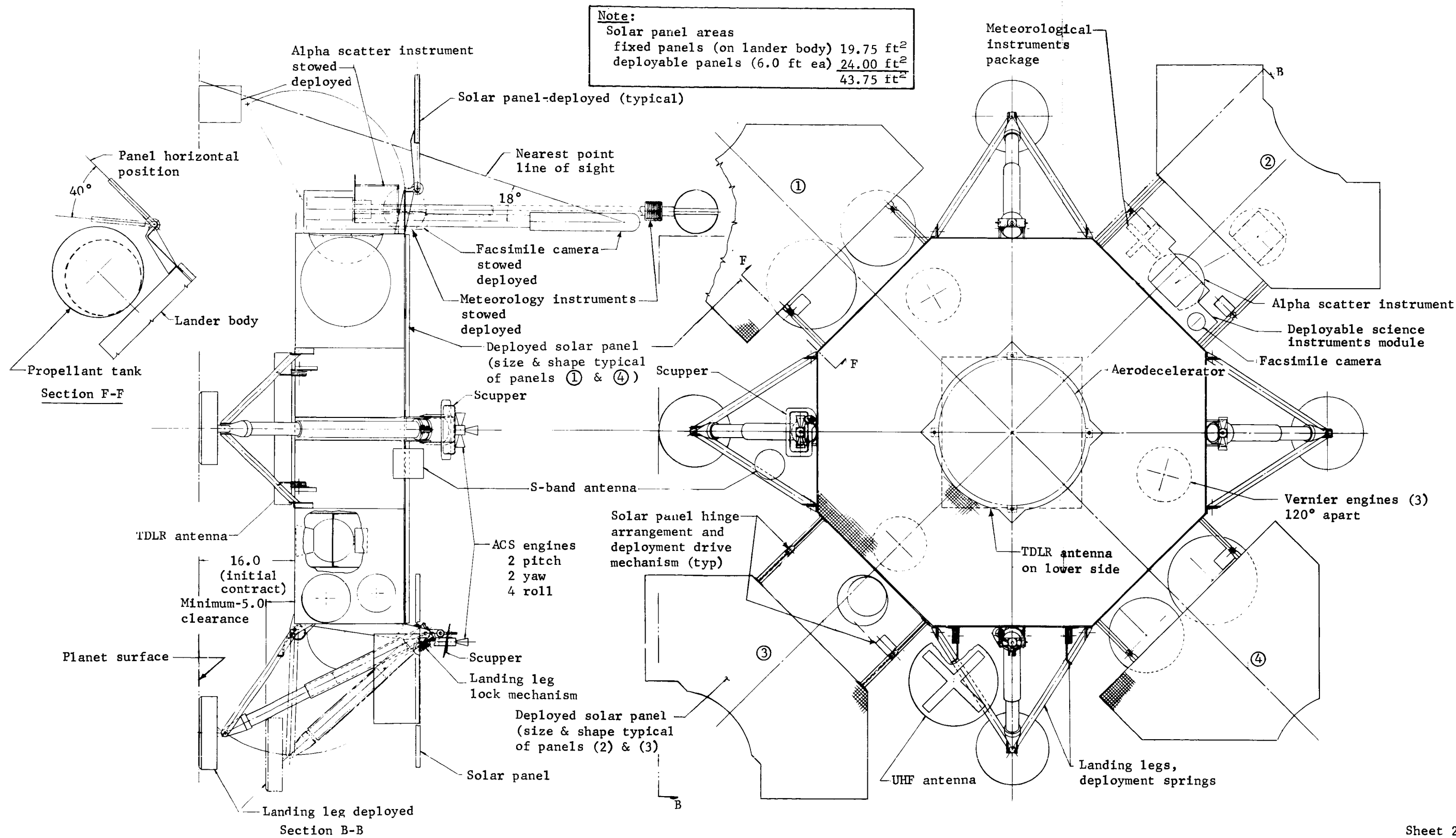
The afterbody is made in two major parts: a lightweight metal shell with a thermal control coating, covering the top of the lander body, and a silicone impregnated fabric that spans the gap from the metal shell to the aeroshell. The use of fabric for this part of the afterbody has several advantages. Since the aeroshell is jettisoned while the vertical velocity of the lander is still high, the fabric will be free to fold back to the relatively streamlined position. A rigid structure capable of surviving the airloads would be heavier than the fabric. In addition, the rigid structure would cause unstable aerodynamic forces on the lander in the time period between aeroshell jettisoning and aerodecelerator jettisoning.

The metal afterbody shell is attached to the lander by a permanent joint to the deflection module support- and compression-carrying standoffs between the lander body and the outer edge of the shell. The fabric portion of the afterbody is permanently attached to the outer edge of the metal shell. At its outer edge, the fabric is welted and retained by a series of fingered spring clips attached



Sheet 1

Figure 98.- Configuration 2A



to an extension of the aeroshell outboard ring-frame. When the aerodecelerator is released from the lander, taking the deflection module support and attached afterbody shell with it, the fabric edge is pulled out from under the clips. Rigid scuppers attached to the ACS nozzle cluster supports provide tight closures and facilitate the use of large clearance cutouts in the afterbody structure to prevent nozzle damage during afterbody jettison. RF transparent and absorbent materials are used at various places on the metal shell to improve the antenna pattern.

Lander structure and related mechanisms (fig. 98, sheet 2): The Configuration 2A lander body is a larger octagonal planform structure than that shown in Configuration 1A. The use of the larger aeroshell allows the lander planform area to be enlarged, which in turn, permits locating the vernier descent engines in the lander body. This avoids the undesireably close proximity of these engines to the lander legs shown in Configuration 1A. Insulation prevents the structure surrounding the engines from overheating. This configuration has a landing stability factor (R/h) of 2.0 and will land stably on slopes to  $32^\circ$  under the same landing conditions as those noted for Configuration 1A.

The lander body houses the same equipment and uses the same thermal control techniques as Configuration 1A. Usable volume within the body is also approximately the same.

One minor difference exists in the landing leg assemblies. No thermal protection is needed on the lander foot since protection is provided by the afterbody.

A total of  $43.75 \text{ ft}^2$  of solar panel area is provided on the lander. A fixed area of  $19.75 \text{ ft}^2$  is located on top of the lander body, and the remaining  $24 \text{ ft}^2$  are provided on four equal area deployable panels. By making the panels in two different shapes, it is possible to avoid stacking the panels in the stowed position that was necessary on Configuration 1A. The panels are hinged outboard of the lander body to provide space for deployment of landed science experiments, and may be driven to any position between  $70^\circ$  above and  $40^\circ$  below the lander horizontal.

The ACS components, landed science module, and antennas are located and mounted in a manner similar to Configuration 1A.

## Propulsion

Functional description.- The direct entry mission mode has no significant effect on the propulsion subsystem other than small changes in propellant quantities and engine thrust.

The landing propulsion subsystem is functionally identical to the system used in Configuration 1A. The only differences are in propellant and pressurant quantities and associated tankage weights and engine thrust and weight.

The deflection propulsion subsystem is functionally identical to the deorbit system used in Configuration 1A. The only differences are in propellant and pressurant quantities and associated tankage weights, and engine thrust and weight. The characteristics of the deflection and landing systems are shown in table 33.

Attitude control system.- The ACS is functionally identical to the attitude control system used in Configuration 1A. The propellant required is reduced compared to Configuration 1A because of the difference in mission mode. A summary of ACS characteristics and propellant use is shown in table 34.

## Guidance and Control

The G&C subsystem is basically the same as for the entry from orbit configuration. The only difference is in the higher deceleration pulse at entry due to the higher entry velocity. This capability would be verified during environmental testing.

## Telecommunications

The telecommunications subsystem is the same for this configuration as discussed under Configuration 1A.

## Power and Pyrotechnics

The power and pyrotechnic subsystem is the same for Configuration 2A as discussed under Configuration 1A.

## Thermal Control

The Mars surface and cruise mode thermal control system for Configuration 2A is the same as for Configuration 1A. The only difference is that Configuration 2A is a direct entry capsule and as a result it has an aerodynamic base heating shield. Therefore, the estimated weight of the thermal control for the descent phase is different than for the out-of-orbit case as described in section 2 of Appendix D.



TABLE 33.- CONFIGURATION 2A PROPULSION SUBSYSTEM CHARACTERISTICS

	Deflection	Landing
Total impulse available, lb-sec . . . . .	13 908	25 870
Maximum thrust per engine, lb . . . . .	540	540
Average delivered specific impulse, sec . . . . .	228	223
Maximum chamber pressure, psia . . . . .	300	300
Nozzle expansion ratio . . . . .	20:1	20:1
Throttling ratio . . . . .	----	5:1
Fuel weight, usable, lb . . . . .	61.0	116
Fuel weight, trapped, lb . . . . .	3.0	5.8
Pressurant weight, lb . . . . .	1.6	3.1
Engine weight, total, lb . . . . .	15.7	47.1
Fuel tank weight (2) total, lb . . . . .	3.9	5.9
Pressurant tank weight (2) total, lb . . . . .	2.5	4.2
Component and line weight, lb . . . . .	13.0	18.3
Engine mount and tank support weight, lb . . . . .	15.8	29.2
Total weight, lb . . . . .	116.5	229.6
Volume per fuel tank, cu ft . . . . .	0.52	1.06
Outside diameter of fuel tank, in. . . . .	12.1	15.1
Volume per pressurant tank, cu ft . . . . .	.31	.62
Outside diameter of pressurant tank, in. . . . .	10.2	12.7
Engine exit diameter, in. . . . .	5.2	5.2
Storage temperature range, (min./max.), °F	40/100	40/100
Operating temperature range (min./max.), °F	40/80	40/80
Fuel tank operating pressure range at 60°F (max./min.), psia . . . . .	500/167	500/167

TABLE 34.- CONFIGURATION 2A ATTITUDE CONTROL SYSTEM

Characteristics		Propellant Schedule	
Measurement	Thrust, lb <sub>f</sub>	Item	Propellant consumed, lb
Pitch and yaw	2.4 to 1.9	Separate from spacecraft  Coast, 30 minutes  Maneuver for deflection  Deflection thrust attitude hold  Coast, 8 hours  Maneuver for entry  Coast, 4 minutes  Rate damping at entry  Landing roll hold  Total required  Contingency (100%)  Total loaded	.03  .04  .05  .77  .04  .05  .03  .66  .43  2.10  2.10  4.20
Roll	3.2 to 2.6		
Measurement	Minimum impulse bit, lb-sec		
Pitch and yaw	.038		
Roll	.052		
Minimum pulse width	20 msec		
Measurement	Pressurization, psia		
Initial GN <sub>2</sub> pressure	360		
Final GN <sub>2</sub> pressure	240		
Blowdown ratio	1.5:1		
Item	Weight		
N <sub>2</sub> H <sub>4</sub>	4.4		
Required	2.1		
Margin	2.1		
Trapped	0.2		
N <sub>2</sub> H <sub>4</sub> tank	.5		
GN <sub>2</sub>	.4		
GN <sub>2</sub> tank	1.0		
Thrusters	6.4		
Components, lines	13.0		
Supports	8.2		
Total	33.9		

### 3. CONFIGURATION 1B DESCRIPTION, OUT OF ORBIT

#### Requirements and Constraints

The requirements and constraints imposed on this configuration are the same as those for Configuration 1A except that a 10% margin is applied to system dry weight and the aeroshell is sized to allow parachute deployment above 20 000 ft.

#### Performance Summary

Table 35 presents pertinent launch-to-landing performance parameters for Configuration 1B.

#### System Definition

This configuration is functionally identical to Configuration 1A. Because of the weight margin allocated to the hardware elements and the higher parachute deployment requirement, the size of many components are larger. The resultant aeroshell diameter is 10.5 ft. The larger aeroshell allows a better packaging concept as explained in the structure description.

The landed equipment weight of 627 lb, including 10% margin, builds up to a total flight capsule system weight of 1982 lb.

#### Functional Sequence

The functional sequence for Configuration 1B is identical to Configuration 1A.

#### Sequential Weight Statement

Table 36 is a summary sequential weight statement of the 1B configuration. A detail flight capsule weight summary is given in section 1 of Appendix D. Because this configuration carries a weight margin on all flight capsule hardware, the weight of landed equipment for this configuration is 627 lb, of which 93.3 lb is allocated to landed science. A total of 19.8 lb including margin would be allocated to entry science, giving a total science allocation of 113.1 lb.

TABLE 35.- CONFIGURATION 1B PERFORMANCE PARAMETERS

Launch vehicle . . . . .	Titan IIIC/Centaur
Launch date . . . . .	July 13, 1973
$C_3$ , (km/sec) <sup>2</sup> . . . . .	16.3
Arrival date . . . . .	February 2, 1974
$V_{HE}$ , km/sec . . . . .	3.15
Injected payload capability, lb . . . . .	8325
Spacecraft weight, lb . . . . .	5770
Space vehicle margin, lb . . . . .	(2555)
$\Delta V_{M/C}$ , mps . . . . .	75
Encounter weight (minus ACS gas), lb . . . . .	5585
$\Delta V_{O/I}$ , mps . . . . .	1350
Orbit characteristics (reference)	
$h_p$ , km . . . . .	1000
$h_a$ , km . . . . .	33 070
P, hr . . . . .	24.62
Spacecraft weight in orbit (minus propulsion), lb . . . . .	3049
Flight capsule weight, lb . . . . .	1982
$\Delta V_{D/O}$ , mps . . . . .	120
$\gamma_e$ , deg . . . . .	-18 (max.)
$V_e$ , fps . . . . .	16 000 (max.)
$B_e$ , sl/ft <sup>2</sup> (10.5-ft-diam aeroshell) . . . . .	0.336
Entry weight, lb . . . . .	1541
Parachute deployment altitude, ft ( $h_T = 0$ ) . . . . .	22 000
$B_{DEC}$ , sl/ft <sup>2</sup> (48-ft-diam chute) . . . . .	0.040
Vernier ignition altitude, ft . . . . .	4000
$W_{LE}$ , lb . . . . .	627

TABLE 36.- CONFIGURATION 1B SEQUENTIAL WEIGHT STATEMENT

Titan IIIC/Centaur capability	(9295)	
Fairing and/or beefup penalty	470	
Adapter	500	
Margin	2555	
Spacecraft weight	(5770)	
Orbiter expendables		
(including 45 lb of N <sub>2</sub> gas)	2171	
Inorbit weight	(3599)	
Orbiter propulsion system	550	
Useful inorbit weight	(3049)	
Useful inorbit orbiter weight	990	
Capsule adapter	77	
Flight capsule weight	(1982)	
Canister	219	
Aft section, body	139	
Forward section, lid	62	
Electrical in canister	18	
Margin	22	
Separated capsule weight	(1741)	
Deorbit structure	31	
Deorbit propulsion system	65.8	
Deorbit propellant	89.0	
ACS propellant	4.0	
Margin	10.0	
Entry weight ( $B_E = 0.331$ )	(1541.2)	
Aeroshell	196.0	
Science in aeroshell	18.0	
ACS propellant	1.5	
Margin	18.0	
Decelerator load	(1307.7)	
Chute weight (48 ft)	90.0	
Margin	9.0	
Verniered weight	(1208.7)	
Vernier propellant	113.0	
ACS propellant	1.0	
Landed weight	(1094.7)	
Propulsion system	124.8	
Useful landed weight	(969.9)	$W_{LE}$
Structure	168.0	
Attitude control system	33.2	
Power system	211.0	211
Guidance and control	131.0	131
Telecommunications	97.4	76.4
Thermal control	91.0	67
Pyrotechnic control	53.5	
Science	84.8	84.8
Margin	100.0	57.0
Landed equipment weight, $W_{LE} = 627.2$ (including margin)		

## Space Vehicle Integration

Figure 99 shows the spacecraft mounted inside the 12.0-ft-diameter bulbous shroud on the Titan IIIC/Centaur launch vehicle. Integration of Configuration 1B is functionally similar to Configuration 2A. The primary difference is the requirement to include additional propulsion capability in the Mariner '73 orbiter for flight capsule orbit insertion.

## Science

The science subsystem is the same for Configuration 1B as discussed under Configuration 1A.

## Structures and Mechanisms

Functional description. - The structure and mechanisms subsystem of the Configuration 1B capsule consists of all elements of the 2A configuration with the exception of the afterbody structure. This structure is not required for orbital entry. Figures 100 and 98 (sheet 2) show the major components of the 1B configuration.

**Sterilization canister:** Because of the smaller aerodecelerator required for Configuration 1B, and the resulting short length of the capsule, the canister is somewhat shorter than that of Configuration 2A. All other features of the design are similar.

**Aeroshell (fig. 100):** The Configuration 1B aeroshell differs from the 2A unit only in diameter (10.5 ft) and that no extension of the outboard ring-frame is required since there is no afterbody.

**Deorbit module (fig. 100):** The appearance of the module is similar, and the mounting and jettisoning features are identical to the Configuration 2A orbit deflection module.

**Aerodynamic decelerator (fig. 100):** Although smaller in size the installation and operation of the aerodecelerator is the same as that of Configuration 2A, except for the deletion of the afterbody structure.

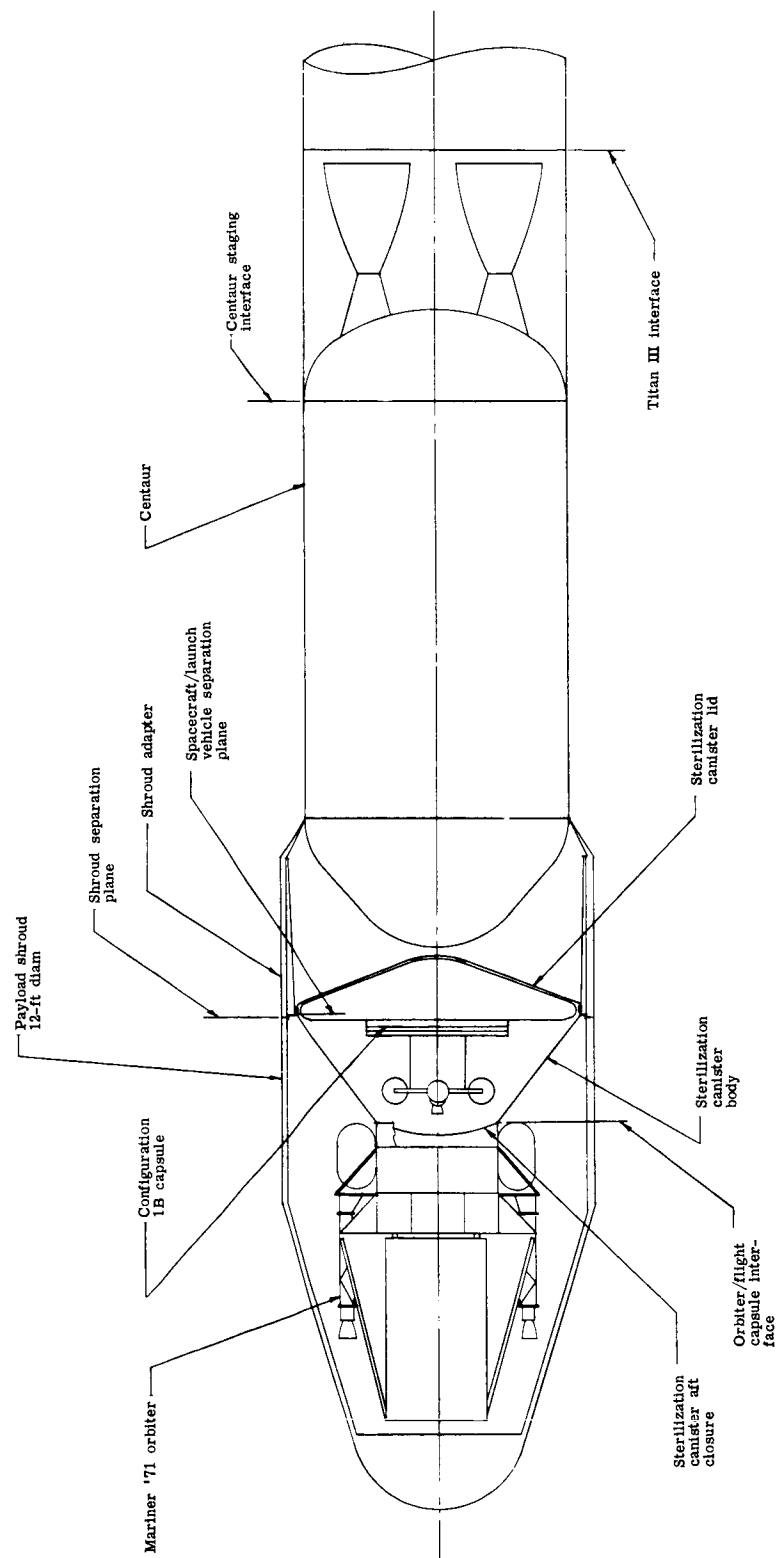


Figure 99. - Space Vehicle Integration, Configuration 1B

Lander structure and related mechanisms (figs. 100 and 98 sheet 2): The configuration 1B lander body is identical in size and shape to the 2A configuration as are the landing leg assembly.

Because of the smaller size aerodecelerator container, more solar panel area is provided than on the Configuration 2A lander. A fixed area of  $20.5 \text{ ft}^2$  is located on top of the lander body, and the remaining  $24.5 \text{ ft}^2$  of the total area of  $45 \text{ ft}^2$  is located on four equal area deployable panels. Other features of the solar panels are identical to those of Configuration 2A.

The ACS components, landed science module, and antennas are located and mounted identically to Configuration 2A.

Landing stability is the same as for 2A.

#### Propulsion

The deorbit, landing, and attitude control systems for this configuration are functionally identical to the systems used in Configuration 1A. Tables 37 and 38 present the characteristics of these subsystems.

#### Guidance and Control

The guidance and control subsystem for Configuration 1B is identical to Configuration 1A.

#### Telecommunications

The telecommunications subsystem for Configuration 1B is identical to Configuration 1A.

#### Power and Pyrotechnics

The power and pyrotechnics subsystem for Configuration 1B is identical to Configuration 1A.

#### Thermal Control

The thermal control subsystem for Configuration 1B is identical to Configuration 1A.



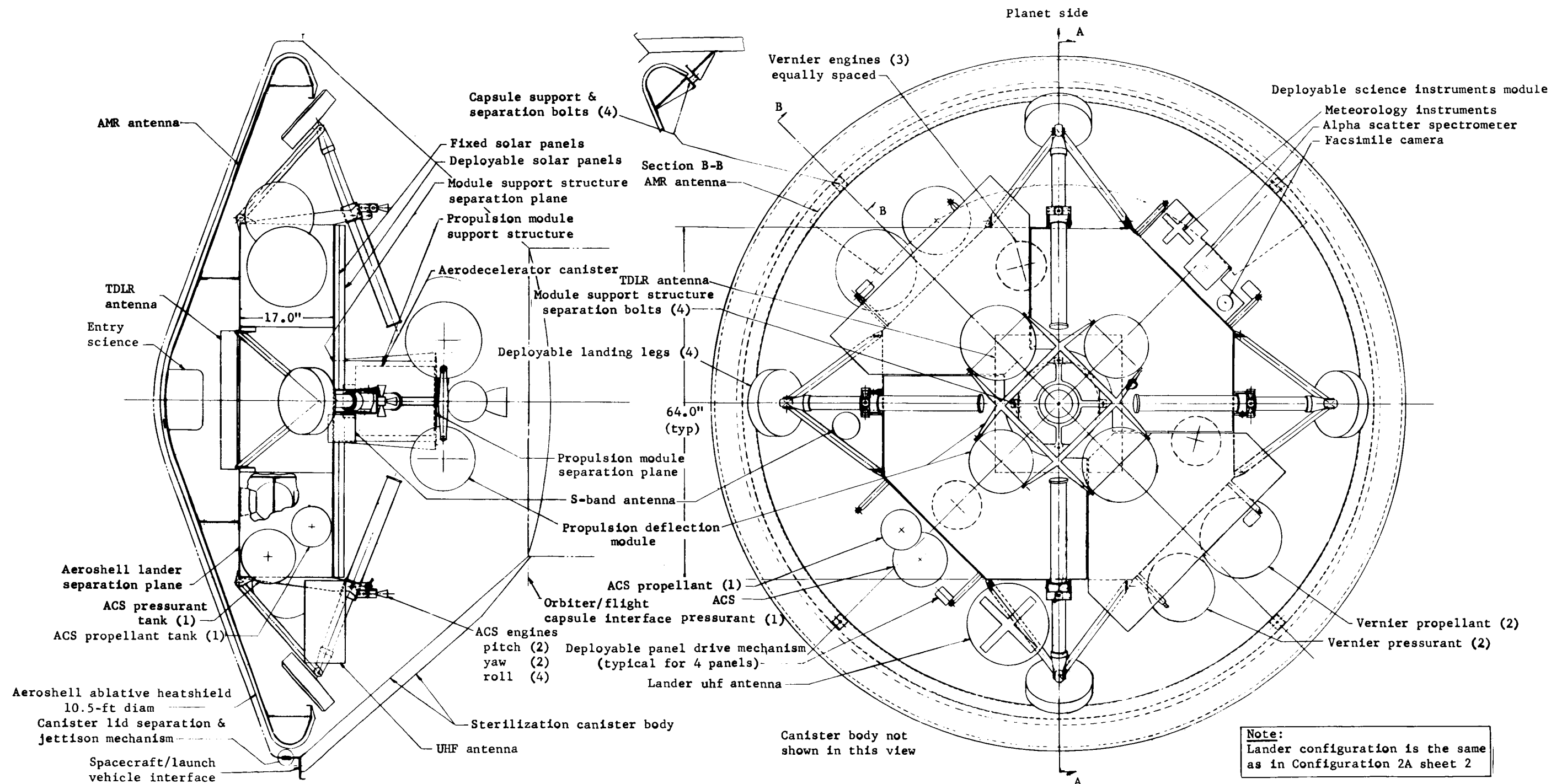


Figure 100.- Configuration 1B

TABLE 37.- CONFIGURATION 1B PROPULSION SUBSYSTEM CHARACTERISTICS

Parameter	Deorbit	Landing
Total impulse available, lb-sec . . . . .	21 292	25 200
Maximum thrust per engine, lb . . . . .	635	635
Average delivered specific impulse, sec . .	228	223
Maximum chamber pressure, psia . . . . .	300	300
Nozzle expansion ratio . . . . .	20:1	20:1
Throttling ratio . . . . .	----	6.3:1
Fuel weight, usable, lb . . . . .	89.0	113.0
Fuel weight, trapped, lb . . . . .	4.4	5.5
Pressurant weight, lb . . . . .	2.4	3.0
Engine weight, total, lb . . . . .	17.9	53.7
Fuel tank weight (2) total, lb . . . . .	5.0	5.9
Pressurant tank weight (2) total, lb . . .	3.2	4.1
Component and line weight, lb . . . . .	13.0	18.3
Engine mount and tank support weight, lb .	17.8	30.2
Total weight, lb . . . . .	152.7	233.7
Volume per fuel tank, cu ft . . . . .	0.78	0.99
Outside diameter of fuel tank, in. . . . .	13.7	14.8
Volume per pressurant tank, cu ft . . . . .	0.47	0.58
Outside diameter of pressurant tank, in. .	11.6	12.4
Engine exit diameter, in. . . . .	5.6	5.6
Operating temperature range (min./max.), °F	40/80	40/80
Storage temperature range (min./max.), °F .	40/100	40/100
Fuel tank operating pressure range at 60°F (max./min.), psia . . . . .	500/167	500/167
Pressurant tank operating pressure range at 60°F (max./min.), psia . . . . .	505/167	505/167

TABLE 38.- CONFIGURATION 1B ATTITUDE CONTROL SYSTEM

Characteristics		Propellant schedule	
Measurement	Thrust, lb <sub>f</sub>	Item	Propellant consumed, lb
Pitch and yaw Roll	3.7 to 2.8 2.2 to 1.7	Separation from spacecraft	0.02
Measurement	Minimum impulse bit, lb-sec	Coast, 30 minutes	0.07
Pitch and yaw Roll	0.056 0.034	Maneuver for deorbit	0.04
Minimum pulse width	20 ms	Deorbit thrust attitude hold	1.77
Measurement	Pressurization, psia		
Initial GN <sub>2</sub> pressure	360	Coast, 8 hours	0.07
Final GN <sub>2</sub> pressure	240		
Blowdown ratio	1.5:1	Maneuver for entry	0.04
Items	Weight, lb		
N <sub>2</sub> H <sub>4</sub>	6.7	Coast, 4 minutes	0.02
Required	3.2		
Margin	3.2	Rate damping at entry	0.73
Trapped	0.3		
N <sub>2</sub> H <sub>4</sub> tank	0.8	Landing roll hold	<u>0.44</u>
GN <sub>2</sub>	0.5		
GN <sub>2</sub> tank	1.3	Total required	3.20
Thrusters	6.4		
Components, lines	13.0	Contingency (100%)	<u>3.20</u>
Supports	8.9		
Total	37.6	Total loaded	6.40

#### 4. CONFIGURATION 2C DESCRIPTION, AUTONOMOUS CAPSULE

##### Requirements and Constraints

Deviations and additions to the requirements and constraints of Configuration 2A are presented in this subsection.

Mission.- The mission deviations and additions for Configuration 2C are:

- 1) Entry will be timed so that an orbiter from a previous launch is available to provide relay communications during entry and for 2 days after landing;
- 2) The canister lid will be ejected before the final launch vehicle burn. The aft canister will remain with the last launch vehicle stage;
- 3) The deflection  $\Delta V$  requirement is deleted. The final midcourse maneuver will put the entire vehicle on the approach trajectory.

System and subsystem.- The system and subsystem deviations and additions for Configuration 2C are:

- 1) A common subsystem will be used for both trans-Mars and Mars entry functions, where practical;
- 2) For the propulsion subsystem there is one midcourse engine with the same design as vernier engines. The trans-Mars ACS provides couples in all three axes;
- 3) For the guidance and control subsystem sun and Canopus sensors are added to provide orientation during cruise. Additional computer capability is required for computation and sequencing;
- 4) The power subsystem will have sun acquisition from trans-Mars to entry using solar cells. Power for entry through the first two days will be supplied by batteries. Long-term operation will be by solar array/battery;
- 5) Communications will be low gain direct and command direct (launch vehicle separation through end of mission except entry to landing). Relay will be used for entry to landing plus two days.

## Performance Summary

Table 39 presents pertinent launch-to-landing performance parameters for Configuration 2C.

TABLE 39.- CONFIGURATION 2C PERFORMANCE PARAMETERS

Launch vehicle . . . . .	Titan IIIC
Launch date . . . . .	July 13, 1973
$C_3$ , (km/sec) <sup>2</sup> . . . . .	16.3
Arrival date . . . . .	February 2, 1974
$V_{HE}$ , km/sec . . . . .	3.15
Injected payload capability, lb . . . . .	2330
Spacecraft weight, lb . . . . .	2281
Space vehicle margin, lb . . . . .	(49)
$\Delta V_{M/C}$ , mps . . . . .	75
Encounter weight, lb . . . . .	2204
$\gamma_e$ , deg . . . . .	-24 (max.)
$V_e$ , fps . . . . .	20 000 (max.)
$B_e$ , sl/ft <sup>2</sup> (11-ft-diam aeroshell) . . . . .	0.346
Entry weight, lb . . . . .	1900
Parachute deployment altitude, ft ( $h_T = 0$ ) . . . . .	12 000
$B_{DEC}$ , sl/ft <sup>2</sup> (73-ft-diam chute) . . . . .	0.021
Vernier ignition altitude, ft . . . . .	4000
$W_{LE}$ , lb . . . . .	570

## System and Subsystem Definition

The autonomous flight capsule is physically very similar to Configuration 2A. Both systems enter directly from the approach trajectory. Again starting with a 570-lb landed equipment weight, the flight capsule system weight for this configuration is 2281 lb.

Although the functional block diagram (fig. 101) indicates only minor changes, many significant changes are required in the operating characteristics of the elements. These are briefly summarized in the following subsections.

Structures and mechanisms.- The aeroshell diameter is increased to 11.5 ft to accommodate the higher entry weight. A second solar array is mounted outside the afterbody for use during the trans-Mars cruise phase. The periphery of the aeroshell and part of the rigid base cover supports these solar panels, the cruise ACS, and the new sun sensors. A Canopus sensor and a cruise mode S-band antenna are mounted on the deorbit propulsion module. Figure 102 shows the major configuration characteristics. Since the capsule and orbiter are combined in this configuration, longerons are not required in the sterilization canister.

Propulsion.- A low thrust cold gas ACS is added to generate couples in all three axes during the trans-Mars cruise period. In addition, the midcourse correction propulsion system (similar in size to the deflection propulsion module of 2A) must be capable of multiple firings, months apart.

Guidance and control.- In addition to the Configuration 1A functions, the G&C subsystem requires interplanetary sequencing capability and sun-Canopus sensors to provide an inertial reference during interplanetary cruise. The sequencing requirement has a negligible effect on the G&C memory capacity; however additional input/output circuitry is required for the added discretes.

All equipment must be sterilized because the entire vehicle is enclosed in the sterilization canister at launch. A potential problem lies in the sterilization capability of the sun-Canopus sensors. At the present time, there are no known sensors that can guarantee performance after being sterilized.

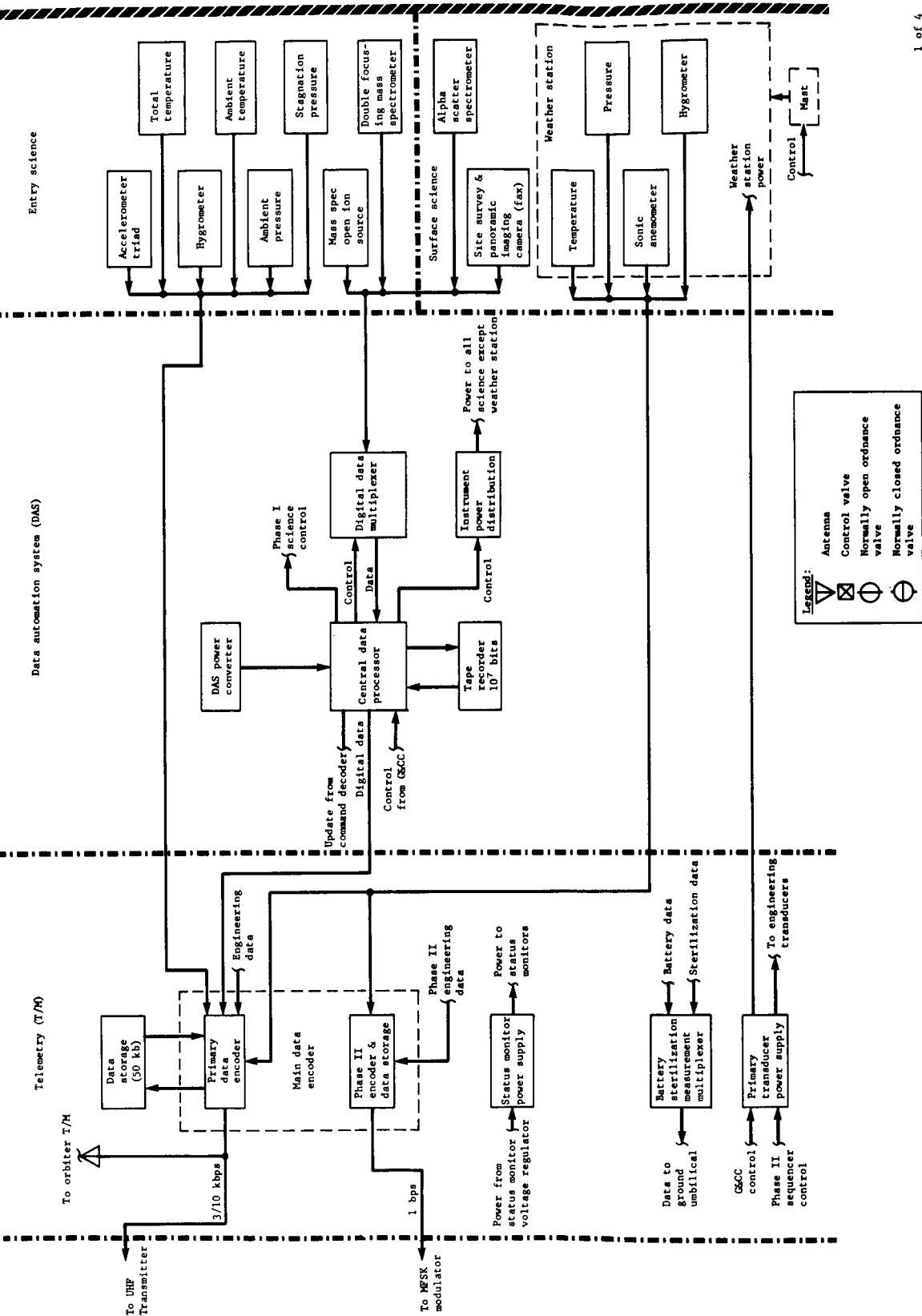


Figure 101.- System Block Diagram, Configuration 2C

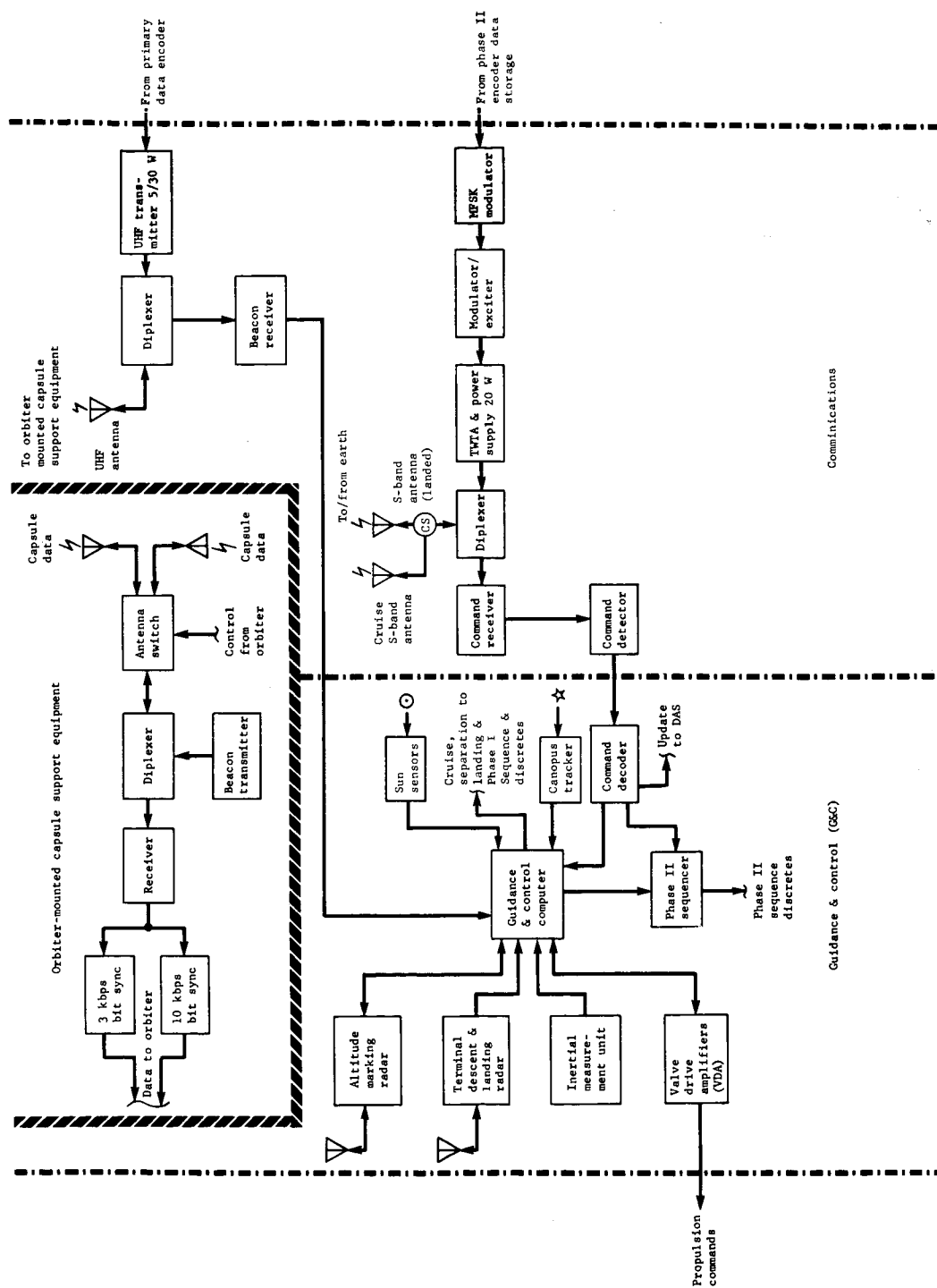


Figure 101.- Continued





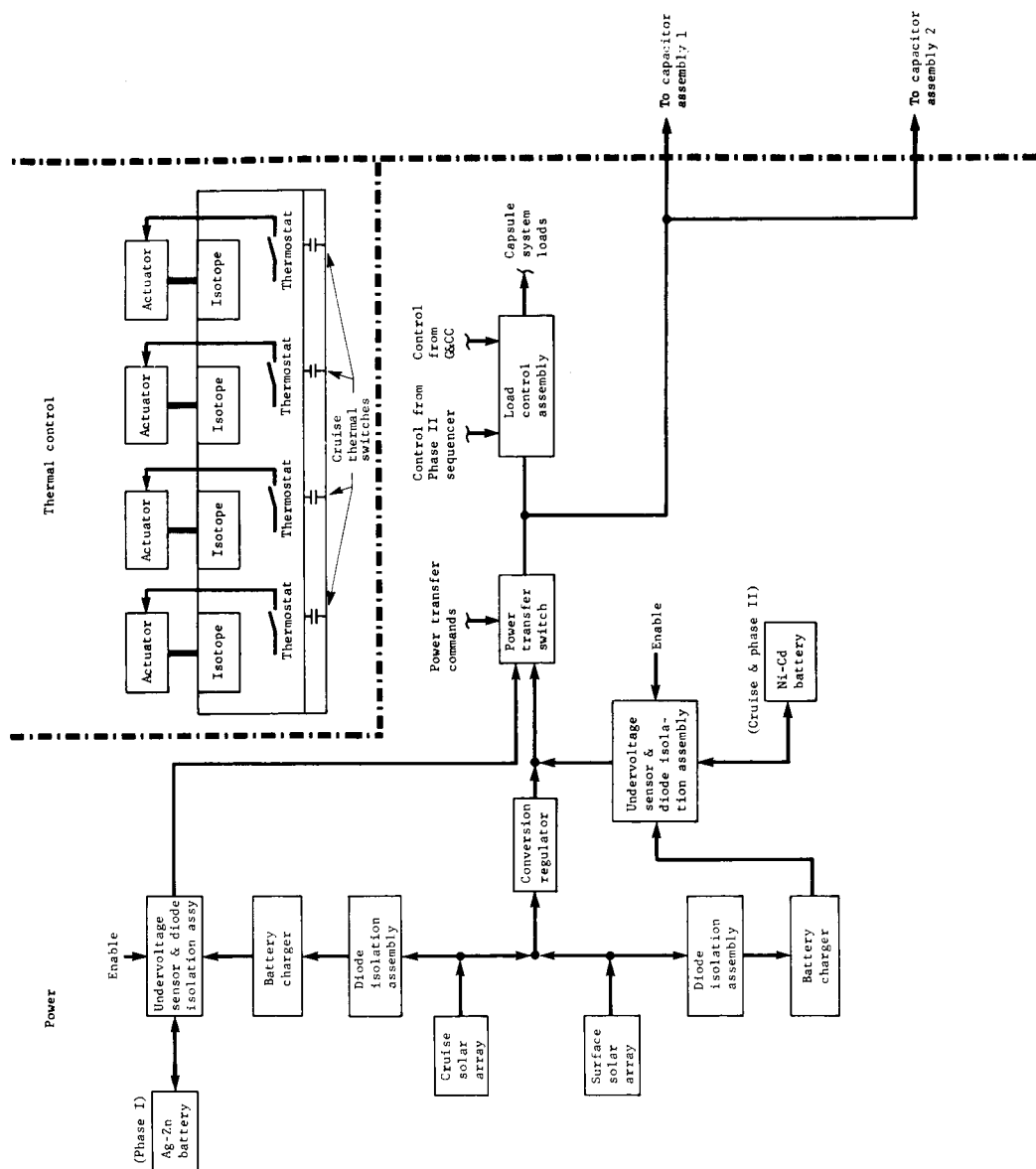


Figure 101.- Concluded

This page intentionally left blank.

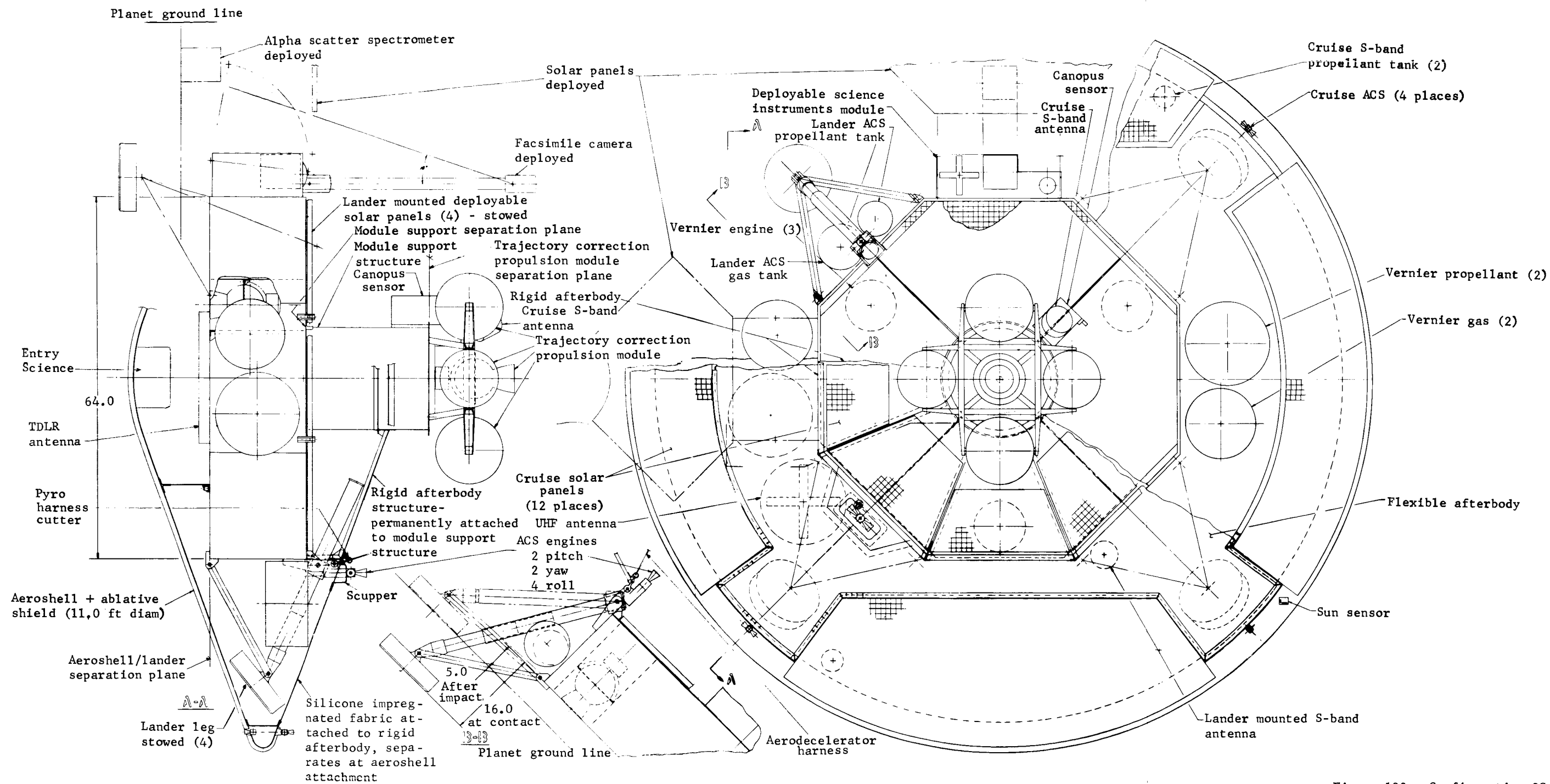


Figure 102.- Configuration 2C

Telecommunications. - The telecommunication subsystem for this configuration is composed of the 1A configuration subsystem elements plus another low-gain S-band antenna and an S-band circulator switch. The second S-band antenna is added to provide the capability of receiving Earth-generated commands and transmitting data back to Earth during interplanetary cruise. The circulator switch performs the function of switching antennas from the interplanetary configuration to the lander configuration.

Power. - The cruise mode solar panels, mentioned previously, are additions to this subsystem, but no other equipment is required to accommodate this source. The status monitor regulator and power management functions are accomplished by other required components and are therefore deleted.

Thermal control. - The major difference between the autonomous capsule and the other configurations is that equipment inside the capsule must be operated during the cruise mode. Therefore, the cruise mode thermal design must be changed to provide for heat rejection.

The autonomous capsule is shown schematically in the cruise mode in Figure 103. The vehicle is maintained in a fixed attitude with the sun along the axis on the aft heat shield, except during initial acquisition midcourse correction and deflection transients. The equipment power is 200 W in addition to 200 W from the lander isotope heaters.

The thermal control approach is to isolate the internal equipment from the sun so that the temperatures will not change appreciably going from Earth to Mars. This is accomplished by using multilayer insulation in areas not occupied by solar cells and using a low  $\alpha/\epsilon$  coating. A stable conversion coating with  $\alpha = 0.42$  and  $\epsilon = 0.7$  is used, which will not degrade after long time exposure to the sun. The equipment and isotope heat is rejected from the system by radiation to the aeroshell and on out to space. A thermal switch device, which is disabled at landing, is needed to provide a high conductance path from the inside of the lander to the bottom surface during the cruise mode. Possible approaches include:

- 1) A conventional heat pipe disabled at landing by an ordnance device to cut the pipe open;
- 2) Mechanical-type switches opened on landing by electrical actuators or by pyrotechnic devices.

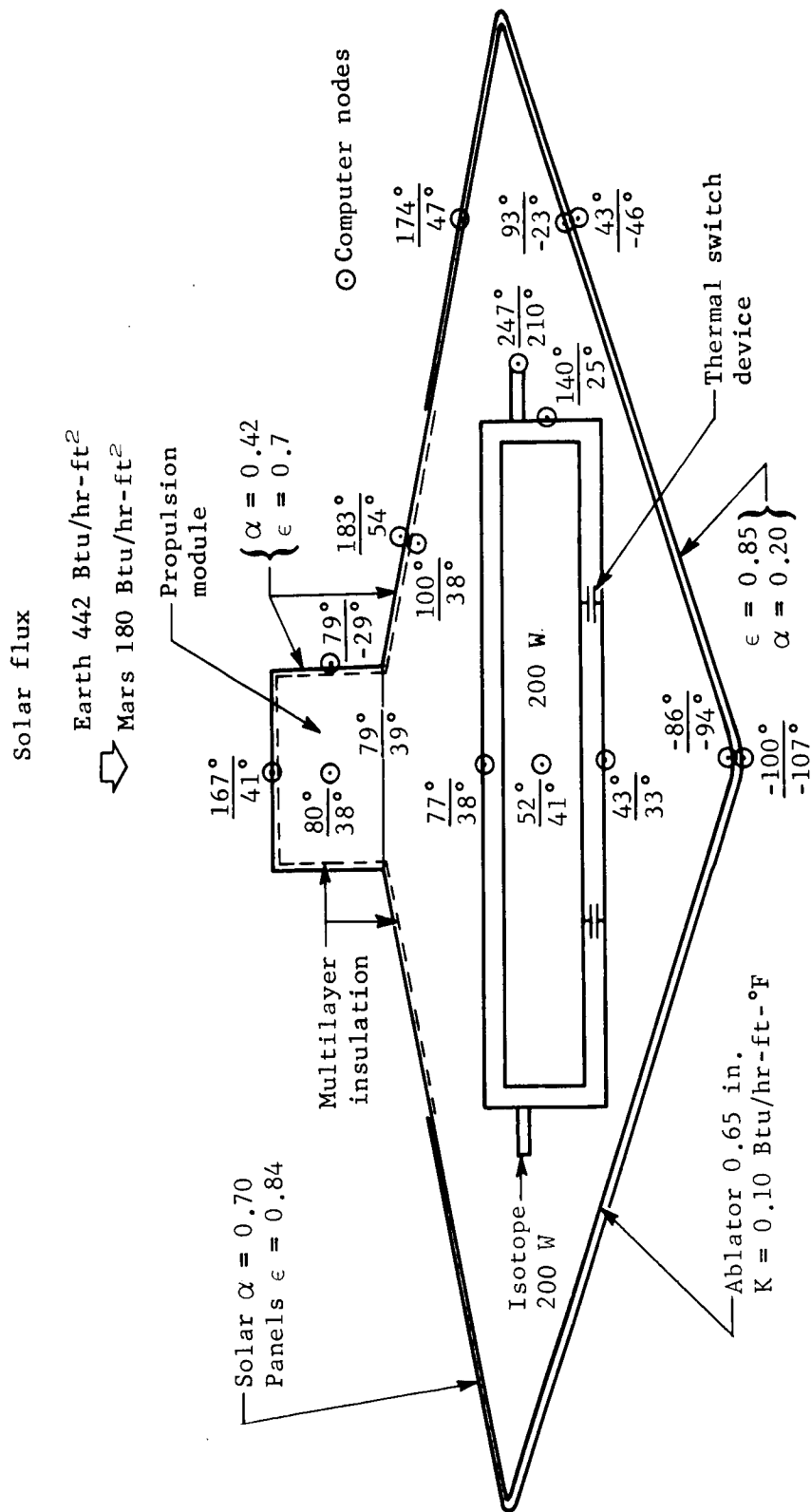


Figure 103.- Autonomous Capsule Thermal Control

A 16-node computer analysis of this design was performed near Earth and near Mars. The results are shown in Figure 103, where the numbers at the top are the temperatures near Earth and the numbers on the bottom are the temperatures near Mars in °F.

The thermal design on the Mars surface is the same as described in Configuration 1A.

### Functional Sequence

Configuration 2C is called the autonomous capsule because the orbiter and capsule functions are combined. However, a cooperative orbiter providing relay communications capability for entry and landed science data is assumed.

The flight capsule mission active phase begins with forward canister separation in earth park orbit. Flight capsule/launch vehicle separation occurs following trans-Mars injection. Subsequent functions include cruise and trajectory correction (mid-course) maneuvers. The flight capsule must perform as many as three trajectory correction maneuvers.

Flight capsule cruise mode is achieved when external references (sun-Canopus) are established. The maneuver mode is established following transfer from the external sun-Canopus references to internal inertial reference (IMU).

Trans-Mars command and communications are provided by the low-gain M'ary FSK link.

The entry mode is established approximately 1 hr before entry. The mission sequence from this point is the same as that described for Configuration 2A.

### Sequential Weight Statement

Table 40 is a summary sequential weight statement of the 2C configuration. The landed equipment weight is 570 lb and the science weight is 84.8 lb landed and 18 lb entry, the same as Configuration 2A. Although work was stopped on this configuration, the weight statement has been updated to account for major changes since that time so that the weights shown are comparable to those of other configurations.

TABLE 40.- CONFIGURATION 2C SEQUENTIAL WEIGHT STATEMENT

Titan III Capability	(2960)	
Fairing penalty	330	
Adapter	300	
Margin	49	
Total flight capsule	(2281)	
Canister structure	189	
Canister electrical	8	
Separated capsule weight	(2084)	
Deflection module structure	36	
Deflection propulsion system	59	
Sun-Canopus sensor	12	
Deflection propellant	69	
ACS propellant	8	
Entry weight ( $B_E = 0.346$ )	(1900)	
Aeroshell	304	
ACS in aeroshell	47	
Solar panels on aeroshell	31	
Science in aeroshell	18	
ACS propellant	4	
Decelerator load	(1496)	
Chute (73 ft diam)	245	
Back face	49	
Insulation and coating back face	11	
Verniered weight	(1191)	
Vernier propellant	119	
ACS propellant	4	
Landed weight	(1068)	
Propulsion	118	
Useful landed weight	(950)	$W_{LE}$
Structure	228	
Attitude control system	28	
Power system	211	211
Guidance and control	136	131
Telecommunication	99	76
Thermal control	107	67
Pyrotechnic control	56	
Science	85	85
Landed equipment weight, $W_{LE} = 570$		



## Space Vehicle Integration

Integration of the autonomous capsule and the launch vehicle is illustrated in Figure 104. The shroud is 12.5 ft in diameter and is functionally similar to the Surveyor-type shroud design. The shroud interfaces at the transtage payload interface.

The spacecraft is mounted forward in the launch position and interfaces with the launch vehicle at the shroud separation plane. Separation energy is provided by spring assemblies at the interface. Shroud L/D is determined by buffeting criteria; however, detailed analysis may allow some reduction of overall length.

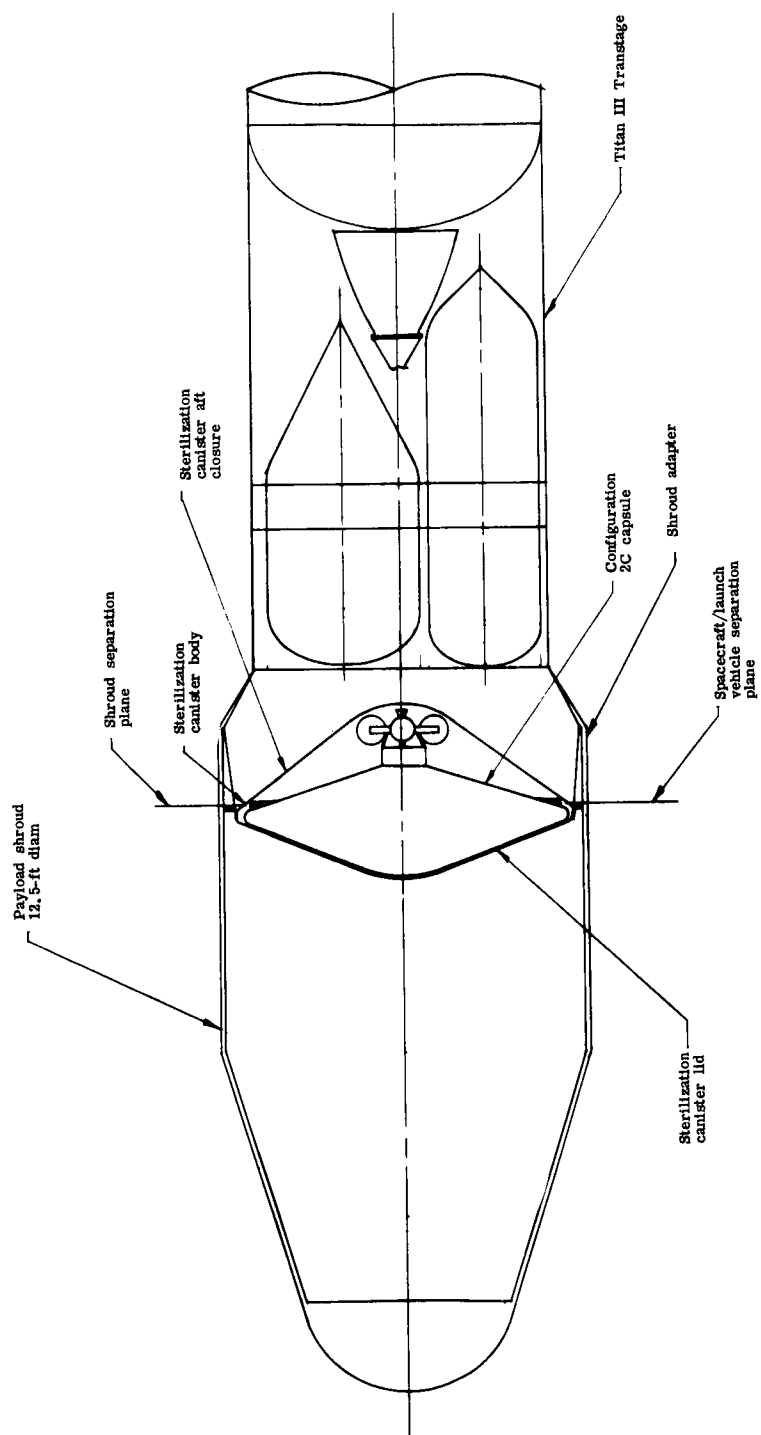


Figure 104. - Space Vehicle Integration, Configuration 2C

## 5. CONFIGURATION 3 DESCRIPTION

### Requirements and Constraints

For the '75/'77 mission, significant changes from the requirements and constraints imposed on the '73 mission are anticipated. Differences from Configuration 1A are listed in the following paragraphs.

Mission. - The mission differences are:

- 1) Trans-Mars trajectory: Type II;
- 2) Deorbit  $\Delta V$ : 300 mps maximum;
- 3) Landing site:  $\pm 60^\circ$  from equator;
- 4) Surface life: > 1 year.

System. - The system differences are:

- 1) Landed equipment weight capability: 1500 lb;
- 2) Structures: Aeroshell diameter compatible with entry conditions, Mach 2 parachute and 1500-lb landed equipment weight;
- 3) Power: RTG/battery;
- 4) Thermal control: RTG heat source;
- 5) Communications: Relay link - entry and postland when orbiter available; low gain direct - postland emergency; high gain direct - postland; direct command link - postland; and data return -  $5 \times 10^6$  bits/day;
- 6) Science: Landed science additions over the Configuration 1A complement are soil organic composition, subsurface temperature and moisture, and soil sample acquisition and processing.

### Performance Summary

Table 41 presents pertinent launch-to-landing performance parameters.

TABLE 41.- CONFIGURATION 3 PERFORMANCE PARAMETERS

Launch vehicle . . . . .	Titan IIIC/Centaur
Launch date . . . . .	August 30, 1975
$C_3$ , (km/sec) <sup>2</sup> , Type II . . . . .	15.5
Arrival date . . . . .	August 4, 1976
$V_{HE}$ , km/sec . . . . .	3.00
Injected payload capability, lb . . . . .	8461
Spacecraft weight, lb . . . . .	8280
Space vehicle margin, lb . . . . .	(181)
$\Delta V_{M/C}$ , mps . . . . .	75
Encounter weight (minus ACS gas), lb . . . . .	8019
$\Delta V_{O/I}$ , mps . . . . .	1350
Orbit characteristics	
$h_p$ , km . . . . .	1000
$h_a$ , km . . . . .	33 070
$P$ , hr . . . . .	24.62
Spacecraft weight in orbit (minus propulsion), lb . . . . .	4470
Flight capsule weight, lb . . . . .	3403
$\Delta V_{D/O}$ , mps . . . . .	300
$\gamma_e$ , deg . . . . .	-18 (max.)
$V_e$ , fps . . . . .	16 000 (max.)
$B_e$ , sl/ft <sup>2</sup> (12.5-ft-diam aeroshell) . . . . .	0.431
Entry weight, lb . . . . .	2813
Parachute deployment altitude, ft ( $h_T = 0$ ) . . . . .	14 000
$B_{DEC}$ , sl/ft <sup>2</sup> (95-ft-diam chute). . . . .	0.020
Vernier ignition altitude, ft . . . . .	4000
$W_{LE}$ , lb . . . . .	1345

## System and Subsystem Definition

This flight capsule uses many of the same design concept as the '73 out-of-orbit systems; however, the increased requirements of the landed mission dictate new power, thermal control, and communications designs. The landed science complement is greatly expanded.

The general configuration of this system is shown in figure 105 and the functional block diagram is shown in figure 106. The 1345 lb allocated landed equipment weight requires an initial flight capsule weight of 3403 lb.

Science. - The expansion of the surface science experiments for this configuration includes the UV spectrophotometer for soil organic composition analysis, the subsurface probe for measurement of temperature and moisture, and the soil sample acquisition device for soil collection and distribution to the soil analyzer. **The size, weight, and instrument interfaces of the DAS will be expanded to accommodate the additional instruments.**

Table 42 lists the 1975 and 1977 extended mission objectives, the measurements that correspond with meeting these objectives, and the measurement life goals.

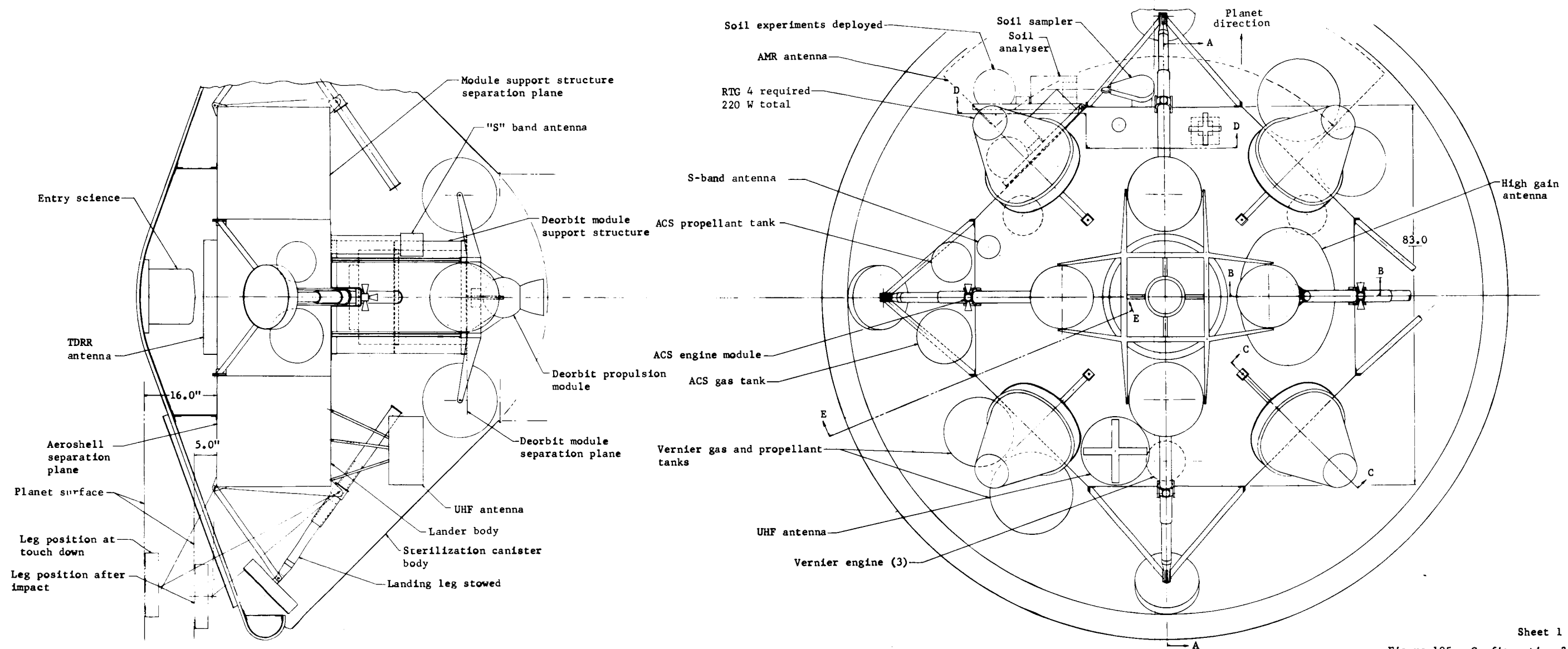
Structures and mechanisms. - All components of this subsystem are similar to Configuration 1B, except in size. The aeroshell is 12.5 ft in diameter and the lander body is a larger octagonal planform structure to house the larger volume of equipment. This configuration has a landing stability factor  $R/H$  of 2.2 and for the landing conditions specified for Configuration 1A will land stably on slopes to  $37^\circ$ .

Telecommunication. - The telecommunication subsystem for this configuration is composed of the 1A configuration subsystem elements and a 2.5-ft-articulated parabolic dish with its associated gimbals, drives, and pointing controls. To transmit data over the high-gain S-band antenna or the low-gain S-band antenna, a circulator switch is added between the TWTA and the diplexer. The sense of circulation is controlled by a direct current control signal. The circulator switch is a three-port latching ferrite switch similar to that used on Mariner '64. The gimbals, drives, and pointing control electronics are sized to accommodate antennas up to 4 ft without redesign. The data rate capability of the high-gain direct link is 240 bps for a coded coherent channel at the maximum range of  $3.96 \times 10^8$  km for a 210-ft DSS antenna. Use of an 85-ft antenna site will reduce the data rate capability by a factor of 10 at the same range.

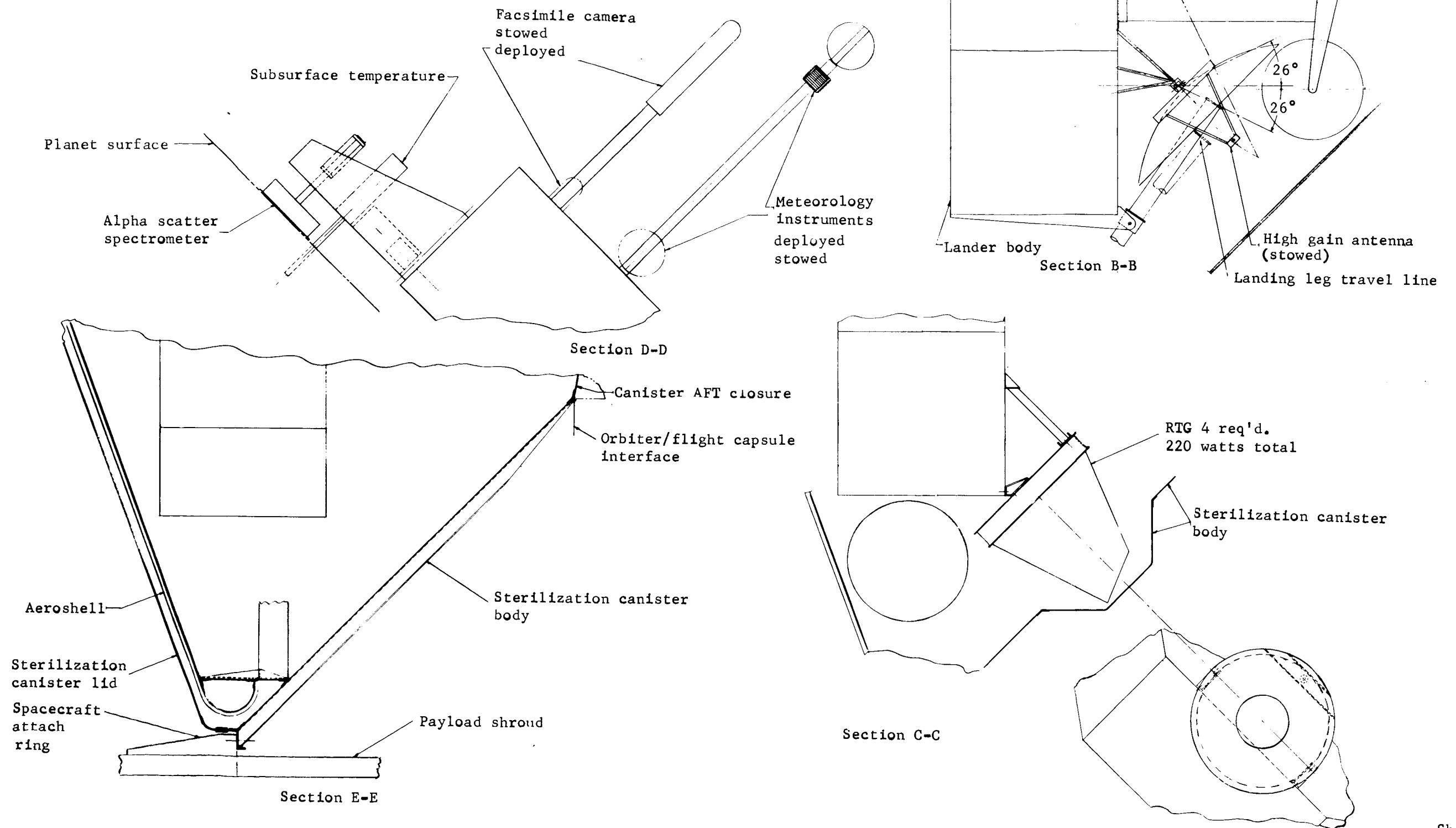
TABLE 42.- EXTENDED CAPSULE MISSION OBJECTIVES AND SCIENCE REQUIREMENTS, 1975 AND 1977

Objectives	Measurements	Life
Soil subsurface environment	Temperature of soil	Minimum 2 diurnal cycles
Soil organic composition	Moisture content of soil	
	Organic compound content of soil	
Atmospheric composition <sup>a</sup>	Composition of the atmosphere at the surface	
Surface imagery <sup>a</sup>	High resolution Low resolution	
Meteorology <sup>a</sup>	Pressure	
	Temperature	
	Humidity	
	Wind	

<sup>a</sup>Designates extended capability for these objectives also shown in Table 12, Capsule Mission Objectives and Science Requirements, 1973.



Sheet 1  
Figure 105.- Configuration 3



Sheet 2  
Figure 105.- Concluded



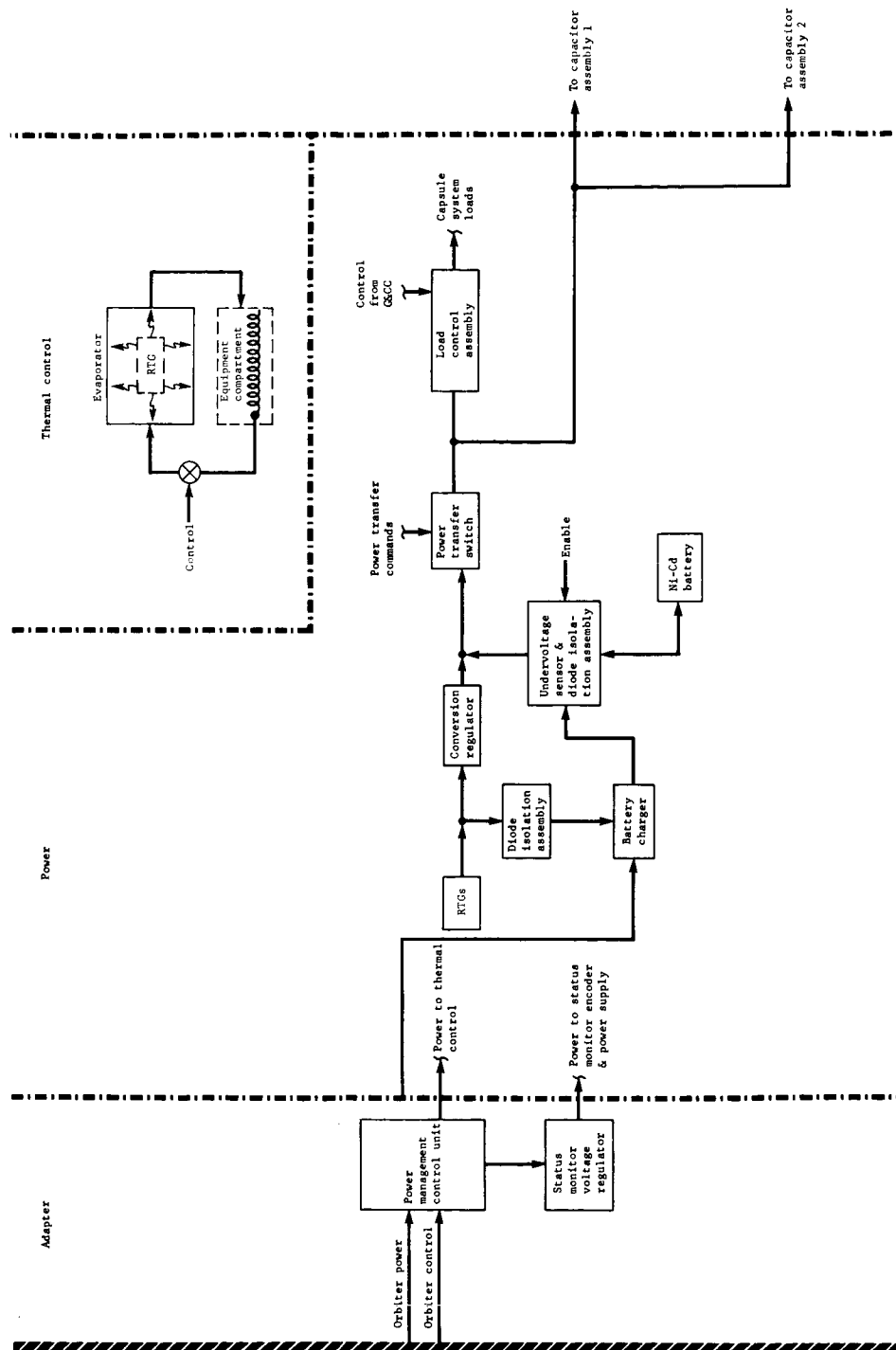


Figure 106.- System Block Diagram, Configuration 3

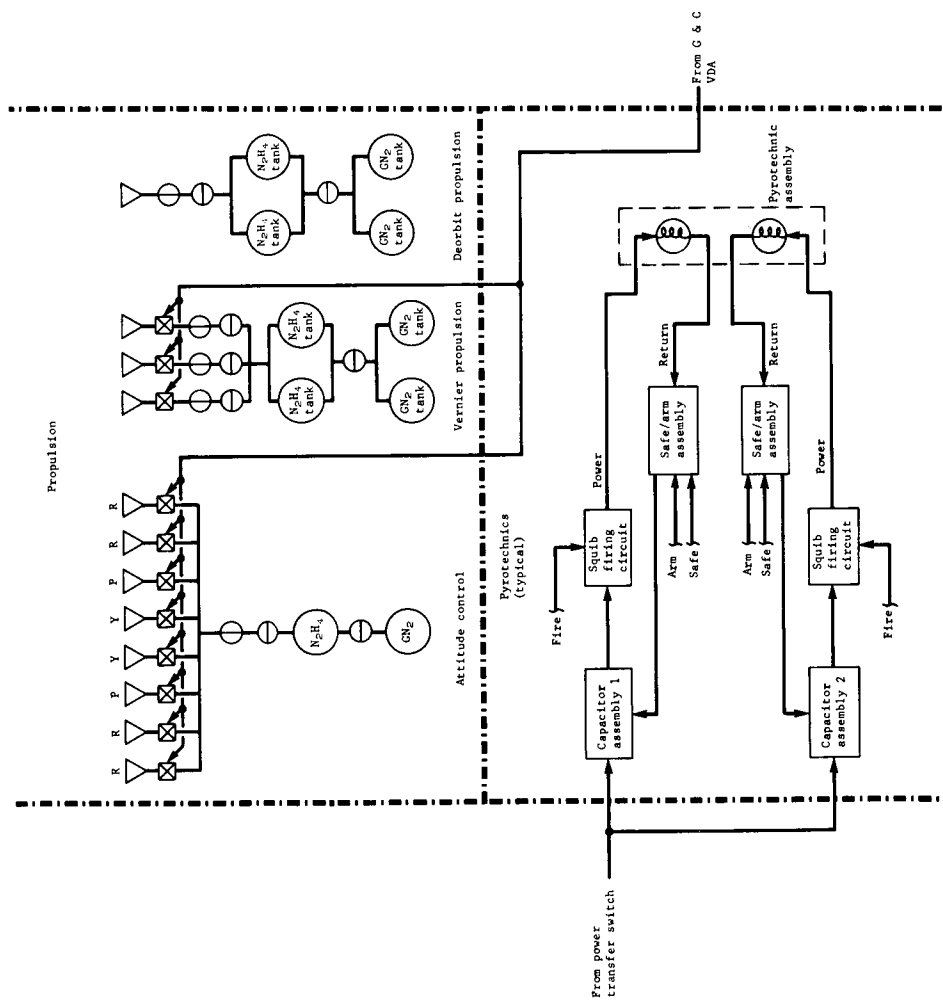


Figure 106. - Continued

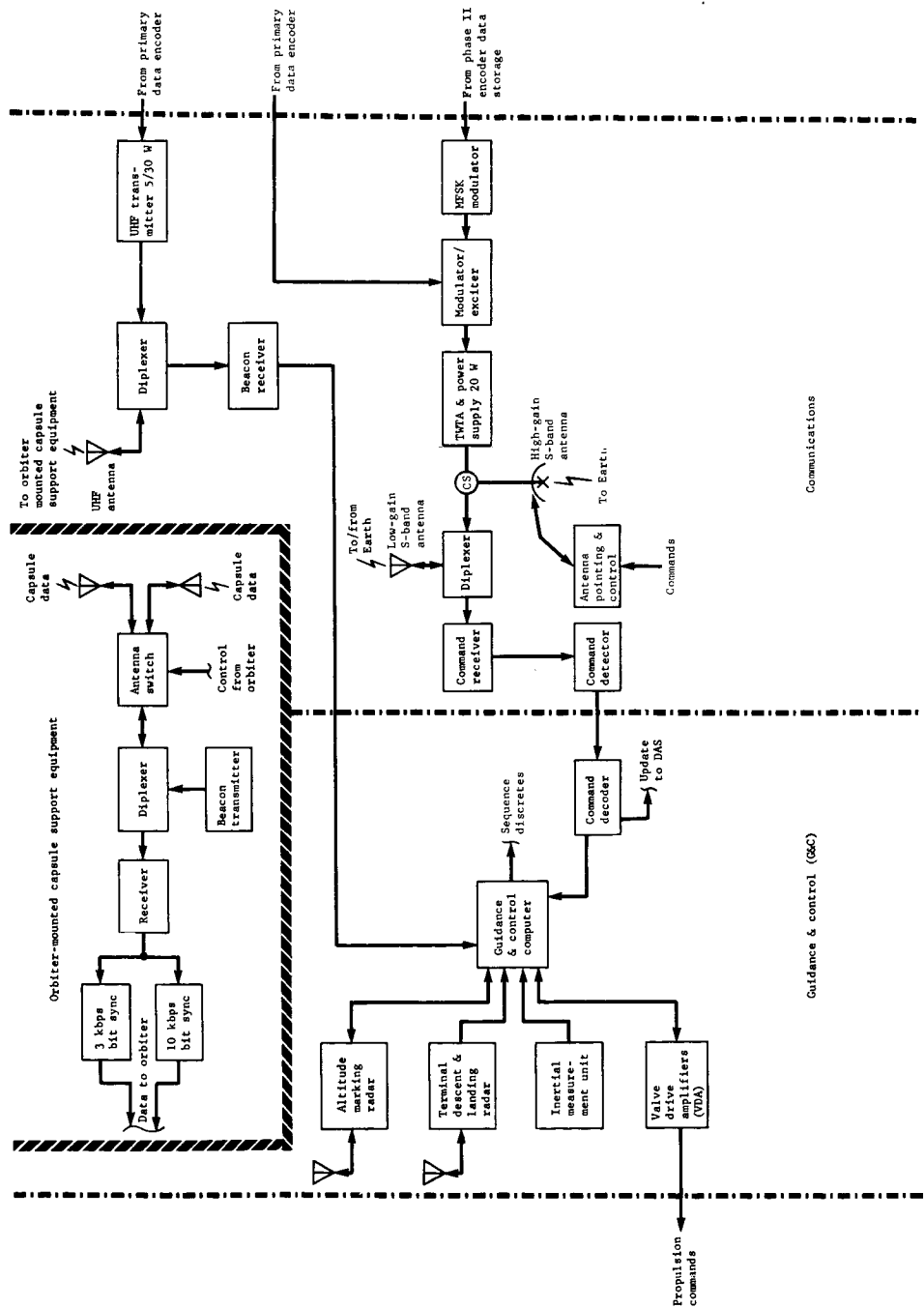


Figure 106.- Continued

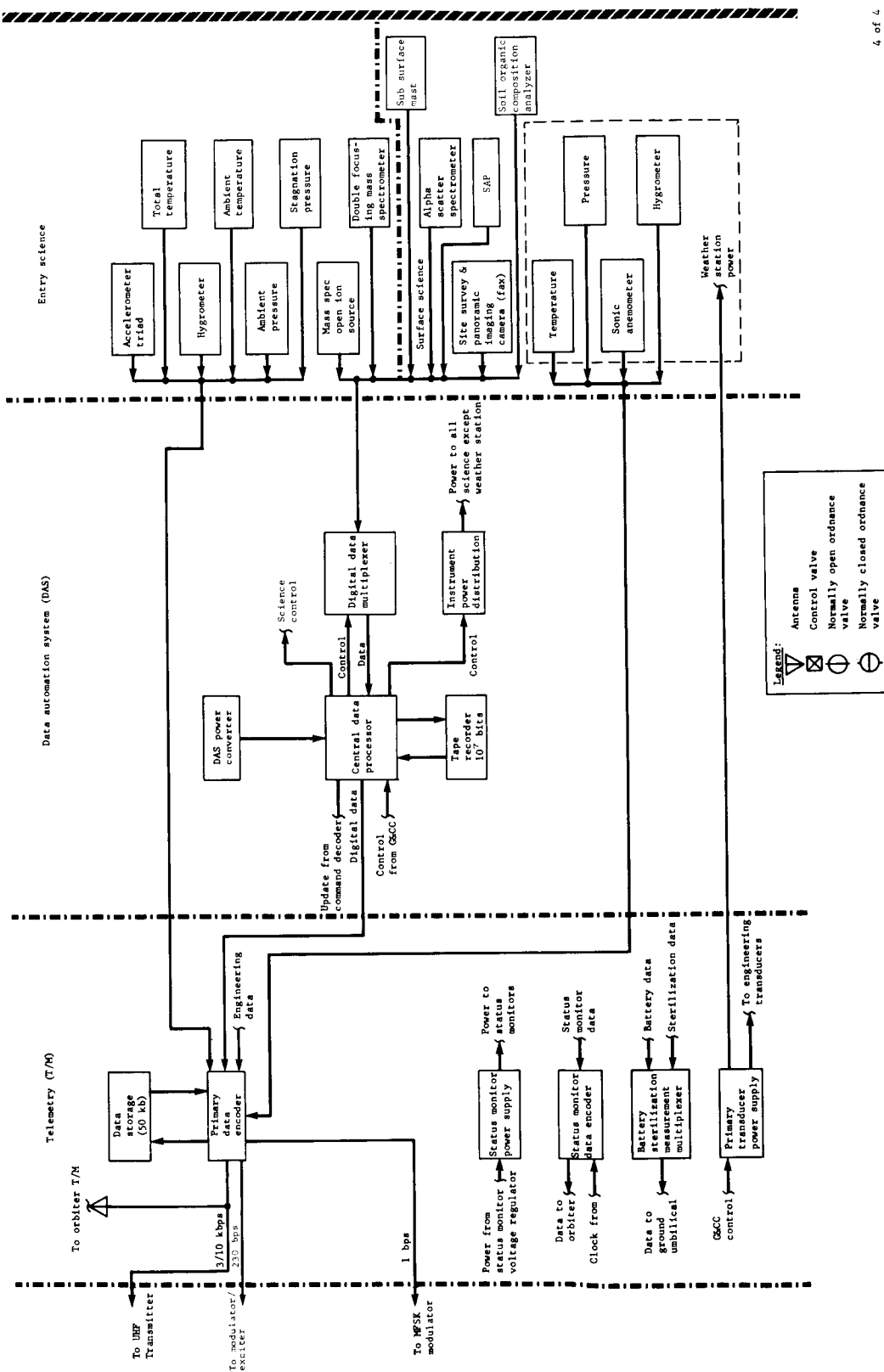


Figure 106.- Concluded

Power. - An RTG/battery power system is dictated by the one-year life requirement since solar array operation cannot be guaranteed in the Mars environment. The system size is based on a 100 W average continuous power and a peak power of 250 W at a 40% duty cycle. Four 50 W RTGs in conjunction with a nickel cadmium battery have been selected to satisfy this power profile. These sources supply not only the landed power requirements, but also the cruise, deorbit, and entry capsule power demands. All power distribution and control concepts are the same as in Configuration 1B.

Thermal control. - The thermal control system consists of a capillary pumped fluid loop that controls the flow of waste heat from the RTG to the lander, insulation, and a phase change material on the transmitter. The procedure described in section 2 of Appendix D was used to estimate the system weights. The capillary pumped fluid loop concept is also described in section 2 of Appendix D. The phase change material and insulation are discussed under Configuration 1A.

Passive cooling of RTGs during the cruise and descent modes were analyzed in detail during the Phase B Voyager studies. The RTG configuration is a scaled-down version of those tested. The shape of the canister is very similar to that used in the tests. The ratio of RTG output to canister area for the test article was  $500/750 = 0.67$ , and for this configuration is  $220/330 = 0.67$ . Therefore, it is expected that the RTG temperatures measured in the tests should be representative of what would be expected in this configuration. The temperatures calculated for the cruise mode were verified in the full-scale tests.

#### Functional Sequence

The mission profile from launch to landing is the same as the profile for Configuration 1A.

Following touchdown, delivery elements of the system are shut down. Before orbiter set, the TV optics are erected and a panoramic survey of the landing site is made and data are transmitted via the relay link. Atmospheric instruments, the alpha-scatter experiment, and the sample acquisition and processing equipment are deployed, activated, and verified operational before orbiter set.

Data are obtained and stored during the night and are transmitted over the high-gain direct link following earth rise and acquisition the morning after landing. A total of  $5 \times 10^6$  bits of data are obtained and transmitted per day to the end of mission.

#### Sequential Weight Statement

Table 43 is a summary sequential weight statement of Configuration 3. The landed equipment weight for this configuration is 1345 lb, and there has been no attempt to break this down. Note that the configuration maintains an entry science weight of 18 lb. Although work was stopped on this configuration, the weights shown have been updated to reflect major changes since that time so that the weights shown are compatible with those of other configurations.

#### Space Vehicle Integration

Configuration 3 utilizes a 14.0-ft-diameter bulbous shroud as shown in figure 107. Integration of this design is functionally similar to Configuration 2A.

TABLE 43.- CONFIGURATION 3 SEQUENTIAL WEIGHT STATEMENT

Titan IIIC/Centaur capability	(9295)
Fairing and/or beefup penalty	515
Adapter	500
Margin	0
Spacecraft weight	(8280)
Orbiter expandables	
(including 60 lb of N <sub>2</sub> gas)	3090
Inorbit weight	5190
Orbiter propulsion system	720
Useful inorbit weight	(4470)
Useful inorbit orbiter weight	990
Capsule adapter	77
Flight capsule weight	(3403)
Canister	274
Aft section, body	175
Forward section, lid	81
Electrical in canister	18
Separated capsule weight	(3129)
Deorbit structure	46
Deorbit propulsion system	98
Deorbit propellant	167
ACS propellant	5
Entry weight ( $B_E = 0.431$ )	(2813)
Aeroshell	262
Science in aeroshell	18
ACS propellant	3
Decelerator load	(2530)
Chute weight (95 ft)	397
Verniered weight	(2133)
Vernier propellant	216
ACS propellant	2
Landed weight	(1915)
Propulsion system	178
Useful landed weight	(1737)
Structure	245
Attitude control system	36
Power system	*
Guidance and control	*
Telecommunication	25*
Thermal control	29*
Pyrotechnic control	57*
Science	*
Landed equipment weight, $W_{LE} = 1345$	
*Only weight not part of landed equipment weight shown.	

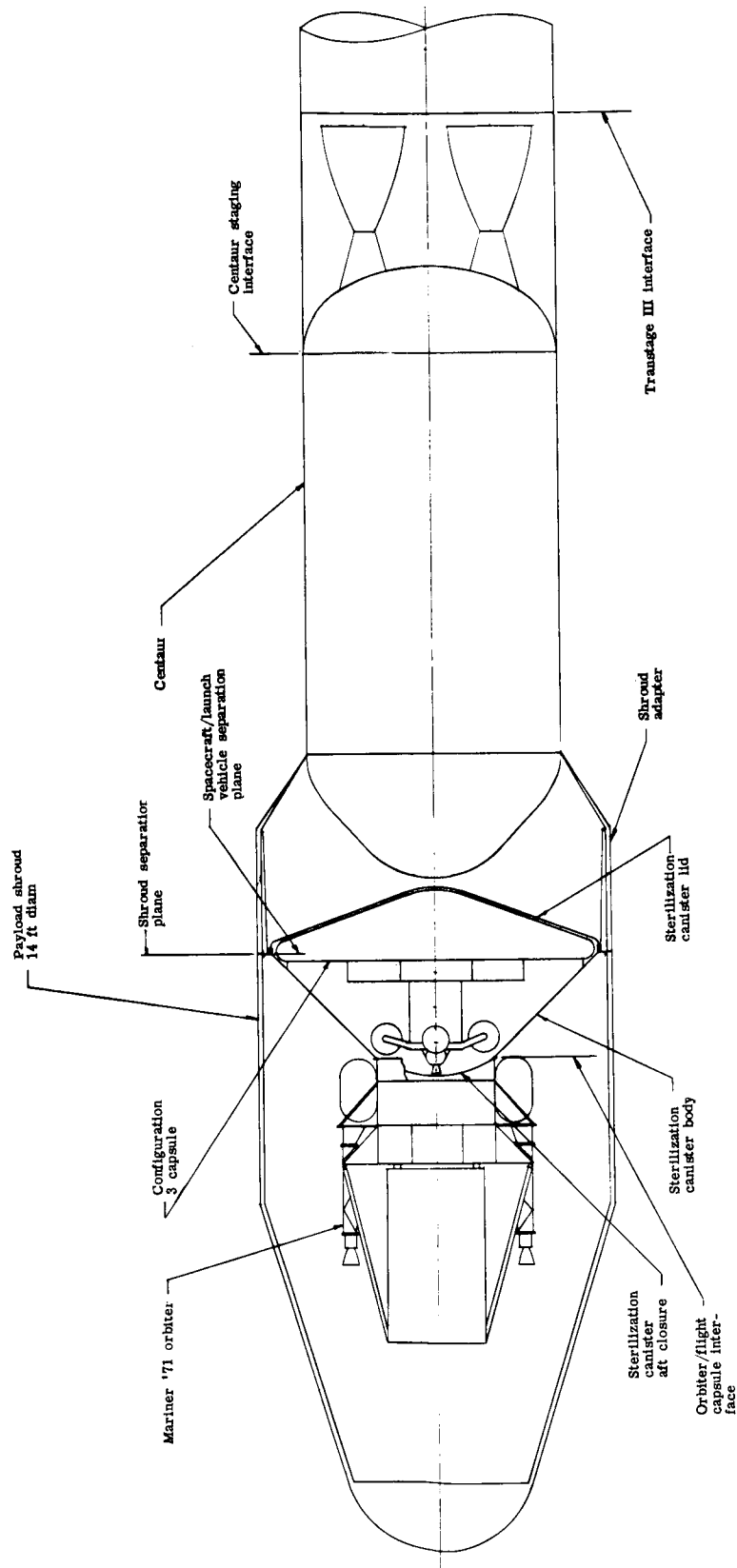


Figure 107. - Space Vehicle Integration, Configuration 3



## 6. CONFIGURATION COMPARISONS

Configuration 1A, 2A, and 1B, which are aimed at the 1973 launch opportunity, have been emphasized during the final phase of this study.

Three other configurations have been studied in lesser detail during this study. These are:

- 1) Configuration 2B - Same capsule configuration as 2A, but with a 600-lb orbiter derived from the 950-lb orbiter (the science and its supporting equipment have been removed). This configuration was eliminated, with Langley Research Center's concurrence, because it was not felt to meet the overall mission objectives.
- 2) Configuration 2C - The autonomous capsule was initially one of the Part II conceptual designs because it required only the Titan IIIC launch vehicle. In the month of study between the first and second oral presentations such serious shortcomings in this configuration were disclosed that it was mutually agreed to stop any further study.
- 3) Configuration 3 - This configuration is representative of later mission capsules using the out-of-orbit mode. Because the emphasis of the present planetary program is aimed at the minimum cost approach for the 1973 launch opportunity, further study of this configuration was terminated at the time of the second oral presentation.

Mission, sequential weight, and subsystem parameters, for the three Part II point designs are compared in table 44. A summary weight comparison for Configuration 1A, 1B, and 2A is given in table 45.

TABLE 44.- MISSION, SEQUENTIAL WEIGHT, AND SUBSYSTEM PARAMETERS, CONFIGURATIONS 1A, 1B, and 2A

Parameter	Orbital		Direct	
	1A	1B	2A	2A
Mission				
Landing site survey before separation	Yes	Yes	No	No
$\Delta V$ deorbit/deflection, m/sec	120	120	75	75
Coast time (max.), hr	8	8	8	8
Targeting $\Delta\beta$ , deg	$a_4$ to 14	$a_4$ to 14	None	None
$V_E$ , fps	$a_4$ to 14	$a_4$ to 14	19 900	19 900
$q_{max}$ , lb/ft <sup>2</sup>	$a_4$ to 14	$a_4$ to 14	380	380
$g_{max}$ , ft/sec <sup>2</sup>	250	180	34	34
$Q$ , Btu/ft <sup>2</sup>	1300	1000	1700	1700
$\dot{q}$ , Btu/ft <sup>2</sup> sec	20	15.5	42	42
$q$ , parachute deployment, lb/ft <sup>2</sup>	16	13	20	20
Time on parachute, sec	40	65	25	25
Vernier ignition altitude, ft	4000	4000	4000	4000
$\gamma_E$ max., deg	-18 -16	-18 -18	-24 -21	-24 -21
Altitude of Mach 2, ft (above MSL)	13 000 16 000	20 000 20 000	11 000 15 000	11 000 15 000
Terrain elevation, ft	0 6000	0 6000	0 6000	0 6000
Weight, lb				
Landed equipment	570	627	570	570
Useful landed	845	970	914	914
Landed	959	1095	1031	1031
Verniered	1068	1209	1148	1148
Entry	1383	1541	1699	1699
Separated	1558	1741	1853	1853
Capsule system	1723	1982	2077	2077
Launch vehicle	TIIC/Centaur	TIIC/Centaur	TIIC/Centaur	TIIC/Centaur
Structures				
Aeroshell				
Diameter, ft	8.5	10.5	10.75	10.75
Ballistic coefficient, sl/ft <sup>2</sup>	.466	.35	.35	.35
Structure weight, lb	72	102	163	163
Ablator weight, lb	44.5	56	83	83
Ablator thickness, in.	.68	.68	.82	.82

TABLE 44.- MISSION, SEQUENTIAL WEIGHT, AND SUBSYSTEM PARAMETERS, CONFIGURATIONS 1A, 1B, and 2A - Concluded

Parameter	Orbital		Direct
	1A	1B	2A
Parachute			
Diameter, ft	65	48	71
Weight, lb	169	90	228
Base cover required	No	No	Yes
Landing slope capability, deg	32	32	32
Shroud diameter	10	12	12
Bulbous	No	Yes	Yes
Science	Entry atmospheric Surface atmospheric Surface imaging Surface composition Isotope heaters, insulation phase change		
Thermal control			
Propulsion	One 510-lb thrust, monopropellant engine, fixed thrust, 3:1 blowdown pressurization	One 635 lb <sup>b</sup>	One 540 lb
Vernier	Three 510-lb thrust, monopropellant engines, 5:1 throttle ratio, 3:1 blowdown pressurization	Three 635 lb	Three 540 lb
ACS	3.7-lb pitch and yaw, monopropellant 2.2-lb roll, monopropellant		
Guidance and control	IMU, TDLR, AMR, computer, science seq		(c)
Telecommunications	UHF relay link Direct M'ary Command		
Power	Ag-Zn (2 days) Ni-Cd/solar array (> 2 days)		
<sup>a</sup> 1000x33 070-km orbit.			
<sup>b</sup> Other than the propulsion thrust levels, all other subsystem parameters are the same.			
<sup>c</sup> Additional and more sophisticated equipment on orbiter for approach guidance.			

TABLE 45.- SUMMARY WEIGHT COMPARISON

	1A		1B		2A	
Total flight capsule	(1723)		(1982)		(2077)	
Canister	165		219		224	
Margin	----		22		----	
Separated weight	(1558)		(1741)		(1853)	
Propulsion and Structure	91		97		91	
Propellant and ACS	84		93		63	
Margin	----		10		----	
Entry weight	(1383)		(1541)		(1699)	
Aeroshell and ACS	128		197		258	
Science in aeroshell	18		18		18	
Parachute	169		90		228	
Base cover	----		----		47	
Margin	----		27		----	
Vernier weight	(1068)		(1209)		(1148)	
Propellant and ACS	109		114		117	
Landed weight	(959)		(1095)		(1031)	
Propulsion	114		125		117	
Useful landed weight	(845)		(970)		(914)	
Structure	156		168		222	
ACS	33		33		32	
Power	211	211	211	211	211	211
Guidance and control	131	131	131	131	131	131
Telecommunications	93	76	97	76	97	76
Thermal control	87	67	91	67	82	67
Pyrotechnic	49		54		54	
Science	85	85	85	85	85	85
Margin	----		100	57	----	
Weight of landed equipment		(570)		(627)		(570)

## CONCLUSIONS

There are no primary flight capsule concept differences resulting from the selection of mission mode. Both the direct and out-of-orbit modes are equally feasible, although the direct mode entry environments are slightly more severe. The main differences between the modes are concentrated in the flexibility and confidence in mission operations. The specific conclusions are tabulated below and on the following page.

Out-of-orbit mode recommended.

Of the point designs studied, Configuration 1B (10.5-ft aeroshell,  $B_E = 0.35$ ) is recommended.

Titan IIIC/Centaur launch vehicle required for either mission mode when orbiter science capability is desired.

Bulbous shroud required for direct mode, and probably required for out-of-orbit mode when using a Mach 2 parachute, VM atmosphere, 6000-ft terrain height, and 10% margins.

Targeting capability is the same in either mission mode when considering only flight profile constraints. However, superimposing any time or orientation constraints decreases the direct mode landing site selection flexibility.

Accuracy of atmosphere structure determination not significantly different between mission modes.

Science, propulsion, telecommunications, power and pyrotechnics, and thermal control (autonomous capsule excepted) subsystems are not affected by mission mode choice.

All subsystem components are either present state-of-the-art technology or can be developed for the 1973 launch opportunity.

Terminal descent and landing radar (TDLR), altitude measuring radar (AMR) antenna, inertial measurement unit (IMU), engines, isotope heaters, sterilizable batteries, sterilizable solar cell adhesives, aerodecelerators, and certain science components are long lead efforts which must start in Phase C.

Out-of-orbit mode	Direct mode
<p>More in-flight mission flexibility</p> <p>Site survey before separation</p> <p>Choose for science objectives</p> <p>Avoid poor capsule surface environment or adverse weather patterns</p> <p>Targeting can be to different site after launch</p> <p>Checkout with time for malfunction correction</p> <p>Second lander can benefit from first lander's data return</p> <p>Can fit within 10-ft shroud; use of a Mach 2 parachute allows for no margins. To provide margins, an 11.5-ft shroud is required</p> <p>Can fit within 10-ft shroud and provide margins by using a Mach 5 ballute</p> <p>Requires additional orbit insertion propulsion added to Mariner Mars '71 orbiter</p> <p>Requires successful orbit insertion maneuver for successful capsule mission</p>	<p>Can use Mariner Mars '71 orbiter, but at sacrifice of targeting and orbital science objectives</p> <p>Slightly larger launch vehicle performance margin</p> <p>More extensive development required</p> <p>Higher entry environment</p> <p>More severe base heating</p> <p>Increased aerodynamic sensitivities to tolerances and misalignments</p> <p>Larger aeroshell and canister</p> <p>More comprehensive aerothermodynamic test program</p> <p>Additional and more sophisticated equipment on orbiter for approach guidance</p>

Martin Marietta Corporation  
Denver, Colorado, June 26, 1968

#### REFERENCES

1. Anon.: Atmosphere of Mars. NASA SP-8010.
2. Schaefer, E. J.; and Nichols, M. H.: Upper Air Neutral Composition Measurements by Mass Spectrometer. J. Geophys. Res., 69, 1964, pp. 4649-4660.
3. Anon.: National Aeronautics and Space Administration Contracts JPL-N-21453, JPL-950267, JPL-950462, JPL-CC-4-321141, JPL-95096, and NASw-1138.
4. Broome, C. G.: Report of Preliminary Studies of Video Data Return for Various Limitations of Total Video Data Bits. LRC Memorandum P/10M-073-GCB, Mar. 12, 1968.